Westinghouse

Approved For Release 2000/05/04 : CIA-RDP67B00657R000300080001-9

Copy 5 of 7.

25X1A

[redacted]

FINAL REPORT

VOLUME II

EQUIPMENT DEVELOPMENT PROGRAMS

Approved For Release 2000/05/04 : CIA-RDP67B00657R000300080001-9

25X1A

[redacted]

Final Report

Volume II

Equipment Development Programs

Prepared by

Westinghouse Research Laboratories

WESTINGHOUSE ELECTRIC CORPORATION

Pittsburgh, Pennsylvania

June 30, 1965

Approved For Release 2000/05/04 : CIA-RDP67B00657R000300080001-9

FOREWARD

25X1A

While the primary aim of the [redacted] was to ascertain the extent of the radar cross-section reduction attainable by an electron cloud, a retrospective examination of the program clearly showed that the development of the specialized equipment to prove the concept in flight required by far the larger portion of the contract effort. During the preparation of the final report, then, it was not surprising to find that there was sufficient material to be documented on the equipment effort alone to warrant an entirely separate volume on that subject. The order of the chapters is generally chronological, beginning with theory and experiments for electron-beam-transmitting windows, following into the window tube work and its more successful successor, the dynamically pumped gun, and concluding with a description of the operation of the equipment in the field.

Every attempt has been made to make the report complete. However, the length of the program and the absence of any formal reporting requirement during its first 80 percent make it entirely possible that those preparing the final report have overlooked important contributions by others, some of whomare no longer even associated with this organization. Where such omissions come to light, the editor will appreciate being so informed, in order that he might arrange for the necessary revisions in the document.

TABLE OF CONTENTS

Approved For Release 2000/05/04 : CIA-RDP67B00657R000300080001-9

Approved For Release 2000/05/04 : CIA-RDP67B00657R000300080001-9

CHAPTER 1
ELECTRON BEAM WINDOWS

1.01. Introduction

The design of a window device for transmitting electron beams into an atmosphere having pressures from several torr to atmospheric pressure depends on several technical factors. The thin foil which constitutes the window should not present an excessive absorption cross-section to the beam. It must be capable of dissipating the power lost by the beam as it traverses the material without excessive thermal gradients and, most important, must be able to withstand the mechanical forces produced by thermal stresses and the pressure of the external atmosphere.

The problem of theoretically computing whether a given window configuration will stand up when transmitting the desired amount of power requires determining the energy losses within the window as a function of the transmitted power, calculating the thermal gradients and mechanical stresses associated with this loading and with the pressure differential across the window and comparing the result with data on mechanical strength of the window material at the temperature in question.

In the sections which follow, the losses associated with the passage of high speed electrons through different materials will be discussed, the thermal gradients associated with different configurations will be computed, the mechanical stresses discussed, and a comparison made with experimental data.

1.02. Assessment of Power Lost by Beam in Al Foil

Bethe[1] has given the following expression for the average energy loss per unit path length for a charged particle traversing matter:

$$-\frac{dE}{dx} = f(E) = \frac{4\ N\epsilon^4}{mv^2}\ \frac{\ln mv^2\sqrt{\frac{e}{2}}}{2\bar{I}} \quad \text{(ergs/cm)} \qquad (1.02.01)$$

where N = number of electrons per cm^3 of matter

ϵ = charge of electron

m = mass of electron

v = velocity of incident electron

e = 2.718

$\bar{I}$ = average excitation energy of the atoms being traversed.

The energy lost by a given particle in traversing a thin section of window material in which electron scattering may be considered negligible can be obtained by integrating Eq. 1.02.01.

$$-\int_{E_1}^{E_o} \frac{dE}{f(E)} = \int_{x}^{o} dx = \int_{E}^{E_o} \frac{dE}{dE/dx} \qquad (1.02.02)$$

where E_o is the energy of the incident particle and E is its energy at a distance x within the material. The $(\frac{1}{dE/dx})$ function easily lends itself to graphical integration methods, so that a convenient solution is available once the dE/dx function has been determined.

1. Bethe, H.A., Handbuch der Physik (Julius Meyer, Berlin, 19663) vol. 24.

Lane and Zaffarano[2] have evaluated Eq. 1.02.01 for electrons traversing aluminum foil and obtained the following equation:

$$\frac{dE}{dx} = (.307)\left(\frac{Z}{A}\right)\frac{1}{\beta^2}\left[\ln\left(51.1\,\beta^2\right) + 3.66\right] \text{ kev/mg/cm}^2 \qquad (1.02.03)$$

where Z is atomic number, A is atomic weight, and $\beta = v/c$ is the ratio of the particle velocity to the velocity of light.

In evaluating Eq. 1.02.01 for Al, they employ the value of 150 ev for $\bar{I}$, and have solved for N as follows:

$$N = \frac{n\rho Z}{A} \qquad (1.02.04)$$

where n is Avogadro's number, and ρ is the density of the material.

Fig. 1.02.01 gives a plot of $\frac{1}{dE/dx}$ vs. kv as derived from Eq. 1.02.03. The upper curve represents the actual curve obtained directly from Eq. 1.02.03. The lower curve incorporates a 1.45 factor reduction obtained by observing the departure of theory from experiment as plotted for Al foil in Figure 19 of Reference 2. Part of the discrepancy between theory and experiment was due to the fact that the electron energy losses determined from the Bethe equation are taken along the actual path of the electrons in their zig-zag course through the material, whereas the desired result relates to the attenuation of beam power with thickness in a given direction through the material. In section 1.04 a more sophisticated theory which takes electron scattering into consideration will be discussed. Use of the corrected curve to obtain the energy loss from the beam as a function of window thickness is exemplified by the cross-hatched area. Determination of this area, of course, represents the integration of Eq. 1.02.02 referred to previously. The area of the cross-hatched section thus

2. R. O. Lane and D. J. Zaffarano, Transmission of 0 to 50 kv Electrons by Thin Films with Applications to Beta Ray Spectroscopy, (U.S. Atomic Energy Commission ISC-439, Dec. 1953.)

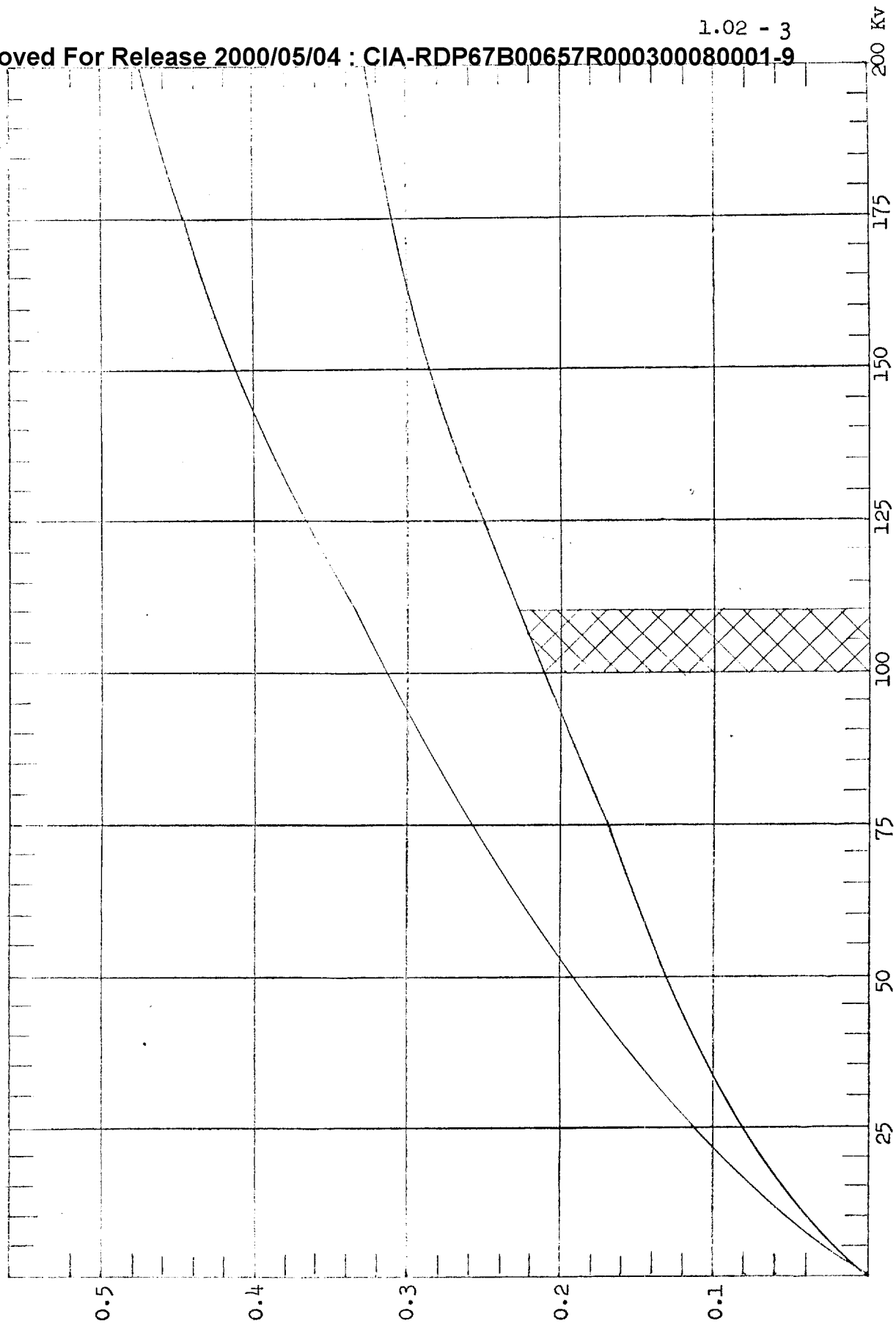

Fig. 1.02.01 $\frac{1}{dE/dx}$ in Reciprocal Kev/mg/cm^2 versus Primary Beam Kv

represents the mg/cm^2 of Al foil which will reduce by 10 kev the average energy of electrons which are incident at 110 kv. From the curve we see that this area turns out to a close approximation to be $(.22)(10) = 2.2\ mg/cm^2$, which corresponds to a thickness of 8.2μ or .32 mil. Thus a 110 kv beam will lose approximately 10 kev in traversing a .32 mil thickness of Al foil. The calculations in section 1.04 on the heat dissipation problem are based on a 10 kev loss in a 1/3 mil foil, corresponding to an 8.5μ thickness. A 110 kv primary voltage is assumed.

On a more formal basis, it is evident that the cross sectioned area of Fig. 1.02.01 represents the window height per unit area M necessary to produce an average energy loss E_1 per electron in a given electron beam. It is given approximately by the product $\frac{1}{dE/dx}$ at the appropriate location of the curve and E_1 the energy loss per electron. Thus the average energy loss per electron can be expressed by the following equation:

$$E_1 = M \frac{dE}{dx} = \rho D \frac{dE}{dx} \qquad (1.02.05)$$

where D is the thickness of window material and dE/dx is the energy loss per unit weight per unit area. For beam current I, the energy per second expended by the electron beam in traversing the window is given by the following equation:

$$W = IE_1 = IM \frac{dE}{dx} = I\rho D \frac{dE}{dx} \qquad (1.02.06)$$

It is apparent that electron range, which is defined as the amount of material necessary to reduce the energy of the incident particles to zero, is obtained by integrating Fig. 1.02.01 over the whole area from the desired incident energy to zero energy.

As a means of obtaining the order of magnitude of the energy losses involved when an electron beam traverses a material, the mg/cm^2 required to achieve a given energy loss in Al foil is plotted in

Fig. 1.02.02 for 100 kv, 125 kv and 150 kv electron beams. These data are obtained using the corrected curve of Fig. 1.02.01 assuming it is linear in the region of interest. The thickness of Al foil necessary to produce a 10 kev energy loss in Al foil is thus 2.1, 2.4 and 2.75 mg/cm^2, corresponding to thicknesses of 7.8, 8.9 and 10.1 microns for 100, 125 and 125 kev electrons respectively.

It is important to note that the loss in the window increases as voltage is decreased. The maximum loading of the window will be determined by the maximum allowable temperature gradient required to dissipate the window heat losses incurred by the beam to an assumed heat sink adjacent to the window. In section 1.05 this maximum loading is assumed to be 30 ma for a primary beam of the order of 110 kv. For 8.5 micron Al foil, the loss per electron is about 10 kev. The heat loss in the window is thus approximately (10,000) (.030) = 300 watts. Table 1.02.01, below, shows how the kev energy loss varies with primary beam voltage, as well as how beam loading must be varied to keep the energy losses at the window constant.

Table 1.02.01 - Energy Loss in 8.5 Micron Al Window, Also Tube Maximum Allowable Current for 300 Watt Loss

Primary kv	Anticipated Energy Loss in Window in kev	Maximum Allowable Current in Tube in ma
149	7.9	38
110	10	30
81.5	13	23
58.3	16.6	18

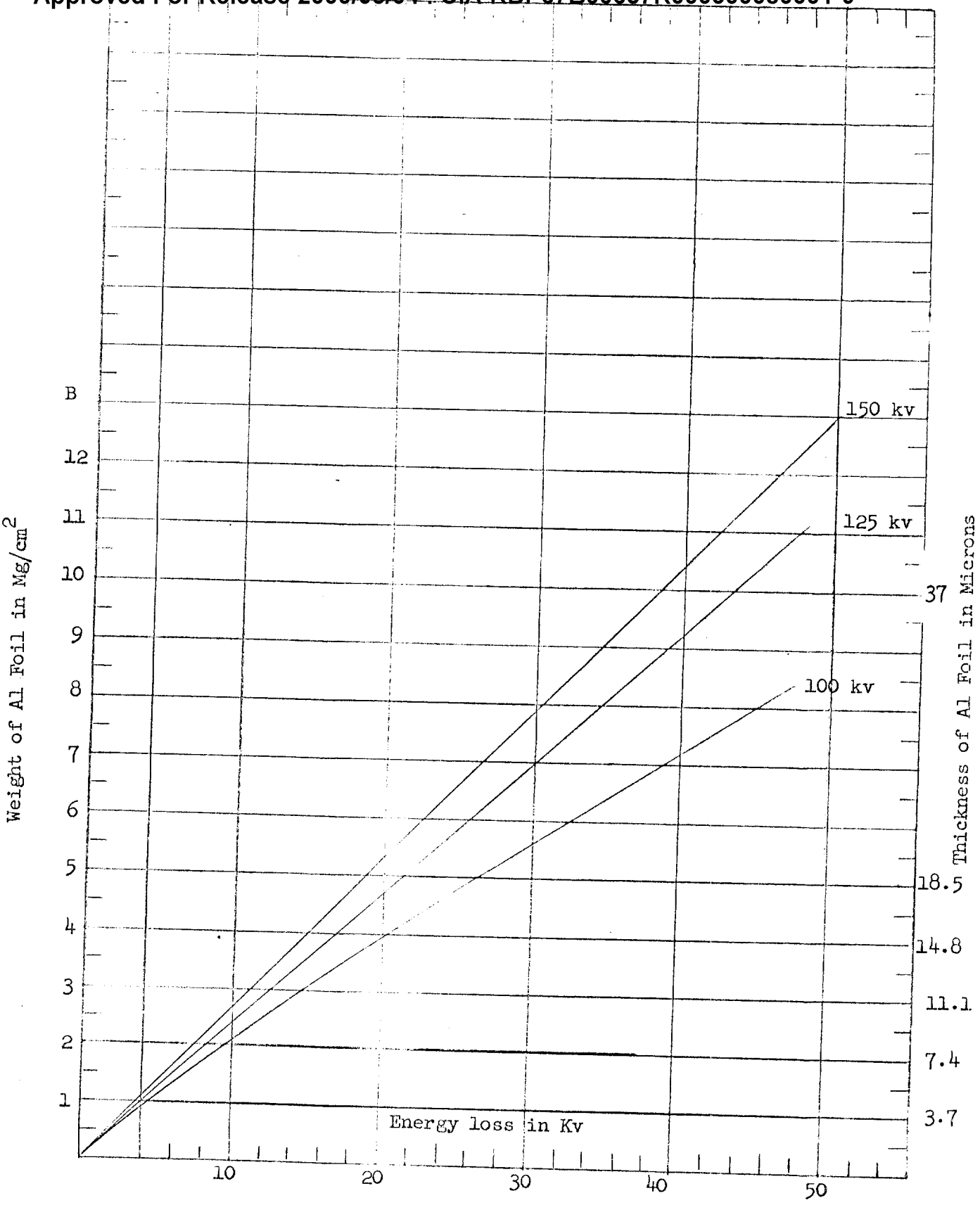

Fig. 1.02.02 Weight of Al Foil which will Produce Given Energy Loss for 100 kv, 125 kv and 150 kv Beams

1.03. Figure of Merits of Different Materials as Electron Beam Windows

Theoretical values of dE/dx and range for a number of different materials have been determined by Nelms[3] as a function of the energy of the incident electrons. Using these data, curves similar to Figs. 1.02.01 and 1.02.02 can be plotted and the energy loss determined as a function of the thickness of the material employed. Theoretical data obtained in this fashion may be subject to the same order of correction which has been made for Al foil in section 1.02. From Fig. 1.02.02, particularly for higher energies, it is evident that the energy loss in traversing a given material can, to a reasonable approximation, be assumed to be linear with the thickness of the material.

The thermal figure of merit can be derived from the following considerations if we neglect all heat losses from the window except thermal conductivity losses. From heat theory the temperature gradient across a window having thermal conductivity k, separated by a distance A from a heat sink, can be expressed by the following equation:

$$\Delta T = \frac{WA}{kLD} \qquad (1.03.01)$$

where W is the energy/sec absorped in the window, L is the length of the beam and D is the thickness of the window.

Substituting Eq. 1.02.06 in Eq. 1.03.01, we obtain

$$\Delta T = \frac{AID\left(\frac{dE}{dx}\right)\rho}{kLD} \qquad (1.03.02)$$

The thickness of the window D, which is present in both denomination and numerator of Eq. 1.03.02, cancels out. Thus the temperature of the window is substantially independent of window thickness. Essentially, this means that the improved thermal conductivity obtained by increasing the thickness of a given window is cancelled out by proportionate increase in the energy losses experienced by the beam as it traverses the thicker window.

3. A. T. Nelms, "Energy Loss and Range of Electron and Position," NBS Circular 577 (1952)

If the thermal figure of merit is taken as being proportional to $1/\Delta T$, then for a given beam size, current and window geometry, we can define an electron beam window thermal figure of merit F by the following equation:

$$F = \frac{k}{\rho(\frac{dE}{dx})} \qquad (1.03.03)$$

where k is thermal conductivity, ρ is the density of the material and dE/dx is the energy loss per unit weight per unit area incurred by the beam in traversing a given window material.

The relevant physical parameters of a number of window materials are listed in Table 1.03.01 including the thermal figure of merit F for 100 kv electrons as defined by Eq. 1.03.03. Since F is proportional to $1/\Delta T$, a knowledge of F permits ready assessment of the maximum temperature associated with different window materials once the temperature gradients associated with one given material have been determined.

The values listed in Table 1.03.01 represent uncorrected values of the electron beam energy loss parameters. For this reason the energy losses associated with aluminum are somewhat lower on this table than the corrected values determined from Fig. 1.02.01. For very thin windows it is believed that the use of Table 1.03.01 to compare the theoretical performance of different materials with the theoretical performance of Al will give reasonably accurate answers when referred to thermal data for Al for which corrected values have been obtained. Since the calculations of section 1.04 are based on corrected values of Al, comparisons of different materials using temperature data taken from section 1.04 will give "corrected" thermal numbers for other materials.

Comparing, for example, the figure of merits of Al vs. Ag, we obtain a ratio of 5.9/3.9 = 1.52 in favor of Al. Thus, if, as discussed in section 1.04, the window has been designed to limit the window temperature gradient to 150°C for aluminum with a 300 watt heat input

Table 1.03.01 - Figures of Merit for Metal Windows for 100 kev Electrons

1	2	3	4	5	6	7	8	9	10	11
Material and Atomic Number	gm/cm^3	k $cal/cm^2/cm/^oC/sec$	k/ρ	dE/dx_2 in kev cm^2/mg	$F = \frac{k}{\rho(\frac{dE}{dx})}$ Thermal Figure of Merit	$F = \frac{1}{\rho(\frac{dE}{dx})}$ Figure of Merit for Absorption Losses for Equal Thicknesses	ΔT Gradient for Window Compared to ΔT = 150°C for Al	Window Thickness in microns to Equal Output of 8.5 micron Al Window	Range at 100 kv in mg/cm	Range at 100 kv in microns
Be 4	1.85	.385	.21	3.4	6×10^{-2}	.16	148°C	12.4	17.3	94
C 6	2.22	.057	.026	3.71	6.9×10^{-3}	.12	1280°C**	9.3	15.9	72
Al 13	2.7	.52	.19	3.24	5.9×10^{-2}	.11	150°C	8.5	18.3	68
Ti 22	4.5	.04	.0089	2.9*	3.1×10^{-3}*	.077*	2860°C**	5.95	--	--
Fe 26	7.87	.19	.024	2.83	8.6×10^{-3}	.045	1030°C**	3.48	21.2	27
Ni 28	8.9	.14	.016	2.8*	5.6×10^{-3}*	.04*	1580°C**	3.1	--	--
Cu 29	8.94	.923	.10	2.72	3.8×10^{-2}	.041	233°C	3.17	22.1	25
Mo 42	10.2	.35	.034	2.46	1.4×10^{-2}	.04	632°C	3.1	24.6	24
Ag 47	10.5	.974	.093	2.40	3.9×10^{-2}	.04	227°C	3.1	25.3	24
W 74	19.3	.476	.025	2.05	1.2×10^{-2}	.025	740°C	1.93	30.1	16
Pt 78	21.45	.166	.078	2.01	3.9×10^{-3}	.023	2270°C**	1.78	30.7	14
Au 79	19.3	.707	.037	2.01	1.8×10^{-2}	.026	492°C	2.0	30.6	16

*By interpolation

**Appreciable radiation loss is neglected

Approved For Release 2000/05/04 : CIA-RDP67B00657R000300080001-9

to the window, then an Ag target would operate with a temperature gradient of (150)(1.52) = 227°C under the same beam and window geometry conditions. As indicated previously, the temperature conditions derivable from the thermal figure of merit are independent of window thickness. For thicker foils with fractional ranges in excess of 0.2 or 0.3, Spencer's theory (section 1.04) showed give more accurate results.

It is evident that the maximum temperature experienced by a window is only one of several parameters which must be evaluated in selecting the window for an electron beam tube. One of the major factors which must be considered relates to the window thickness required to withstand the pressure differentials across the window at the temperatures associated with operation of the tube under maximum loadings. Still another important parameter relates to the output power which is transmitted through the window at the thickness in question, which is, of course, the total beam power minus the energy losses incurred in the window. An even more important factor are the thermal stresses incurred as related to the physical properties of the window at the temperatures in question.

Taking subscript 1 to apply to Al, and subscript 2 to apply to Ag, the ratio of the window absorption losses in Al to those in Ag from Equation (5) are as follows:

$$\frac{(E_1)_1}{(E_1)_2} = \frac{\rho_1 D_1 \left(\frac{dE}{dx}\right)_1}{\rho_2 D_2 \left(\frac{dE}{dx}\right)_2} \qquad (1.03.04)$$

It is evident that we can define still another electron beam window figure of merit which will permit direct comparison of the absorption losses incurred by the beam in traversing equal thicknesses of different materials. From Eq. 1.03.04 for a given value of D, this figure of merit which applied only for very thin parts is given by the following equation:

$$E = \frac{1}{\rho(\frac{dE}{dx})} \qquad (1.03.05)$$

Values of this figure of merit are also listed in Table 1.03.01. It is important to bear in mind in using E to compare the electron absorption losses of given materials that window thickness must be taken into consideration, whereas, the use of the F figure of merit for thermal gradient comparisons is independent of window thickness.

Returning to the comparison of Al and Ag, we observe E_1/E_2 = .11/.04 = 2.75. Thus, if a 10 kev loss is incurred by a 110 kv electron beam in traversing an 8.5μ thickness of Al, a 27.5 kev loss will be experienced by the beam in traversing an equal thickness of Ag for thicknesses where scattering is not excessive. In order to obtain the same power output through the Ag window as is obtained through the 8.5μ Al window, the Ag window thickness according to the simple theory must be reduced by a 2.75 factor to 8.5/2.75 = 3.1μ. The 3.1μ window must be able to withstand the required pressure differentials at 227°C compared to similar requirements on the 8.5μ Al window at 150°C.

Column 8 of Table 1.03.01 lists the relative temperature gradients computed for different window materials on the basis of the thermal factors F assuming that the beam and window geometry will produce a 150°C temperature gradient for Al foil. This column is independent of window thickness for the range of thickness for which the linear approximation holds. Column 9 gives the window thickness of different materials required to produce electron beam power outputs equivalent to that obtained for 8.5 micron Al foil for which a 10% power loss has been calculated.

Materials having low figure of merits F will have temperature gradients which are so high that other means of heat dissipation such as radiation cooling can no longer be considered negligible. The total area of the window bombarded by the beam is .3 cm^2 on the basis of assumptions made later. A black body having this area at

1000°C will radiate 4.5 watts. At 2000°C a black body having this area will radiate 45 watts. Thus, heat dissipation by radiation does not get to be a very major factor for window inputs of the order of 300 watts.

Column 10 gives the total 100 kv range of different window materials computed by Nelms,[3] and column 11 gives these range data in microns.

While data in this report are restricted to metal foils, promising materials are by no means limited to metals. A major problem associated with non-metallic materials relates to the low thermal conductivities frequently associated with them. However, some such materials have relatively high thermal conductivities. For example, the thermal conductivity of BeO at room temperature is comparable with Be. Unfortunately, the thermal conductivity of BeO drops from .63 at 20°C to .07 at 800°C making it more difficult to capitalize on the superior high-temperature properties of this material.

Data of the type shown in Table 1.03.01 can be used to make a direct comparison of materials for thin foil windows. Column 9 of the table represents the approximate thickness of a given material which will produce a 10% loss in an electron beam operating in the 100 to 110 kv range. Column 8 indicates the temperature gradient from the center of the window to its edge which the window will assume under operating conditions. As noted previously, this temperature is substantially independent of window thickness.

Columns 8 and 9 in a sense may be considered as defining the requirements on the material imposed by the conditions of service. It is then only necessary to consider the strength of the material as a function of its thickness at the required operating temperature for the thermal loading stresses produced in order to compare different

window materials. An extra premium results if a material will meet the operational conditions in a thickness which is less than the 10% loss thickness defined by column 9 of the table. Thus, if 1.5 microns of silver will meet operating conditions, then it is evident that the power loss to the window will be reduced by a factor of 2 from 10% to 5% of the total beam power.

1.04 Spencer Thick Target Theory

Spencer[4][5] has developed a theory from which energy losses incurred by high speed electrons as they traverse a plane perpendicular target of infinite thickness can be calculated as a function of their fractional range. It was felt that computations based on his data could be used with a fair degree of confidence for thicker targets (in excess of 0.2 to 0.3 fractional range) since fairly good correlation with experimental results were obtained. A brief review of the calculations based on Spencer's data follows using the following definitions:

Let $I(z)\,dz$ be the energy dissipated per square centimeter in a plane layer between z and $z + dz$. $I(z)\,dz$ represents the average energy per electron dissipated in the plane layer between z and $z + dz$, $r_o = r(E_o)$ is the residual range of the electrons, as measured along their path.

$\left(\frac{dE}{dr}\right)_{E_o}$ = the stopping power of electrons at the initial energy of the source E_o.

$x = \frac{z}{r_o}$ the fractional range or thickness z transversed through material divided by residual range for initial energy E_o.

$J(x) = I(z)/\left(\frac{dE}{dr}\right)_{E_o}$ is the de-dimensionalized energy distribution for the plane perpendicular case.

To obtain the energy loss $(\Delta W)_L$ incurred in penetrating a given material to a thickness z_1, it is necessary to integrate $I(z)\,dz$

4. L. V. Spencer, "Energy Dissipation by Fast Electrons," NBS Monogram No. 1, Sept. 10, 1959.
5. L. V. Spencer, Phys. Rev., 98, 1597 (1955).

$$(\Delta V)_L = \int_{z_1}^{o} I(z)\, dz$$

By substitution, recognizing that $dz = r_o\, dx$, we obtain:

$$(\Delta V)_L = \int_{x_1}^{o} J(x)\left(\frac{dE}{dr}\right)_{E_o} r_o\, dx.$$

For a given r_o and $\left(\frac{dE}{dr}\right)_{E_o}$ are constants. The curves of A_E versus fractional range for Pb, Sn, Cu, Al, C and Au shown on Fig. 1.04.01 were obtained from the tabulated values for J(x) published in Spencer's report using Simpson's rule for accomplishing the integration. Spencer gives his data as a function of increments Δx of .025. Some loss in accuracy was incurred in the interest of saving time by making the calculation using $\Delta x = .05$ as the basic increment for the integrations. When $\left(\frac{dE}{dr}\right)_{E_o}$ is expressed in mg/cm^2, $(\Delta V)_L$ is determined directly in kv.

The concept of fractional range is used to eliminate beam voltage as a parameter on the graphs. For voltages of present interest, say 50 to 200 kv, there is little change in the data represented in Fig. 1.04.01 with change in beam energy. The decrease in the fraction of beam energy absorbed with increase in voltage is determined by the decrease in fractional range which occurs for a given thickness material as the voltage is increased due to the increase in range with voltage. The dashed lines in Fig. 1.04.01 represent the fraction of the total energy reflected at high values of fractional range.

In interpreting Fig. 1.04.01 it is important to keep in mind that Spencer's "thick" target assumption gives larger values of A_E for a given value of x than would be expected for a foil of comparative thickness. For example, the 31% of electron beam energy absorbed in traversing 20% of the range is based on the assumption

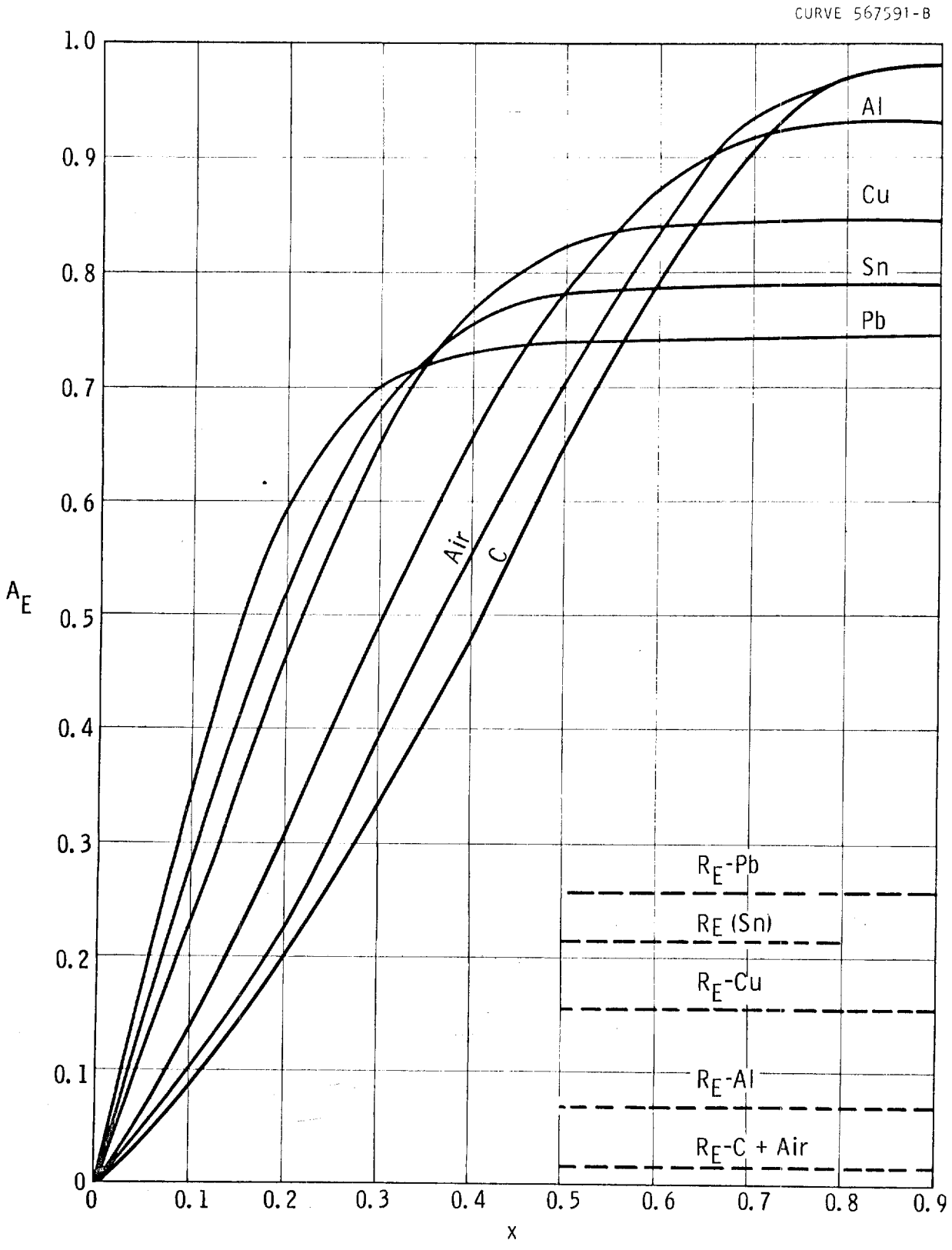

A_E and R_E versus fractional range x for thick materials

that the actual material is thicker than the fractional range thickness under consideration. Thus the 31% absorption figure includes some backscatter from sections of the material which are thicker than the 0.2 fractional range for which A_E is determined. A foil having a thickness corresponding to fractional range of 0.2 would lose less energy than would be expected on the basis of Spencer's thick target theory since it does not have thicknesses beyond 0.2 of the fractional range to cause scattering back into the thickness of interest.

Berger has applied a Monte Carle method in the application of the transport of fast charged particles to compute reflection and transmission characteristics of thin aluminum foils. His data which has fairly good agreement with experiment, include quantitative information on electron beam energy changes as will numerical information on changes in numbers of electrons as a function of the direction of the incident electron beam and its initial energy. Fig. 1.04.02 gives a direct comparison of Berger's results for electrons have a 90° angle of incidence with Spencer's results which also assumes normal incidence.

The following definitions are used in Fig. 1.04.02:

A_E = fraction of beam energy absorbed

A_N = fraction of total number of electrons absorbed

R_E = fraction of beam energy reflected

R_N = fraction of total number of electrons reflected

T_E = fraction of beam energy transmitted

T_N = fraction of total number of electrons transmitted

As would be expected, the fraction of energy absorbed, A_E, predicted by Berger for thin foils is significantly less than is obtained by Spencer on the assumption of electrons impinging as a material of infinite thickness. The fractional absorption loss for a foil having a fractional range thickness of 0.2 is only about 22% as compared to the 31% obtained from Spencer's thick target theory.

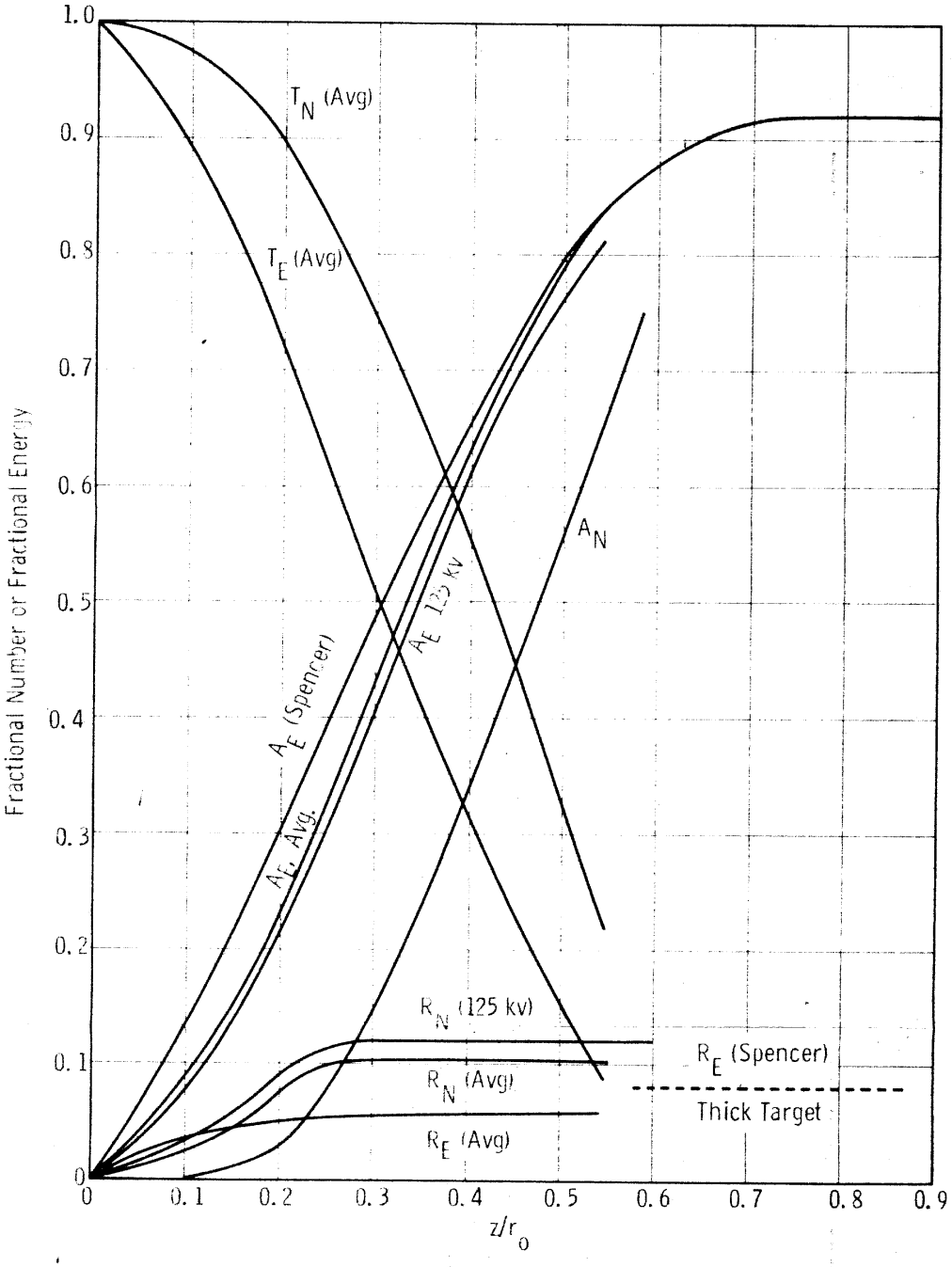

-Comparison Berger and Spencer data for Al
All curves Berger data except as noted

Fig. 1.04.02

From Berger's data in Fig. 1.04.02 about 90% of the electrons are transmitted through a thin foil having a thickness of 0.2 of the fractional range, but only about 72.5% of the energy is transmitted. About 8% of the electrons are reflected. These reflected electrons take with them about 5% of the total incident energy. Two percent of the electrons are neither accounted for by transmission or reflection and thus are assumed to be captured within the boundries of the foil.

In Fig. 1.04.03 the fraction of beam energy absorbed, A_E, is plotted as a function of atomic number for different values of fractional range for a target of infinite thickness. The fractional reflected energies corresponding to large values of fractional range are shown at the top of the figure. As shown in Berger's data in Fig. 1.04.02, full reflection takes place once the thickness of a given material approaches about 30% of the fractional range.

In order to simplify obtaining data for different materials, range data obtained by Nelm's are plotted in Fig. 1.04.04 as a function of atomic number for different values of kv. Nelm's data on range translated in thickness of foil in mils as a function of kv in the voltage range of interest are shown in Fig. 1.04.05.

Spencer's data are applied to foils of different materials to give the sum of A_E as a function of foil thickness for the 125 kv electrons plotted on Fig. 1.04.06. Since the ranges of different materials have roughly the same variation with change in kv, the thickness of foils corresponding to the A_E values shown in the curves can be estimated for 150 kv and 100 kv by multiplying the thickness of foil as given in the absence of Fig. 1.04.06 by 1.3 for the 100 kv case and by .7 for the case of 150 electrons.

Fig. 1.04.06 can be used for comparing absorption raises for Al foil with those obtained in the earlier discussion. The comparison tabulated below for .32 mil Al indicates that the estimate first obtained for Al was reasonable.

CURVE 567593-B

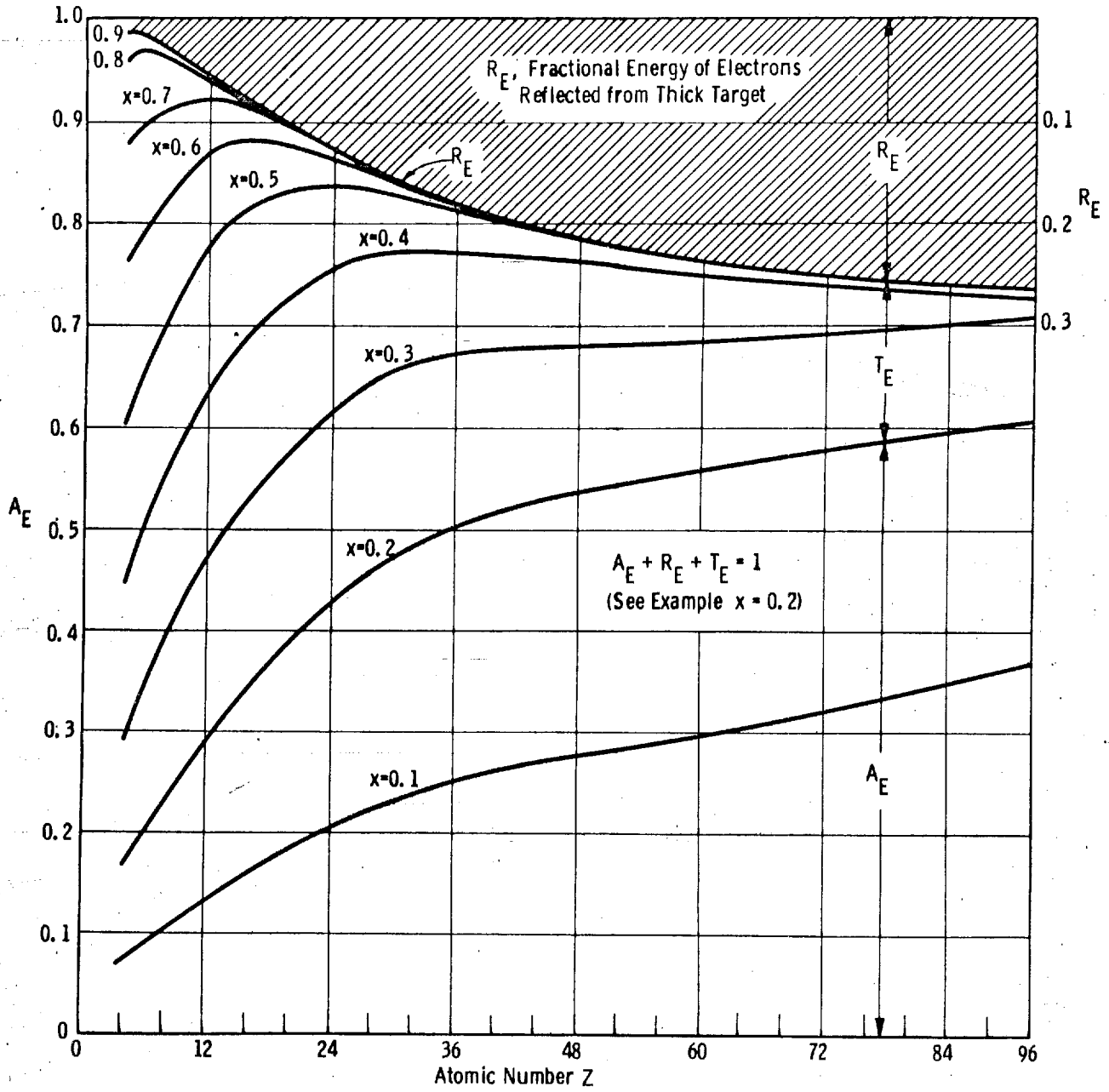

A_E, fractional energy absorbed and T_E fractional energy transmitted as function of fractional range x

Fig. 1.04.03

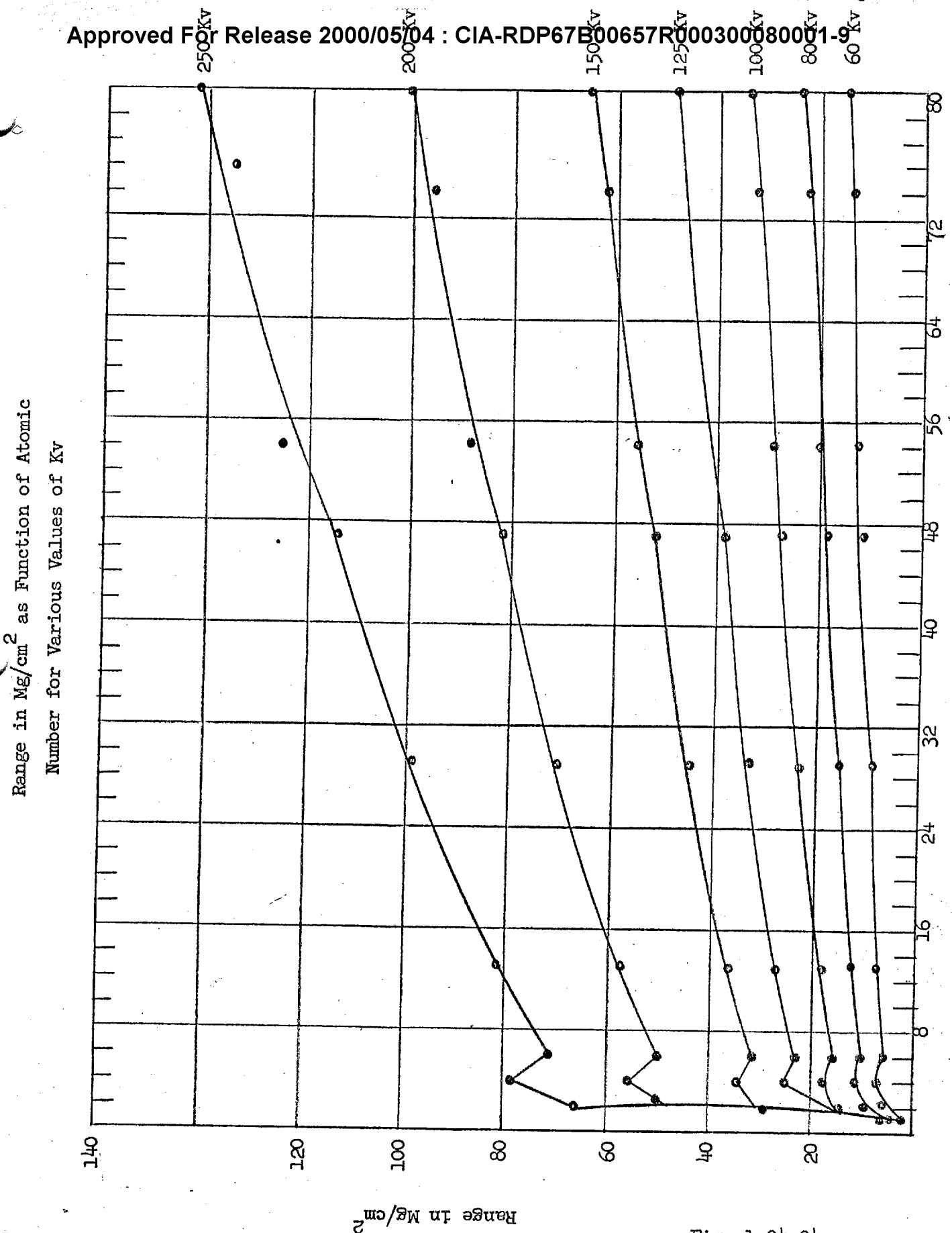

Range in Mg/cm^2 as Function of Atomic Number for Various Values of Kv

Fig. 1.04.04

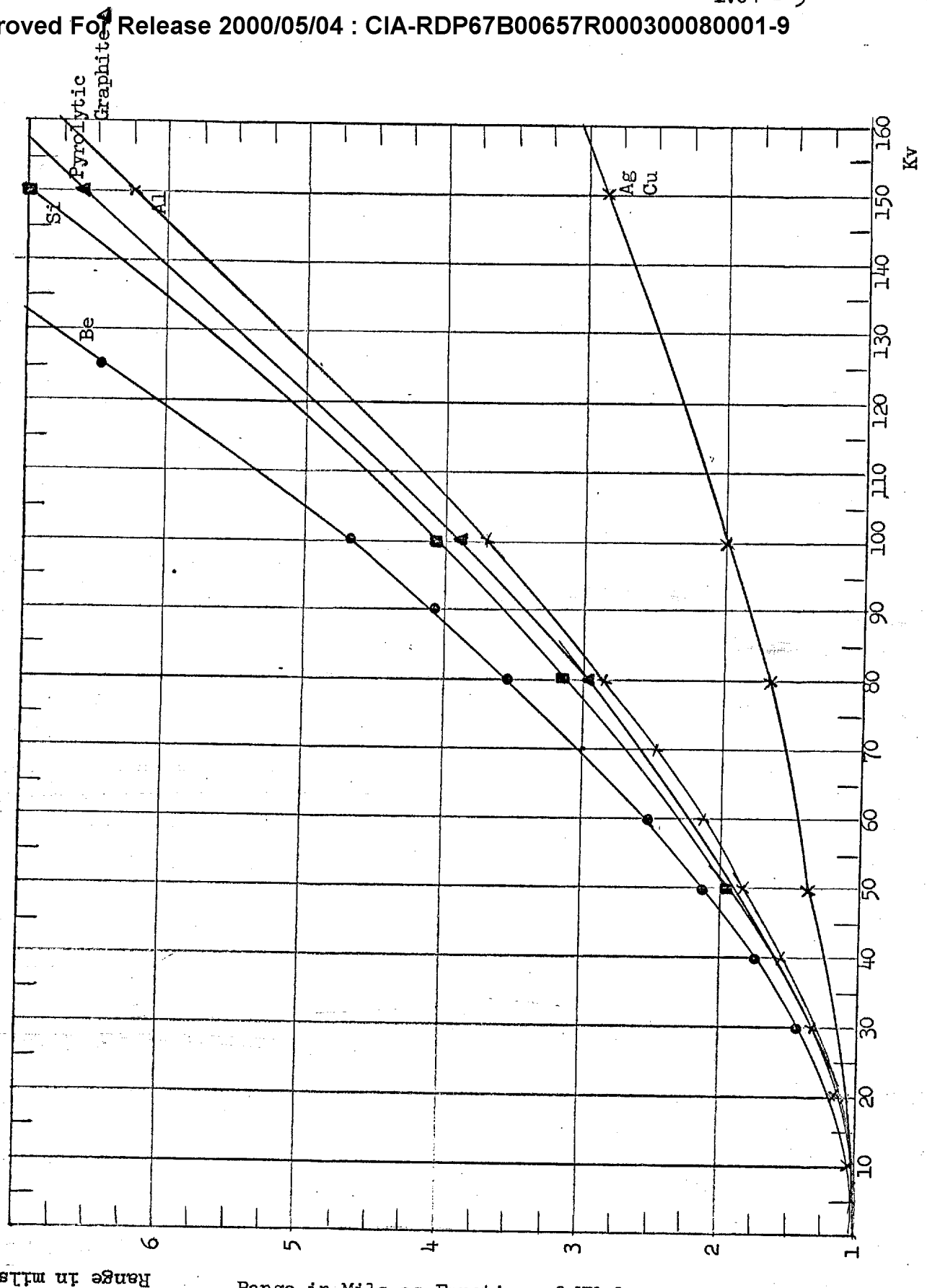

Range in Mils as Function of KV for
Be, Si, Pyrolytic Graphite, Al, Ag and Cu

Fig. 1.04.05

A_E, Fractional Absorption Loss for 125 Kv Electrons as Function of Foil Thickness in Mils for Different Materials - Solid Lines Thick Target Theory (Spencer)

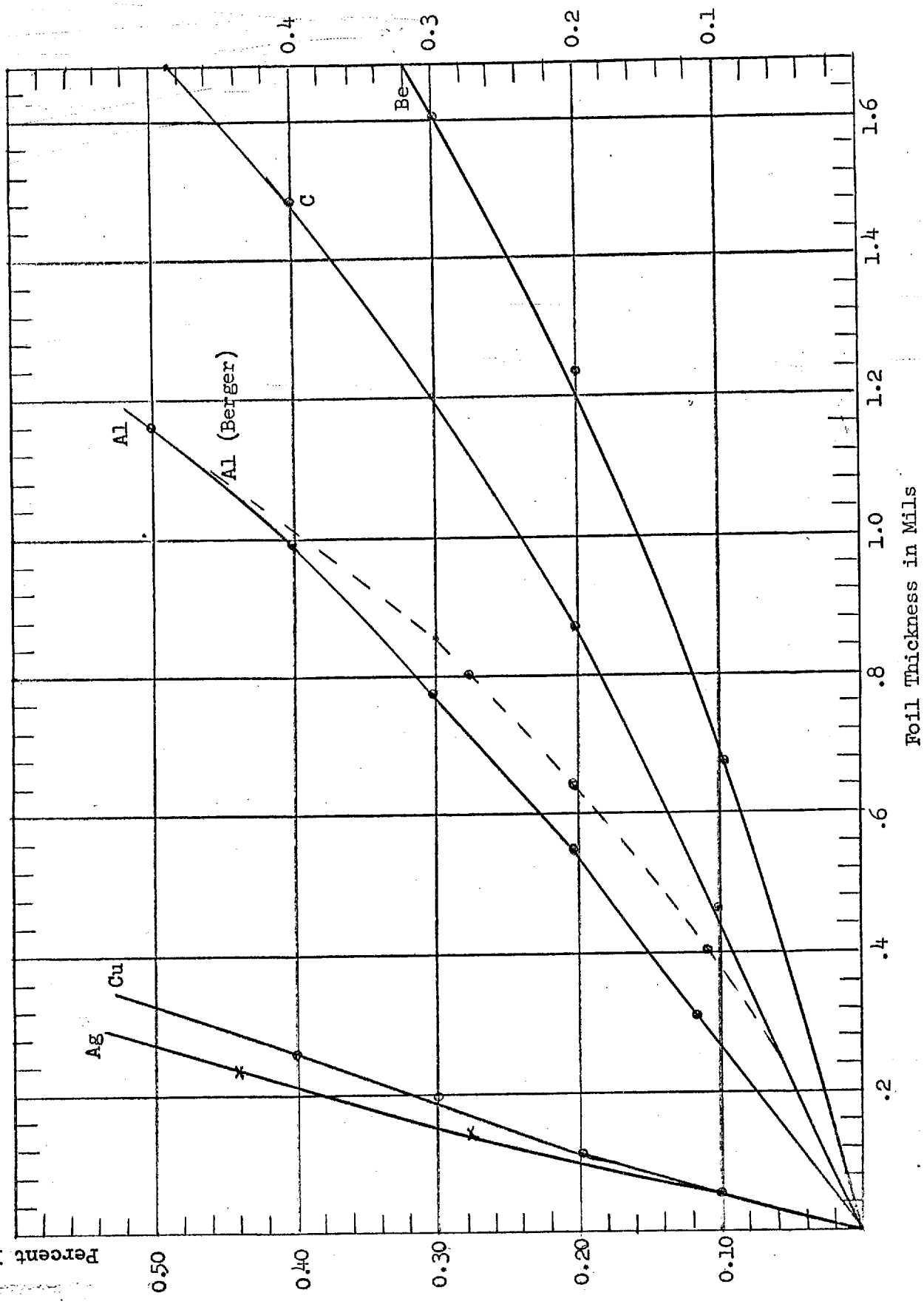

Fig. 1.04.06

Source of Information	KV	A_E
Fig. 1.02.01	110	.091
Spencer	125	.116
Spencer	100	.150
Berger	125	.08
Berger	100	.102

In this report unless specified otherwise, Berger's data will be used for Al. Data for all other materials will be based on Spencer's thick target theory. For low atomic number materials where back reflection is minimal, excessive loss of accuracy would not be entailed. However, for high atomic materials such as Cu and Ag, serious errors may be incurred for thickness corresponding to low values of fractional range. For very thin materials at high atomic number it is possible that more accurate estimates can be made from eq. 1.02.06.

In order to apply the consideration on losses just discussed usefully, it is desirable to have available the constant of proportionality between the power lost in a given window, Q, and the useful transmitted power U. This constant of proportionalities is derived as follows:

The total input of the beam $W_B = Q + U + W_R$ where W_R is the power reflected from the window and Q is the power lost in the window proper. From consideration of Fig. 1.04.01 and 1.04.03 the absorbed energy becomes prohibitively high as atomic number is increased. For lower atomic number to which our attention is restricted, the fraction of electrons reflected is less than 10% and is neglected in these considerations.

$$W_B = Q + U \qquad 1.04.01$$

$$Q = A_E W_B \qquad 1.04.02$$

By substitution for W_B in eq. 1.04.01

$$U = Q \frac{(1 - A_E)}{A_E} = Q(f) \qquad 1.04.03$$

where $f = \frac{(1 - A_E)}{A_E}$ is the constant of proportionality between useful and absorbed power.

In applying the data derived in this section and practical windows it is important to make sure that electrons scattered in traversing a given window are transmitted as a result of the particular window configuration employed.

Values of f as a function of kv are plotted in Fig. 1.04.07 for different thicknesses of Be and Al foil. It is interesting to note that the power transmitted through a 0.5 mil Be foil at 150 kv is 19 times the power absorbed. Thus a window design having 0.5 mil Be which will dissipate 200 watts should transmit almost 4 kw of power. A half mil Al window will transmit about half this power for the same absorbed power.

Factor f (by which Power Absorbed Must be Multiplied to Obtain Useful Power) as Function of Kv for Different Thicknesses of Be and Al Foil

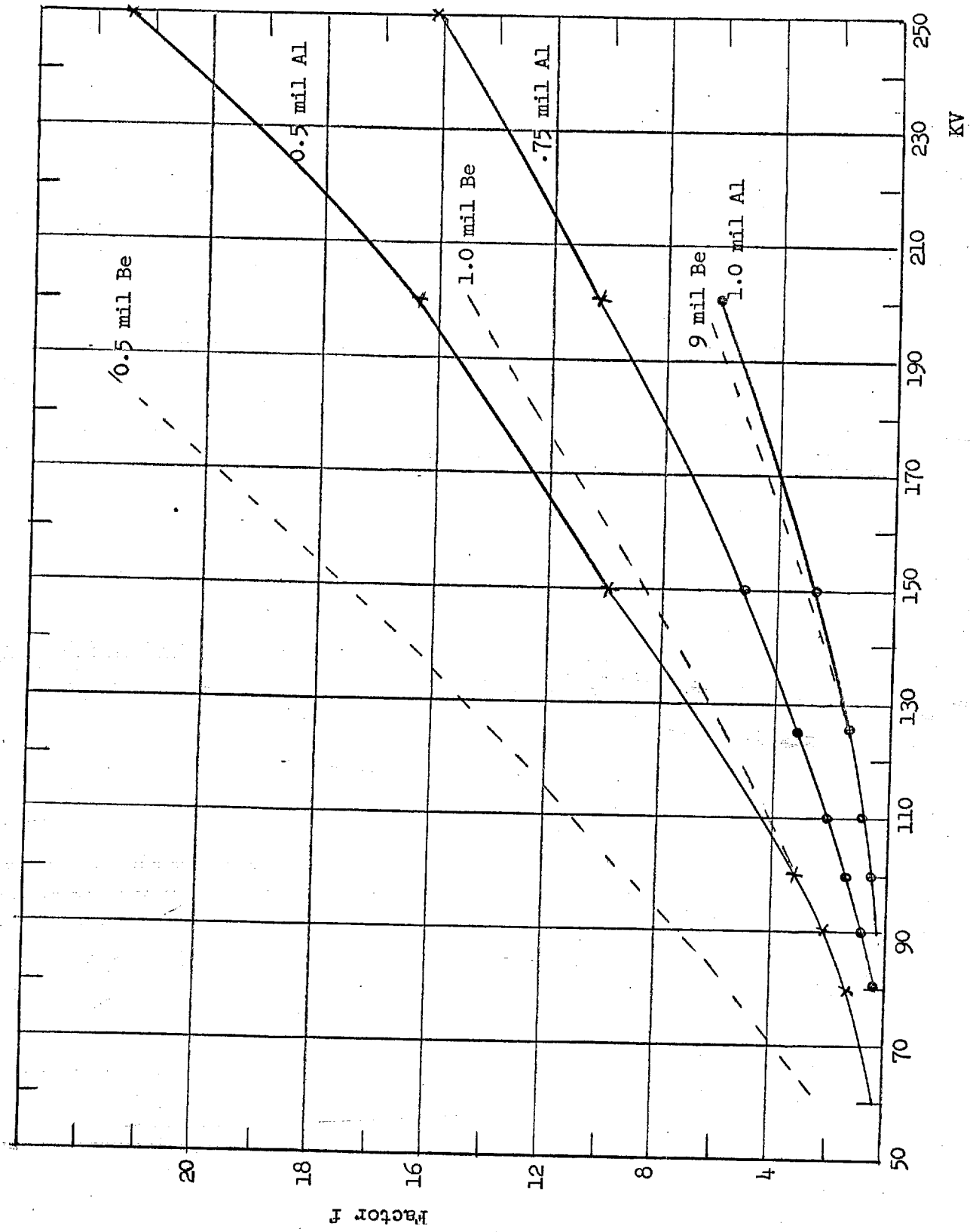

1.05. Estimated Thermal Gradients for Thin Foil Windows

Assumption of Negligible Thermal Gradient Across Beam:

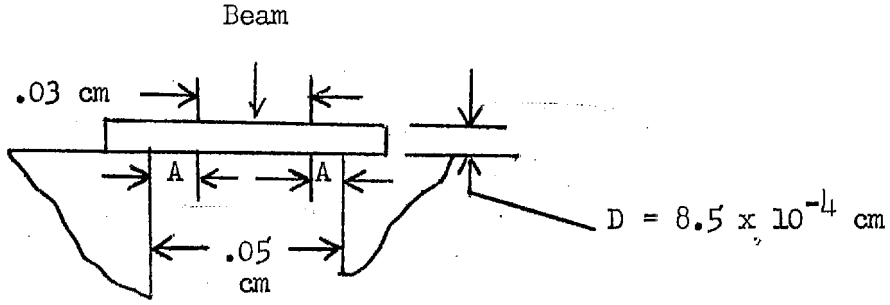

Assume 0.3 mm wide beam landing on the Al foil window shown. The power absorbed in window will dissipate to the wall according to the equation:

$$\Delta T = \frac{W}{2} \frac{A}{kLD} \qquad (1.05.01)$$

where W is power in calories/sec absorbed in window, k is thermal conductivity, ΔT is the thermal gradient across window, L is the length of spot and D is thickness of window. Substituting in Eq. 1.05.01 on the assumption that 300 watts = 72 calories per second is absorbed in the window, A = .01 cm, D = 8.5×10^{-4} cm, k = 0.5 cal/cm^2/sec, and solving for L for ΔT = 150°C, we obtain L = 5.6 cm = 2.2". The assumption of 300 watts dissipation is, of course, equivalent to a tube loading of 30 ma for a 10 kev energy loss per electron. In the previous sections, it was determined that a 10 kev loss is reasonable for the assumed thickness of foil for primary beams of the order of 110 kev.

The power dissipated by radiation and other mechanisms for removing energy from the window have been neglected in these calculations.

Determination of Thermal Gradient From Center to Edge of Beam for the Condition Above:

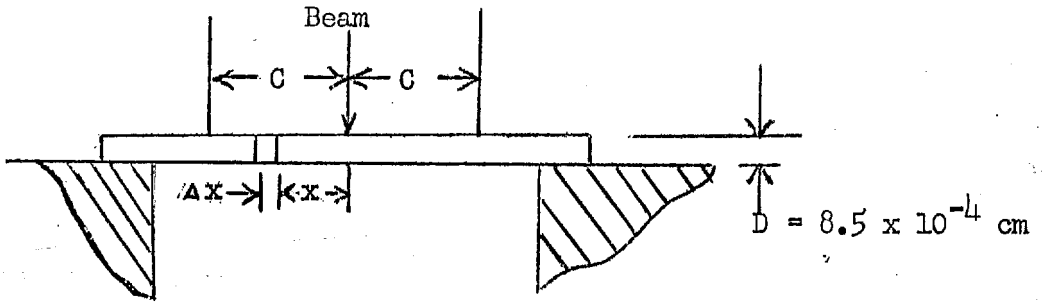

Let $Q_o = \frac{W}{2LC}$ = power density in calories/sec/cm^2, assumed uniform, being absorbed by window in the region of direct beam landing, where C = .015 cm is the 1/2 width of beam, and Q = xQ_oL is the absorbed power which is flowing through differential element dx at distance x from center of beam toward the edge of window. From heat conduction theory:

$$\frac{dT}{dx} = \frac{Q}{kLD} \qquad (1.05.02)$$

and

$$\Delta T = \int_T^{Tm} dT = -\int_C^o \frac{Q_o\, Lxdx}{kLD} = -\int_C^o \frac{Q_o\, xdx}{kD} = \frac{C^2 Q_o}{2kD} \qquad (1.05.03)$$

where Tm and T are steady state temperatures at x = o and x = C respectively. For the example cited first, $Q_o = \frac{72}{(5.6)(.015)(2)}$ = cal/cm^2/sec. Substituting in Eq. 1.05.03, we obtain ΔT = 114°C.

Total Thermal Gradient From Center of Beam to Edge of Window:

From the results above, the total temperature gradient ΔT from the center of window to edge of spot is equal to 150°C + 114°C = 264°C for a beam that is .03 cm by 5.6 cm long which impinges on an Al window 8.5 x 10^{-4} cm thick. To drop ΔT from 264°C to 150°C requires

lengthening the beam from 5.6 cm to 9.9 cm or 3.9". For a 10 cm beam, the thermal gradient from the center to edge of beam will be 65°C, and the gradient from edge of spot to edge of window will be 85°C or 150°C total temperature gradient. It will be observed that temperature gradient from center of beam to edge is about 43% of the total gradient from center to edge of window, and thus the temperature gradient across area of window irradiated by beam is by no means negligible.

Effect of Thermal Heat Capacity on Window Loading:

Assume that the bombarded area of an Al window, which is 10 cm long by .03 cm wide by 8.5 microns in thickness, has negligible heat dissipation, what exposure time at 300 watt loading will bring the window to 100°C? The heat capacity of Al is taken as .225 calories/gram.

The volume of window affected by this assumption is $(10)(.03)(8.5 \times 10^{-4}) = 2.55 \times 10^{-4}$ cm^3, and weighs $(2.7)(2.55 \times 10^{-4}) = 6.9 \times 10^{-4}$ grams. Heat input is 300/4.18 = 72 calories/sec.

The calories required to heat the window to 100°C are given by $(.225)(6.9 \times 10^{-4})(100) = 1.55 \times 10^{-2}$ calories. The time in seconds required to equal 1.55×10^{-2} calories at an input of 72 calories/sec is $1.55 \times 10^{-2}/72 = 2.16 \times 10^{-4}$ seconds = .22 milliseconds = 220 microseconds.

Thus, significant increases in loading are possible for exposures in the microsecond region. A 3000 watt heat input to the window should be permissible for exposures of 22 microsecond duration having a 10% duty cycle.

Temperature Gradients Across Different Window Configurations:

(a) Slotted Configuration:

Let Q_B be the power absorbed by a given beam width 2C impinging on a window of width w. As shown in Fig. 1.05.01a the clearance between beam and window is given by dimension A. The beam density in watts/cm^2 is assumed to be uniform over the cross sectional area of the line focus and is defined as Q_o. As outlined above, the total temperature

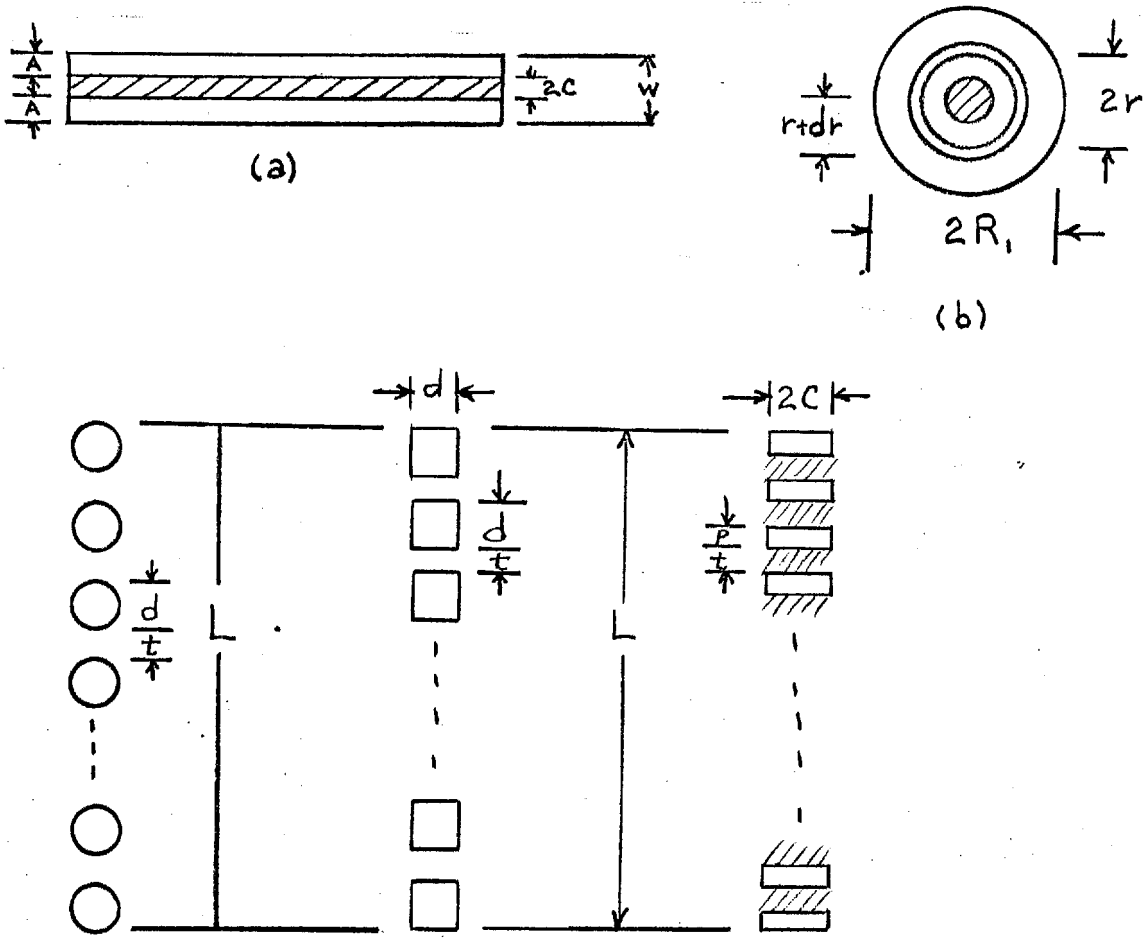

Window Configurations for Which
Transmission Coefficient Is Computed

Fig. 1.05.01

gradient $(\Delta T)_T$ from the center of the window of length L to its edge is given by

$$(\Delta T)_T = \frac{Q_B A}{2kLD} + \frac{C^2 Q_o}{2kLD} \qquad (1.05.04)$$

Since $Q_o = \frac{Q_B}{2CD}$ By substitution using Eq.

$$(\Delta T)_T = \frac{Q_B}{2kDL}\left(A + \frac{C}{2}\right) = \frac{U(A+C/2)}{F(2kDL)} \qquad (1.05.05)$$

where K is the thermal conductivity in $cal/cm^2/°C/sec/cm$* and the power is expressed in cal/sec, and D is window thickness. All dimensions are in cms. The first term in the above equations represents the temperature gradient from the edge of beam to the window; the second term the gradient from the center of beam to edge.

(b) Circular Windows

Referring to Fig. 1.05.01b let us assume a beam which loses a total power of Q_b calories in traversing a thin foil having a circular cross section area of diameter $2R_o$. The tital diameter of the window is $2R_1$. A heat sink is assumed to be attached to the periphery of the window. The temperature gradient in the area directly loaded by the beam is derived as follows: The temperature drop across a circular strip dr located at a distance r from the center is given by

$$dT = \frac{Q dr}{2\pi r k D}$$

where Q is total loading in a circle of radius r

but $Q = \pi r^2 Q_o$,

*Note that k is in general a function of T.

where Q_o again represents the power density in calories/cm^2, assumed uniform. Substituting for Q and integrating, one obtains for the temperature gradient from the center of the beam impingement location to its periphery.

$$(\Delta T)_1 = \frac{Q_o r_o^2}{4kD} = \frac{Q_B}{4\pi kD} \qquad (1.05.06)$$

It is interesting to note that the temperature gradient from the center of the beam to its periphery is independent of beam diameter. Thus the temperature gradient across a circular window assumed to have the same size as the beam depends only on the total loading, the thickness of the window, and its thermal conductivity, and not on the window diameter. This provides an opportunity for obtaining a high total loading by using many small diameter windows at relatively high loading.

If the beam diameter is smaller than the diameter of the window, we must also compute the temperature gradient $(\Delta T)_2$ between the periphery of the beam and the edge of the window. We assume that the area being loaded corresponds to a circle of diameter $2R_o$ for a window diameter $2R_1$

$$(\Delta T)_2 = \int_{r_o}^{r_1} \frac{Q_B\, dr}{2\pi r kD} = \frac{Q_B}{2\pi kD} \ln\left(\frac{R_1}{R_o}\right) \qquad (1.05.07)$$

$$= \frac{r_o^2 Q_o}{2kD} \ln\left(\frac{R_1}{R_o}\right) \qquad (1.05.08)$$

Thus the total thermal gradient $(\Delta T)_T$ is given by $(\Delta T)_T = (\Delta T)_1 + (\Delta T)_2$.

$$(\Delta T)_T = \frac{Q_o r^2}{2kD}\left(\frac{1}{2} + \ln \frac{R_1}{R_o}\right) \qquad (1.05.09)$$

$$= \frac{Q_B}{2\pi kD}\left(\frac{1}{2} + \ln \frac{R_1}{R_o}\right) \qquad (1.05.10)$$

Terms involving power in any of the above equations can be converted to watts by substituting the loading in watts and multiplying the value of watts by $\frac{1}{4.18} = 0.24$.

(c) The Registration Problem:

Eq. 1.05.05 and Eq. 1.05.10 demonstrate the nature of the registration problem. If the beam is made significantly smaller than the window, the extra $(\Delta T)_2$ term in these equations must be used to compute the additional gradient associated with the fact that the window is larger than the beam. If the window is diminished in size until it coincides with the window, this additional temperature gradient goes to zero. Exact coincidence between the window and the beam cross-sectional areas represents the ideal case. It is also possible to make the beam larger than the window to make the registration problem less critical. This of course is accomplished at the expense of requiring additional power, which serves no useful purpose, except to simplify the problem of registry between beam and window.

The registration problem must be considered not only in the light of accomplishing registration at the beginning of service, but also of maintaining registration under conditions of useful life.

(d) Multihole Configurations:

Referring to Fig. 1.05.01c, let us assume a line focus from having uniform power density impressed into a single line of holes. In the initial assessment of temperature gradients we assume the main heat sink is relatively thick and ignore temperature gradients due to the width of the web t between individual holes. We also assume that a beam of width d and length L is impressed on this series of holes

in exact registration with them. An exactly registered configuration in which the beam exactly matches each hole is of course much more efficient and more difficult to realize in practice.

The fraction of the beam which impinges directly on the windows will define the "optical" transmission, T of the window geometry which is given by:

$$T = \frac{\pi}{4}\left(\frac{d}{d+t}\right) = .785\left(\frac{d}{d+t}\right) \qquad (1.05.11)$$

Strictly speaking this value of transmission assumes that the beam is equal to L + t. Since t is $\ll$ L, it is ignored compared to L.

The corresponding "optical" transmission T_w of the window for the line of square holes defined by Fig. 1.05.01d is about 25 percent more efficient and is given by

$$T = \frac{d}{d+t} \qquad (1.05.12)$$

The length L of a given number of holes or square apertures N may be expressed as follows:

$$L = (N-1)(d+t) + d \qquad (1.05.13)$$

or

$$N = \frac{L-d}{d+t} + 1 \qquad (1.05.14)$$

Table 1.05.01 gives pertinent characteristic data for a series of N round 1 mil Be windows per inch of total window lengths separated by 2 and 5 mil webs. The corresponding "optical" transmissions factor T is given for a square aperture foil as a matter of interest. Temperature gradients are calculated using Eq. 1.05.06.

TABLE 1.05.01

Characteristic Data for Window Configuration Consisting of N Round Hole Per Linear Inch. (U is Power Transmitter, W_B is Total Input, ΔT is Temperature Gradient from Center of Window, d is Diameter of Holes, t is Thickness of Web Between Holes.)

d (Mils)	t (Mils)	N Per Inch	T Round Hole	T Square Hole	Assuming 1 Mil Round Be Window			
					(ΔT)	U/Inch (Watts)	W_B/Inch (Watts)	U/W_B
5	2	143.	.56	.715	19.5°C	1215	2430	.5
5	5	100.5	.394	.500	19.5°C	854	2430	.35
10	5	67.	.52	.67	19.5°C	569	1220	.466
10	2	83.5	.65	.83	19.5°C	710	1220	.682
15	5	50.0	.59	.75	19.5°C	425	810	.525
15	2	58.5	.69	.88	19.5°C	497	810	.614
20	5	40.	.63	.8	19.5°C	340	610	.557
20	2	46.	.715	.91	19.5°C	390	610	.640
25	5	33.5	.655	.83	19.5°C	285	485	.587
25	2	37.	.73	.93	19.5°C	314	485	.646
30	5	28.	.67	.86	19.5°C	238	400	.595
30	2	31.	.735	.94	19.5°C	264	400	.660
35	5	25.	.685	.875	19.5°C	212	350	.605
40	5	22.	.700	.89	19.5°C	187	300	.624

Approved For Release 2000/05/04 : CIA-RDP67B00657R000300080001-9

Temperature gradients for the square apertures would be slightly higher. In order to obtain the useful power per individual window we need only to know f, the proportionality constant between transmitted useful power and absorbed power. From Fig. 1.04.07 this is taken as 8.6 for 1 mil Be at 150 kv based on A_E of .104 and 10.0 for 0.5 mil Al at 150 kv, based on A_E of .091. The useful power per individual, multiplied by the number of holes gives the total useful power U transmitted through the window configurations and is shown in the appropriate column.

The figure for W_B, the total watts beam input per inch of window is obtained by observing that U is related to W_B for the assumed geometry by the equation:

$$U = W_B \, T \, (1-A_E) \qquad (1.05:15)$$

The values shown for W_B, the total impressed power to the window is obtained, by use of values of T listed for the round windows and the values of A_E given above.

It is interesting to note that substantial power is transmitted in the case of small holes (order of 1000 watts) for rather modest temperature gradients (19.5°C). The power transmitted for this temperature gradient is substantially greater for the instance of 143 5 mils holes than for the other extreme in Table 1.05.01 of 22 40-mil holes, even though the ratio of useful transmitted power to input power U/W_B is higher for the case of the larger diameter windows.

In the calculations above the assumption of perfect registration between a line focus beam of uniform density and the line of circular windows is assumed. In addition, temperature gradients along the web between the windows are neglected. Obviously transmitted power can be increased by use of a sufficient number of inches of window of a multihole configuration, and by increasing the allowable temperature gradient

across the window. Because this approach looked very promising it was considered desirable to make more rigorous calculations on the temperature gradients to be expected.

(e) Calculation of Temperature Gradients in a Single Row of Rectangular Slots

Consider the structure shown in Fig. 1.05.01e consisting of a row of slots of length L, width 2c, web width t, having a length of individual slot p, along the axis. Let the thickness of web and its thermal conductivity be D_1 and K_1 and the corresponding quantities for the window be D_2 and K_2 respectively. Assume perfect registration of beam with slots. To a close approximation the optical or windowless beam transmission is given by

$$T = \frac{p}{p+t} \qquad (1.05.16)$$

Assume total beam power is W_B, beam power density is W_o, and that the reflection of electron beam power from the window and web are negligible.

In order to estimate the temperature gradients, we assume that all power absorbed in the window, which is given by $TA_E W_B$, is dissipated laterally to web. Negligible dissipation to the side of the row of slots is assumed. This assumption not only simplifies the calculation but should make the results conservative. The accuracy should increase as 2c becomes large compared to p. In the next section, a comparison is made with results based on a more rigorous approach. It turns out that good agreement is achieved.

The total temperature gradient is taken as the sum of the gradient to the center of web $(\Delta T)_{WB}$ plus the temperature gradient to the center of the window $(\Delta T)_{WN}$.

The power going to the web from the window by this assumption must be added to the loading the web assumes by direct beam impingement, which is given by W_B (1-T). Thus the total loading, $Q_{\ }$, which must be dissipated by the web is given by

$$Q_W = TA_E W_B + W_B(1-T) = W_B(TA_E + 1-T) \qquad (1.05.17)$$

By direct substitution for W_B using the following equation:

$$U = W_B T(1-A_E), \qquad (1.05.18)$$

we obtain

$$Q_W = \frac{U(TA_E + 1-T)}{T(1-A_E)} \qquad (1.05.19)$$

The effective density of power on the web, $(Q_W)_o$ may be obtained by dividing Q_W by the area of the web:

$$(Q_W)_o = \frac{Q_W}{2LC(1-T)} = \frac{U(TA_E + 1-T)}{T(1-A_E)(1-T)2LC} \qquad (1.05.20)$$

From equation 1.05.04 we obtain the formulation for the temperature gradient for the web under the condition of uniform density $(Q_W)_o$. (The first term in this equation is zero since perfect registration is assumed)

$$(\Delta T)_{WB} = \frac{C^2(Q_W)_o}{2K_1 D_1} = \frac{CU(TA_E + 1-T)}{4K_1 D_1 LT(1-A_E)(1-T)} \qquad (1.05.21)$$

The temperature gradient from the center of window to the web is obtained in a similar manner using a computed value of uniform density of absorbed power. As indicated previously the power dissipated to the edge of the row of slots is neglected. The density of power being absorbed by window $(Q_{WN})_o$ is given by

$$(Q_{WN})_o = \frac{TW_B A_E}{2LCT} = \frac{W_B A_E}{2LC} \qquad (1.05.22)$$

Substituting in Eq. 1.05.04 we obtain:

$$(\Delta T)_{WN} = \frac{p^2 (Q_{WN})_o}{8\ K_2 D_2} = \frac{p^2\ A_E\ U}{16\ K_2 D_2 LCT(1-A_E)} \qquad (1.05.23)$$

As indicated previously the total temperature gradient is conservatively assumed to be equal to the sum of the web gradient plus the window gradient, or

$$(\Delta T)_T = (\Delta T)_{WN} + (\Delta T)_{WB} \qquad (1.05.24)$$

To simplify the resulting equation, we lump all geometrical variables except C, D, and L together into two new constants:

$$Z = \frac{(TA_E + 1-T)}{T(1-A_E)(1-T)} \qquad (1.05.25)$$

and

$$X = \frac{A_E p^2}{T(1-A_E)} \qquad (1.05.26)$$

Thus eq. 1.05.24 becomes:

$$(\Delta T)_T = \frac{CUZ}{4K_1 D_1 L} + \frac{UX}{16K_2 D_2 LC} \qquad (1.05.27)$$

Equation 1.05.27 was used to determine temperature gradients for a series of different window configurations using a computer program. The temperature gradients plotted in Figs. 1.05.02 through 1.05.05 as a

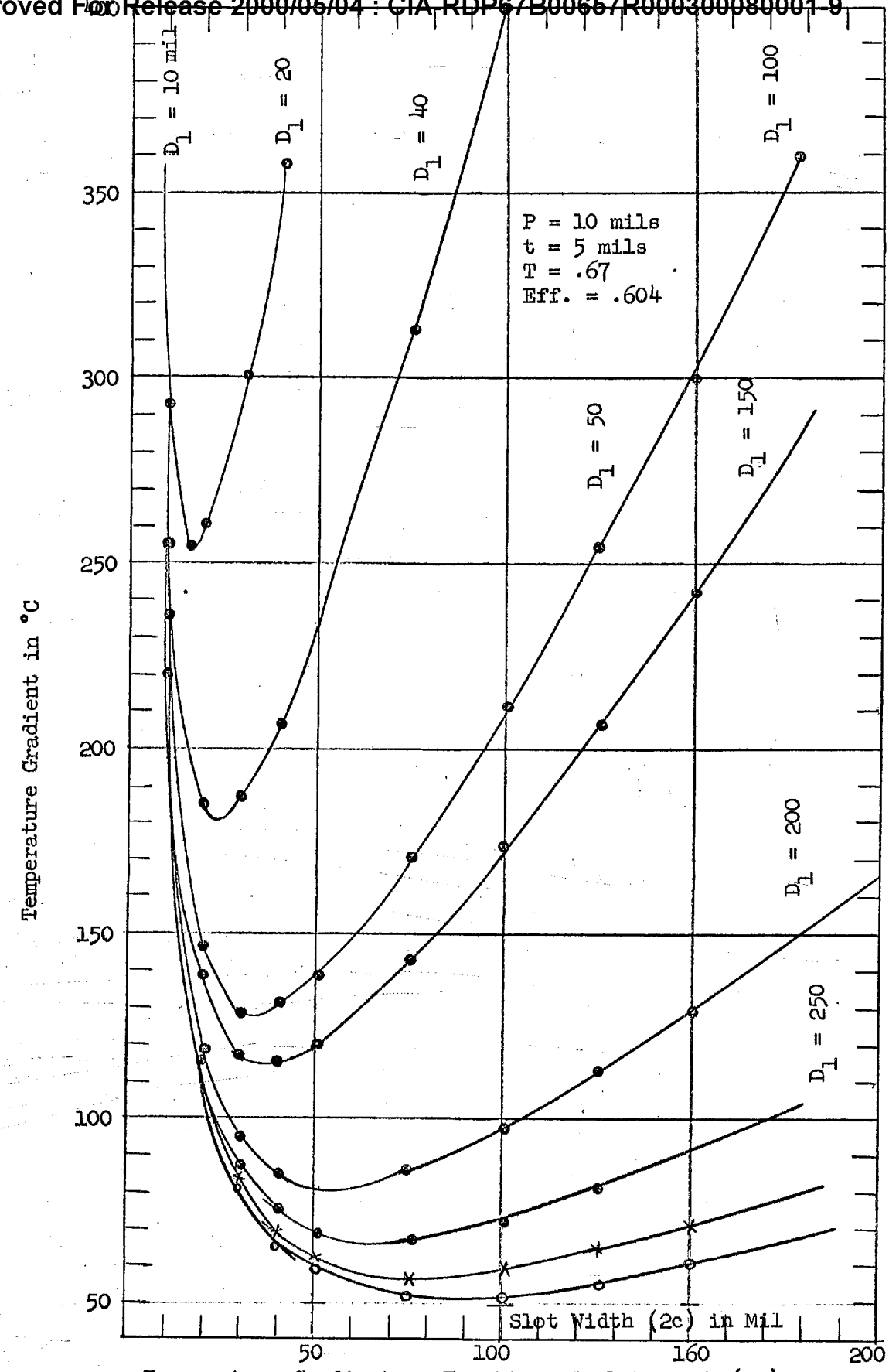

Temperature Gradient as Function of Slot Width (2c) for 3000 watt Output Loading per Linear Inch, Cu webb, 1/2 mil Al Window, P = 10 mils

Fig. 1.05.02

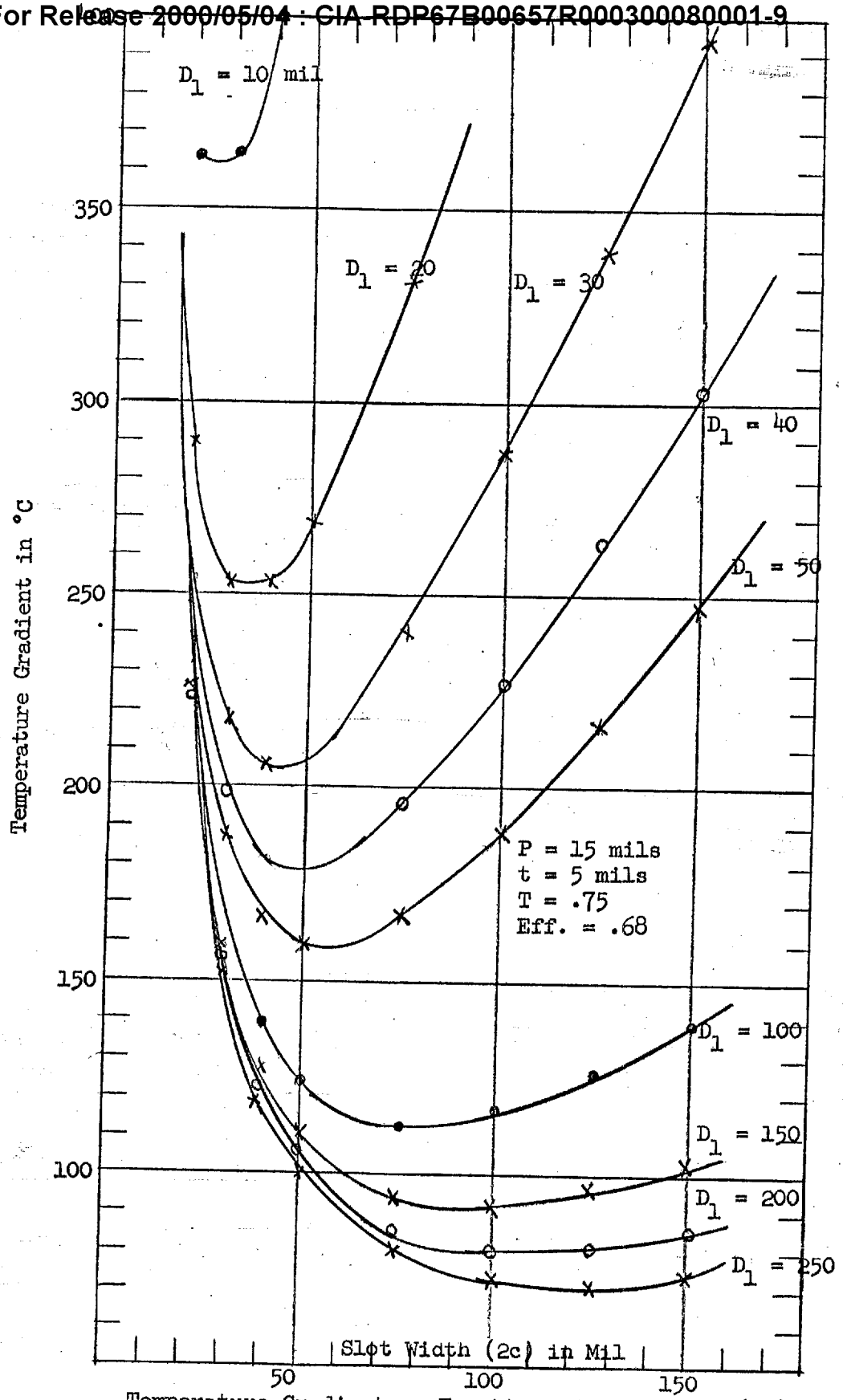

Temperature Gradient as Function of Slot Width (2c) for 3000 watt Output Loading per Linear Inch, Cu webb, 1/2 mil Al Window, P = 15 mils

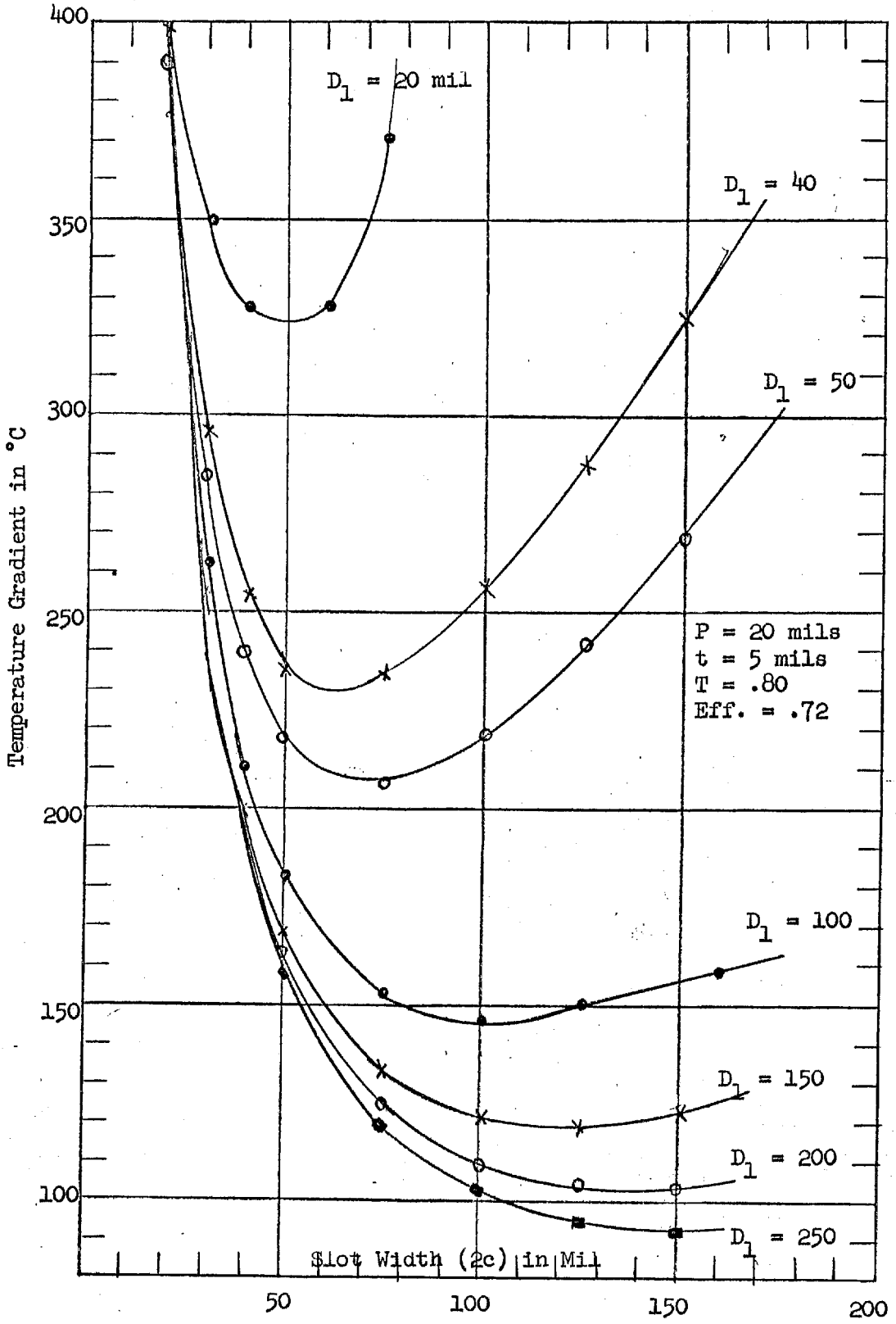

Temperature Gradient as Function as Slot Width (2c) for 3000 watt Output Loading per Linear Inch, Cu webb, 1/2 mil Al Window, P = 20 mils

Fig. 1.05.04

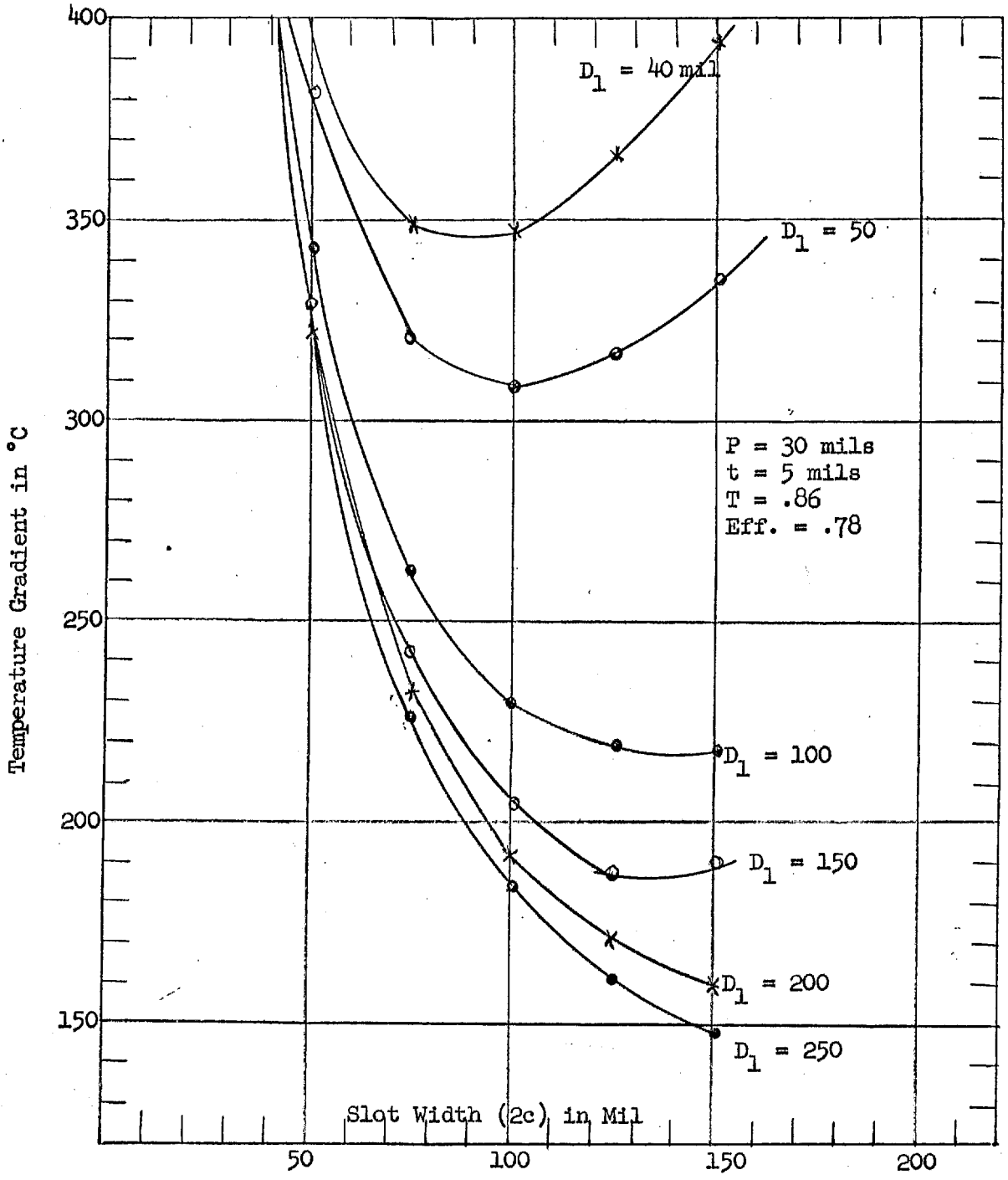

Temperature Gradient as Function as Slot Width (2c) for 3000 watt Output Loading per Linear Inch, Cu webb, 1/2 mil Al Window, P = 30 mils

Fig. 1.05.05

function of total slot width 2c are based on the use of a copper web of width t = 5 mil, an 0.5 mil aluminum window and a 1000 watt of the curves are based on obtaining useful output power U for a length of slot L = 1/3 inch. (The length L was selected to correspond to 1/3" because the 1" long filament used in the experimental tube program to be described later consisted for all practical purposes of two filament sections in series, each having a 1/3" length of effective electron emission).

Each of the graphs consists of a series of individual curves giving the temperature gradient from the center of window to web for fixed values of p and for different values of D_1, the thickness of the web. As indicated previously the window configuration must be designed so that electrons scattered from the window are not intercepted by the walls of the web. Unlimited thickness of web is not possible both because of such scattering limitations and because of practical limitations in fabrication of the configuration. At large values of thickness D_1, the temperature gradient through the thickness of web must be taken into consideration also. As can be observed from the curves, large values of web thickness are very desirable. In order to avoid interception of the scattered beam some tapering of the web geometry is desirable. (In actual practice it is difficult to fabricate the web without some tapering).

From the graphs it is evident that a temperature minimum exists for each value of p and D_1 at a given value of total slot width 2c. Thus an optimum width exists for each fixed value of P_1, D_1, t, and window materials, which we define as $(2c)_{OPT}$. The optimum width turns out to be given by the following expression:

$$(2c)_{OPT} = \sqrt{\frac{K_1 D_1 A_E p^2 (1-T)}{K_2 D_2 (TA_E + 1-T)}} \qquad (1.05.28)$$

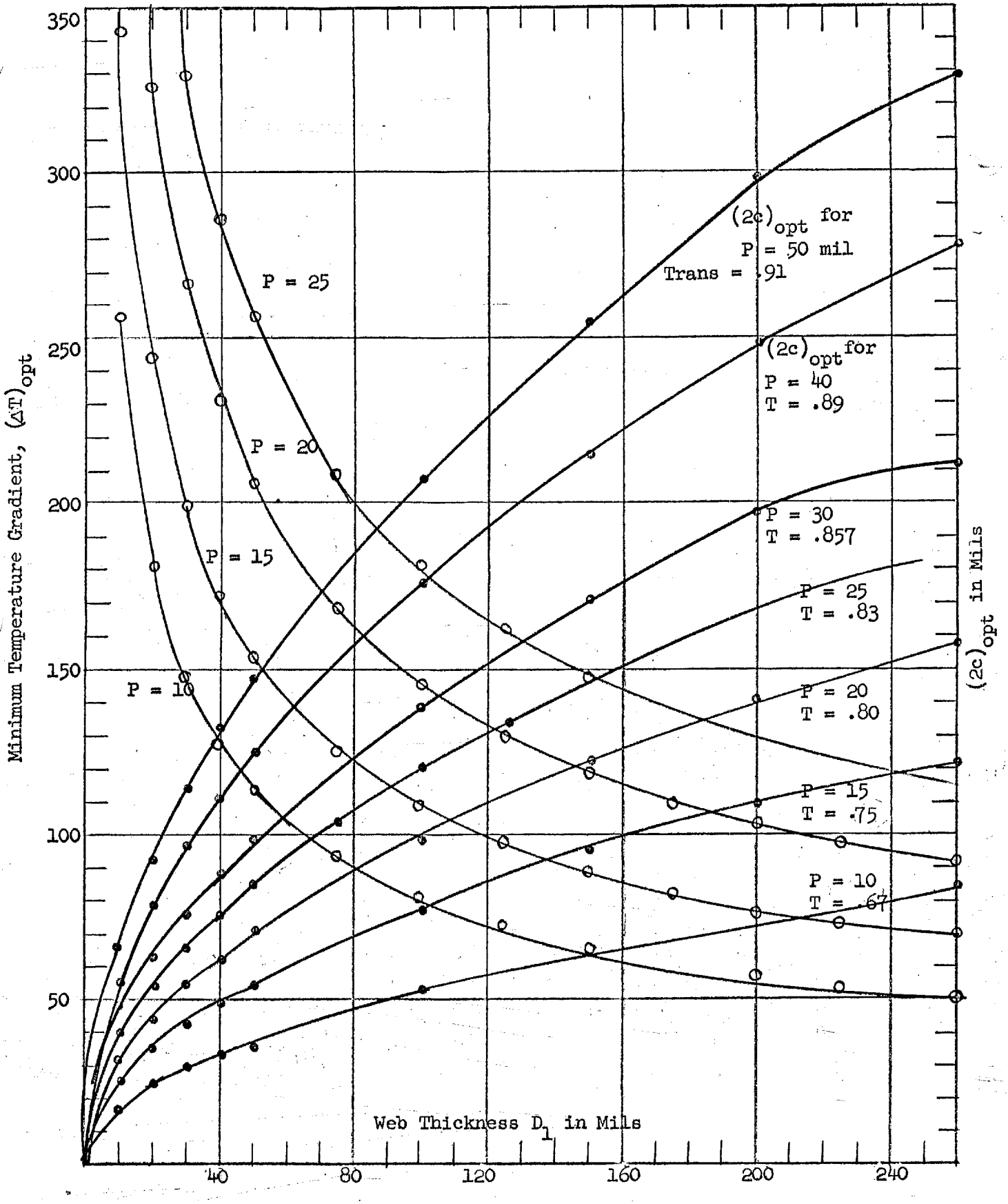

Maximum Temperature and Optimum Slot Width $(2c)_{opt}$ as Function D_1 Thickness of Cu Webb for Various Values of Slit Width P at 3000 watts/inch (1/2 mil Al Window and Rectangular Slots)

Fig. 1.05.06

By substituting $(2C)_{OPT}$ in eq. 1.05.27 we obtain for $(\Delta T)_{MIN}$, i.e. the minimum temperature on curves like those plotted in Figs. 10-13:

$$(\Delta T)_{MIN} = \frac{UP}{4LT(1-A_E)} \sqrt{\frac{A_E(TA_E + 1-T)}{K_1 D_1 K_2 D_2 (1-T)}} \qquad (1.05.29)$$

At $(\Delta T)_{MIN}$, $(\Delta T)_{WN} = (\Delta T)_{WB}$

The optimum value of slot width $(2C)_{OPT}$ for given values of D_1 and particular values of P the individual slot width is plotted in Fig. 1.05.06 for a window configuration consisting of 0.5 mil Al and a copper web. The corresponding minimum temperature gradients are plotted in the same figure for 1000 watt useful output power U and the previously mentioned condition of 3000 watts per linear inch of slotted window configuration. The transmission T_1 and the efficiency of power transmission $(E)_F = \frac{U}{W_B} = (1-A_E)T$ are also indicated on the curves.

From the graphs it is evident that the temperature gradient drops markedly as p decreases, and that the efficiency of transmission of power also decreases with decreasing p.

As an example of data which can be read off Fig. 1.05.06 the optimum total width of slot $(2C)_{OPT}$ corresponds to a 60 mil copper web turns out to be 60 mil for an individual slot width p of 15 mil. The corresponding temperature gradient from the center of window to the edge of the multislot configuration is 140°C, a temperature gradient which is very reasonable for the 0.5 mil Al window.

Thus 3" of this multiaperture window should be capable of transmitting of the order of 9 kw useful power continuously.

The computations associated with obtaining the thermal gradients plotted in Figs 1.05.02 to 1.05.05 were based on the assumption of perfect registration which is difficult to achieve in practice. Since it was considered desirable to allow some leeway

for registration, a series of computations were made with the beam 30 mil smaller in width than the window, thus increasing the thermal gradients associated with transferring absorbed power from the window and web by the temperature gradient across a 15 mil extent of web.

Referring to Fig. 1.05.01f, the temperature gradient across width B of web due to the above stipulated registration requirement is given by

$$(\Delta T)_B = \frac{(TA_E + 1-T)W_B B}{2K_1 D_1 L\ (1-T)} \qquad (1.05.30)$$

$$= \frac{(TA_E + 1-T)UB}{2K_1 D_1 L(1-T)T(1-A_E)} \qquad (1.05.31)$$

Eq. 27 must now be rewritten and becomes:

$$(\Delta T)_T = (\Delta T)_{WN} + (\Delta T)_{WB} + (\Delta T)_B \qquad (1.05.32)$$

The total gradient based on eq. 1.05.32 is plotted for a copper web and 1/2 mil Al window, in Fig. 1.05.07. The values of $(2C)_{OPT}$ plotted in Fig. 1.05.07 do not include 15 mil value of B used in determining the total thermal gradients. Thus total slot width corresponding to the temperature gradients shown in these figures is equal to $(W_{OPT} + 30)$ mils.

(f) Cross-Check on Computations for a Single Row of Rectangular Slots

The problem of obtaining a rigorous calculation on a rectangular window having width 2c in one direction and p in the other direction mounted on web of width t and thickness D_1 is very similar to the problem of determining the equipotential plot of a given electrode configuration once the boundary conditions have been determined. For the equilibrium condition it amounts to solving the following differential equations

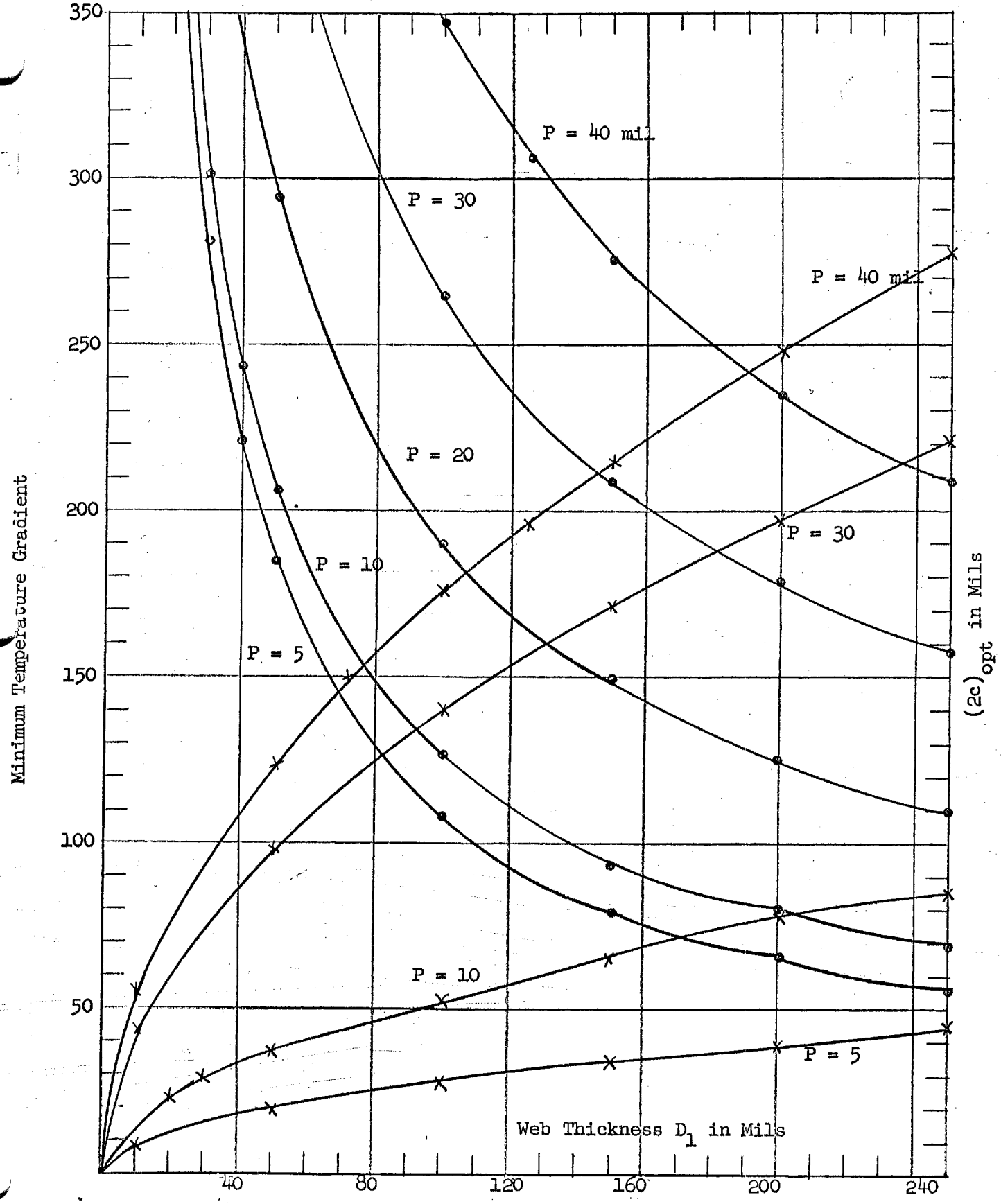

Maximum Temperature of Window and Opt. Slot Width $(2c)_{opt}$ as Function of Web Thickness D_1 for Cu Web for Different Values $(2c)_{opt}$ (Beam width is $(2c)_{opt}$. Window width = $(2c)_{opt}$ + 30 mils) Assumes 3000 watt Output per Linear Inch

Fig. 1.05.07

due to Fourier in 2 dimensions for the case of a geometry with an internal heat source:

$$\frac{\partial^2 T}{\partial x^2} + \frac{\partial^2 T}{\partial y^2} = - \frac{Q}{K} \quad , \qquad (1.05.33)$$

where Q is the power released per unit volume, and K is the thermal conductivity.

In this laboratory a relaxation technique for solving LaPlace's equation for a 2 dimension cross-section of cylindrically symmetrical geometry has been set up as a computer program. A similar technique in rectangular coordinates has been applied to a simple slot configuration such as one considered previously, consisting of a 1/2 mil Al window, a Cu web 200 mil thick having width t = 5 mil. Loading conditions were fixed to correspond to 3000 watts useful power per inch. Under these conditions, the maximum temperature gradient in the window corresponding to p = 15 mil, and 2C = 40 mil was 120.5°C. This temperature gradient can be checked with those of the previous section by referring to Fig. 1.05.03 for the same geometrical condition. For 2C = 40 mils and D_1 = 200 mil, the temperature corresponding to the assumed window configuration is 121°C which is in excellent agreement with the temperature gradient of 120.5°C derived by the more accurate relaxation technique using eq. 1.05.33.

(g) Multiaperture Configuration Consisting of N rows of Slots

Consider N rows of square slots of length L and width p separated by uniform web width t from adjacent slots as shown in Fig. 1.05.01g. All of the power absorbed by the windows and the web is assumed to be dissipated laterally to the edge of the configuration via the single hatched section of the web. Since the length of the configuration is assumed significantly larger than the width 2c of the configuration, negligible dissipation of power is assumed along the length L of each

individual longitudinal web. This assumption should help make the calculated temperature gradients obtained more conservative since appreciable power is lost longitudinally in practice.

Assume perfect registration of the beam with the slot array. The total beam power is W_B. Beam density is assumed uniform over the window configuration and the reflection of beam power from the web and window are considered negligible. The power absorbed in the windows of the array is $W_B TA_E$; the beam power absorbed directly by the web configuration is $W_B (1-T)$. The total power which must be dissipated by the single-hatched section of the web to the side of the configuration by reason of the assumptions made above is $WB (TA_E + 1-T)$.

Assume there are N_v slots in the vertical direction in Fig. 1.05.01g. By inspection of the figure:

$$N_v = \frac{L-p}{p+t} + 1 \qquad (1.05.34$$

The directly loaded area of the web corresponds to the single-hatched sections of the figure and is equal in area to $(N_v-1)\ 2ct$. The loading density on the web $(Q_{WB})_o$ assumed uniform is this:

$$(Q_{WB})_o = \frac{WB(TA_E + 1-T)}{(N_v - 1)2ct} \qquad (1.05.35)$$

Substituting for N_v in eq. 1.05.34, and using eq. 1.05.15 for W_B

$$(Q_{WB})_o = \frac{U(TA_E + 1-T)(p + t)}{(1-A_E)T(L-p)2ct} \qquad (1.05.36)$$

From eq. 1.05.04

$$(\Delta T)_{WB} = \frac{c^2(Q_{WB})_D'}{2K_1D_1} = \frac{CUZ'}{4K_1D_1(L-p)} \qquad (1.05.37$$

where

$$Z' = \frac{(TA_E + 1-T)(p+t)}{(1-A_E)(Tt)} \qquad (1.05.38)$$

The maximum temperature gradient is taken as the sum of the gradient to the center of the web plus the gradient to the center of the window. To obtain the gradient from the web to the center of a given window we assume circular windows of diameter P. The density of loading on the windows is equal to $\frac{W_B}{2LC}$. The density of loading absorbed in the window is given by

$$(Q_{WN})_o = \frac{W_B A_E}{2LC} = \frac{U A_E}{(1-A_E)T2LC} \qquad (1.05.39)$$

From eq. 1.05.06 the temperature gradient across a circular window of diameter p is

$$(\Delta T)_{WN} = \frac{(Q_{WN})_o p^2}{16K_2D_2} = \frac{U_p{}^2 A_E}{(1-A_E)TK_2D_2LC(32)} \qquad (1.05.40)$$

$$= \frac{UX'}{32K_2D_2LC}$$

where

$$X' = \frac{p^2 A_E}{(1-A_E)T} \qquad (1.05.41)$$

In computing the above, the area of the window was assumed to be given by $\frac{\pi p^2}{4}$ instead of p^2 the actual area of the square hole. Making this $\frac{4}{\pi}$ correction to compensate for the greater area of the square hole and the consequent greater absorption of power we obtain in place of eq. 1.05.40:

$$(\Delta T)_{WN} = \frac{UX'}{8\pi K_2 D_2 LC} \qquad (1.05.42)$$

$$(\Delta T)_T = (\Delta T)_{WN} + (\Delta T)_{WB} = \frac{UCZ'}{4K_1 D_1 (L-p)} + \frac{UX'}{8\pi K_2 D_2 LC} \qquad (1.05.43)$$

where Z' and X' are defined by eq. 1.05.38 and 1.05.41 respectively.

The geometrical transmission of a window configuration consisting of N rows of square slots of width p separated by a distance t is given to a close approximation of the following equation:

$$T = \frac{p^2}{(p+t)\left[p+\frac{(N-1)}{N}t\right]} \qquad (1.05.44)$$

Plots of the temperature gradients for 1/2 mil Al windows and a copper web as obtained on the basis of a computer program using eq. 1.05.43 are given in Figs. 1.05.08 to 1.05.12 as a function of the number of rows N for p = 5, 10, 20, 30 and 40 mil and web thickness t = 5 mil and different values of web thickness D_1. The curve marked $D_1 = \infty$ corresponds to the temperature gradient across the windows only, i.e. the web here corresponds to an infinite heat sink. Since the temperature gradients listed are based on adding the temperature gradient of the window to the temperature gradient of the center of the web the results are slightly off for even number of rows. The transmission values corresponding to the different number of rows is indicated at the top of the graphs. Temperature gradients through the thickness of the web are neglected.

The curves have the same type minima which were characteristic of the single row configuration previously discussed when the temperature gradients are plotted as a function of row width 2c. For low values of web thickness the minimum temperature gradients usually occur at 1 row.

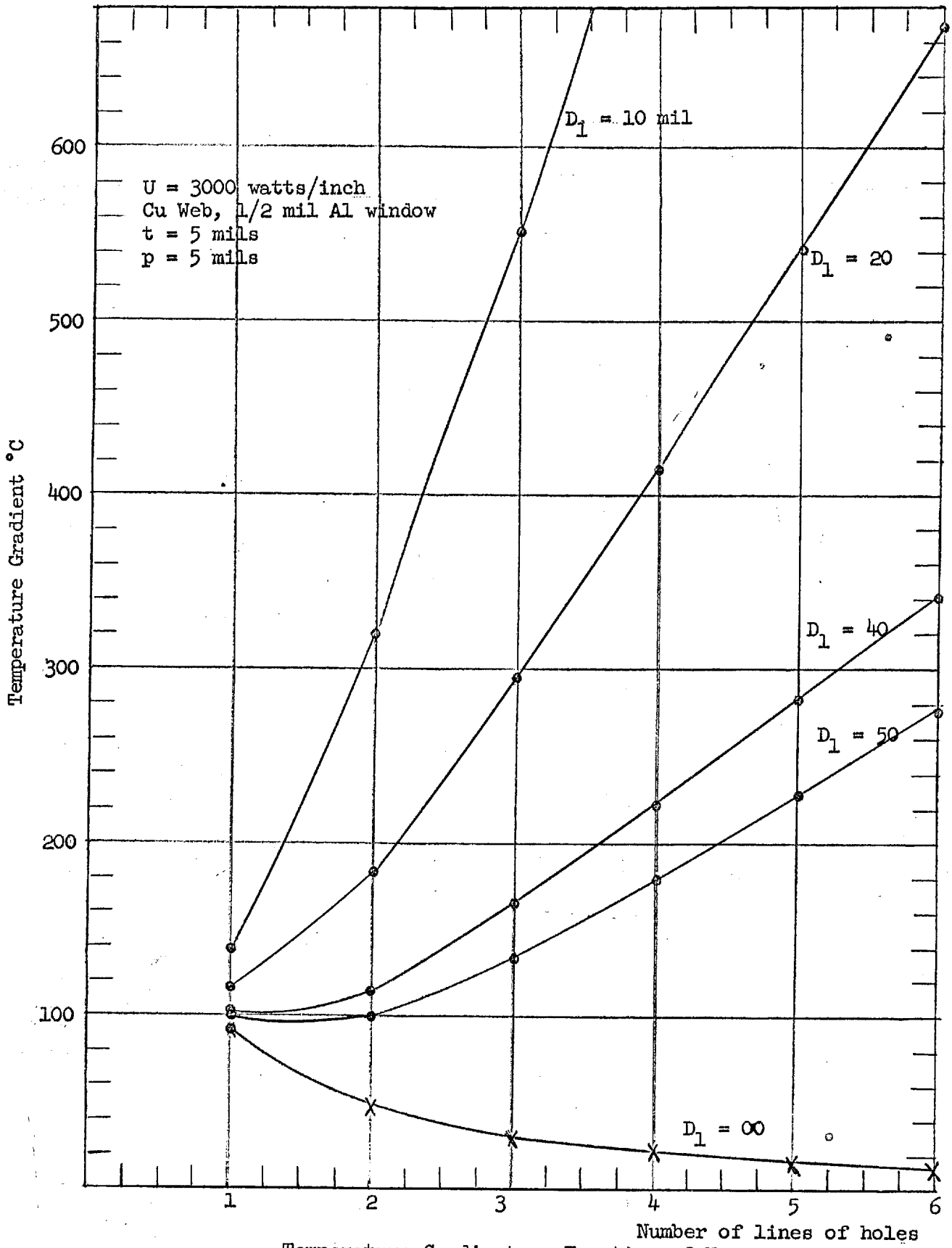

Temperature Gradient as Function of N
Number of Lines of Square Holes

Fig. 1.05.08

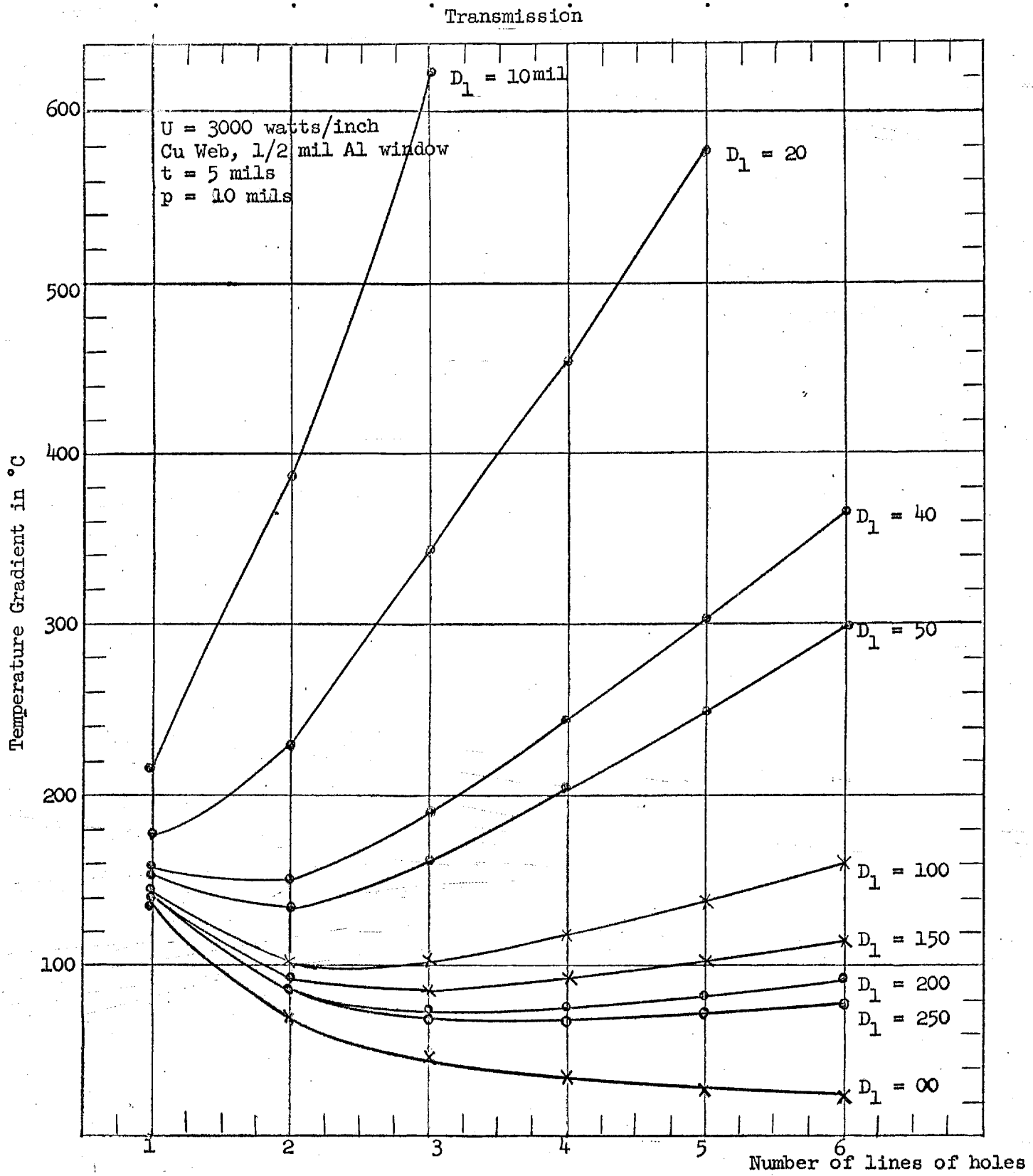

Temperature Gradient as Function of N
Number of Lines of Square Holes

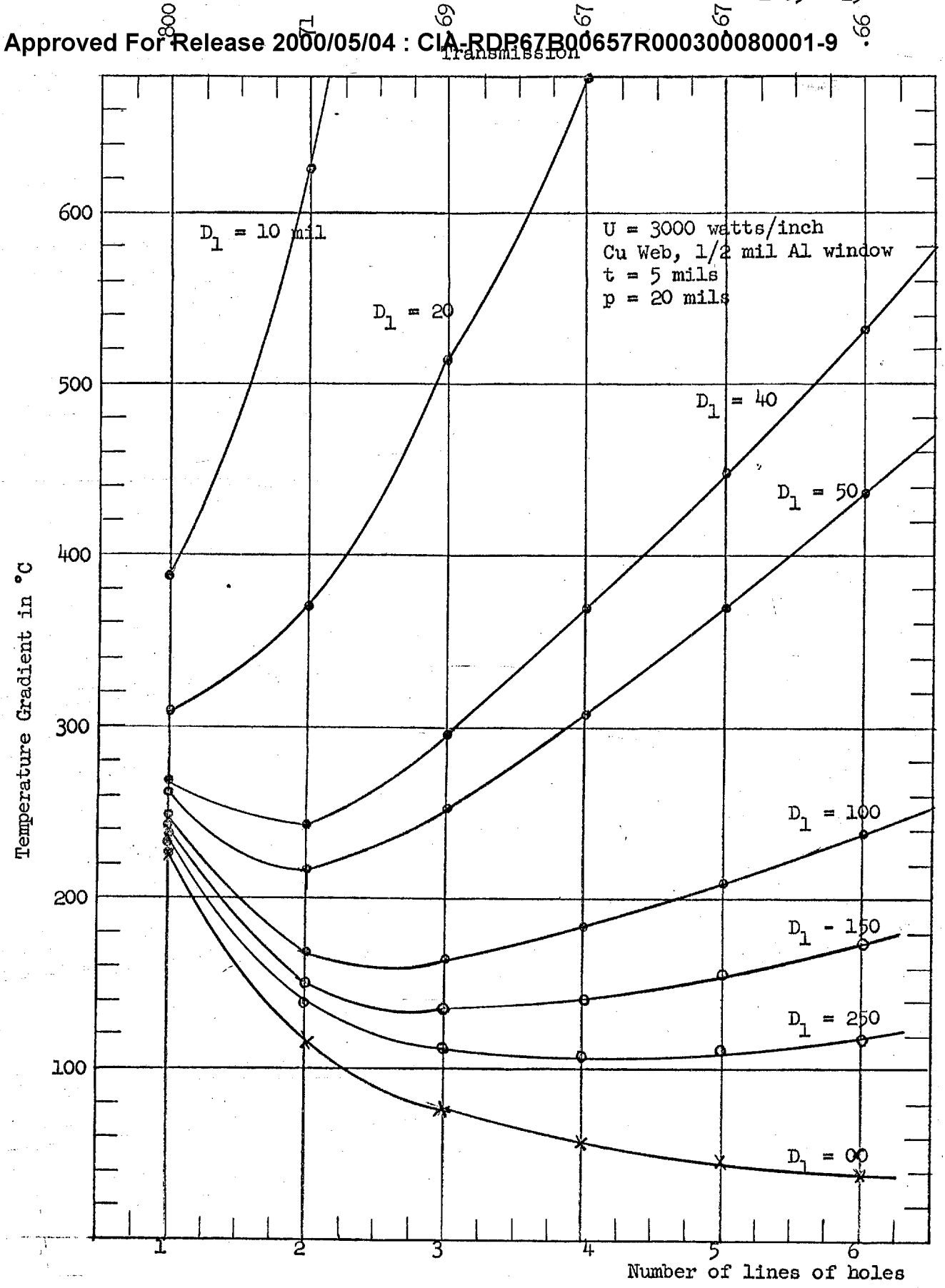

Temperature Gradient as Function of N
Number of Lines of Square Holes

Fig. 1.05.10

.66 .79 .77 .76 .76 .75

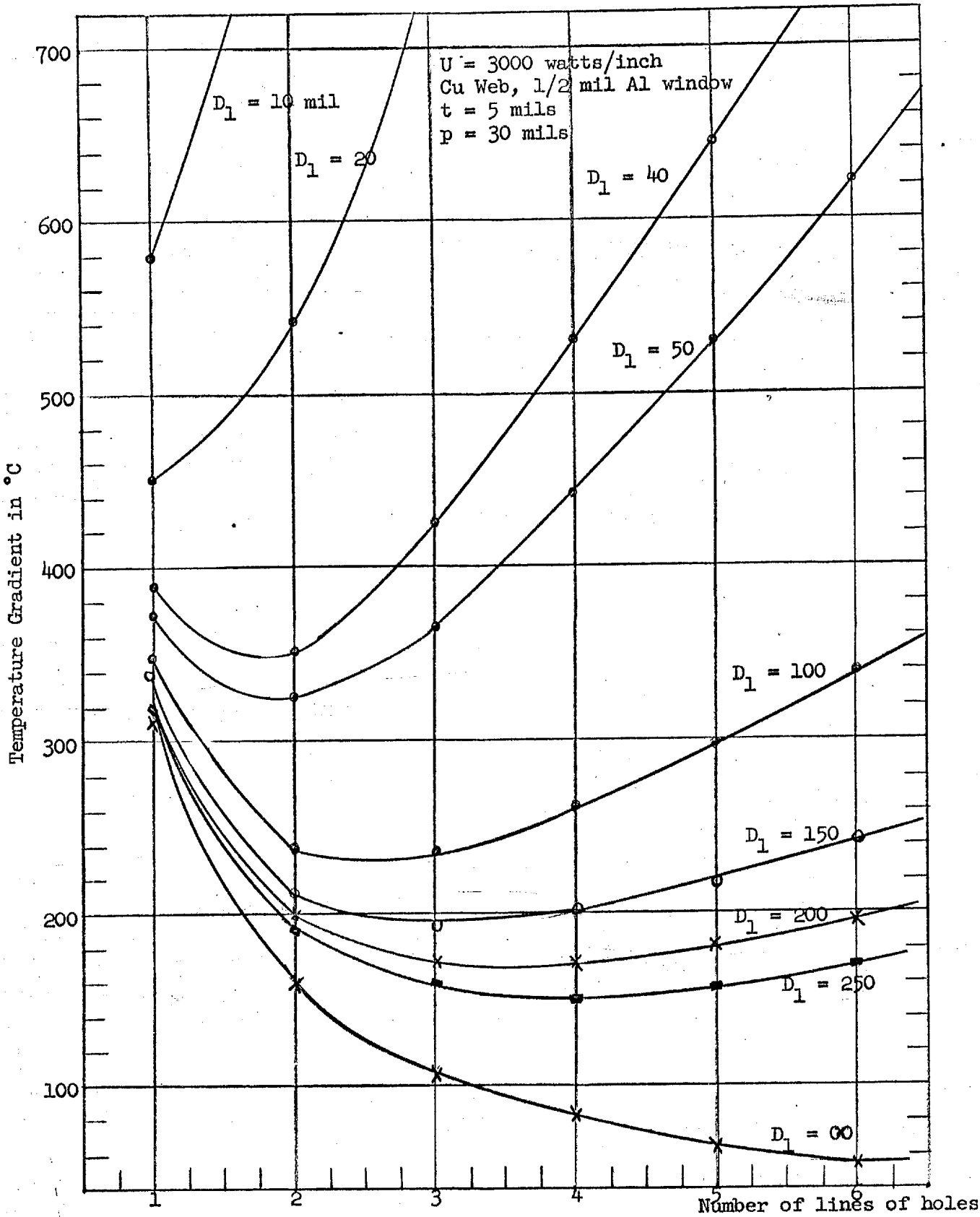

Temperature Gradient as Function of N
Number of Lines of Square Holes

Fig. 1.05.11

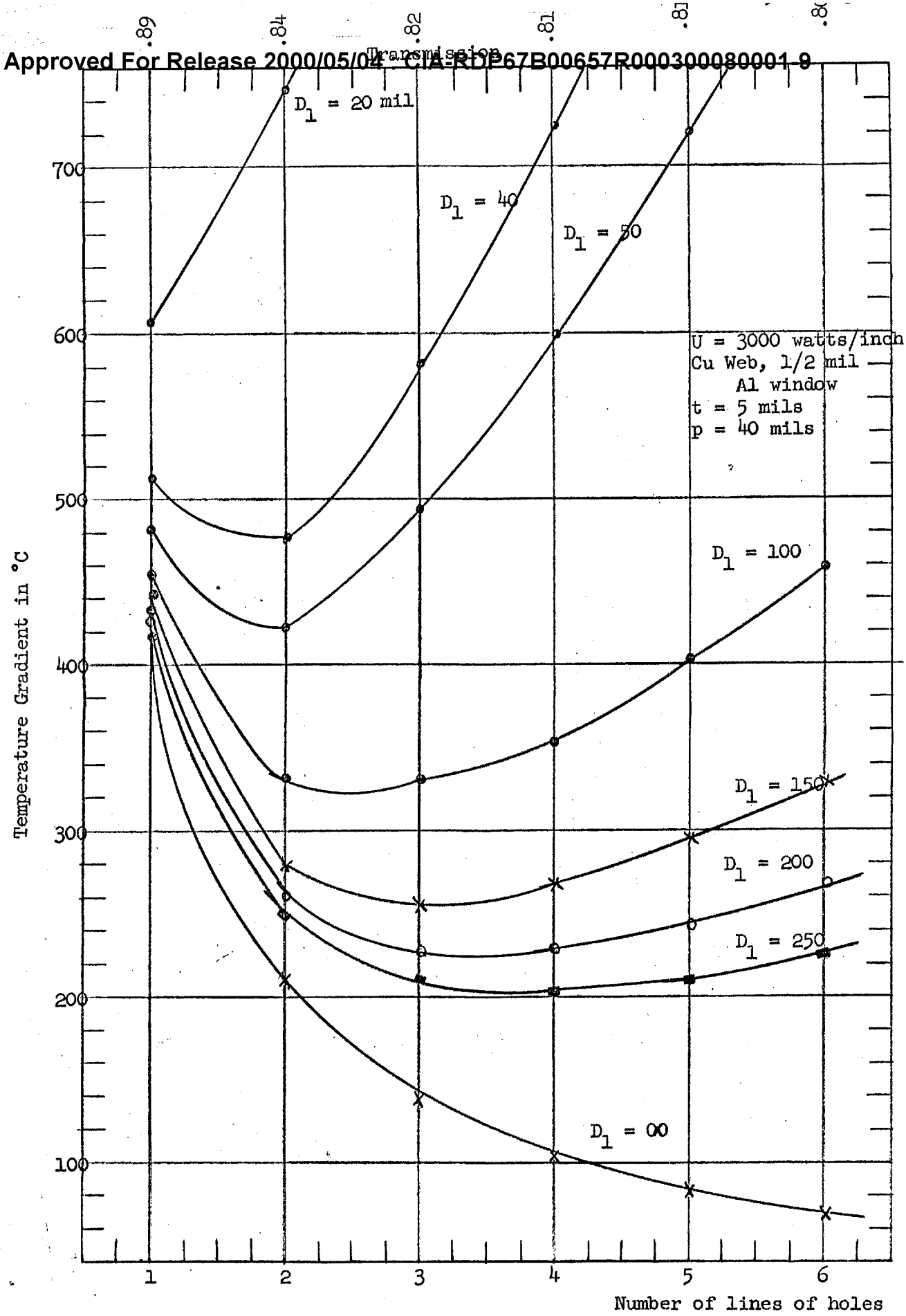

Temperature Gradient as Function of N
Number of Lines of Square Holes

Fig. 1.05.12

For higher thicknesses the minima occur at several rows, corresponding roughly to the configuration which might be expected from the value of $(2c)_{OPT}$ for the single row case.

It is interesting to compare results of calculations of the multirow configuration with the single row calculations in the previous section. A comparison is given in Table 1.05.02 for a 1/2 mil Al window, 5 mil width copper web, 50 and 100 mil in thickness. It is evident from the table that the temperature gradients corresponding to the single rows at optimum values of row width have temperature gradients which are lower than the minimum temperature gradients occurring for the multiplerow case. It is reasonable to believe that the multiple arrays would exhibit lower temperature gradients if the dissipation of power in the longitudinal direction were taken into consideration in the calculations. These structures, however, are more difficult to machine and it is considerably more difficult to make vacuum seals to them. For this reason most of the later work on window design was concerned with fabricating and testing single slot window configuration arrays.

TABLE 1.05.02

Comparison of Temperature Gradients for Single Rows of Rectangular Slots Versus Multiple Rows of Square Slots for 1/2 mil Al Window, Copper Web 5 mil Thick, 3000 Watts Transmitted Output per Inch, °C

		Temperature Gradients for Single Rows At Optimum Value of Slot Width		Max. Temperature Gradients for Different Numbers of Rows N					
p	D_1	$(\Delta T)_{OPT}$	$(2C)_{OPT}$	N = 1	N = 2	N = 3	N = 4	N = 5	N = 6
10	50	115	38	153	133	161	202	247	296
10	100	81	54	146	101	104	118	138	159
20	50	206	70.2	261	217	252	306	369	435
20	100	146	99	246	166	164	182	208	237
40	50	420	124	491	422	494	600	720	848
40	100	297	176	453	315	316	352	402	458

1.06. Mechanical Stresses

Introduction:

In the following section an analyses is made of the mechanical stresses to which the window of a beta ray tube is subjected. Of necessity, many simplifying assumptions are made in this analysis in view of the complexity of the stress situation. The conclusions in some cases do not jibe with the observed facts. For example, the conclusion is reached in the analysis that Si should be superior to Be or Al as a window foil. In actual practice all of the silicon windows which were fabricated proved to be extremely fragile and tended to shatter at nominal loadings. However, many of the conclusions of the analysis of mechanical stresses have been verified. For example, the conclusion is reached that narrow slots are not only subject to lower temperature gradients but have significantly lower mechanical stresses. Narrow slots in practice, as will be noted in a later section, have appeared to be a very promising approach.

The three basic stresses in the window are:

1. Brazing stress - caused by differential expansion between window and anode (supporting structure) on cooling from the freezing temperature of the braze to room temperature.

2. Pressure stress - caused by pressure difference between external environment and high vacuum inside tube (maximum of one atmosphere).

3. Thermal stress - caused by thermal absorption of portion of incident radiant beam in the window which induces differential expansion between various parts of the window (and the anode).

The analyses assume that stresses and strains are perfectly elastic (Hooke's Law) and that superposition applies. (The sign convention used is positive values for tension and negative for compression). The analyses further assume in general that the anode or window supporting structure is perfectly rigid, i.e. all strains are taken up by the window. However, the effect of a flexible structure is considered for a specific case of a rectangular beryllium window in the section discussing thermal stresses.

Two window geometries are considered in this report: the flat rectangular plate and the flat circular disk. The possibilities of other geometries obtainable by dishing and corrugating have been considered but comparative analysis indicates that only minor thermal and brazing stress reduction is obtainable relative to the flat case. Some reduction in pressure stress is obtainable, however, as the pure membrane condition is approached.

PRESSURE STRESSES

Considering the rectangular window as a flat plate clamped along all edges, the stress due to a uniform pressure P across the window can be expressed as:(7)

(7) Don Hartag, "Advanced Strength of Materials" p. 134

$$\sigma_p = \pm \frac{6\gamma P (2c)^2}{h^2}$$

where γ = .0833 (for a long narrow plate).

P = external pressure (psi)
c = half-width of window (in.)
h = thickness of window (in.).

The maximum stress for an evacuated tube would occur when P is one atmosphere. Therefore,

$$\sigma_p = \pm 29.4 \left(\frac{c}{h}\right)^2$$

Since the stress occurs as a bending stress, the maximum value will occur at the outer fibers and will be tension on the one side of the window and in compession on the other.

Considering the case of the round window, the stress for a circular plate with clamped edges is given by (reference 7., page 128)

$$\sigma_p = \pm \frac{3 P b^2}{4 h^2}$$

where b = radius of the window
h = thickness of the window
and for one atmosphere

$$\sigma_p = \pm 11.3 \left(\frac{b}{h}\right)^2.$$

The stress for one atmosphere pressure loading as a function of window width for several window thickness are plotted in Figs. 1.06.01 and 1.06.02 for the rectangular and circular cases.

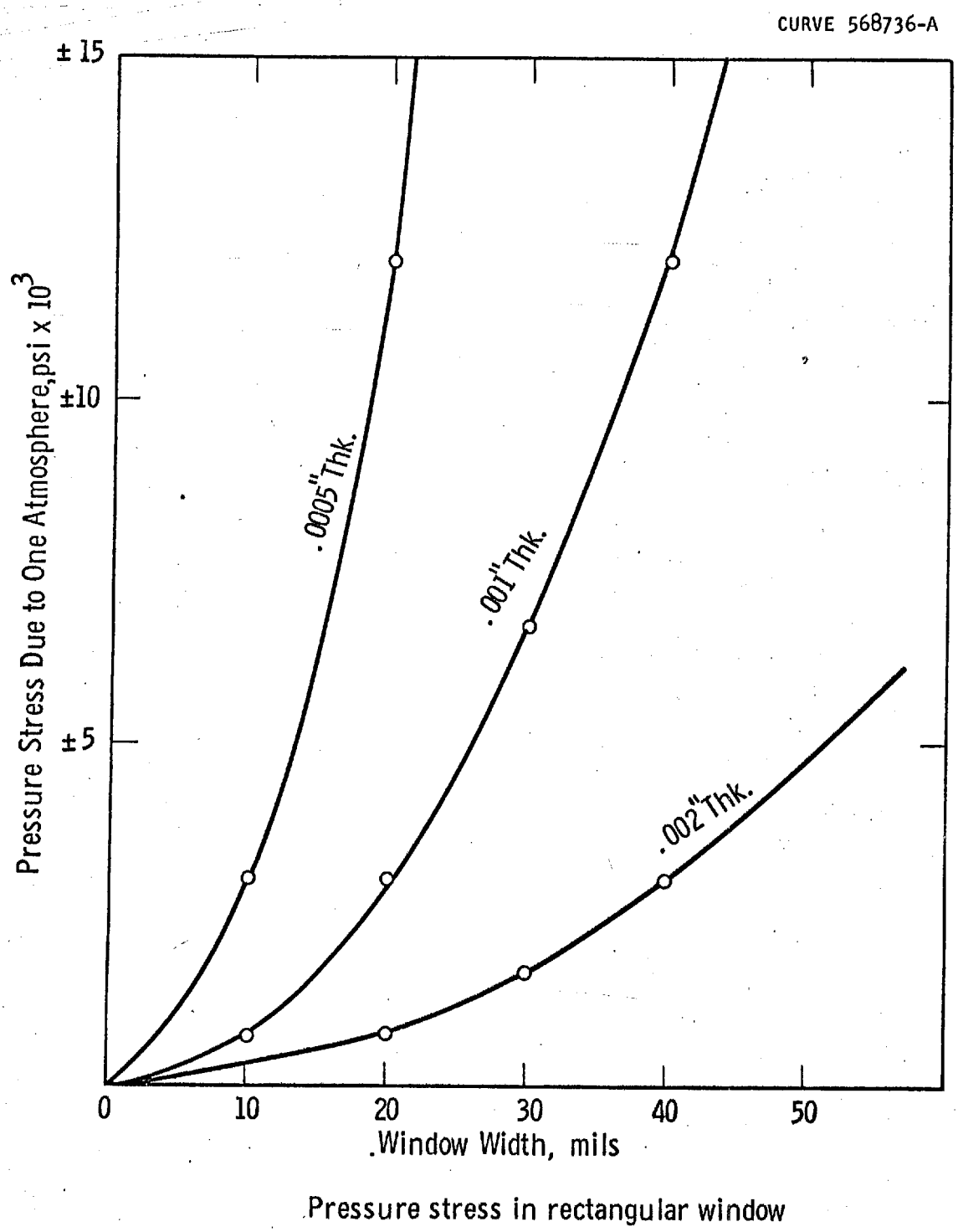

Pressure stress in rectangular window

Fig. 1.06.01

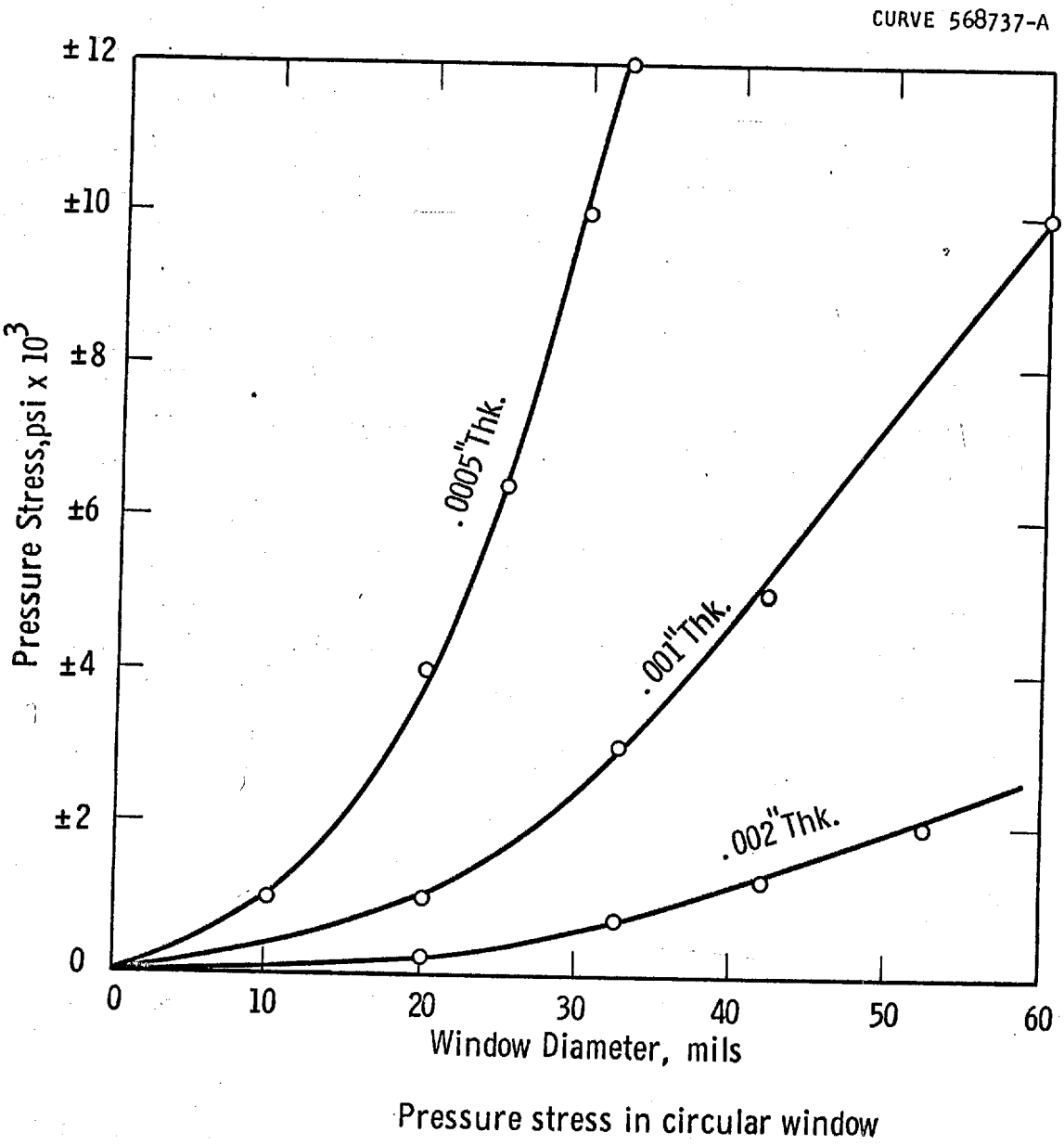

Pressure stress in circular window

Fig. 1.06.02

In the case where the windows are preformed so that they fulfill the conditions for membrane analysis (a section of a cylinder for the plate and a section of a hemisphere for the disk, where the thickness of the window is very much less than its other dimensions) we have for both cases the purely tensile stress (reference 7, page 75),

$$\sigma = + \frac{Pc}{2h} \text{ or } \frac{Pb}{2h}.$$

In this instance (for the nominal dimensions practical from considerations of thermal stress and absorption) we have stresses less than 1,000 psi (since b is in tens of mils and h is in mils) and they may be neglected.

BEAM LOADING TEMPERATURES

Rectangular Window

Assuming the beam to be uniformly distributed and centrally located on the window, the temperature distributors across the beam width (y - direction) is parabollically symetrical for conductive cooling, i.e.,

$$T_y - T_{edge} = \frac{q_o}{2Kh} (c^2 - y^2)$$

and

$$T_{center} - T_{edge} = \Delta T_y = \frac{q_o c^2}{2Kh}$$

where q_o = thermal absorption of beam (watts/in^2)
K = thermal conductivity of window material (watts/in-C°)
ΔT_y = maximum temperature difference in y-direction (°C).

This, of course, further assumes that the window width is equal to the beam width. If the beam is narrower than the anode slot, a further temperature drop must be included to allow for conduction between the beam edge and the side of the slot. Since the thermal stress calculations are relatively insensitive to the exact shape of temperature distribution but are mainly affected by the total temperature difference, the drop to be used in the actual calculations should be the sum of the two individual drops. When the beam is wider than the slot, the slot half-width should, of course, be used in the temperature equation.

Circular Window

In the case of a round window the temperature distribution is given by

$$T_r - T_{edge} = \frac{q_o}{4Kh} (b^2 - r^2)$$

and

$$T_{center} - T_{edge} = \Delta T_r = \frac{q_o b^2}{4Kh} = \frac{Q_{total}}{4\pi Kh}.$$

The same comments concerning overlap and underlap apply in this case. An interesting fact with this geometry is the independence of ΔT_r on the radius for fixed total heat inputs.

THERMAL STRESSES

Rectangular Window

The maximum stress caused by a uniform temperature difference between a rectangular window (with all edges built-in) and its rigid supporting structure is given by:(8)

$$\sigma_x = \sigma_y = \frac{-\alpha E \Delta T}{1 - \mu}$$

where μ = Poissons ratio for the window material

E = modulus of elasticity (psi)

α = coefficient of thermal expansion (in/in-C°).

(8) Boley and Weiner, "Theory of Thermal Stresses" [illegible]

It should be emphasized that this expression covers the case when the entire window area is raised a given ΔT above the supporting structure. In the actual case there is, of course, a thermal gradient in the y - direction (i.e. across the narrow portion of the window). In the x - direction; the gradient is essentially zero except for end effects. In the case where the window is only built in at the ends and there is a symmetrical gradient in the y - direction the maximum stress is given by(9)

$$\sigma_x = -\alpha E \Delta T_y.$$

Therefore, we may bracket the value of the maximum stress:

$$-\frac{\alpha E \Delta T_y}{1-\mu} \geq \sigma_{x\,(max)} \geq -\alpha E \Delta T_y.$$

For most metallic materials, $\mu = 0.3$ (beryllium being one extreme exception with a value of 0.05) so that the difference between the stresses in these two cases is at most, one-third. However, since the expression on the left most closely approximates the actual conditions and gives a conservative value, it is used in the calculations throughout this memorandum.

Expressing this value of stress in terms of the thermal input, we have (dropping the subscript ΔT),

$$\sigma_{x(max)} = -\frac{\alpha E \Delta T}{1-\mu} = -\frac{\alpha E\, q_o c^2}{2\,Kh\,(1-\mu)} = -\frac{\alpha E\, Q_{total}(c)}{2\,Kh\,\ell\,(1-\mu)}.$$

Thus, it is apparent that the stress in the rectangular window varies directly as the slot width for a given total heat input and inversely as the thickness and length.

Table 1 gives stress values which would occur in a flat rectangular beryllium window as a function of thermal flux density. To obtain a total wattage input value, a one-inch long slot was chosen. Both thermal and pressure

(9) Gatewood, "Thermal Stresses," page 9

TABLE 1.06.01

CALCULATED STRESSES (psi) RECTANGULAR BERYLLIUM WINDOW

Window Thickness h (inches)	Heat Flux q_o (watt/in^2)	.020 in. Window Width				.30 in. Window Width				.040 in. Window Width			
		σ_{th}	σ_p	$\sigma_{th}+\sigma_p$	Watts*	σ_{th}	σ_p	$\sigma_{th}+\sigma_p$	Watts*	σ_{th}	σ_p	$\sigma_{th}+\sigma_p$	Watts*
.0005	1000	-13,800	±12,000	-25,800	20	- 31,100	±27,000	- 58,100	30	- 55,200	±48,000	-103,200	40
.0005	2000	-27,600	±12,000	-39,600	40	- 62,200	±27,000	- 89,200	60	-110,400	±48,000	-158,400	80
.0005	4000	-55,200	±12,000	-67,200	80	-124,000	±27,000	-151,000	120	-220,800	±48,000	-268,800	160
.001	1000	- 6,900	± 3,000	- 9,900	20	- 15,500	± 7,800	- 23,300	30	- 27,600	±12,000	- 39,600	40
.001	2000	-13,800	± 3,000	-16,800	40	- 31,100	± 7,800	- 38,900	60	- 55,200	±12,000	- 67,200	80
.001	4000	-27,600	± 3,000	-30,600	80	- 62,200	± 7,800	- 70,000	120	-110,400	±12,000	-122,400	160
.002	1000	- 3,500	± 800	- 4,200	20	- 7,800	± 1,700	- 9,500	30	- 13,800	± 3,000	- 16,800	40
.002	2000	- 6,900	± 800	- 7,700	40	- 15,500	± 1,700	- 17,200	60	- 27,600	± 3,000	- 30,600	80
.002	4000	-13,800	± 800	-14,600	80	- 31,100	± 1,700	- 32,800	120	- 55,200	± 3,000	- 58,200	160

Formulae Used in Calculations:

$$\sigma_{th} = \frac{-\alpha E}{2K(1-\mu)} \left(\frac{q_o c^2}{h}\right) = -69 \left(\frac{q_o c^2}{h}\right)$$

$$\sigma_p = \pm 30 \left(\frac{c}{h}\right)^2$$

*Assumed window length of one inch

stresses are given as well as their total. Assuming an allowable maximum stress for beryllium between 30,000 and 40,000 psi, an estimate of allowable wattages may be made for the various slot widths and window thicknesses. Fig 1.06.03 to 1.06.05 are plots of the results of the calculated values given in Table 1.

Table 1.06.02 and Fig 1.06.06 present the results of similar calculations for Si. Table 1.06.03 gives the materials properties used in these and the other calculations in this report.

The effectiveness of flexibility introduced into the supporting structure to reduce these stresses is hampered by the thermal conductance and strength requirements of any such supporting structure. In the limit, a totally unrestrained plate with a temperature distribution of this type (about the x-axis) would have a stress given by (reference 9, page 9).

$$\sigma_x = \frac{-\alpha E q_o c^2}{6Kh} .$$

Comparison of this expression with the value used previously shows that a factor of three to four between the completely restrained and completely unrestrained case. However, rough calculations show that even in the case of supporting structures with cross sections only several times the window thickness that reductions of only 10 to 15 per cent appear feasible with the geometries acceptable for brazing and forming. Consequently, such structres would probably introduce more difficulties, problems, and thermal impedence than the slight obtainable reductions in stress would warrant.

Another problem which must be considered in determining the effects of thermal loading is the possibility of buckling of the window under thermal stresses. The critical temperature difference is given by (reference 9, page 175):

$$\Delta T_{cr} = \frac{\pi^2 k^2}{4\alpha c^2} = \frac{\pi^2}{8\sqrt{3}\alpha}\left(\frac{h}{c}\right)^2$$

where k = radius of gyration.

CURVE 568740-A

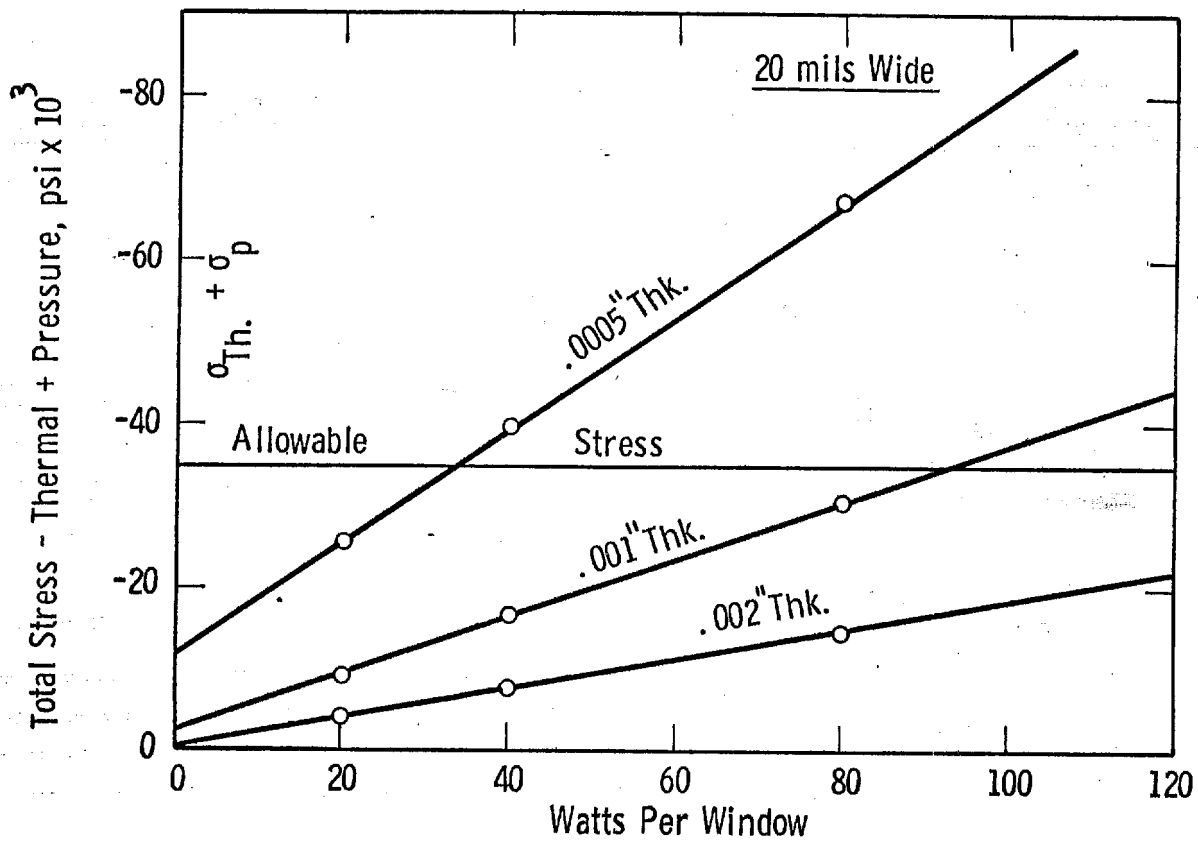

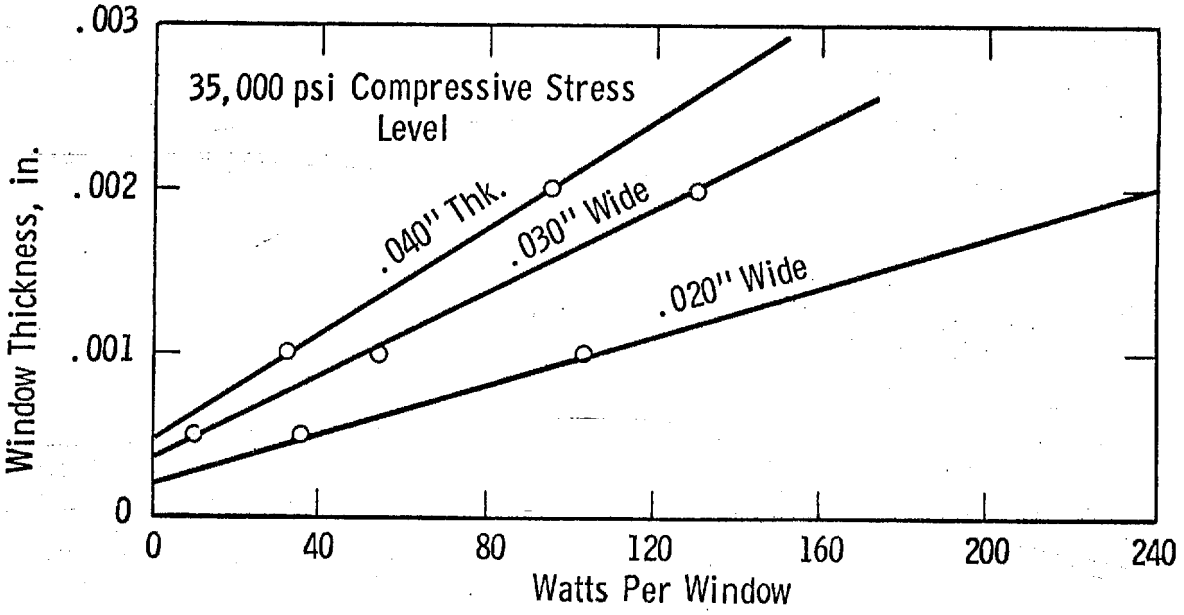

Rectangular Be Window (1 inch long)

Fig. 1.06.03

CURVE 568739-A

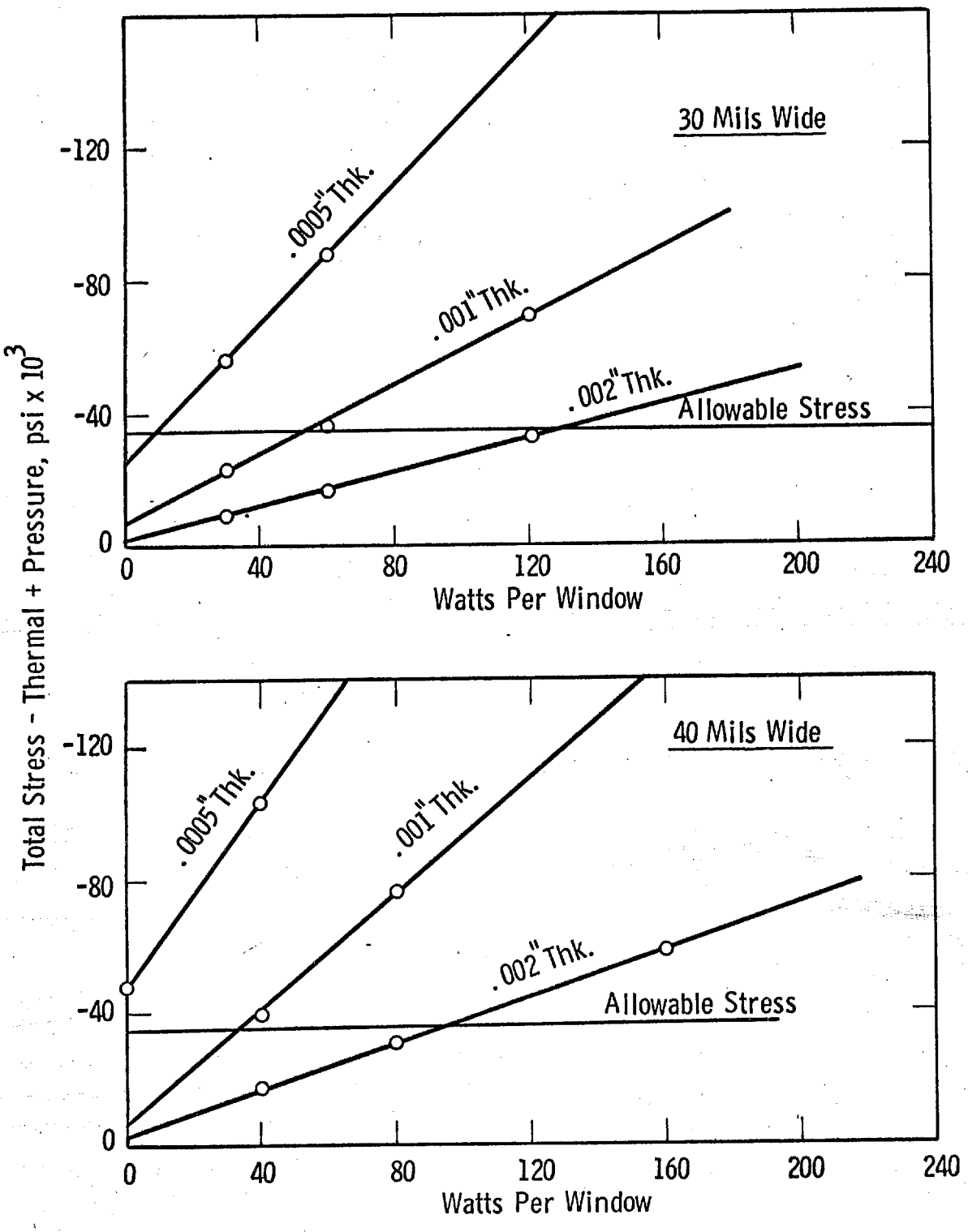

Rectangular Be Window (1 inch long)

Fig. 1.06.04

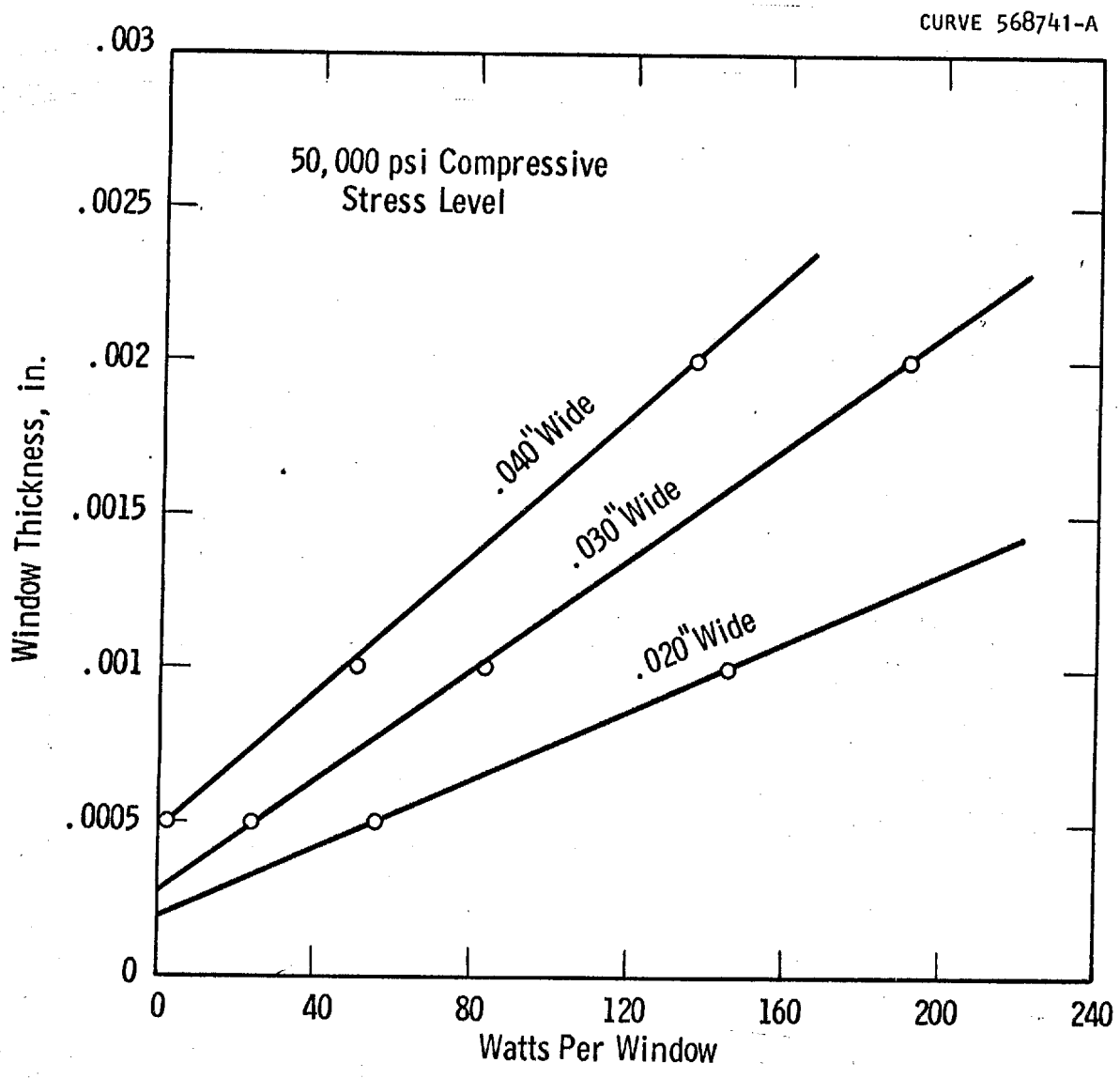

Rectangular Be Window (1 inch long)

Fig. 1.06.05

TABLE 1.06.02

CALCULATED STRESSES (psi) IN SILICON WINDOW

Window Thickness h (inches)	Heat Flux q_o	.020 In. Width				.030 In. Width				.040 In. Width			
		σ_{th}	σ_p	$\sigma_{th}+\sigma_p$	W per Window	σ_{th}	σ_p	$\sigma_{th}+\sigma_p$	W per Window	σ_{th}	σ_p	$\sigma_{th}+\sigma_p$	W per Window
.0005	1000	- 2,060	±12.0	-14,060	20	- 4,650	±27,000	-31,650	30	- 8,300	±48,000	-56,300	40
.0005	2000	- 4,240	±12.0	-16,240	40	- 9,300	±27,000	-36,300	60	-16,600	±48,000	-64,600	80
.0005	4000	- 8,480	±12.0	-20,480	80	-18,600	±27,000	-45,600	120	-33,200	±48,000	-81,200	160
.0005	6000	-12,720	±12.0	-24,720	120	-27,900	±27,000	-54,900	180	-49,800	±48,000	-97,800	240
.001	1000	- 1,030	± 3.0	- 4,030	20	- 2,320	± 6,750	- 9,070	30	- 4,150	±12,000	-16,150	40
.001	2000	- 2,060	± 3.0	- 5,060	40	- 4,640	± 6,750	-11,390	60	- 8,300	±12,000	-20,300	60
.001	4000	- 4,120	± 3.0	- 7,120	80	- 9,280	± 6,750	-16,030	120	-16,600	±12,000	-28,600	160
.001	6000	- 6,180	± 3.0	- 9,180	120	-13,920	± 6,750	-20,670	180	-24,900	±12,000	-36,900	240
.002	1000	- 515	± .75	- 1,265	20	- 1,160	± 1,700	- 2,860	30	- 2,070	± 3,000	- 5,070	40
.002	2000	- 1,030	± .75	- 1,780	40	- 2,320	± 1,700	- 4,020	60	- 4,140	± 3,000	- 7,140	80
.002	4000	- 2,060	± .75	- 2,810	80	- 4,640	± 1,700	- 6,340	120	- 8,280	± 3,000	-11,280	160
.002	6000	- 3,090	± .75	- 3,840	120	- 6,960	± 1,700	- 8,660	180	-12,420	± 3,000	-15,420	240

Equations Used

$$\sigma_{th} = \frac{\alpha E}{2K(1-\mu)} \left(\frac{q_o c^2}{h}\right) = -10.3 \left(\frac{q_o c^2}{h}\right)$$

$$\sigma_p = \pm 30 \left(\frac{c}{h}\right)^2$$

Approved For Release 2000/05/04 : CIA-RDP67B00657R000300080001-9

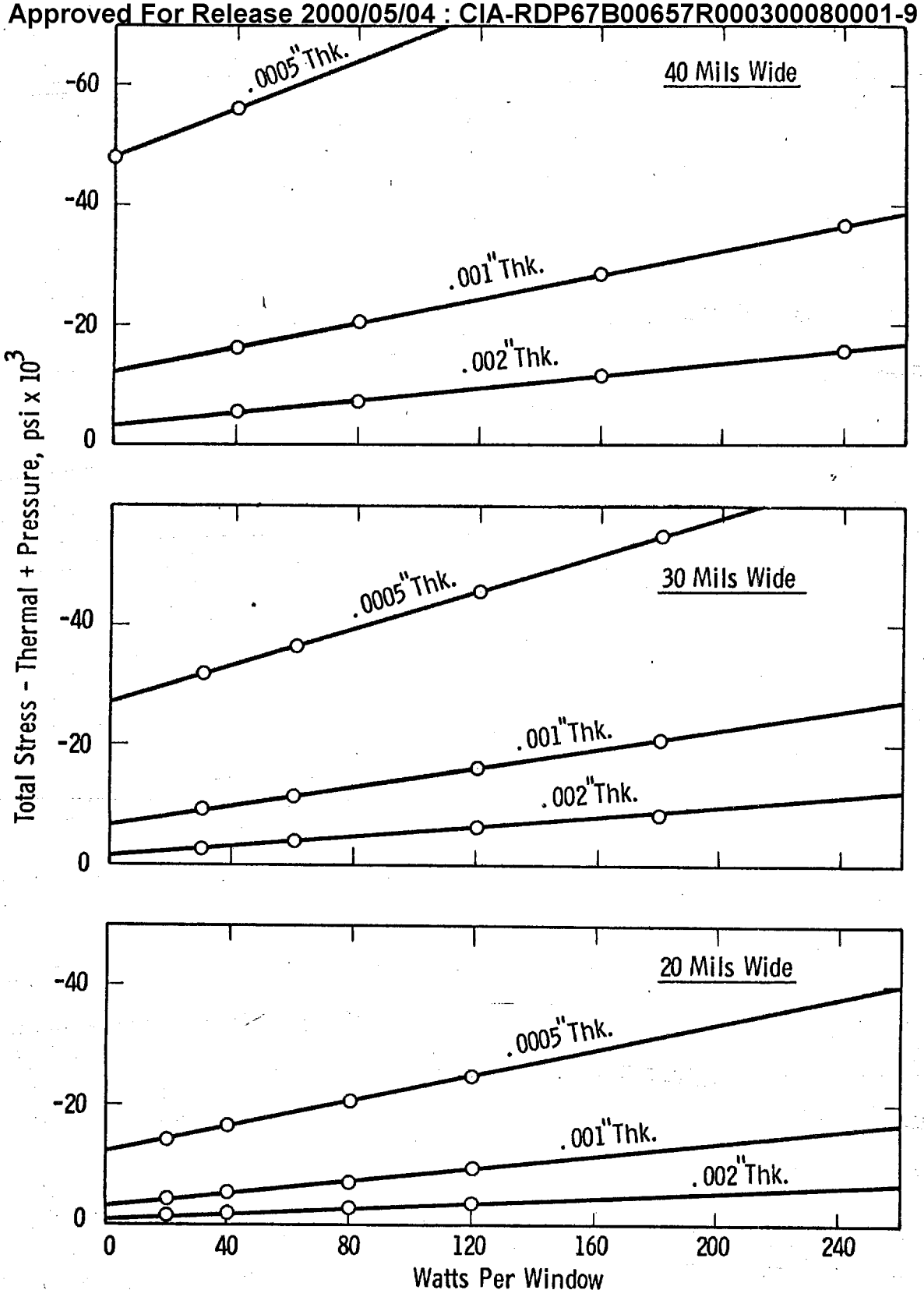

Rectangular silicon window (1 inch long)

Fig. 1.06.06

TABLE 1.06.03

Properties of Possible Window Materials

	$\alpha \times 10^{-6}$ @20°C	$\sigma_{allow.} \times 10^{-3}$	K Watt In.°C	$(1-\mu)$	E $\times 10^{-6}$ psi	M* Thermal Stress Figure of Merit	ρ gm/cc
Be[3,4,6]	12.2	35	3.73	.95	40	870	1.85
Si[3,6,7,8]	2.2	45	2.12	.82	16.3	8720	2.30
Mo[5]	5.4	80	3.48	.68	47	2980	10.2
Al[2] (6061-T6)	23.6	40	3.63	.67	10.0	1650	2.70
Ag[6]	19.4	18	11.0	.63	10.3	2500	10.5

* M (Thermal Merit Factor) = $\frac{4K(1-\mu)\sigma_{allow.}}{E}$

1. Eng. Mat. Handbook
2. Reynolds' Aluminum Data Book
3. Am. Inst. of Phys. Handbook
4. Data from Brush Bey Corp.
5. Sylvania Brochure
6. Metals Handbook
7. J.A.P. 31, 211, Jan. 1960
8. Phys. Rev. 83, 1080 (1951)

Approved For Release 2000/05/04 : CIA-RDP67B00657R000300080001-9

This is based on the classical Euler relationship for critical buckling which is seen when solving for the critical stress.

$$\sigma_{crit} = \alpha E \Delta T_{cr} = \frac{\pi^2 E}{8\sqrt{3}} \left(\frac{h}{c}\right)^2.$$

The critical stresses for the geometries and materials under consideration are far in excess of the ultimate strengths of the materials indicating that yielding and/or fracture should occur long before buckling can take place. This is analogous to a column with low slenderness ratio which would yield or fail from compressive stress before it would buckle. However, windows operating at excessively high thermal fluxes will exhibit buckling and they may be so operated through a number of thermal cycles without fracture if they are sufficiently ductile. Such operation is extremely difficult to analyze since the geometries become exceedingly complex and the results are extremely dependent on the past history (rolling, heating and cooling rates during brazing, etc.) of the material. Furthermore, the normal mechanical properties have very little meaning or use under such conditions and specific bend and flexure data would be needed. If such operation (thermal loading above the elastic limit) is contemplated, the best approach would be an experimental one using actual windows. However, the brittleness of most of the materials presently being considered for this application appear to be much too high to withstand such flexing.

Circular Window

The stress in a circular window with built-in edges with a thermal gradient as described previously is given by (reference 10).

$$\sigma_r \text{ (radial)} = -\frac{\alpha E q_o}{8 Kh} \left(\left[\frac{1-\mu-\mu^2}{1-\mu} \right] b^2 + \frac{b^2}{2} - \frac{r^2}{2} \right)$$

$$\sigma_t \text{ (tangential)} = \frac{\alpha E q_o}{8 Kh} \left(\left[\frac{1-\mu-\mu^2}{1-\mu} \right] b^2 + \frac{b^2}{2} - \frac{3r^2}{2} \right)$$

(10) Temoshenko "Strength of Materials, Vol. II, p. 263 ff.

The σ_r in this case is approximately 1.5 times as great as in the unrestrained case. However, σ_t goes into tension at the outer edge in the unrestrained case; this is undesirable for most of the materials being considered. In addition, the number of such windows required to provide the desired output precludes the possibility of using flexible supports for the circular geometry. Consequently, only the restrained case is given further attention. The maximum stress for the restrained case occurs in the middle and is given by

$$\sigma_{th} = \frac{3\alpha E\, q_o b^2}{16\, Kh} = \frac{-3\alpha E}{16\pi Kh}\, Q_t .$$

Table 1.06.04 and Figure 1.06.05 show the results of calculations for round Beryllium windows. One interesting result which was not tabulated in the calculations on the rectangular geometry is the low temperature rises required to introduce excessive stresses in the window materials.

The critical buckling stress is given by (reference 11)

$$\sigma_{cr} = \frac{4E\, h^2}{3b^2(1-\mu^2)} .$$

As in the rectangular case, the stresses computed for the geometries being considered give values in excess of the maximum allowable stress and similar comments apply.

A direct comparison of the two geometries may be obtained by reference to Table 1.06.05 which shows the number of beryllium windows required to obtain a 6 KW output. Rough efficiency estimates were used to allow for the increased absorption in the thicker windows.

BRAZING STRESSES

The brazing stress is a locked-in stress due to the difference in expansion between the window material and the anode. As the two metals cool from the solidus of the brazing material, the higher expansion member will

(11) Temoshenko "Theory of Plates and Shells", p. 323

TABLE 1.06.04

CALCULATED STRESSES (psi) IN ROUND BERYLLIUM WINDOWS

Window Thickness h(inches)	Heat Input Q_T(W)	.010 In. Window Dia.				.020 In. Window Dia.				.030 In. Window Dia.			
		ΔT	σ_{th}	σ_p	$\sigma_{th} + \sigma_p$	ΔT	σ_{th}	σ_p	$\sigma_{th} + \sigma_p$	ΔT	σ_{th}	σ_p	$\sigma_{th} + \sigma_p$
.0005	1	42	-15,400	±1,200	-16,600	42	-15,400	-4,800	-20,000	42	-15,400	-10,800	-26,200
.0005	2	85	-30,800	±1,200	-32,000	85	-30,800	-4,800	-35,600	85	-30,800	-10,800	-41,600
.0005	3	127	-44,200	±1,200	-45,400	127	-44,200	-4,800	-49,000	127	-44,200	-10,800	-
.0005	4	170	-61,600	±1,200		170	-61,600	-4,800	-	170	-61,600	-10,800	-
.001	1	21	- 7,700	± 300	- 8,000	21	- 7,700	±1,200	- 9,000	21	- 7,700	± 2,700	-10,400
.001	2	42	-15,400	± 300	-15,700	42	-15,400	±1,200	-16,600	42	-15,400	± 2,700	-18,100
.001	3	63	-22,100	± 300	-22,400	63	-22,100	±1,200	-23,300	63	-22,100	± 2,700	-24,800
.001	4	84	-30,800	± 300	-31,000	84	-30,800	±1,200	-32,000	84	-30,800	± 2,700	-33,500
.002	1	11	- 3,900	± 100	- 4,000	11	- 3,900	± 300	- 4,200	11	- 3,900	± 700	- 4,600
.002	2	21	- 7,700	± 100	- 7,800	21	- 7,700	± 300	- 8,000	21	- 7,700	± 700	- 8,400
.002	3	32	-11,100	± 100	-11,200	32	-11,100	± 300	-11,400	32	-11,100	± 700	-11,800
.002	4	42	-15,400	± 100	-15,500	42	-15,400	± 300	-15,700	42	-15,400	± 700	-16,100

$$\sigma_{th} = -\frac{3\alpha E}{16\pi Kh} Q_T = -\frac{7.74}{h} Q_T$$

$$\sigma_p = \frac{3P}{4}\left(\frac{b}{h}\right)^2 = \pm 11.3 \left(\frac{b}{h}\right)^2$$

$$\Delta T = \frac{Q_T}{4\pi Kh} = 0.0212 \left(\frac{Q_T}{h}\right)$$

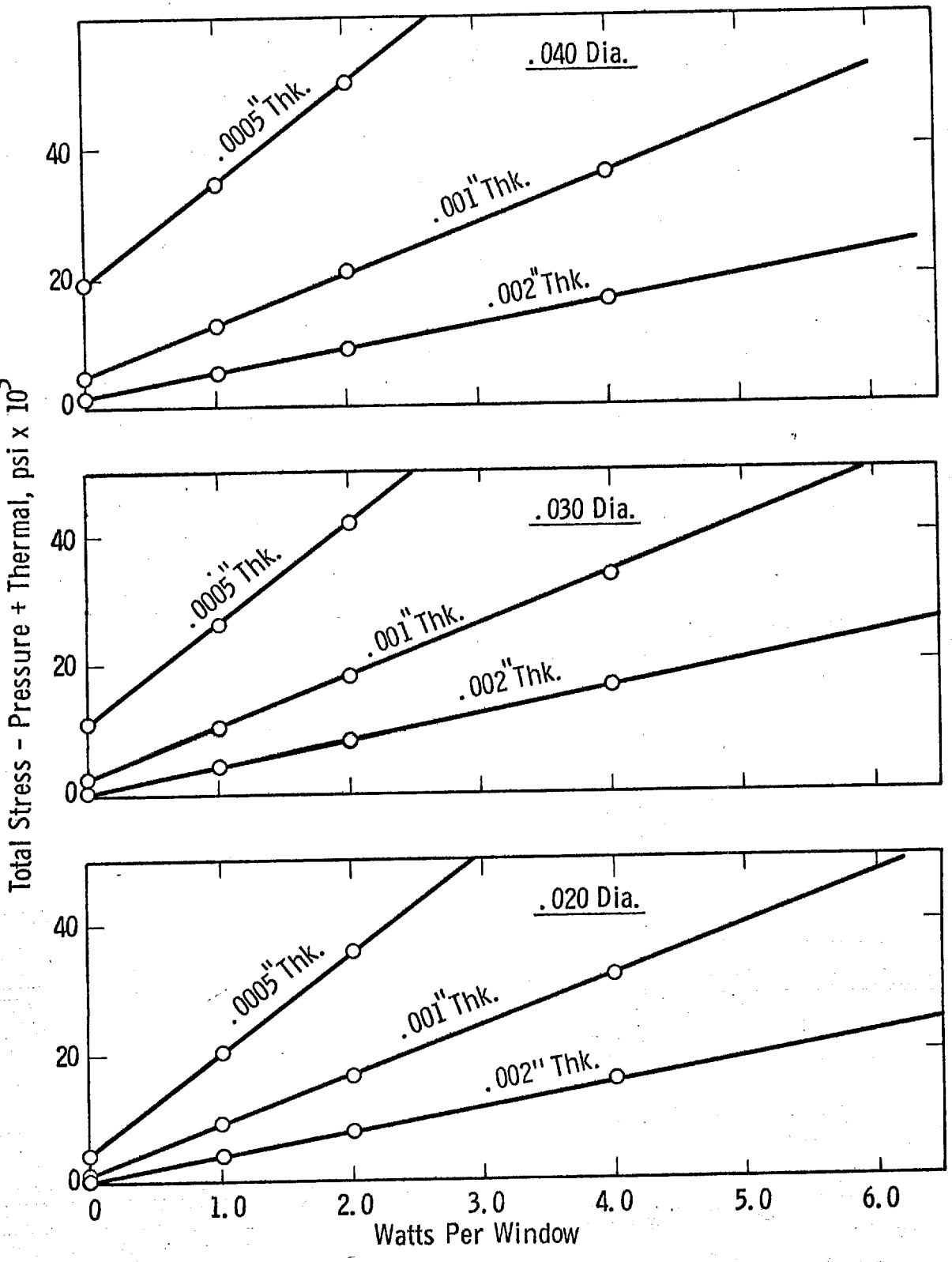

·Circular Be window

Fig. 1.06.07

TABLE 1.06.05

COMPARISON OF RECTANGULAR Vs. CIRCULAR Be WINDOWS FOR CONSTANT OUTPUT (6KW)

(Allowable Stress Level of 35,000 psi)

Window Thickness h (in)	Assumed* Eff. (%)	Watts Absorbed		Rectangular Slot Width .020	.030	.040	Circular Window Dia. .010	.020	.030
.0005	.90	667	watts/window	39	10	0	2.2	2.0	1.6
			no. needed	17	67	-	303	333	417
.001	.80	1500	watts/window	106	52	34	4.5	4.3	4
			no. needed	14	29	44	333	350	375
.002	.60	4000	watts/window	240	130	95	9.0	9.0	8.9
			no. needed	17	31	42	445	445	450

*For these calculations absorption was assumed to vary linearly with window thickness. In some of the later calculations account is taken of the non-linearity.

contract more and cause a stress to be developed. This stress will vary with temperature as both the expansion and modulus vary. On reaching room temperature, the strain (expansion difference) induced in the window can be expressed as

$$\epsilon_x = \frac{\sigma_x}{E} - \mu \frac{\sigma_y}{E} \text{ and } \epsilon_y = \frac{\sigma_y}{E} - \mu \frac{\sigma_x}{E}$$

where ϵ_x and ϵ_y are the difference in expansion per unit length. Since the rectangular window is clamped at all edges; a symmetrical, two-dimensional stress situation exists in which the stresses and strains in the x and y directions are equal.

Therefore, in the x and y directions

$$\sigma_B = (1 + \mu)\, \epsilon\, E \qquad \text{(Rectangular Case)}$$

where the subscript B indicates brazing.

For the circular window the maximum brazing in both the radial and tangential directions is given by

$$\sigma_B = \frac{\epsilon E}{1-\mu} \qquad \text{(Circular Case)}$$

This stress is comparable to that in the rectangular window and no further differentiation is made between the two cases in the remainder of this section. It should be noted here that both these analyses assumed a completely rigid anode which does not deform due to the thermal stress and all of the strain is transmitted to the window.

Figures 1.06.08 and 1.06.09 show the expansion of various possible anode material that might be used with beryllium and silicon windows over the temperature range in question. In calculating the brazing stress for beryllium, the curve for wrought sheet was used.

An examination of Figure 1.06.10 will show that the induced brazing strain for the beryllium to copper combination results in an extremely high stress situation which would normally indicate failure of the window member. The fact

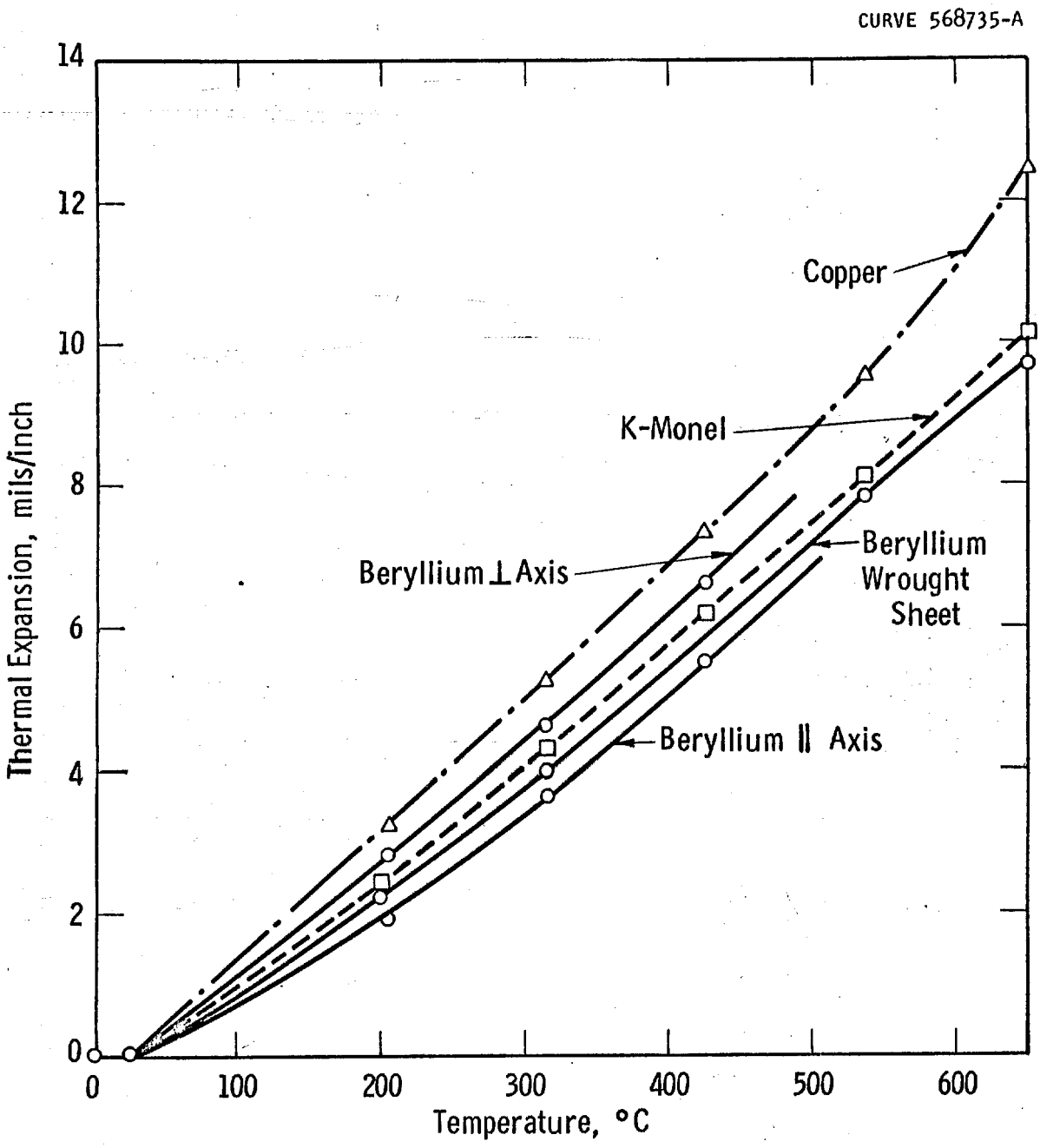

Thermal expansion of beryllium and possible anode materials

Fig. 1.06.08

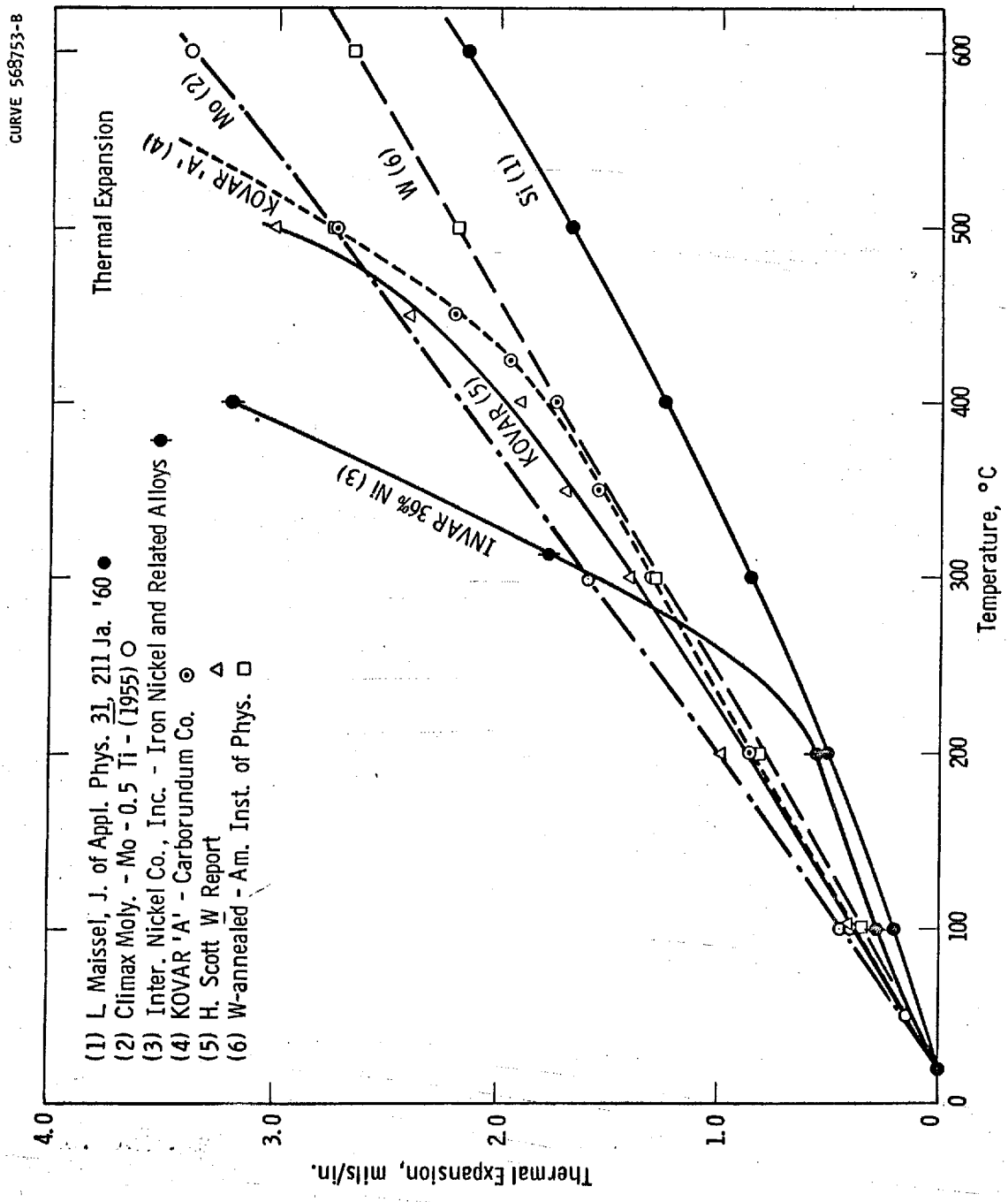

Fig.1.06.09Thermal expansion of silicon and possible anode materials

CURVE 568738-A

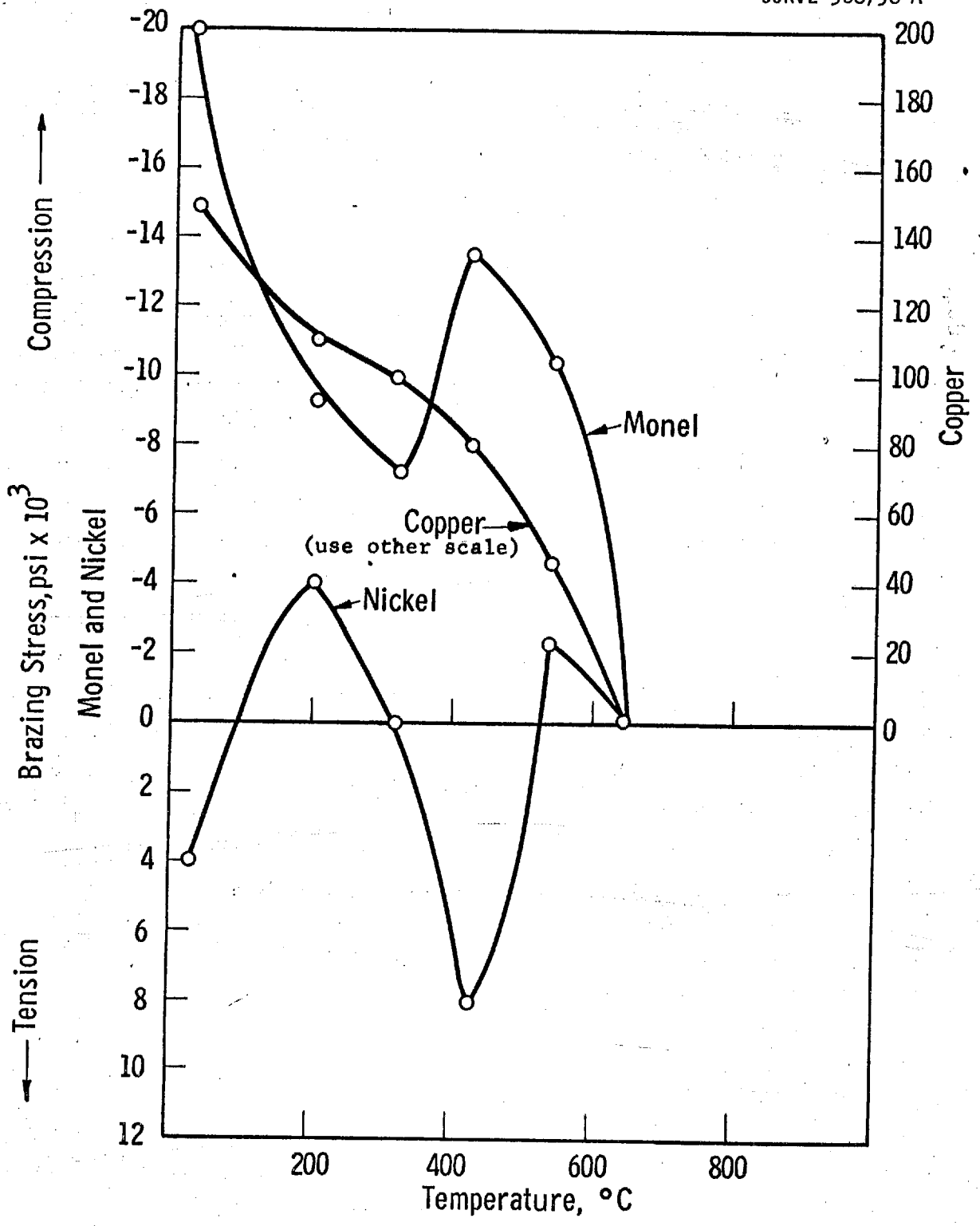

Brazing stress for rectangular beryllium window assumes 650 °C brazing temperature

Fig. 1.06.10

that this combination has been successfully brazed would indicate that a purely elastic analysis is not adequate to explain the stress picture. It is therefore theorized that some yielding is taking place in the beryllium window at the higher temperatures after the joint is formed. Since beryllium does exhibit some elongation at the higher temperature, the actual thermally induced strain may be at a lower level than elastic analysis indicates. If elongation occurs, the locked-in stress would equal the yield stress at the temperature level where an equilibrium is reached between the thermal strain and yield strength. In addition to yielding, buckling of the window could absorb or alleviate the induced strain. This situation would induce further buckling on thermal loading of the window and result in premature failure. A combination of the two modes of stress relief is most likely occurring in the actual situation and may be the cause of some of the scatter in the actual testing of beryllium windows.

The silicon- molybdenum combination has a similar problem but to a much lesser degree. Figure 1.06.11 shows that Kovar would be a likely choice of anode material with tungsten somewhat more desirable. For low brazing temperatures (400°C) Kovar is acceptable; however, being of the low expansion iron-nickel family, it exhibits an inflection temperature at approximately 410°C where its thermal expansion increases very rapidly. For brazing temperatures above 400°C, tungsten (or molybdenum) is a much better choice of materials. Invar would, of course, be undesirable except for soft solders because of its very low inflection point.

MAXIMUM POWER OUTPUT

Rectangular Windows

If a safe, allowable total compressive stress level, σ', chosen based on the mechanical properties of a given window material, then a maximum allowable thermal stress level is determined by

$$\sigma_{th}' = \sigma' - \sigma_p - \sigma_B$$

with the prime superscript indicating "maximum allowable."

CURVE 368734-A

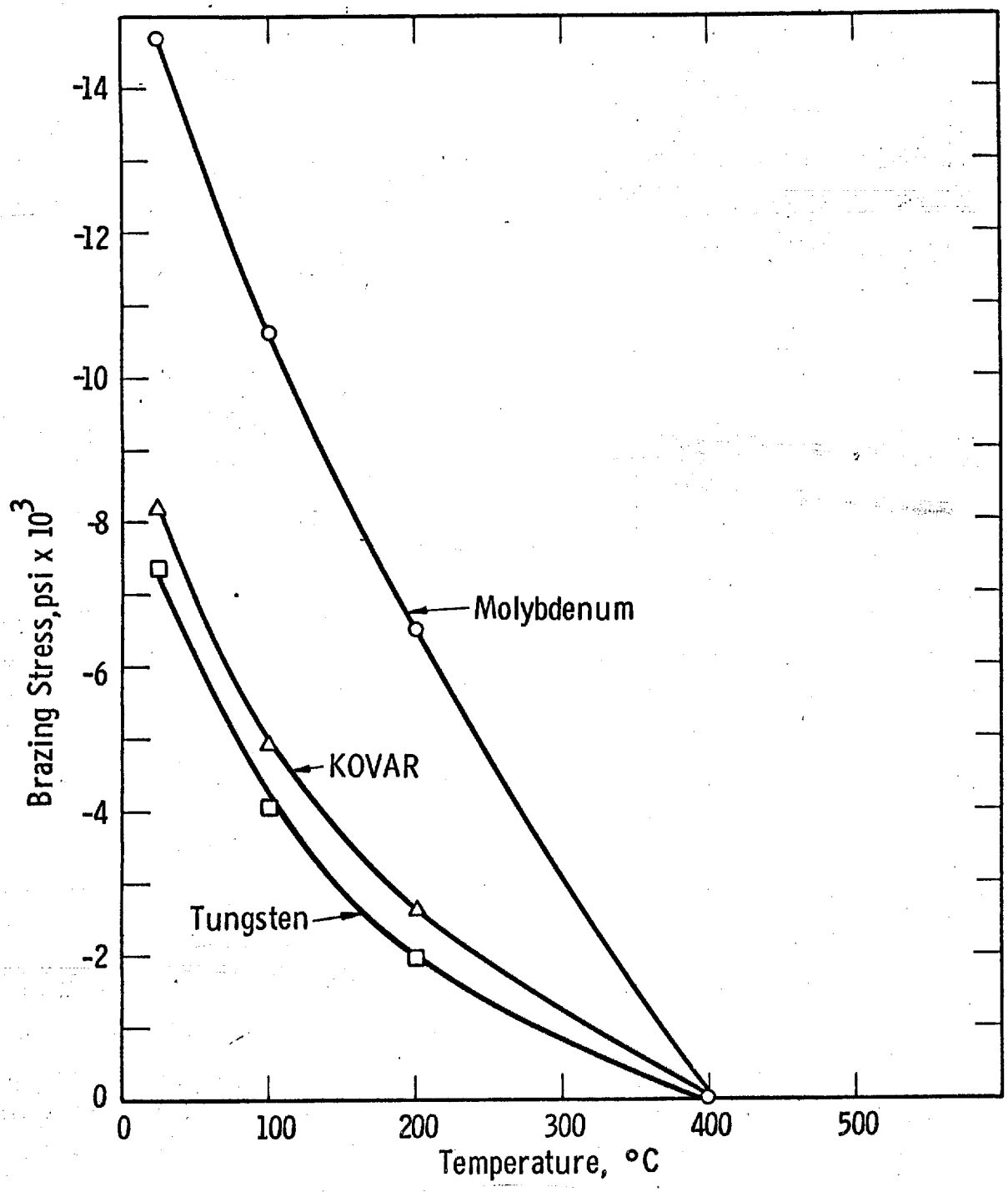

Brazing stress for rectangular silicon window assume 400 °C brazing temperature

Fig. 1.06.11

Once σ_p and σ_B are computed for a given geometry and material combination, the allowable heat absorption in the window corresponding to the maximum allowable thermal stress level may be determined from the following relation:

$$\sigma_{th} = \frac{\alpha E q_o c^2}{2Kh(1-\mu)}$$

The power absorbed in the window (watts) is given by:

$$W_{abs} = (2\, q_o\, c\, \ell)$$

Thus,

$$W'_{abs} = \left(\frac{4K\,(1-\mu)}{\alpha E}\right)\left(\frac{\ell h}{c}\right)\quad \sigma'_{th}$$

If the beam transmitting properties of the window are known, we may write the transmission-absorption ratio, R, as

$$R = \frac{W_{out}}{W_{abs}} = \frac{\epsilon}{1-\epsilon}$$

where ϵ = fraction transmitted through the window, being a function of incident energy level of beam, the window material (density, atomic number, etc.) and window thickness. (In the sense used here, the fraction transmitted means the ratio of that portion of the total beam input which is not converted into heat to the total beam input).

Then

$$W_{out} = \left(\frac{4\,K(1-\mu)\sigma'}{\alpha E}\right)\quad\left(\frac{\sigma'_{th}}{\sigma'}\right)\quad\left(\frac{\ell h}{c}\right)\quad\left(\frac{\epsilon}{1-\epsilon}\right).$$

The first term in this expression is dependent only on materials properties and essentially is a thermal stress merit factor. Values of the thermal stress merit factor for various materials are given in Table 1.06.03.

These are computed using room temperature values since allowable stress levels only permit attaining a maximum ΔT across the windows in the range of 50 to 100°C.

The second factor in the expression for the power output indicates the percentage reduction in the maximum allowable stress caused by the presence of pressure and brazing stresses.

The last term is the ratio of energy absorbed to energy transmitted. Transmission curves for various materials at 125 KV are given in Figure 1.06.12. The curve for aluminum is taken from data in a NBS report, and the curves for silicon and beryllium are based on the aluminum curve using a density ratio correction. However, the curves for molybdenum and silver are probably too high since their higher atomic numbers would reduce their transmission characteristics more than the simple use of density ratios would indicate. Corresponding transmission-absorption ratios are given in Figure 1.06.13 considerable error may exist for very thin windows because the values were determined by differences using Figure 1.06.12.

A plot of allowable power outputs for beryllium as a function of window thickness is given in Figure 1.06.10 for slot widths of 20 and 30 mils neglecting any brazing stress. The reduction in power output for the thin windows is due to the increase importance of pressure stress in this region. The obtainable power outputs for the case of zero pressure stress (i.e. vacuum on both sides of the window) is indicated by the dashed curves. It is apparent that for window thickness less than one mil, the effect of compressive pressure stress becomes more and more pronounced.

Figure 1.06.15 is a similar plot for a rectangular silicon window. Here, the dashed lines indicate the reduced allowable power output when an 8,000 psi brazing stress (silicon to tungsten at 600°C) is taken into account. The maximum allowable power output is calculated to be several times that of beryllium for comparable geometries.

Figure 1.06.16 gives the corresponding values of allowable power output of an aluminum window. The properties of a heat treatable low alloy aluminum, 6061-T6, were used in these calculations (see Table 1.06.03) and can be considered typical of what might be used. The value of maximum allowable stress used was

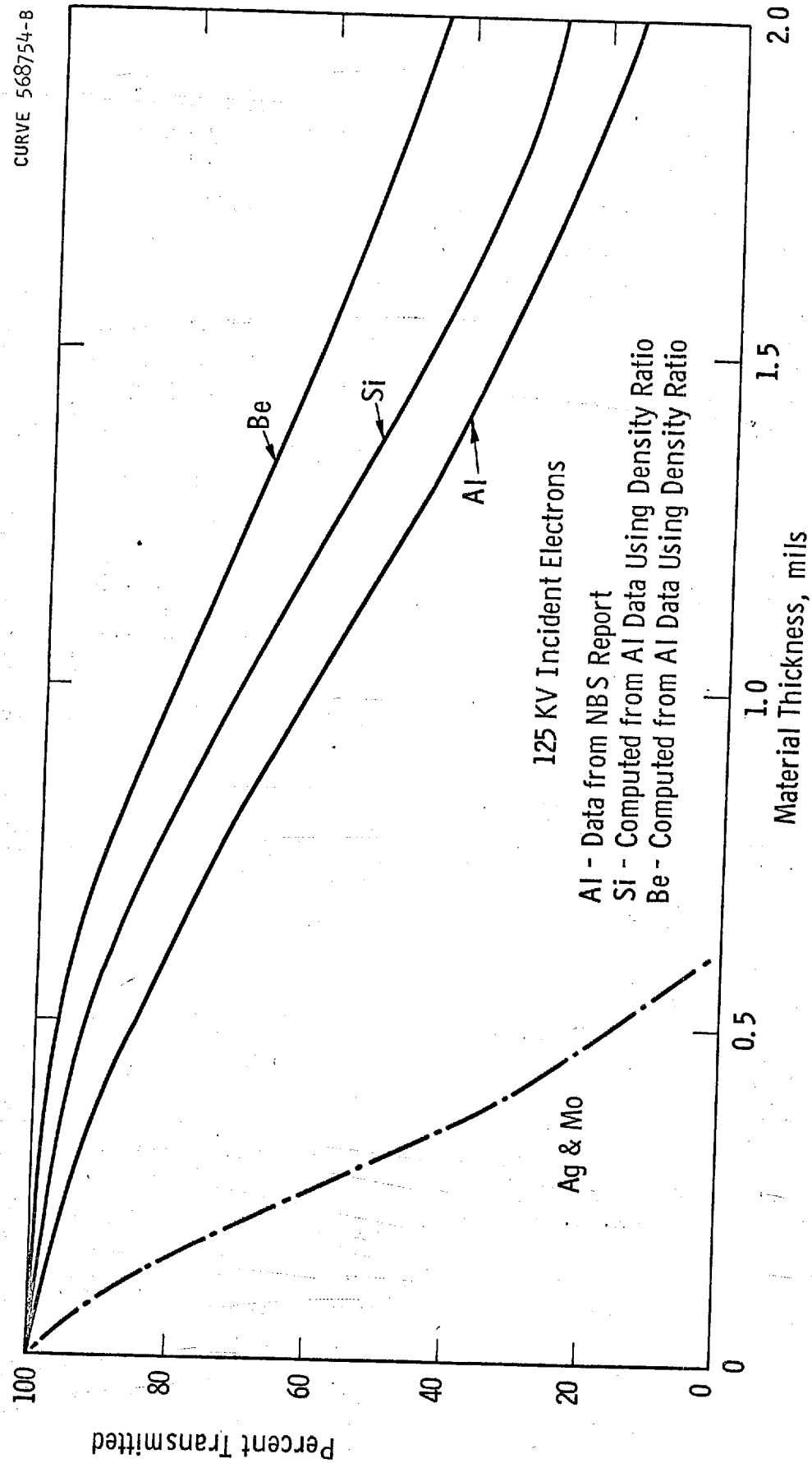

Fig. 1.06.12 Transmission curves of various possible window materials

Approved For Release 2000/05/04 : CIA-RDP67B00657R000300080001-9

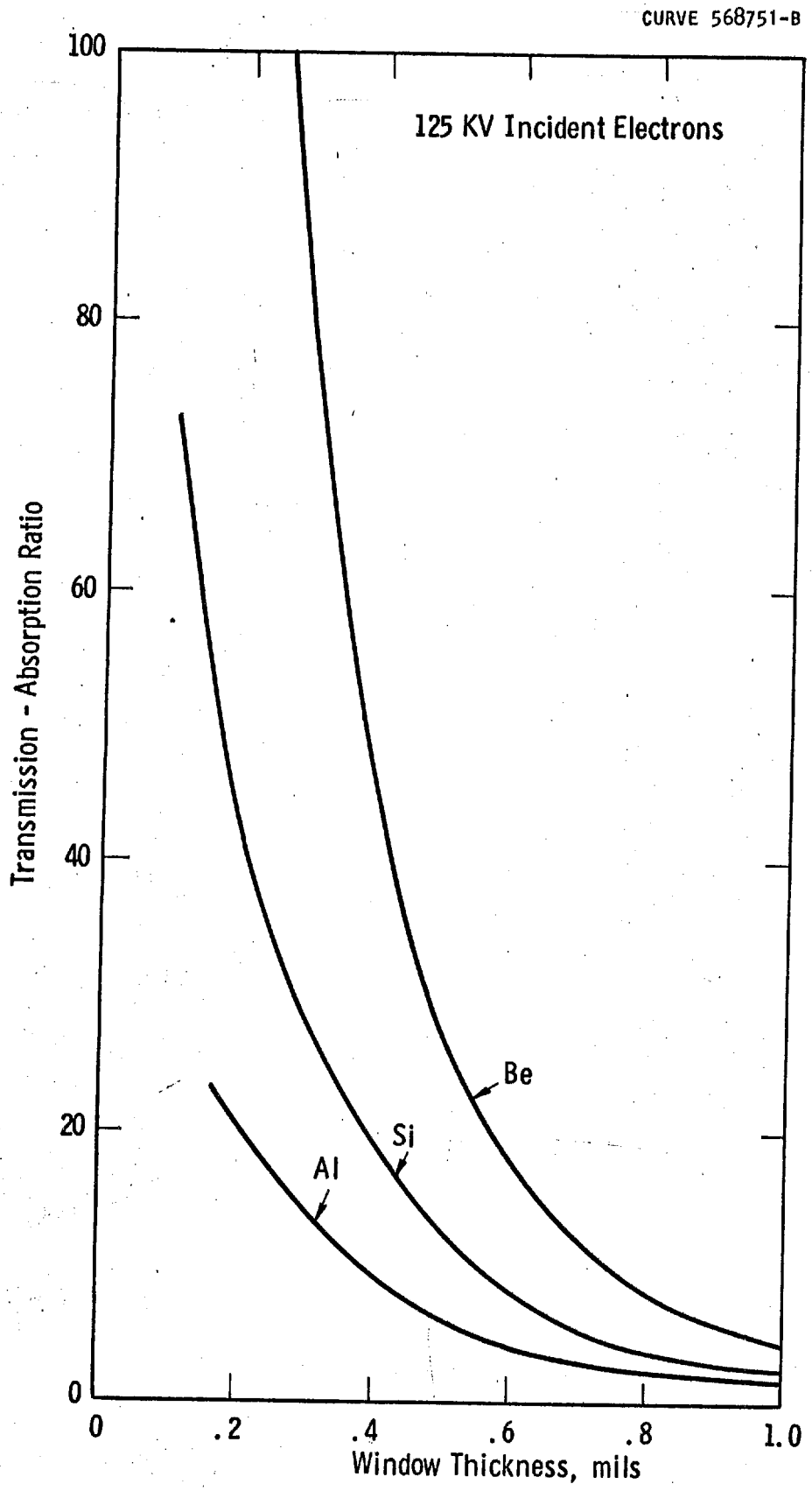

Transmission - absorbtion ratio of several window materials

Fig. 1.06.13

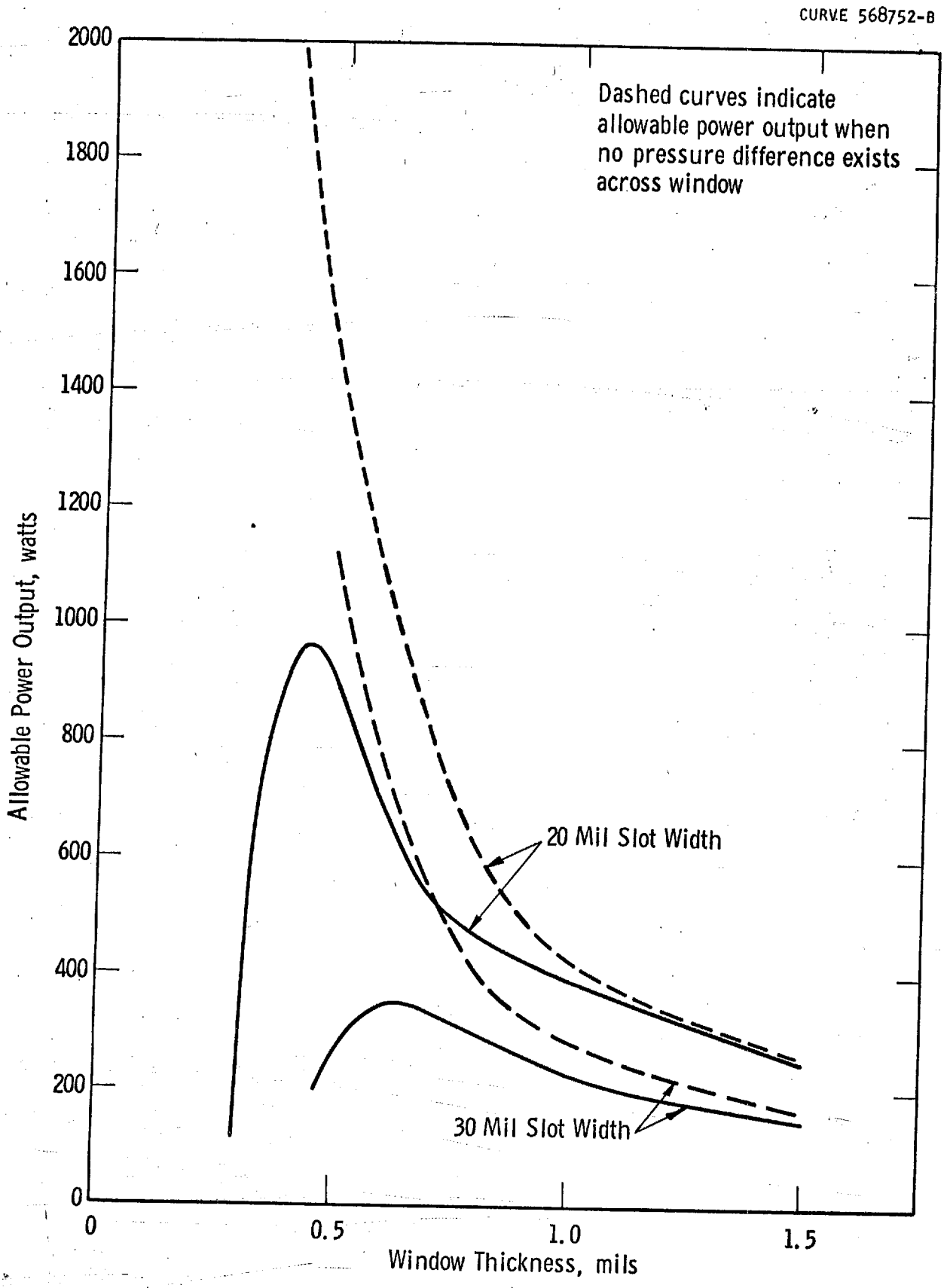

Rectangular beryllium window (1 inch long)

Fig. 1.06.14

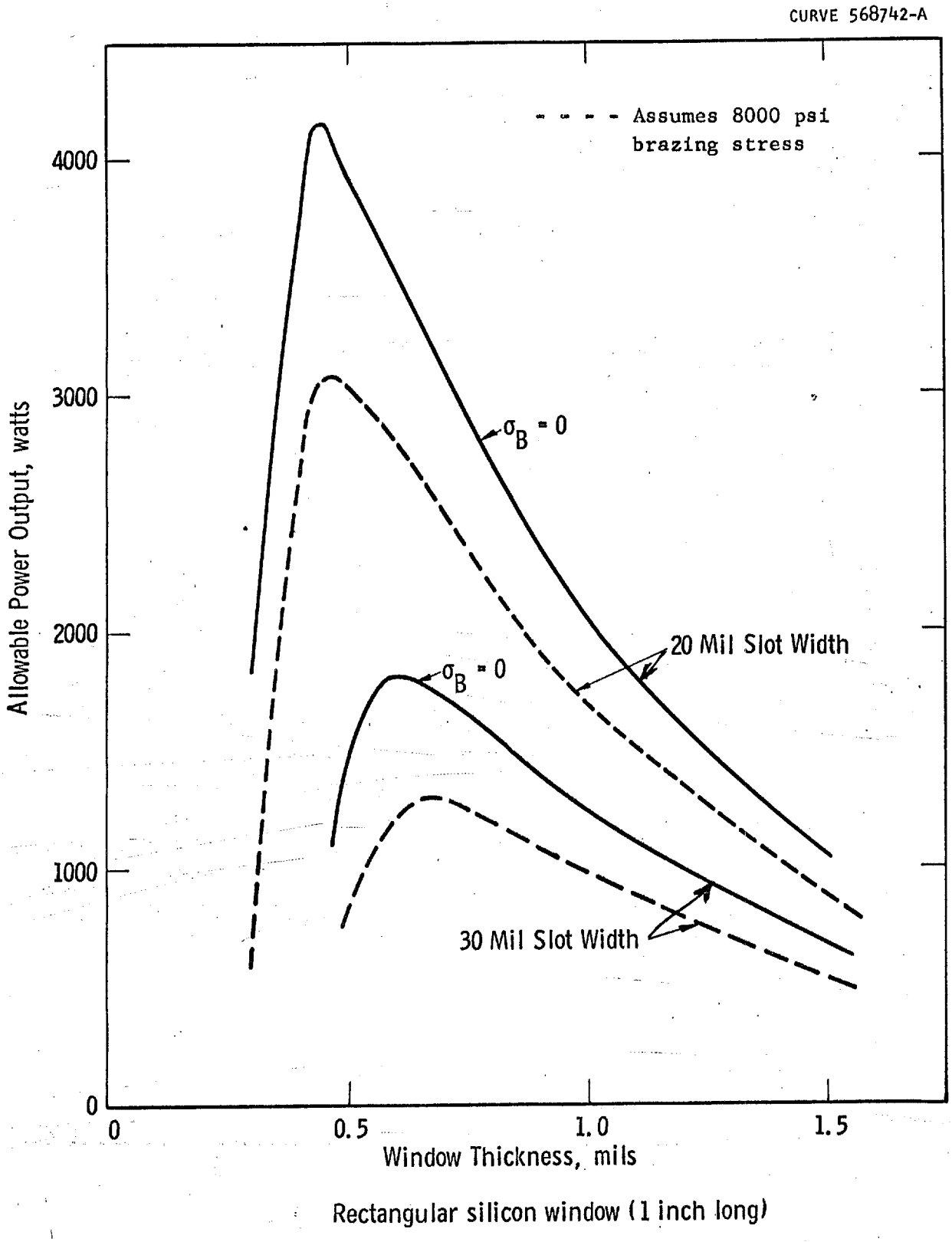

Fig. 1.06.15

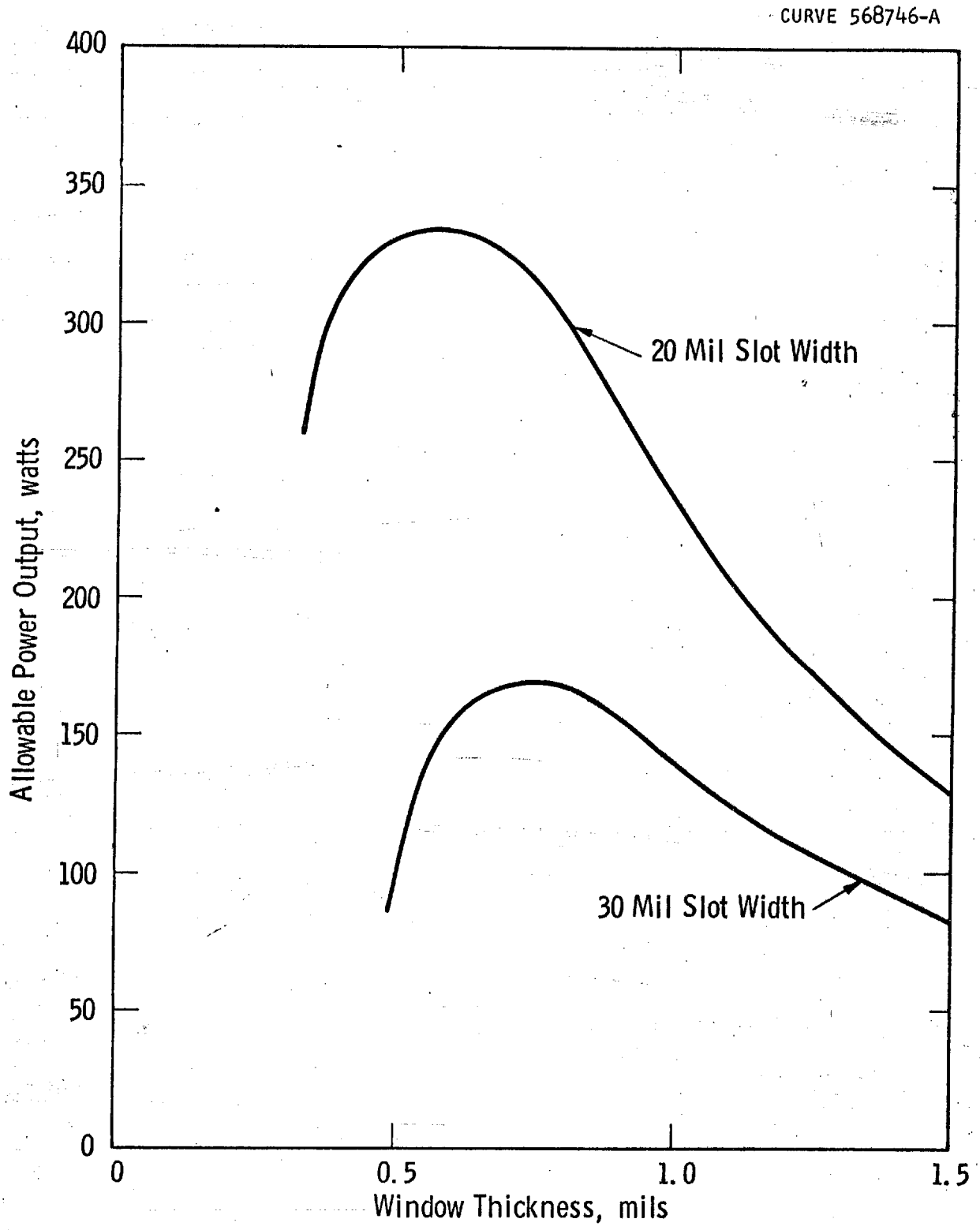

Rectangular aluminum window (1 inch long)

Fig. 1.06.16

the yield point of the material but considering the value of elongation (12 per cent) and corresponding ductility of this material, considerably higher thermal inputs could be used. The problem then becomes one of buckling and fatigue as described previously. The most straight forward way of evaluating operation at such levels is experimentation with actual aluminum windows. Pure aluminum or some other alloy than the 6061 may be preferable for such thermal inputs because ductility, elongation, cold working, and fatigue become increasingly more important.

Figures through are plots of the allowable power absorbed for the three window materials discussed.

Circular Windows

Similarly, a formula may be developed for the maximum allowable power output for a round window:

$$W_{out} = \left(\frac{16\pi K\sigma'}{3\alpha E}\right)\left(\frac{\sigma_{th}'}{\sigma'}\right)\left(\frac{\epsilon}{1-\epsilon}\right) \quad (h)$$

This equation differs from the rectangular case in that the power output is affected by the diameter only, as this linear dimension determines the pressure stress; otherwise, the output is a function of the window thickness alone. The change in geometry also modifies the thermal stress merit factor in that the effect of Poisson's ratio is reduced to the point where it may be neglected in these calculations.

Plots of allowable power outputs of circular windows using silicon and beryllium are given in Figures 1.06.20 and 1.06.21. It can be seen that for thicker windows the magnitude of the pressure stresses are reduced to the point where the allowable power outputs are essentially independent of diameter, as is to be expected.

CONCLUSIONS

Based on the stress calculations, it would appear that silicon is the best window material to use to obtain the desired 6KW output. This could be done with two windows one inch x .020 inches x .00075 inches. The next best

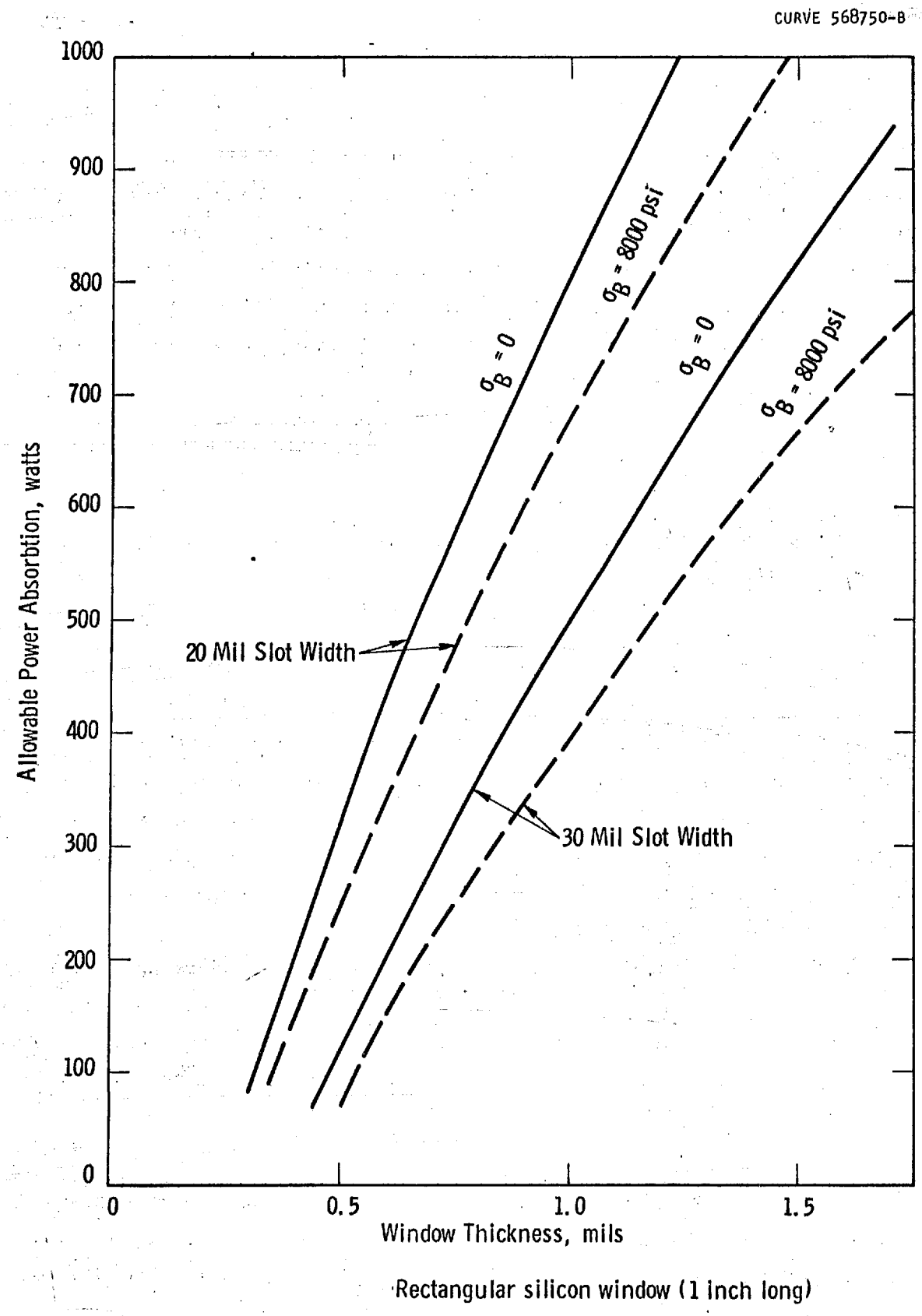

Fig. 1.06.17

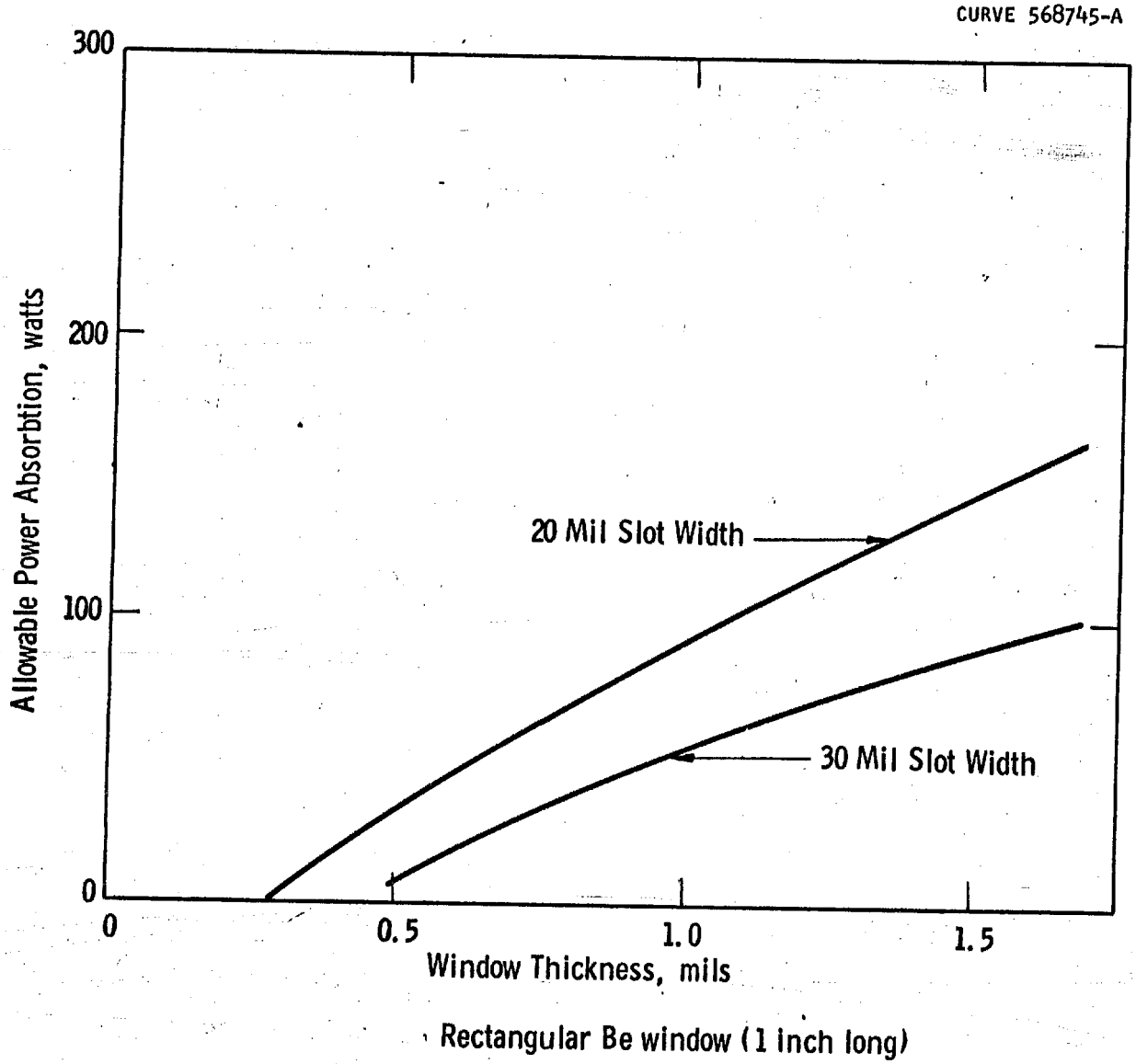

Fig. 1.06.18

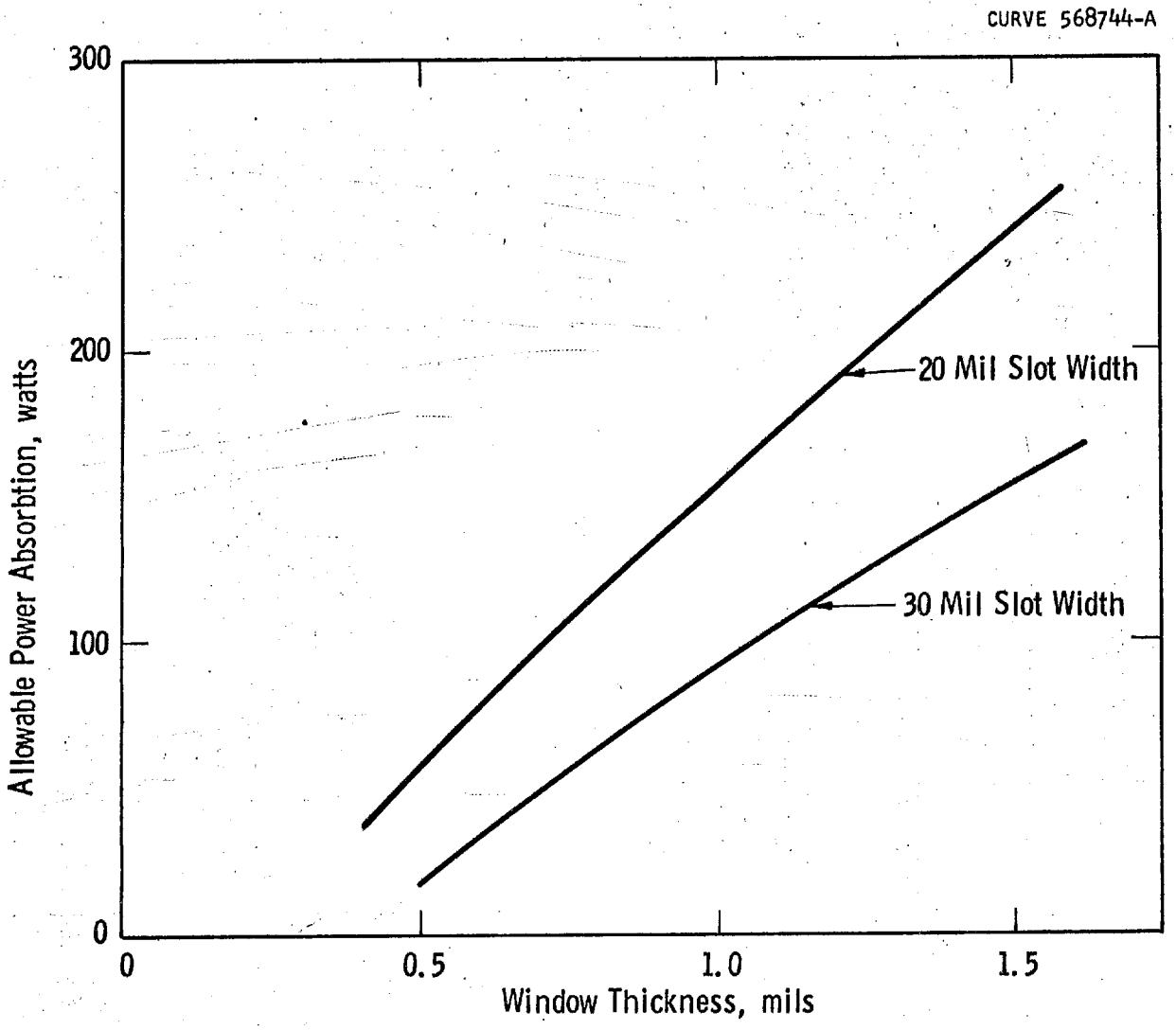

·Rectangular Al window (1 inch long)

Fig. 1.06.19

CURVE 568747-A

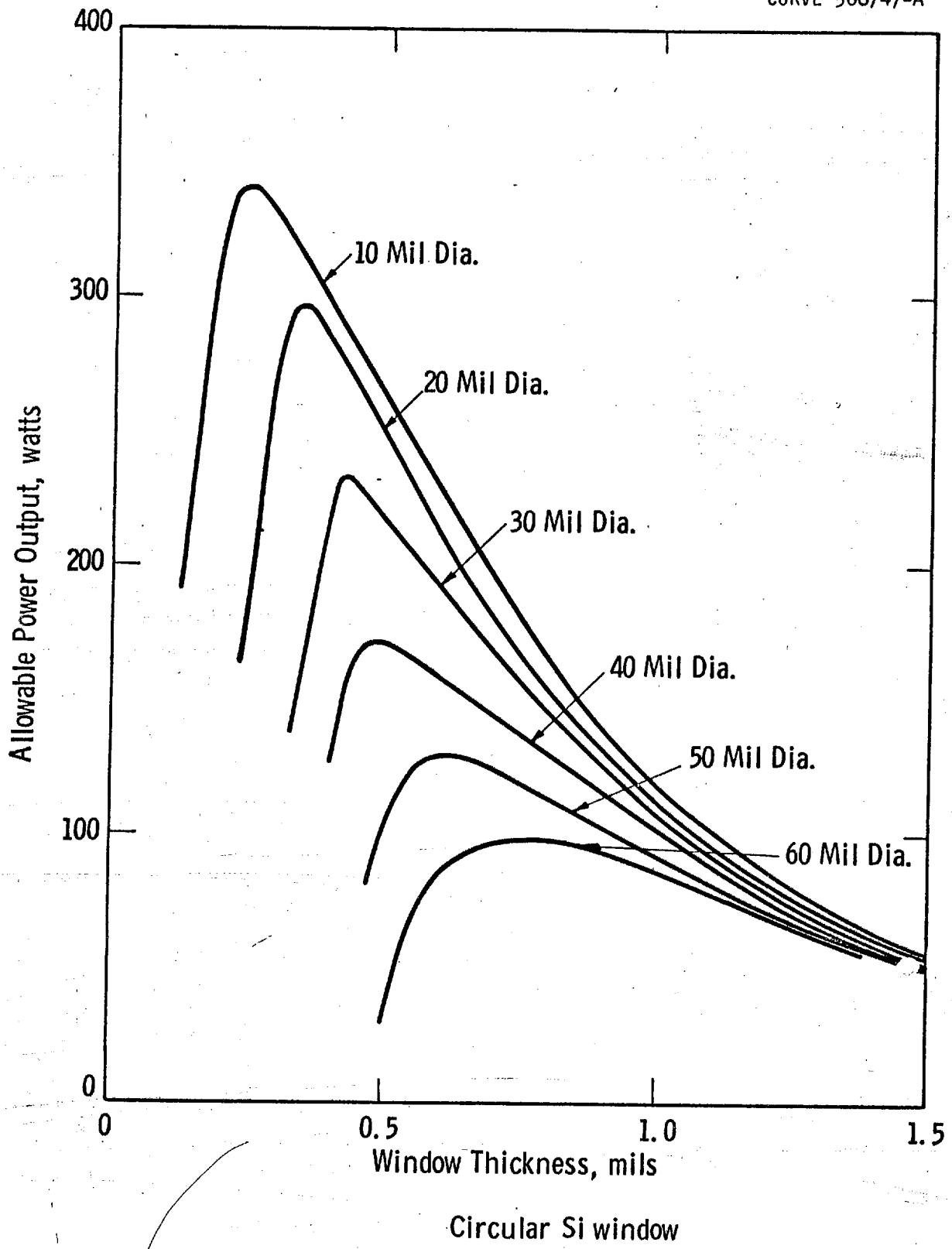

Fig. 1.06.20

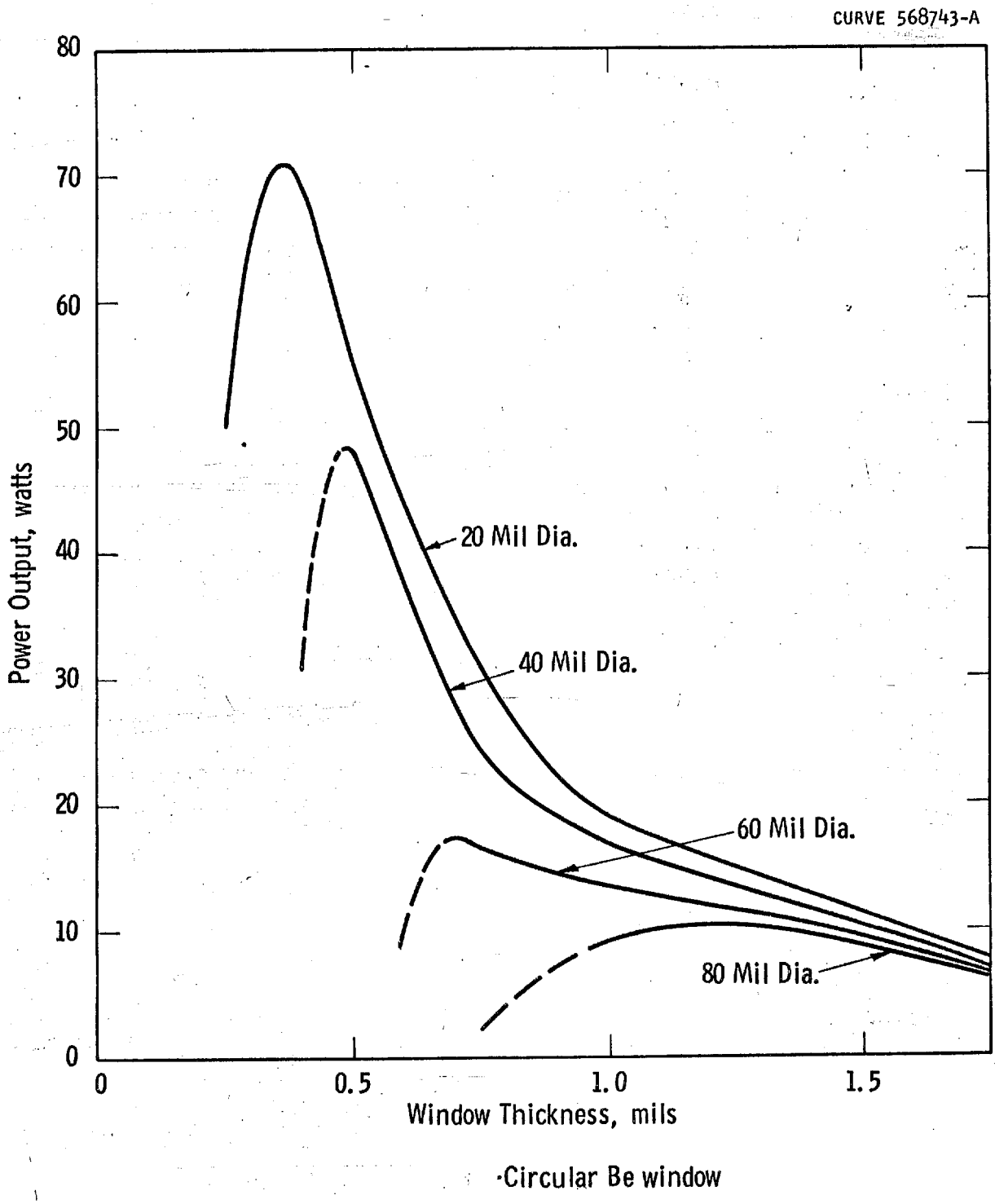

Fig. 1.06.21

material of those considered would be aluminum. No estimate can be made from this limited analysis as to how much more output could be obtained safely if the aluminum were run at an absorption level in excess of the yield point.

Beryllium is definitely the least desirable of the three. Because of its brittleness, it cannot be operated much in excess of its yield point or calculated values of power input without a good chance of fracture.

The rectangular geometry appears to be satisfactory from the stress point of view as far as obtaining the desired output with a practical number of slots. The circular geometry would require a large number of windows (thirty in the case of 0.5 mil thick silicon with a 20 mil diameter). Such a decision is basically determined by the feasibility of the electron-optics involved.

The use of geometries other than the flat are not recommended as very little stress advantage can be obtained from any of those suggested and the forming and brazing complications are increased.

1.07. Be as a Window Material

Be Foil:

In the original survey on window materials, Be turned out to have most promising properties. It has a low atomic number, a high ratio of thermal conductivity to density, excellent mechanical strength, a high recrystallization temperature, and low vapor pressure at high temperatures. A one mil thickness of aluminum window has 2.5 times greater absorption losses to a 125 kv electron beam than a one mil thickness of Be foil. For a given power lost in the window, one mil of Be window will transmit about 3.5 times more power than the same thickness of Al window. Correcting for the higher thermal conductivity of Al, a one mil Be window configuration at a given temperature will transmit about 2.5 times as much power as an Al window of the same thickness and operating with the same temperature gradient.

Most of the material tested in this program was purchased from Brush Beryllium. At the beginning of this program Brush Beryllium appeared to be the only company that could supply thin Be foil that was vacuum tight. Later in the program it developed that rolled Be foil was available from other suppliers as well, notably the Beryllium Corporation of America and Pechiney Company. The types of Brush material which were available in increasing order of purity were S200, S100 and N50. According to Brush specifications, as confirmed by our own analysis, these range in minimum Be assay from 98.5% to 99.0%, the remainder of the compositions being mainly BeO.

The original brazing experiments started with 0.5 mil and 1.0 mil S100 Be foil made from a powder compact. Because of excessive alloying in the brazing materials experienced with the thin Be foil, the experimental program on brazing was diverted temporarily to developing brazing techniques for 5 mil Be. The thin 2 mil sections of Be required for electron beam transmission were EDM'd (electric discharge machined) after the brazes were completed. These windows cracked during electrical operational tests. The cracking failures were attributed to the formation of stress raisers in the edge between the two thicknesses and to

the natural poor ductility of the beryllium employed. After some experimentation, described in later sections, techniques were developed for vacuum brazing 2-mil Be both in the flat configuration and in the "V" shapes described in more detail in a later section. V-shape structures were employed to minimize expansion problems as the Be was heated. The first "V" shaped structures were produced at the Brush Beryllium Co. Later window structures were produced in these laboratories. It was necessary to design special dies so that the hot forming of the windows could be accomplished at temperatures of the order of 1100°F in order to prevent cracking of the beryllium. With better brazing techniques, improved mechanical configurations, and possibly as the result of going to a purer Be material (N50 instead of S100), the mechanical breakage situation improved.

Pinhole Leaks:

Around this time considerably more difficulty was noted with very tiny leaks appearing in the windows. Instead of cracking at tests, failures now were largely due to pinhole leaks developing through the windows. These pinholes were first noticed when the brazed assemblies were leak checked. A technique for determining the location of pinhole leaks using a penetrant dye was developed. Previously it had proved very difficult to leak-check the window foil itself unit it had been sealed to its support. Even then it was quite difficult to distinguish between leaks in the brazed joint and leaks in the window proper due to the small sizes of the ports. The dye penetrant test not only aided in determining the exact location of the leak in a given window assembly, but also permitted testing the foil as received and in all stages of our processing prior to brazing.

Pinhole leaks now showed up at various stages of processing when the penetrant dye test was applied. Some showed up as the material came in from the supplier or when it was cupped into the "V" shape; other pinhole leaks showed up when the Be was cleaned for brazing, still others occurred later in the processing or at test.

There was some evidence that later shipments of Be (after the supplier had experienced a strike of hourly workers) were inferior in quality to material obtained earlier when the brazing techniques were first being developed. Unfortunately, in the earlier period it had not proven feasible to mass-spectrometer-leak-check the individual windows as received from the supplier, and the dye penetrant test was not available at that time.

Extensive metallographic studies at these laboratories, including sectioning and radiography, as well as discussions with Brush, Beryllium Corp. of America, Goddard Space Flight Center, Pechiney (General Astrometals), Franklin Institude, Lawrence Radiation Laboratory, Navy Bureay of Weapons, Temescal Metallurgical Co., WADC and Nuclear Metals ultimately led to the conclusion that inclusions in the Be, which are characteristic of the powder fabricated variety, exercise a major role in the troubles experienced.

These inclusions appear to be largely oxides of beryllium and intermetallics. It is not clear whether microcracks are formed around the inclusions due to differences of expansion with the parent metal or whether they represent temporarily plugged leak paths which open up as the result of processing. The formation of oxides or other compounds may play significant roles in the leaks which develop during processing. From the observation made in our experimental work and from data in the literature, it appeared that best results could be obtained with very pure beryllium, vacuum cast to avoid oxides. The material should be rolled to size in inert-gas-filled, tightly closed cans. It appears that additional ductility of the powder product may be obtained by recrystallization at high temperatures, 1000-1100°C, but attaining this without further oxidation may be difficult because of the inherent affinity of beryllium for oxygen.

Improved Materials:

In our efforts to obtain better quality Be we contacted the Pechiney Beryllium Company through their distributer in this country, the

General Astrometals Corp. Their quotes for Pechiney products were high and they could not guarantee foils of thickness less than .010" to be vacuum tight.

The Beryllium Corporation of America were much more receptive. Early shipments from them had an excessive percentage of leakers. However, there was some evidence that later vacuum cast materials in which processing was tightened up were better in vacuum tightness, ability to take loading, and in improved ductility. The curtailment of the window program did not permit evaluation of some of the later shipments, in which the supplier modified his processing in order to improve the material, nor was there an opportunity to look into the feasibility of using ultra-purity materials such as zone refined metals, which have higher ductilities than the material available heretofore. While the higher purity materials have lower mechanical strength, the indications are that their mechanical strength should be adequate to the application. The strike at Brush Beryllium continued for the duration of the remainder of the program, so that an opportunity was not afforded to evaluate regular production Be, i.e., material made by their regular operators.

1.08. The Be Joining Program

The methods considered for making vacuum tight seals between Be foils and the window support were brazing, soldering, arc welding, diffusion bonding, spot welding, electron beam welding and ultrasonic welding. It is important to appreciate that it was not only necessary to obtain a vacuum tight seal to the window at the time of joining but that good thermal contact was mandatory between the edge of the window and the main body of the window support to avoid excessive thermal gradients. The brazing approach had promising results from its inception and thus proved to be the area in which most effort was invested. It did prove feasible as a result of the development effort to develop techniques for fabricating reasonably reliable vacuum seals for the window application by brazing in a pure H_2 atmosphere. As indicated previously the major problem at the termination of the program were the pinhole leaks in Be proper which showed up in various stages of processing, including in the completed tubes.

Welding:

As a result of the promising results obtained with brazing this phase of the project did not reach the experimental stage. It appeared particularly difficult to effect a good thermal seal between the window to the supporting member using this technique.

Spot Welding:

It has been found possible to spot weld copper-plated beryllium to copper. In this experiment, a 0.0005" thick piece of Incusil 15 brazing alloy was placed between the copper and beryllium and the spot weld was made with a capacitor discharge welder; bare beryllium was not exposed during welding.

Electron Beam Welding:

Some preliminary work was done at Hamilton Standard on the electron beam welding of one mil beryllium foil to copper. A complete leak-tight weld was not achieved. Best results were obtained by welding

through a 7-mil thick copper mask, on top of the beryllium, through the beryllium into the base metal. In some areas the beryllium was melted but it did not join to the weld pool. Power levels, welding speeds, and other parameters were varied but leak-tight welds could not be produced. The major problem with this technique was the maintaining good contact between the beryllium and copper so that a weld could be formed between the two matrices. It was difficult to maintain this contact. When it was not maintained the molten beads of copper and beryllium did not coalesce. Even when the beryllium was tightly sandwiched between two pieces of copper, complete bonding between the two metals was not achieved in 100% of the required area.

Diffusion Bonding:

Diffusion bonding was used for making several leak-tight joints in test specimens consisting og a 1/4" square of 0.0005" thick beryllium mounted between two pieces of solver-plated copper 3/8" in diameter by 1/2" high with a 1/8" hole through the longitudinal axis. The parts were joined in a pressure bonding apparatus. Parts were assembled beneath a hydraulic ram, loaded to 200 lbs, heated to 790°C, and held at temperature for one minute. The silver-copper eutectic formed and caused the parts to braze together. When micrographs were made, it was found that beryllium had also been dissolved and probably formed a ternary eutectic. The beryllium foil dissolved right up to the edge of the brazed joint. However, two of the three experimental assemblies were vacuum tight.

On the basis of these experiments, an experimental window assembly was joined using the same technique. In this assembly a 1-1/4" square of 0.0005" thick beryllium was joined to a silver-plated copper support about 1/2" thick and 4" in diameter. The beryllium was placed so as to cover the slits which were centrally located on the copper piece. Results were poor. The foil buckled and cracked. Better results were obtained on a similar assembly in which individual pieces of beryllium were cut to just cover the holes, but the joints were not leak tight.

Several attempts were made to diffusion bond beryllium foil directly to the copper without the use of the intermedeary silver layer. This was not completely successful. One small specimen was leak tight, but in larger units buckling of the foil was encountered.

In summary, the diffusion bonding was promising but needed considerably more work, including better pressure bonding equipment than was employed in the tests. Accurate fit up of parts was a major consideration. However, formation of a liquid phase during this process may help to minimize tolerance problems.

Brazing of Beryllium:

Brazing trials were made originally in vacuum to obtain wetting. Three brazing alloys, 80% copper-15% silver-5% phosphor (1185-1300°F); 72% silver-28% copper (1435°F), and 62% silver-23% copper-15% indium (1274-1320°F), i.e., Incusil 15, were tried. In the experiments, the brazing alloy, usually 0.0005 to 0.002" thick was preplaced between the beryllium and copper to preclude the necessity of alloy flow. All three alloys wet the beryllium but also dissolved it.

To obtain better control of the time the beryllium was in contact with the molten brazing alloy, the experimental window assemblies were brazed in a vertical furnace containing a hydrogen atmosphere of unusual purity. This furnace consisted of a pedestal about 5 ft high over which the hydrogen-filled, vertical furnace could be lowered. The lower part of the furnace was cold and the upper part was at about 1900°F. Thus, the work was placed on the pedestal and the cool zone placed over the pedestal for purging. Then, the hot zone was lowered over the work until the alloy was observed to melt. As soon as the alloy had melted and flowed, the heated portion of the furnace area was raised and the work passed into the cooling zone.

It was found that the brazing alloys would not wet the beryllium in hydrogen so the beryllium was plated with about 0.00001" of silver. In early trials with 0.005" thick beryllium the alloy was preplaced under the beryllium and vacuum tight joints were obtained. Later, when the beryllium

(0.002") was curved longitudinally, the alloy was preplaced over the edges of the beryllium on the copper and flowed into the joint. Vacuum-tight joints were made between beryllium foil 0.002 and 0.005" thick and the two copper sheets used in the window support.

Since the initial tests on the brazing of 1/2 or 1 mil beryllium were not completely successful, effort was concentrated on brazing 5 mil sheet to obtain a sound sealing joint. About eight helium tight window assemblies were fabricated using the following procedures:

a. The copper assembly was pretinned with 1/2-mil thick Incusil 15, then more 1/2-mil thick Incusil foil (1/8" wide) was preplaced by spot welding.

b. Two pieces of beryllium about 1/4" x 1-1/4" were copper plated and laid on the preplaced foil in the proper location. Then another strip of 1/2-mil thick Incusil 15 foil (1/8" wide) was placed over the edge of the beryllium and tack welded to the copper.

c. The unit was brazed in the "vertical" hydrogen atmosphere furnace referred to above. Although the furnace temperature was maintained at 950°C the brazed assemblies did not reach this temperature. Dwell time in the furnace, determined experimentally, was just long enough to melt and flow the brazing alloy.

In another method, the beryllium was plated with copper or silver then nickel and the copper inserts were tinned with Incusil 15 (15% indium, 24% copper, 61% silver - MR 635 - 705°C). Incusil 15 was also used for final brazing and was preplaced above or at the edge of the beryllium to form a fillet. A weight of 70 ounces was used to hold the beryllium in place, to insure maximum contact between the beryllium and copper surfaces, and to obtain thermal contact as close as possible to the slits. Five units produced by this technique have been satisfactory for test but not leak tight to helium.

In still another second method, the silver and nickel plated beryllium was brazed directly to copper not previously tinned. The brazing alloy was preplaced under the beryllium and the same weight was applied. Several units made by this technique have been leak tight to dye check but not to helium. The units, however, could be pumped to a pressure less than 10^{-5} mm of Hg.

Further experimentation, tighter controls, more attention to the cleaning of the Be and the quality of the plating greatly improved the quality and reliability of the brazing. The major problems experienced in brazing of thin beryllium foils to copper were as follows:

a. The foil was easily dissolved by the brazing alloy.

b. The foil wrinkled and buckled upon cooling from brazing temperature.

c. The amount of alloy used had to be adequate to make a joint and to fill gaps made by wrinkles of the foil, but still small enough to minimize solution.

d. Holding the edges of the foil in the brazing alloy was a problem.

As indicated previously, solution of beryllium foil because of poor temperature control and cooling in vacuum forced the selection of the vertical hydrogen furnace where heating and cooling could be easily controlled. However, wetting of the beryllium in hydrogen could not be obtained until it was electroplated with about 0.0005" of silver. The adhesion of the silver plating was only fair but was satisfactory. The silver promoted wetting but dissolved in the brazing alloy. Diffusion treatment improved adhesion of the silver plating but did not improve the overall results.

Some solution of the beryllium occurred in the brazing alloy, but it was limited and did not appear to interfere with the end product. The alloy formed was probably a quaternary eutectic of silver-copper-indium-beryllium. Mechanical properties of the brazing joints were not determined but performance in tests indicated they were satisfactory. The major difficulty at the end of the program was the formation of pinhole leaks in the beryllium during processing. As indicated previously these leaks were probably caused by micro-cracks, inclusions, diffusion, oxidation, or corrosion. The indications were that given a pinhole-free Be material, it would be possible to make satisfactory thermal contact to the window support.

Ultrasonic Welding:

Some preliminary experiments using ultrasonic welding were conducted in these laboratories. Initial results did not look promising. The Aeroprojects Company was contacted on this problem, and some tests with aluminum foils were conducted.

One of the major problems with this technique appeared to be in making the seal close enough to the edge of the window support so that prohibitive thermal gradients could be avoided. In view of promising work with the Be brazing this approach was discontinued.

1.09 Testing of Experimental Be Windows

Method and Apparatus:

In the evaluation of a given window design, the following tests were performed:

a) The window and seal were checked for vacuum tightness.

b) The ability of the window to stand up under continuous and intermittent loading as a function of time was determined.

c) Measurements on beam transmission for different thicknesses of window were made.

The vacuum tightness tests were straightforward and could be performed with ease using a conventional helium leak detector and appropriate fixturing. After a study was made of different techniques for simulating the kind of window loading that an electron beam would produce under operating conditions, the decision was made to test experimental windows by using the proposed electron beam configuration directly in a demountable design in which the experimental window assemblies could easily be installed. The decision was based on the excessive amount of development required to perfect a test for simulating the loading effect of the beam and the considerable degree of uncertainty that would be involved in interpreting how the simulated test would apply to the loading stresses produced by the electron beam in the final tube. The experimental arrangement permitted testing the windows under almost exact operating conditions. Details of the structure and use of the demountable tube appear in Chapter 2.

Test Results:

All of the results of the comprehensive series of hundreds of tests on the ability of different Be materials sealed to window configurations of various designs to stand up under continuous and pulsed loadings are too extensive to be included here. Suffice it to present some of the tests conducted on flat Be windows brazed to solid copper anodes via an intermediate .020" thick copper sheet, shown in Table 1.09.01, these being the most promising of the series. For the .002" Be,

TABLE 1.09.01

Loading Test on Flat Copper Demountable
Using Flat Intermediate Copper Sheets

Number	Window and Material	Configuration	Braze	Threshold	Loading in Watts		Remarks
F 13	2 Mil Be	Flat .020 Cu insert .010" slot	I-15	64 kv	50w-1/2 hr 75 -1/2 hr 100 -1/2 hr 125 -1/2 hr 150 -1/2 hr 175 -1/2 hr 200 -1/2 hr 250 -1/2 hr 300 -1/2 hr Failed on Cooling	350w-1/2 hr 400 -1/2 hr 450 -1/2 hr 500 -1/2 hr 550 -1/2 hr 600 -1/2 hr 700 -1/2 hr	Long Longitudinal Crack
F 20	.002" Flat Be Berylco Vac. Cast	Same as F 13 .030 slot	I-15	65	50w-1/2 hr 75 -1/2 hr 100 -1/2 hr 125 -1/2 hr 150 -1/2 hr 175 -1/2 hr 200 -1/2 hr 225 -1/2 hr 250 -1/2 hr 300 -28 min Failed		Slight He Leak Initially
F 24 Window I	.0016 Flat Be Vac. Evap. (Lawrence Rad. Lab.)	Same as F 20		54 kv	50w-15 min 75 -30 min 100 -30 min 125 -30 min 150 -30 min 175 -30 min 200 -1/2 min Failed		Slight Initial Leak Longitudinal Crack P = 20 Torr

Approved For Release 2000/05/04 : CIA-RDP67B00657R000300080001-9

TABLE 1.09.01 (cont'd)

Number	Window and Material	Configuration	Braze	Threshold	Loading in Watts	Remarks
F 24 Window II	.0016 Flat Be Vac. Evap. (Lawrence Rad. Lab.)	Same as F 20		58 kv	50w-15 min 75 -30 min 100 -30 min 125 -30 min 150 -30 min 175 -30 min 200 -30 min 225 - 1 min Pressure Rises	P = 20 Torr Slight Initial Leak

Approved For Release 2000/05/04 : CIA-RDP67B00657R000300080001-9

the values of transmitted power at 150 kv corresponding to any given test the table can be obtained by multiplying the absorbed, or loading power by 3.1. Thus, for example, a loading of 100 watts absorbed power per window corresponds to a transmitted loading of 620 watts for a double focal window, and an absorbed loading of 200 watts corresponds similarly to 1240 watts of transmitted power.

Results on window F13 must be discounted somewhat since only about 40% by the beam power noted impinged on the window due to the .010" slot which was being investigated. This window, however, was operated at 1/2 hour steps to an estimated value of absorbed loading of 240 watts for 7-1/2 hours, and then for an additional half hour at 280 watts absorbed power on window. These results certainly make the possibility of obtaining high transmitted loading capability by means of very narrow long beams appear to be very attractive.

Window F20, a vacuum cast Be from Berylco also looked promising. It operated from 5 hours as it was raised in 1/2 hour steps to 300 watts, where it operated for almost a half hour before developing a leak large enough to affect its performance. Since no visual damage was noted, the indications were that it developed a pinhole leak. The Be foils in experimental windows F24 of Table XIV were vacuum evaporated samples which were fabricated at the University of California. Be foil we received from LRL had quite a few pinhole leaks. The windows were cut so as to avoid major areas of leaks.

The general conclusion from the tests on the Be windows indicated that further development work on the production of Be foils in the .001" to .002" range of thickness which would eliminate the pinhole leak problem would have a very beneficial effect on the loading these windows would take without vacuum failure, particularly if good quality foils become available in .001" thickness. The indication from the early work at Berylco was that as further increase in quality of Be was realizable by further development of the techniques for rolling vacuum cast materials, techniques for purifying the Be further such as

the use of zone refining passes as part of the vacuum casting process should be investigated as part of any future possible program on windows.

As for the specific geometries tested the indication was that the flat Be structure on a .020" flat copper intermediate sheet employed in the tests of Table 1.09.01 was probably superior to most of the other structures tested in the Be program. An additional very promising direction for increasing loading is through the use of narrower line focus beams and narrower slots.

1.10. Aluminum Windows

Comparisons with Be:

As indicated in Fig. 1.04.07, a 1/2-mil Al window has a higher f factor, i.e., a higher ratio of transmitted to absorbed power, than a 1 mil Be window.

Since the thermal conductivity of Be is only slightly less than Al (.385 as compared to .520 in calories/cm^2/sec/cm), yet it is twice as thick, the 1 mil Be window will transmit more power (28% more) than the 1/2-mil Al window will for the same temperature gradient. The crucial factor in assessing the performance of a given window, however, comes down to the question of what power the window has the capability for transmitting without damage to itself in the required loading period. In the tests we conducted this was determined experimentally by measuring power absorption and using the f factor to estimate power transmission capabilities.

A study of the tensile strength of pure Al foils as a function of temperature revealed that aluminum unlike Be, rapidly loses its tensile characteristics with increase in temperature. Since small amounts of alloying elements contributed substantially to increased strength at high temperatures, foils with small amounts of alloying agents appeared to be called for. An attempt was made to minimize the amount of high atomic number materials in the interest of reducing the cross-sectional losses to beta rays.

Al alloy 3003 and 1100 aluminum were selected for these tests on the basis of composition and availability. The 3003 material consists of 1.2% manganese, the remainder is aluminum. The 1100 material is essentially standard Al foil and has a minimum of 99% aluminum. Some of the loading tests made use of EC aluminum, which is still purer, having a 99.45% minimum content of aluminum.

Joining Problem:

A number of approaches to the problem of joining the thin foil to the window support were investigated including mechanical seals, brazing,

diffusion bonding, and electron beam welding.

Diffusion bonding appeared to offer the most promise in initial attempts. Early trials were made by placing the aluminum foil and silver insert between two stainless steel blocks which were bolted together and heated in hydrogen at the desired temperature. Temperatures tested were from 200° to 500°C and times were from 1/2 to 4 hours. Best conditions appeared to be from 1/2 to 2 hours at 400°C but results were erratic. A new vacuum diffusing bonding apparatus was built , both to permit closer control of atmosphere and pressure. The unit is illustrated in Fig. 1.10.01.

Helium tight joints were obtained on aluminum foil to copper and aluminum foil to aluminum insert joints, as well as on the aluminum to silver units. Plating improved the bonding but introduced a pinhole corrosion problem. The best conditions for the diffusion bonding appear to be around 6000 lbs. load (about 9500 psi), and temperatures of 300°C or above. Higher pressures could be used but the width of the slits would be reduced significantly but not uniformly. A temperature limit of 325°C was set after a literature survey indicated that recrystallization and grain growth of 3003 occurred above this temperature. Higher joining temperatures also promoted some flow of the silver and closing of the slits.

The following conclusions were reached:

(1) Leak tight joints between 3003 aluminum foil and silver-copper or aluminum inserts can be made by a hot pressing or diffusion technique. A temperature of 300°C and pressure of 6000 lbs. appear to produce leak tightness with the desired shape of the aluminum foil cross section.

(2) Joints made below 400°C are mainly mechanical.

(3) Window assemblies made at either 300 or 400°C have maintained leak tightness after being exposed to 400°C in air for 5 to 14 hours.

(4) Sandwich type structures appear promising for straight slit construction.

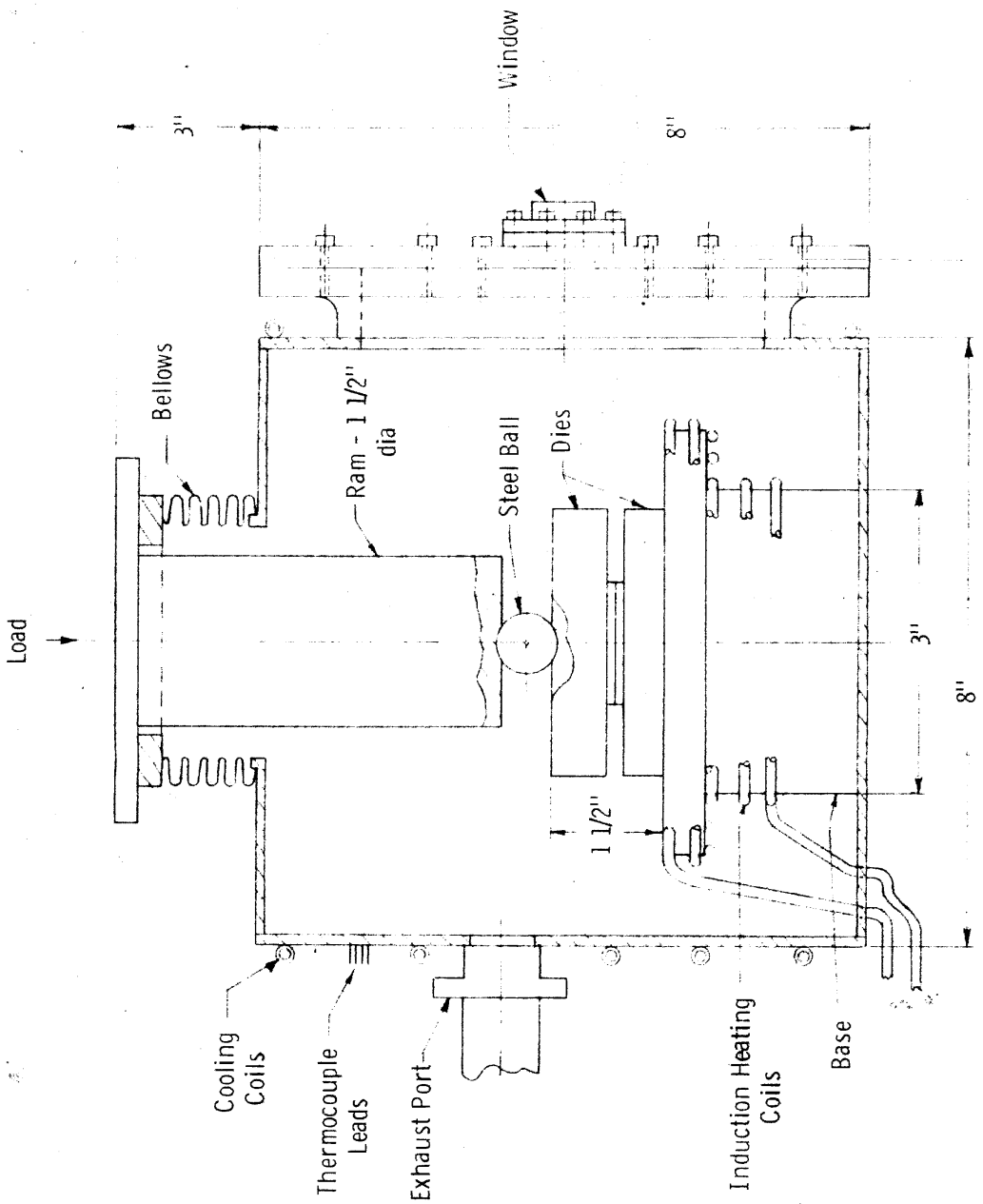

Apparatus used for diffusion bonding aluminum foil to silver, copper or aluminum

Fig. 1.10.01

Coined Al Window Approach:

As a parallel technique, a series of tests were conducted to investigate the feasibility of "coining" or forming the thin window segment in a sheet of .010" or so aluminum foil. It proved possible to coin 1/2-mil Al windows out of .010" sheets, thus simplifying the problem of joining to the main window support.

Testing of Al Windows:

In excess of 20 experimental diffusion bonded Al assemblies were tested using 3003 Al, 1100 Al windows and also a purer EC variety. Several of these were operated for substantial times in excess of 100 watt absorption. For example, window ALD-52 (1/2-mil Al 3003) operated 1/2 hour intervals at 50, 100, 125 and 150 watts of absorbed power, and finally at 20 minutes at 175 watts. This loading corresponds to 3500 watts of transmitted power for a double beam tube operated at 150 kv. Almost all windows demonstrated the ability of withstanding loadings in excess of 100 watts. Results with 10 coined windows were comparable.

1.11. Miscellaneous Window Materials and Techniques

Lockalloy:

Samples of a new alloy (70% beryllium-30% aluminum), 0.030" thick, were obtained from Lockheed Company for testing. The material was rolled to 0.002" thickness by heating to 400-500°F between passes of about 20% reduction. Edge cracked material was trimmed off and the 1/4" x 1" pieces were joined to a copper anode support by diffusion bonding. The Lockalloy was plated with copper, the copper support was plated with silver and both placed between bolted stainless steel blocks and heated for 1 hr at 500°C in hydrogen. A liquid zone of copper-silver-beryllium-aluminum was formed and acted as a brazing alloy. The joints made were found to be leak tight and the window assemblies were used for loading tests.

Eight windows were given standard loading. In general, the material was not as satisfactory as the Be windows in terms of capability of standing up under loading. This result is particularly unfavorable since the ratio of transmitted to absorbed power is lower than for Be.

The material was in an early stage of development at time of test. It is possible that more recent materials would be of better quality. In a visit to Berylco we were informed that they had alloys of similar composition under development.

Silicon:

While this material appeared to be very promising in view of its high strength, low atomic number, low thermal expansion coefficient, and apparent low stresses under loading, it proved to be very disappointing in preliminary loading tests. The silicon window tended to shatter very easily in handling and test. A systematic investigation of techniques for joining it to matching materials, such as tungsten and molybdenum was discontinued in view of unfavorable initial results.

Ag-Mg:

While pure silver drops excessively in mechanical strength as temperature increases, several hardening alloys are available having

0.1 to 0.3% Mg, which have tensile strengths in excess of 30,000 psi at temperatures in excess of 300°C. These materials are hardened by the simple process of heating in an oxidizing atmosphere.

It was necessary to develop techniques for joining the Ag-Mg foil to the window support materials. This was accomplished by vacuum brazing the plated foil with Incusil "10". The material demonstrated satisfactory ability to take loading when 1/2 mil thick. At this thickness transmitted power was insufficient to merit further work. Thinner material was obtained from a supplier, but was not satisfactory from the standpoint of pinhole leaks.

Pyrolytic Graphite:

Pyrolytic graphite is a unique form of graphite which is produced by the pyrolytic deposition process. It has unusual anisotropic properties. In the "a" direction, parallel to the deposition surface, it has a thermal conductivity which is higher than copper in the room temperature region and a factor of 200 lower thermal conductivity in the direction normal to the original disposition surface. In view of its low atomic number and unusual thermal conductivity, an investigation of a preliminary nature was conducted to assess its potentialities.

Pyrolytic graphite flakes procured from High Temperature Materials, Inc. in 1/2 mil to 1 mil thickness were checked to be leak tight on the helium leak detector. Several attempts were made at High Temperature Materials to deposit a thin pyrolytic film over slot configurations such as employed in the experimental demountable anodes. They did not succeed in producing films suitable for test.

Vacuum Evaporated Be Foil:

Several suppliers suggested that vapor-deposited material might be suitable for the window application, an idea strengthened by a Russian publication(12). This material, when evaporated on to backing plates held above 850°C, could be bent several times over a templet 1 mm

12. V. M. Amonenko, A. A. Kruglykh, V. S. Pavlov, and G. F. Tikhinskii, "Production of Be Foil," Zavodskaya Laboratoria, Vol. 26, 625 (May 1960)

in diameter. The foils were reported to be vacuum tight in thicknesses down to 1-1/4-mil of Be when evaporated on to plates held below 300°C. The plasticity of these foils could be enhanced by suitable annealing in the temperature range between 700°C and 800°C for 3 to 6 hours. In the Russian process, the Be is rolled after evaporation.

Dr. R. V. Bunshah of the Lawrence Radiation Laboratory, Livermore, Calif., was contacted to see if LRL might provide samples of Be evaporated foils. From the information he provided, it appeared that the Livermore process was similar to that employed by the Russians. The samples provided had an excessive number of pinholes as received. However we were impressed by the good flexibility of this particular foil. Results on testing were comparable if not superior to standard Be foil as obtained from the Brush Beryllium Company.

Cryogenic Approach to High Power:

From curves of the variations in the thermal conductivity and expansion of Be with temperature, it is evident that the advantages of lowering the temperature of the Be window foil to the cryogenic temperature range would be considerable. In the first place for pure Be the thermal conductivity would be down by a factor of 5 to 25, depending on the purity, and thus greatly reducing thermal gradients or permitting substantial increase in loadings. Secondly, the slope of the linear expansion curve of Be decreases significnatly with temperature. Thus a given temperature gradient at low temperature would be expected to produce lower mechanical stresses than the same temperature gradient at high temperatures.

A loading test was performed on a window fabricated from a Berylco vacuum cast copper using liquid N_2 cooling. Threshold KV of window was 60 kv. The window was given 25 cycles at the 50 and 75 watt loading levels and 50 cycles respectively at the 100, 125, 150, 175 and 200 watt levels. Failure occurred after 48 cycles at 225 watts as the result of an overheated spot in the loaded zone.

A second loading test using the deep 0.1" R demountable design was conducted using .005" thick Be material which has been thinned by electric discharge machining to two mil. The threshold voltage was 76 kv. Liquid nitrogen cooling was used. The temperature was observed

to be -180°C. The window was subject to 25 cycles at 50 and 75 watt loadings followed by 50 cycles respectively at 100, 125, 150, 175, 200 and 225 watts. Failure occurred after 7 cycles at 250 watts as a result of an overheated spot in the loaded zone. It was interesting to note that most evidence of heat was on the atmosphere side of window.

A rough estimate was made on the weight of liquid N_2 coolant which would be required for this use. If a 10°C temperature rise were permitted, it would require about 400 pounds of liquid N_2 an hour to handle 1 kw of absorbed power. For 2 mil Be this would correspond to 3.1 kw of transmitted power, and 8.6 kw of transmitted power for .001" Be. Since the heat of vaporization of liquid N_2 is 100 times greater than its heat capacity, considerable economy of weight could be effected by allowing the liquid N_2 to vaporize into the ambient environment.

Conclusions:

In assessing the window program on the basis of the results reported, it is important to recall that its termination was dictated by the realization of an alternative system, which, although more complex and bulky, did satisfy the requirement of immediate availability. A number of the window ideas mentioned in this last section are felt to hold considerable competitive promise, although not without extensive developmental effort. It is, therefore, suggested that the question of additional window work be re-examined at a future date, when a better assessment of the operational advantages to be gained by utilizing window tubes can be made.

CHAPTER 2

WINDOW TUBES

2.01 Introduction and Summary

The pivotal element of an electron beam generating tube is the window, covered in Chapter 1, but other elements must be provided: a cathode, means to connect the cathode to the power supply, electrical insulation for the connection, and a pump to keep the tube evacuated in the face of leakage or perfusion of gas through the window.

Demountable tubes were used to test experimental windows without committing more than a minimum of material and labor to an expendible part. These tubes were provided with the same cathodes used in the prototype tubes and simulated the prototype tubes in all details but the arrangements for vacuum.

Difficulties in obtaining and keeping good registration of the two beams on the two window slits inspired the development of an adjustable cathode, in which the two filaments, carried in their focusing grid cups, could be translated normal to their length for accurate registration on the slits of a window.

As it became evident that the quality of available window material made a supply of enough tubes for a successful field test program improbable, several methods of accommodating to the situation were proposed. Not even enough good windows to try those methods were obtained, but the ideas are discussed here, since they might prove useful in any future window program.

The insulation system adopted was dictated more by the limited space available than by direct choice. The cable connectors made by R. Seifert of Hamburg, Germany are about the only item available for 150 kv service in such small size. They were used on the tube packages, power supplies and later on the Heraeus electron beam gun.

2.02 Machlett Cathodes

Cathodes built to the design illustrated in Fig. 2.02.01 were purchased from Machlett Laboratories, Inc. for incorporation in both experimental and prototype tubes. A pair of filaments and focusing structures; adapted from Machlett line-focus x-ray tubes, was spaced a convenient distance apart, which became the spacing between windows in the anode. The cathodes were supplied on a glass stem as shown for sealing into tube envelopes. One of the leads was connected to one end of each filament, another to the two free ends, permitting series, or parallel or individual operation of the two filaments. The post at the center of each filament gave mechanical support only and was insulated from the focus cup, permitting a bias voltage, introduced on the fourth lead (not shown in the drawing), to be used to control the distribution of the focal lines on the windows.

Because of the large calculated sensitivity of beam focus to depth of the filament in the focusing cups, several different depth settings were ordered. Pinhole radiographs of the focal spots confirmed the prediction of an optimum filament depth for a given anode-cathode spacing, but differences in filament depth were obscured by other effects in performance of actual windows. For example, it proved impossible to focus the beams routinely on both window slits with the precision necessary to achieve acceptable transmission through the windows and to maintain the design values of thermal gradient. To accommodate all the sources of variation, adjustable cathodes were designed and built.

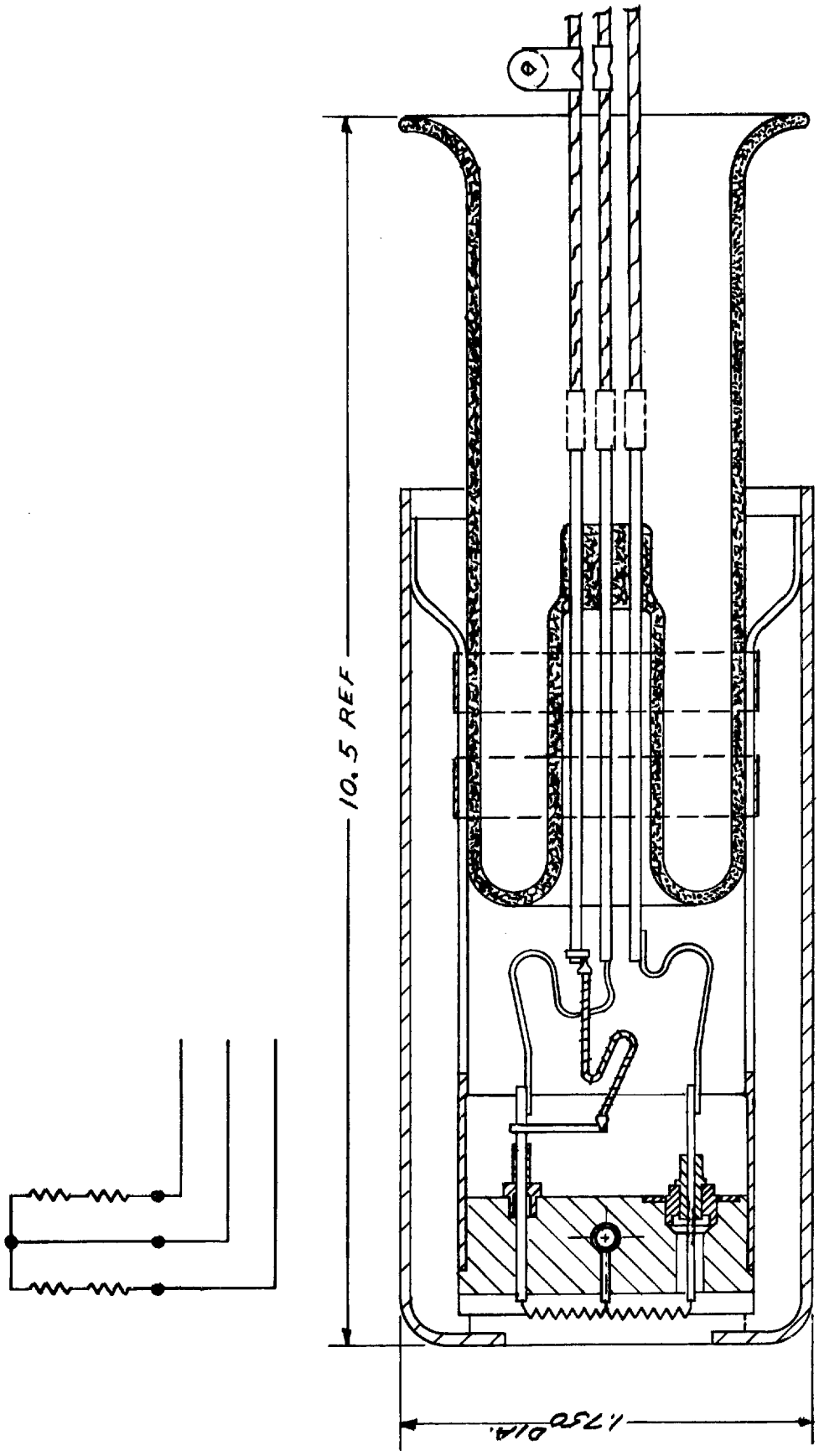

Fig. 2.02.01

Machlett Cathode

2.03 Adjustable Cathode

Design:

The most serious problem encountered in the use of the Machlett cathodes was the loss of transmitted power due to small errors of registration of the beams on the windows of the prototype tubes. A cathode was needed which would have its filaments sufficiently adjustable to allow for proper beam alignment after initial test, when it could be rigidly fixed for continued operation.

The basic design is shown in the upper illustration of Fig. 2.03.01. Two Machlett focusing cups were mounted on rods pivoting on knife edges to accomplish the required lateral movement. The opposite ends of the pivoted rods were threaded and moved in slots in a phenolic plastic cap attached to the end of the tube with a high temperature cement. A nut on the rod clamped it in position; a drop of cement held it there. The rods were vacuum sealed with metal bellows, and the electrical leads were brought in with glass or ceramic feedthroughs as shown in the two lower views of the figure. The filaments were run in series to eliminate the need for another feedthrough in this design. With the potentiality of perfect alignment it was not necessary to be able to operate just one filament.

Fabrication:

The initial step was a high temperature braze of the internal parts to the supporting plate. Next, the stem was attached in a glassing operation, after which the feedthrough(s) could be installed and the cathode finished by spot welding the focus cups, electrical leads and shield. Care was taken to keep the cathode extremely clean at all times, and leak checking was done at appropriate stages of assembly to insure quality comparable to the commercial fixed cathodes.

Testing:

The cathode structure was subjected to some limited vibration testing in the design stage in the form of a model. Natural frequencies

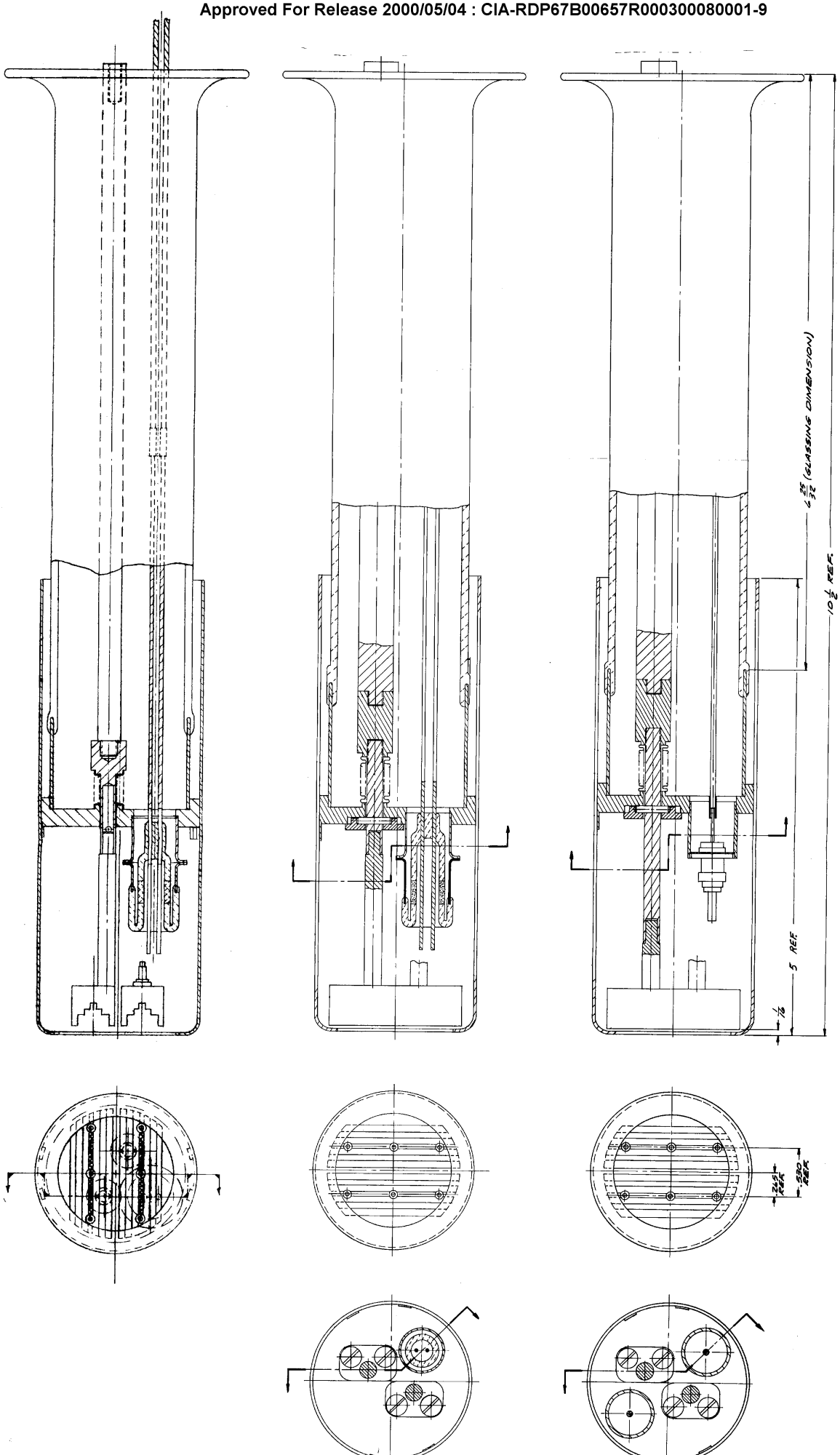

Fig. 2.03.01

Adjustable Cathode

of low amplification were found in the critical range of the design vibration envelope, but clearance in the pivots caused variations in the response.

The means of clamping and of movement to correct observed errors in registration were satisfactory, but the clearance in the pivots allowed angular misalignment and also axial movement that changed both focus and perveance.

Focus cups were joined to the pivot rods by a spot weld on a sleeve joint; this loosened in some units.

Aside from these malfunctions in specific units, the design performed as intended and did correct the troublesome discrepancies of registration.

Modifications Recommended:

A modified design of the pivot, which never was built, provides for positive retention of the pivot in its seat. This change and a reduction of weight of the focusing cups should remove all the deficiencies observed.

Adjustable Optical System:

Late in the window tube program, a need was seen for a means of varying not the beam alignment but its geometry. In size and in axial current distribution, the focal spots produced by the standard cathodes were not optimum for many desired tests. A broader beam of uniform current density was needed for multi-aperture windows, and a much narrower beam was desired for other special designs. Since direct calculation of exact cathode element spacings was impracticable, they were determined by experimenting with combinations established by simpler methods.

A test setup was designed around a piece of pyrex pipe, which served as vacuum envelope, cathode insulation and anode-cathode spacer. The pipe stood on the surface plate of a bell jar system, and the cathode was suspended inside on a stem containing electrical feed-throughs and adapters to make connections to the filament and to position the grid. An anode, supported by an adjusting screw, was mounted inside the pipe on the base plate. Magnet coils could be dropped over the tube to produce an axial field at the accelerating gap.

The straight filament, one inch in length operated within a rectangular slot cut in the grid, which was a plate thicker than the slot width, so that the filament was in a kind of well.

The anode was a two pound cylinder of copper to eliminate the need for cooling requirements. A heavy gold plating on the target surface gave good, sharp x-ray images which were recorded with a pin-hole camera outside the envelope. From the camera dimensions and image measurements, focal spot sizes could be calculated with good accuracy down to 1 - 5 mil widths. Below this limit, thin aluminum foil was stretched across the anode, and the burned-through areas were taken as direct measures of focal spot size. Widths as low as 0.0005 inch were measured by this method.

Some representative results are collected in Table 2.03.01. All of the dimensions given are referenced to the face of the grid closest to the anode, as shown in the inset.

TABLE 2.03.01

BEAM WIDTH AS FUNCTION OF FILAMENT DEPTH, GRID BIAS, AND AXIAL MAGNETIC FIELD: All Dimensions in Inches

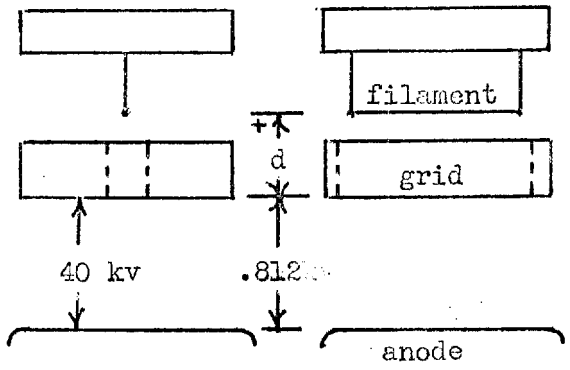

Fil Depth d (in)	Flux Density B (gauss)	Grid Bias v dc +510	+90	+45	0	-45	-90
$-1/2$	0		.240	.245	.250	Negative bias cut off beam	
	350		.050	.027$^{\omega}$	.006$^{\omega}$		
	700		.014	.006$^{\omega}$	.006$^{\omega}$		
$-1/4$	0	.200			.288	.250	
	300	.180			.065	.047	
	550	.087			.040	.033	.027
	700						.014$^{\omega}$
$-1/8$	0				.335$^{\alpha}$		
$-1/16$	0				.390		
0	0				.710		
$+1/16$	0				.813		
	55				.813		
	110				.773		
	165				.731		
	220				.690		
	440				.196		
	550				.143		
	605				.130		

α: Very nonuniform distribution

ω: These figures based on assumption of 3° tile of camera axis. If tilt is zero, beam width should be reported 0.001.

2.04. Demountable Tubes

Since the demountable tube was intended to provide data for prototype cathodes and windows, its construction, Fig. 2.04.01, deviated from the prototype design concept only where its different role made the change unavoidable.

The cathode is supported and positioned by a glass stem, axially re-entrant in the cylindrical tube envelope. An exhaust arm leaves the side of the envelope and connects to the evacuation stand. The cylindrical envelope terminates at a seal to a thin Kovar cylinder, which is brazed into a flange. This flange carries a groove for an O-ring, which seals the anode plate, and a bolt circle for the clamp by which the anode plate is located and fastened.

Everything pertaining to the window was contained in the anode plate, which was provided with a smooth inner face for efficient sealing, cooling coil(s) if required, and the window under test. In addition, a bolt circle was usually provided on the external face to permit the use of a protective cup, which could be evacuated, or filled with an inert gas, to mitigate the effects of window failure on the cathode.

The windows were located by an extremely simple technique. Lines were scribed across the face of the tube flange, parallel to a diameter and offset by half the spacing between filaments. Corresponding lines were scribed on the cylindrical lip of the window plates, marking the centerlines of the two slits.

With the clamp screws holding the window plate lightly against the O-ring, finger pressure produced motion without stick-slip, and the four pairs of scribe marks could be aligned by eye within about .004 inch. Occasionally, distortions from brazing or small machining errors would make registration of both window slits impossible. When all the error was imposed on one slit, it would show the error clearly on test while the other performed well. This was taken as validation of the method for normal cases.

When a demountable tube was provided with a new cathode or had been open for some time, it was baked out as well as its silicone O-ring permitted. This was followed by high voltage seasoning, with the cathode cold and a large protective resistor in series with the power supply. Normally, a brief cold seasoning was all the treatment required since about 120 kv, depending on weather, was the flashover limit of the air termination between cable and tube. This proved adequate for laboratory use.

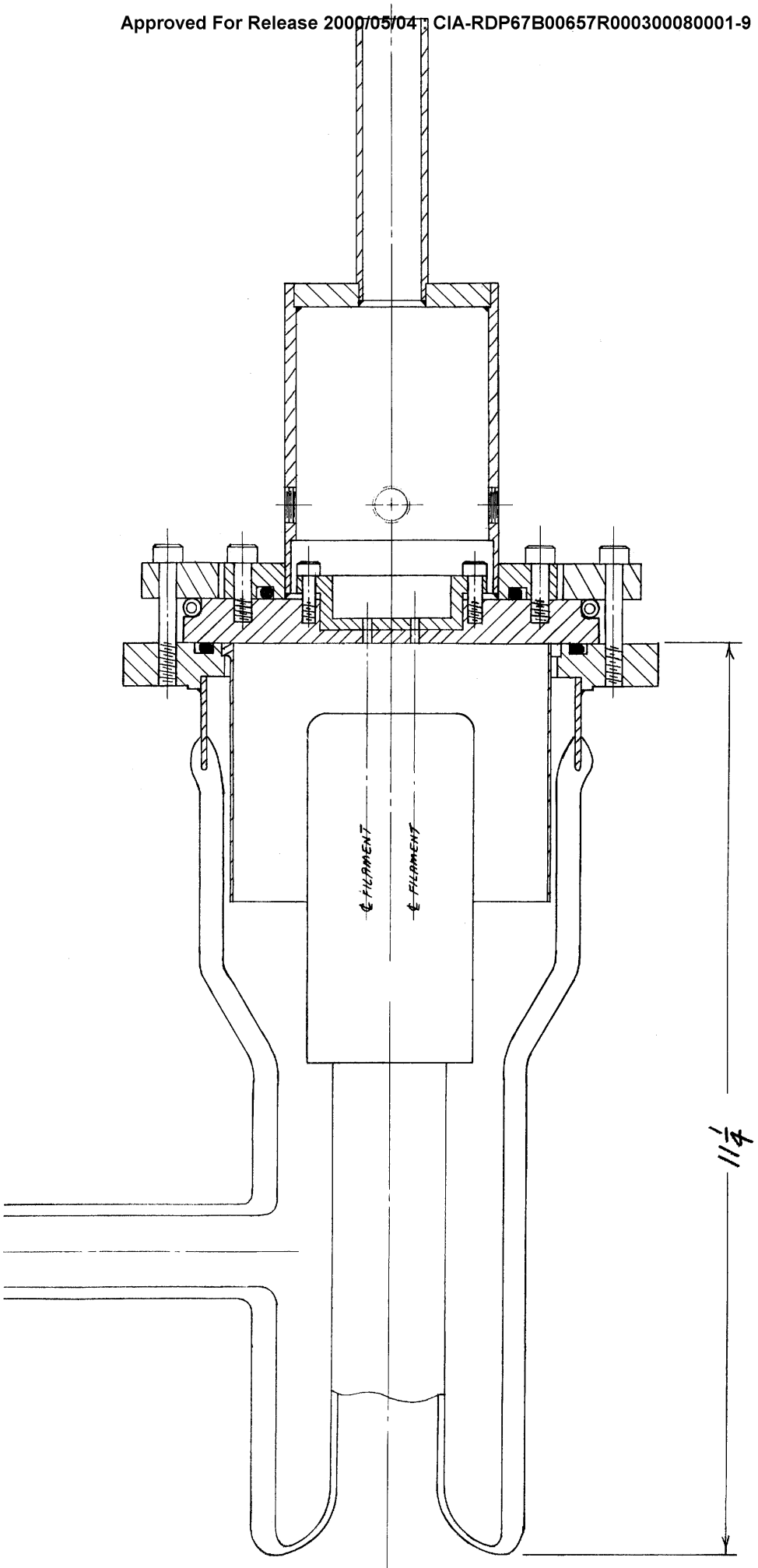

Fig. 2.04.01

Demountable Tube

2.05. Testing Windows with Demountable Tubes

After evacuation and cold seasoning, the first step was to verify the window registration by means of pinhole radiographs. The camera shown in Fig. 2.05.01 is typical of the several models used. Those beams which are well centered and those which are not are easily told apart in the radiographs of Fig. 2.05.02. In the ideal case, four separate lines can be seen, showing the four separate images of the filament produced in perfect focus.

The next step was determination of the window penetration threshold voltage. At a current level below one milliampere, the accelerating voltage was slowly raised until a glow in the gas at the window indicated electrons were penetrating. An alternative detector was a thin film of zinc oxide, which gave a brilliant white fluorescence when excited by electrons. Unfortunately, the two methods did not give exactly the same results, differing by two or three kv in 40-60 kv. The gas glow required a small excess of electron energy to produce a glow discernable against the red hot window. The phosphor, on the other hand, began to glow just before complete penetration, because of the copious soft x-rays generated just beneath the surface of the window. A little experience quickly provided a feeling for the voltage to be subtracted from the gas glow figure to give an accurate report of the threshold electron energy.

Various thermal tests usually followed, always run at voltages below the threshold so that the absorbed power could be estimated with greater accuracy. The soundness of the window attachment was measured by continuous operation or by cycling on and off with a period of several seconds. Faster pulsing, which measured the thermal shock resistance of the window material itself, required full power operation, for which prototype tubes were used.

Another test, run slightly over threshold, gave indications of the rate of gas leakage and/or perfusion through windows. Absolute readings were hard to make, since the beam produced enough ions to

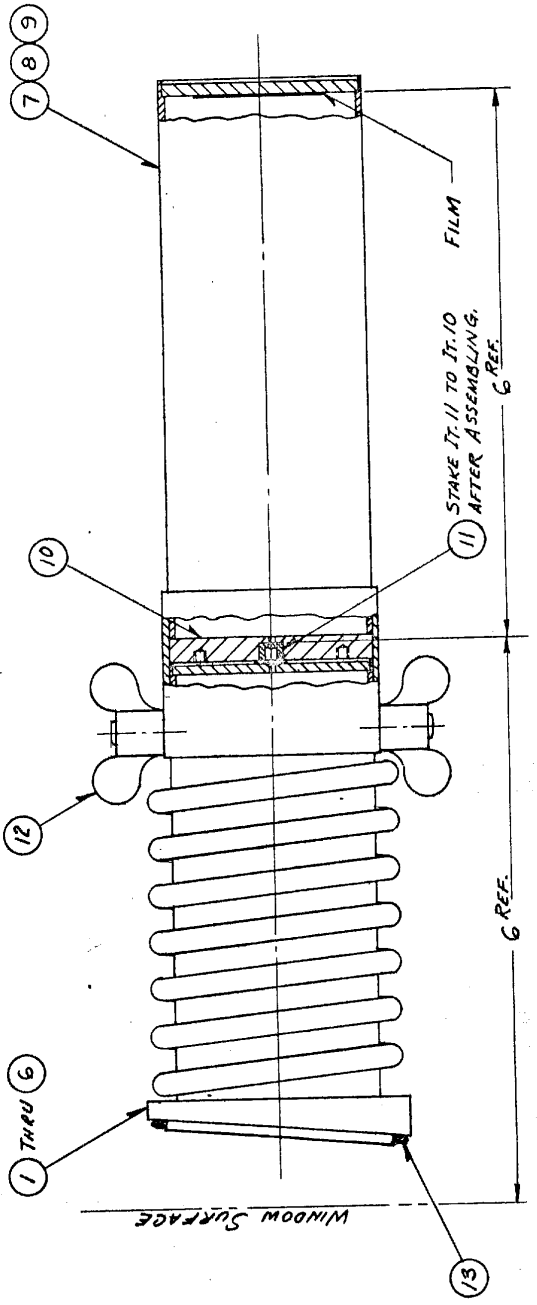

Fig. 2.05.01

Pin Hole Camera

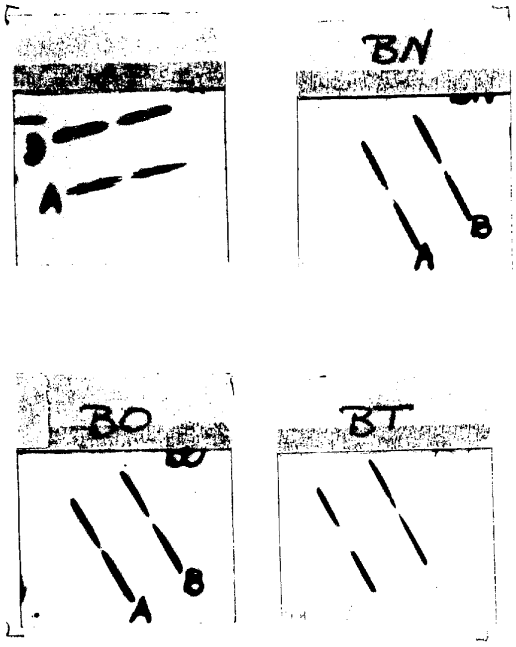

Pinhole Radiographs

Fig. 2.05.02

affect the indication of the vacuum gages, but comparative readings were possible, by which the different windows could be ordered from the most pervious to the least.

The thermal loading tests were usually run with the protective cup installed, so that failure of the window would not admit air, which would have ruined the hot cathode. The post mortem analysis of failed windows was ordinarily confused by events taking place after the actual failure. Gas streaming through a crack in the window would encounter the beam and be heavily ionized, concentrating the subsequent current surge of the flashover directly on the parts wanted for examination. For this reason the protective cup was frequently evacuated to a few microns pressure when the exact mode of window failure was in question.

2.06. Prototype Tubes

Introduction:

The prototype tubes, which the demountables simulated, consist of the following sub-systems: cathode, anode with windows, cooling, electrical insulation and connection, and vacuum holding. All these except the insulating oil expansion tank are shown in Fig. 2.06.01. The anode is shaped to fit into the installation with cooling coils directly behind the mounting flange to absorb the window power losses. Directly above the anode is a cylindrical section in which are brazed tubulations for exhaust and vacuum maintenance. The shield, which protects the glass-to-metal seal from the electric field, is heliarc welded to the other two at the edge of the three-ply flange which doubles as the sealing surface for the insulating oil tank.

Assembly:

The cathode and envelope assembly and the anode and flange assembly were joined in a fixture which permitted exact alignment of the cathode filaments and window slits. The focusing track of a microscope was set up parallel to the axis of the cathode and a reticle centered on one filament. Then the microscope was raised, and the anode assembly was set on the tube and shifted around until the reticle could be focused on the corresponding window slit. Clamps held the two parts together until tack-weld beads could be run to hold the tube together for the final sealing weld with inert gas in the tube.

Vacuum System:

A one liter per second Varian VacIon pump was mounted on the tube package to maintain the vacuum against small leaks. The tubes were exhausted with a Varian VacSorb roughing pump and a 15 liter/sec VacIon pump. This arrangement insured absolute freedom from contamination by pump oil, as the VacSorb pump removes gas by adsorbing it on molecular sieve, an artificial zeolite, chilled to liquid nitrogen temperature. The VacIon pump is just as clean, since it pumps by burying gas molecules in sputtered titanium.

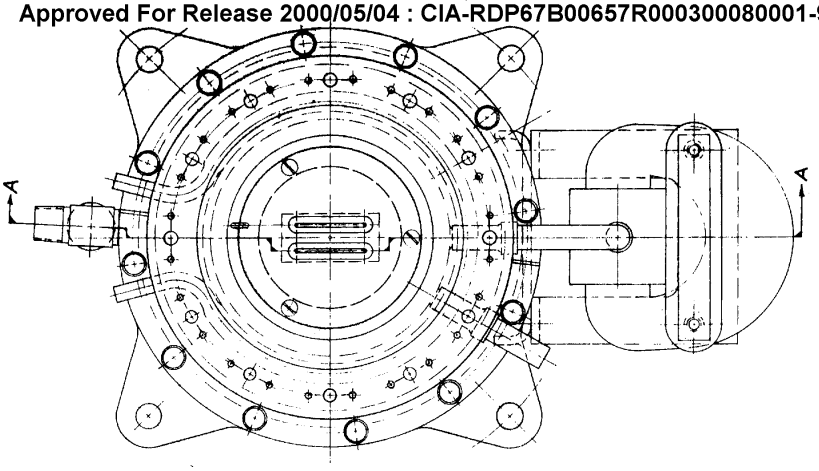

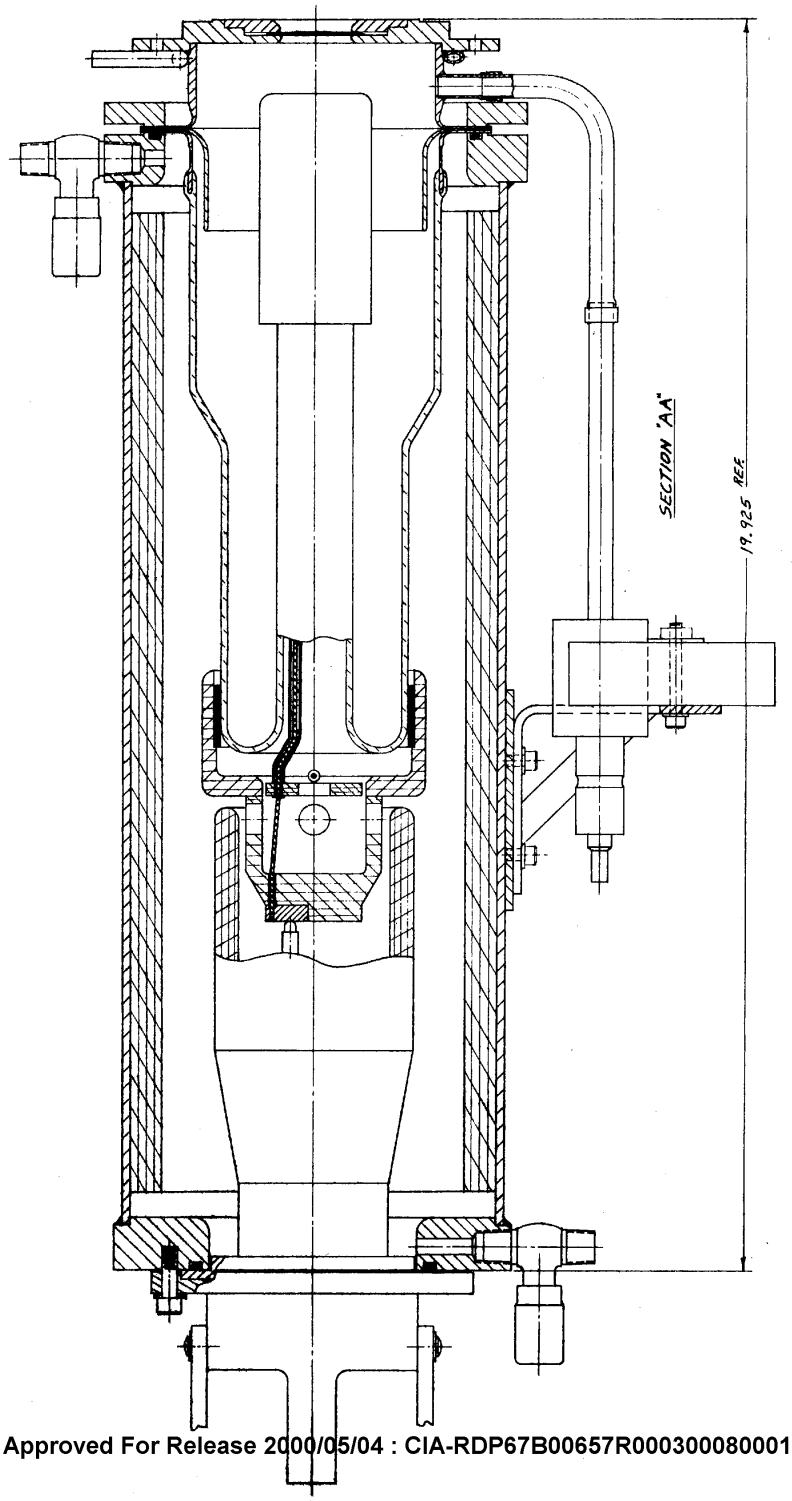

Fig. 2.06.01

Prototype Tube Package

The high electrical and thermal conductivity of the OFHC* copper tubulations made silver brazing the exhaust and maintaining pumps to the tubulations a problem. It was solved by pressing a steel ring over the joint to concentrate heat from an induction heating coil.

There was a possibility that the stray field of the magnet required for the VacIon pump would be strong enough at the accelerating gap to ruin the beam registration. Measurements made with a pump and tube shield in operating spatial relationship gave field densities of one to two gauss at the cathode position, too little to deflect the beam significantly for the way the slits and magnet were oriented.

The tubes were processed on an exhaust stand in which the pumps were mounted under an insulating panel on which the tubes could be set up. This construction permitted an oven to be dropped over the tube for outgassing without affecting the vacuum pumps.

After a VacSorb pump had pumped the system down to 10 microns, a 15 liter per second VacIon pump took over. This pump is capable of pumping the system down to approximately 2×10^{-9} torr or a pump current of less than 1 microampere. On the initial pumpdown if the tube system functioned properly with no vacuum leaks, the oven was dropped over the vacuum stand for bakeout.

Bakeout or outgassing was done in two steps. First, the external baking oven was used and then the inner metal surfaces were outgassed using rf heating.

The oven bakeout was done using an oven that fitted over the complete tube assembly. The 15 liter per second pump and VacSorb are mounted under the transite system base for maximum heat isolation.

Whether temperature was controlled meanually or automatically, the rate of oven temperature rise was guided by the vacuum system pressure. In order not to contaminate the vacuum system the pump current was held to 4 ma or less. This is approximately 2×10^{-5} torr. The bakeout in the automatic mode is covered in the following section.

*Oxygen-free high conductivity

For manual bakeout, visual recorded data determined the times that temperatures were increased. The approximate time to reach 400°C in either mode was 6 hours. Variations in bakeout time depended on the cleanliness of the tube and vacuum system during assembly.

An extremely high rate of outgassing occurs at a temperature of 200 to 300°C. The time spent pumping in this range was much longer than at the lower or higher temperatures. Baking at 400°C was maintained for a period of approximately 8 hours or until the vacuum system pressure dropped to 3×10^{-6} torr. At this point the oven temperature was slowly decreased to room temperature over an average time of 4 hours. The oven was then removed and the system prepared for rf heating. An rf generator was used to outgas the metal surfaces and shields within the tube. Parts were heated to approximately 400°c and controlled to limit the pump current to 5 ma or a pressure of 3×10^{-5} torr. Cathode filament current was maintained at 4 amperes during the rf outgassing operation. Rf cycling required approximately 8 hours.

Automatic Baking:

To minimize the amount of attention needed for tube treatment a system was devised to monitor temperature against pressure and progressively drive the temperature to the upper limit of baking. An added feature enabled the tube to be baked eight hours or to a predetermined vacuum pressure and then cooled to 50°C at which time the equipment was de-energized.

Constant vacuum check was maintained on the system through the current of the 15 liter/sec VacIon pump. A signal was taken from the VacIon power supply and fed to a transistorized amplifier. The amplifier was used to trigger the temperature controller three ways: run up, stop or run down. At the completion of the run down cycle all temperature controlling equipment was automatically turned off. After the initial equipment startup all functions are automatic and further attendance is not required.

During the run up cycle the recorder controller is gear driven upward to a temperature of 400°C. As outgassing starts, causing the pressure in the system to rise, the sense circuit will stop the recorder drive. A current of 2.5 ma (approximately 10^{-5} torr in the vacuum system) is the point of stopping. This point is adjustable.

While in the stop portion of the cycle the system remains stationary until the pumping system pressure has dropped to a predetermined value. A current of 1 ma or a pressure of approximately 6×10^{-6} is the lower stop limit. The upper stop limit is set at 4 ma or a pressure of approximately 2×10^{-5}. The upper and lower trigger points or bandwidth is adjustable. A standard strip chart temperature controller (0-500°C) was slightly modified in this system. A low limit switch set at 50°C, a upper limit switch set at 400°C and an override switch set at 420°C were added. Two toggle switches were also installed, one to change the recorder controller from automatic to manual, and the other to provide a reversible manually controlled drive.

Insulation System:

In order to have the beam generator a convenient package, a high voltage cable connector was required. From the standpoint of reliability in minimum size, the connectors manufactured for their x-ray equipment by Richard Seifert Co. of Hamburg, Germany are the best available commercial units. This receptacle and cable-end combination provides three conductors (two filament leads and a common) insulated for 150 kv dc. The x-ray tubes for which this connector is intended have a three-pole terminal which makes pressure contact with three spring pins in the receptacle. A similar terminal was provided for the tube as shown in Fig. 2.06.01.

Some difficulty was encountered in fixing the cap firmly to the tube envelope without inducing cracks when the temperature rose. This was finally accomplished by using a resilient intermediate member of cork between the tube wall and the cup.

Because of size limitations, oil spaces around the tube were not great enough to satisfy clearance requirements, so a barrier of rolled up polyethylene sheet was added. This was generally quite successful, although in one tube the insulating oil (Wemco C) softened the plastic at high temperature, apparently without significantly degrading its insulating properties.

Vacuum degassing, filtration and circulation of the oil, for several days achieved insulation qualities required for 150 kv operation. The solid fill required an expansion tank, which was connected by a hose to one of the valves shown in Fig. 2.06.01.

Testing Window Tubes:

After evacuation and thorough outgassing, the tubes were given a cold seasoning treatment, and the window registration was checked with the pinhole camera. If acceptable on this score, the tube might be given some further test such as thermal loading of the windows, but usually the tubulation to the exhaust stand was pinched off at this point, and the tube was ready to be installed in a package and subjected to full load. The tubes were tested in a lead-lined booth to protect personnel from any x-rays that might escape the shielded beam current receiver.

One of the most important variables to be measured in full load testing was the transmission, in terms both of energy and current. A carbon target in the current collector clamped over the window minimized backscatter for accurate current measurement, and the energy received was absorbed by a stream of cooling water instrumented to permit the power reaching the water to be calculated. This number, plus a similar quantity for the anode dissipation, usually agreed with the electrical input within the power which could reasonably be attributed to convection loss or pickup.

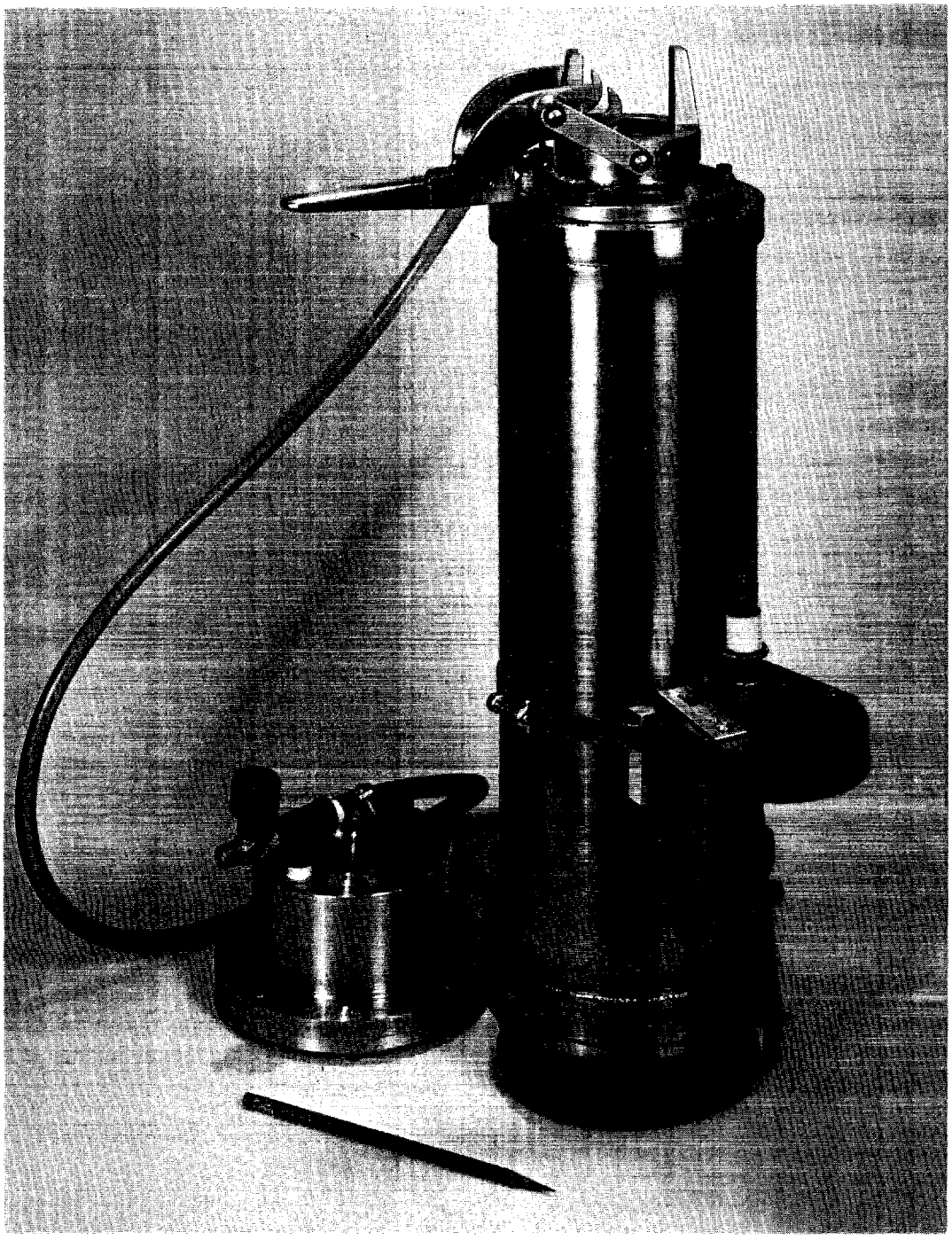

Completed Prorotype Window Tube

2.07. Tube Shipment

A relatively simple package was made for each individual tube, utilizing a double suspension system. The ends of the tube were capped with fitted styrofoam blocks and placed in a carton padded externally with rubberized hair. This in turn was placed in another carton to complete the package. Thus the styrofoam and matting amply supported the tube in three directions. All parts necessary for the operation of the tube, but not a true physical part of it, were shipped in the same package in recesses cut in the styrofoam block or inner carton. These parts included the oil expansion chamber and a power pack for the 1 liter/sec pump. A battery operated power supply was used to maintain pumping in transit. A sealed 12-volt lantern battery proved to have more than adequate life for the longest reasonable trip.

2.08. Flight Tests of Dummy Tubes

In order to check out the power supply, control, telemetry and other support equipment in flight without risking a good tube, which might meet with an accident in such preliminary tests, a dummy tube with a blank anode was fabricated, tested, shipped and installed. In all, five flights were made with this tube operating, and a number of troubles in the other elements of the system were uncovered. The actual power was limited for this tube to a level that the cooling system could handle, corresponding to the window and interception losses in a standard tube.

2.09. Alternate Approaches

When it became evident that material quality of beryllium would make it impossible for a single tube to supply reliably all the power required for the tests, an alternate scheme was devised to mount two or more tubes in a cluster and run each at the appropriate fraction of the desired power level. This entailed the provision of multiple outlets on the power supply and filament supplies to regulate each tube at its share of the total load. An actual modification of one power supply was made to accommodate two tubes, but a reliable pair was not obtained until after work had begun to convert the test configuration to the Heraeus gun. Because of the success of the latter, no subsequent attempt at flight tests using window tubes was made.

At the same time that clustering was being considered, it was noticed that the windows almost always failed during a downward temperature excursion, and that the cracks were usually small enough that a 5 liter/sec pump could cope with the leak from 20 torr pressure. A design was made incorporating such a pump, and later a 15 liter/sec unit, but then the approach was abandoned when the program emphasis was shifted away from window tubes.

CHAPTER 3

DYNAMIC PRESSURE STAGING AND HERAEUS GUN

3.01. Introduction

The transfer of an electron beam through a series of aligned orifices contrasts strongly with almost every aspect of transfer through a window. Power density is no longer a limitation. Instead, the objective is maximum density in a small beam cross section with 'tails' of minimum intensity outside the nominal beam envelope. The simplicity of a sealed vacuum system is replaced by a whole range of pumps to remove gas from the chambers between orifices. Pure tungsten cathodes must be used in place of more efficient emitters that would be injured by exposure to atmospheric pressure and ion bombardment. Along with more complicated structure go more complicated operating procedures. One requirement in common is accurate positioning of the beam, but in the pumped gun a little error is not immediately fatal, and all the pieces can be replaced if any are damaged.

Design of the pumping system for the Heraeus gun is based on the work of B. W. Schumacher[1]. For the existing set of orifices, the weight of the ducts and pumps was minimized within the practical requirements of accessibility, available fabrication techniques, and the limited space for the installation.

1. B. W. Schumacher, "Dynamic Pressure Stages for High Pressure/High-vacuum Systems" in 1961 Transactions of Eighth Vacuum Symposium and Second International Congress (Pergamon Press, N.Y., 1962), pp 1192-1200.

3.02. Pumping Design

To maintain the required vacuum of 10^{-4} torr or better in the beam generating and accelerating chamber of a dynamic system requires the application of several vacuum pump-orifice combinations. By proper vacuum pump selection and orifice design an optimum number of stages can be selected to meet space and weight requirements.

For the design of the dynamic pressure stages the gas conductance of the orifices and ducts must be known over the full range of operating pressure and flow regions. Two basic flow conditions are encountered in the dynamic system:

1) Free molecular flow, which is found at extremely low pressures. In this type of flow the collisions between gas molecules are considered negligible as compared with collisions of gas molecules with the tube walls. The tube conductance for this flow is independent of pressure.

2) Viscous flow, which is found at higher pressures and where the collisions between molecules are no longer considered negligible. The conductance for this flow becomes pressure dependent.

In the viscous flow regions, three different types of flow occur; laminar, turbulent and effusive. Laminar flow occurs at slow speeds and forms a parobolic velocity profile across the tube, with parallel flow lines. At higher speeds the laminar flow profile is no longer stable and turbulent flow begins. Turbulent flow will not be encountered in the dynamic pumping systems, so no further consideration is necessary. Effusive flow or enthalpy controlled flow occurs when the flow of gas through the tube or orifice is limited by the fact that the kinetic energy of any mass element of the gas at any one point in the flow cannot become higher than the difference in enthalpy between that point and the stagnating gas.

In the free molecular flow region of a gas of molecular weight M and temperature T °K, the kinetic gas theory gives an exact value for the flow conductance of an orifice of area A in a thin wall:

$$m_{F_0} = A\ v/4 = 3.638\ A(cm^2)\ \sqrt{T/M}\ \text{liter/sec} \qquad (3.02.01)$$

where v is mean molecular speed, $14551\ \sqrt{T/M}$ cm/sec.
For air at 25 °C,

$$m_{F_0} = 11.67\ A(cm^2)\ \text{liter/sec.} \qquad (3.02.02)$$

The conductance of a tube of length ℓ with diameter d can be found by multiplying m_{F_0} by an empirical factor k, known as Clausing's factor[2], which gives the conductance of a tube in the molecular flow region:

$$m_F = k\ m_{F_0}, \text{ where k is a function of } \ell/d. \qquad (3.02.03)$$

For laminar flow from pressure P_1 to P_2, the Hagen-Poiseuille Law[2] for a compressible gas of kinematic veiscosity η gives the conductance of a tube:

$$l_F = \frac{\pi}{8\eta}\frac{d^4}{16\ell}\frac{P_1+P_2}{2}\ \text{liter/sec.} \qquad (3.02.04)$$

For air at 25 °C and $P_2 << P_1$,

$$l_F = 89\ d^3\ \frac{d}{\ell}\ P_1\ \text{liter/sec.} \qquad (3.02.05)$$

For viscous effusion or enthalpy controlled flow, the basic laws of energy conservation give the conductance of an orifice:

$$e_{F_0} = \left(\frac{2}{\gamma+1}\right)^{1/(\gamma-1)} A \left(\frac{2\gamma}{\gamma+1}\cdot\frac{RT_1}{M}\right)^{1/2} \text{liter/sec} \qquad (3.02.06)$$

where γ is the ratio of specific heats, C_p/C_v, and R is the gas constant.
For air at 25 °C,

$$e_{F_0} = 20\ A(cm^2)\ \text{liter/sec.} \qquad (3.02.07)$$

The conductance of a tube, based on work by Frössel[3], is:

$$e_F = \mathcal{V}\left(\frac{\ell}{d}\right) e_{F_0}\ \text{liter/sec} \qquad (3.02.08)$$

2. S. Dushman, Scientific Foundations of Vacuum Technique (John Wiley and Sons, Inc., New York, 1962), 2nd ed.
3. W. Frössel, Forschung, 7, 75 (1963)

where $\nu\left(\frac{\ell}{d}\right)$ is the coefficient derived from data by Frössel.

Eq. 3.02.03, 3.02.05, and 3.02.08 can be represented in a graph with F and $\frac{\ell}{d}$ as axes and D as a parameter as shown in Fig. 3.02.01 (a,b,c). Knowing the conductance F as a function of geometry, ℓ/d and d, for the three principle types of flow, it is possible to describe the complete conductance curve for any orifice or duct as a function of pressure on the diagram with F and P as axes. Some approximation must be made to get the proper conductance line for the transition regions where flow changes from one type to another. There ${}^{l}F$ and ${}^{m}F$ lines meet, the laminar and molecular flow components must be added, i.e., F must be multiplied by 2. Through this new point, then a smooth curve is drawn tangent to the ${}^{l}F$ and ${}^{e}F$ Sections. A number of such curves are shown as the generally horizontal lines in Fig. 3.02.01(d).

In this diagram are also shown the 45°-slanted lines of constant throughput, Q. By definition the mass of gas, Q, flowing through a tube per unit time is determined by the pressure difference P_1-P_2 and the conductance, F, of the tube:

$$Q = F(P_1-P_2) \qquad (3.02.09)$$

For the case of a dynamically pumped vacuum system, it may be assumed that $P_2 << P_1$. This assumption simplifies the expression to

$$Q = F\,P_1 \qquad (3.02.10)$$

This approximation is the basis for the use of Fig. 3.02.01 in the designing pumping systems.

Given an orifice and the upstream pressure, the throughput is determined. Downstream of the orifice will be the pressure at which the system beyond the orifice can accept the throughput. In order to make this comparison conveniently, vacuum pump characteristics, normally supplied by the pump manufacturer in the form of pumping speed vs. pressure may be plotted on the PQF diagram. If fore-pressure tolerance is specified for a given pump, this must be known exactly and taken into consideration during pump selection and application, for the PQF diagram does <u>not</u> provide a constant reminder of fore-pressure requirements.

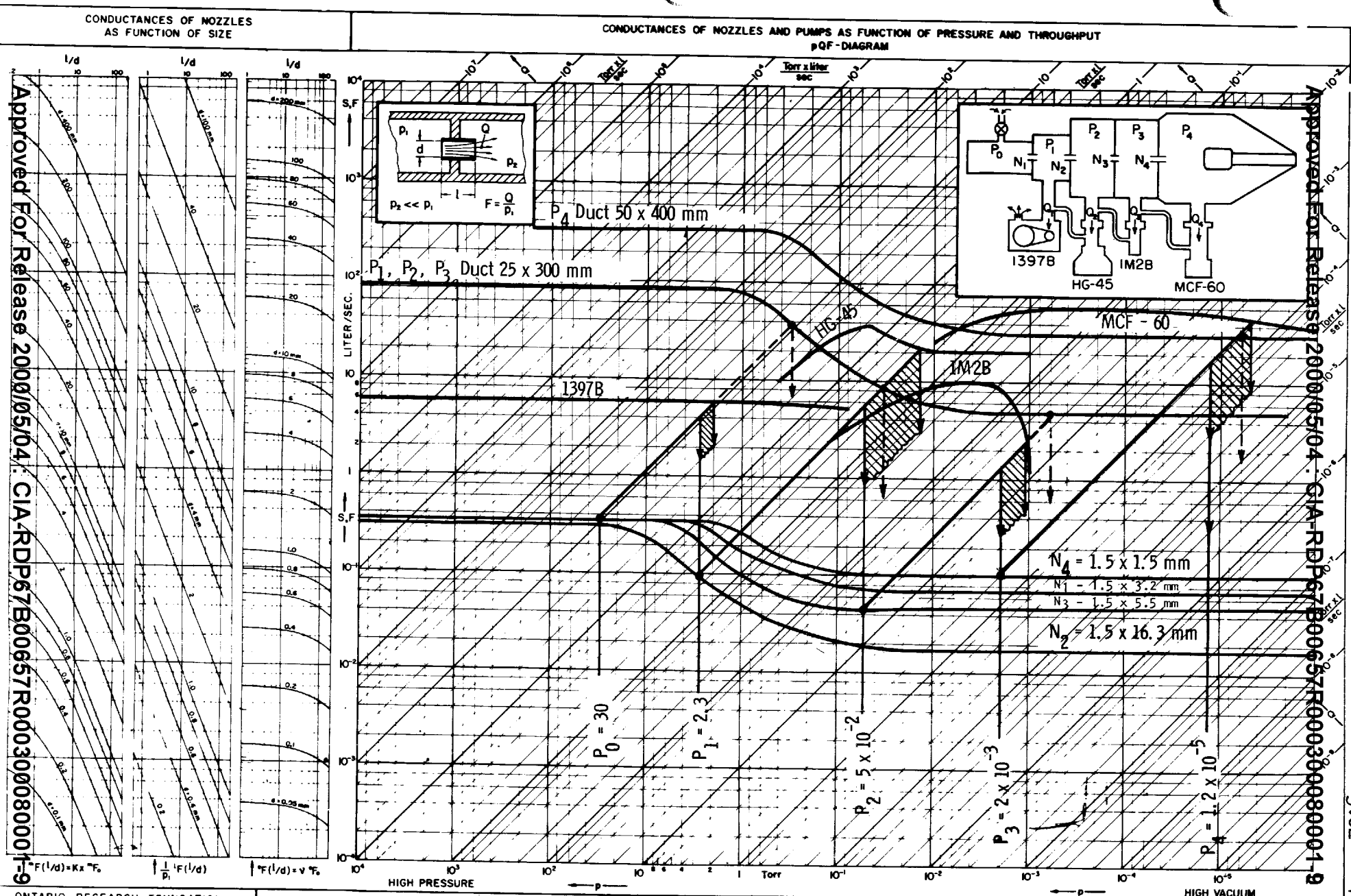

3.03. Design Diagram for Dynamic Pressure Staging

The use of the PQF diagram in designing a system of dynamic pressure stages is best illustrated by following through the system represented by Fig. 3.02.01. The conductance curves for the apertures and pump ducts, calculated from their dimensions, are shown on the diagram and labeled to correspond to the inset system schematic. Also shown are the characteristics of the pumps taken from the manufacturers' published data.

An assumed external pressure P_0 = 30 torr, established by the valve shown in the schematic, causes a throughput of 10 torr-liter/sec through the orifice N_1. This is the intersection of the N_1 characteristic and the 30 torr lines. This throughput line is continued until it meets the mechanical pump characteristic, labeled 1397B.

Mechanical pumps, in general, are used to pump to atmosphere and provide a suction pressure in the low vacuum range. This type is also used to provide the fore-vacuum required by other pump types, such as mercury or oil diffusion pumps. The mechanical pump characteristic, i.e., pumping speed as a function of inlet pressure, is relatively flat over its full operating range and drops abruptly at the high vacuum end. The Roots type mechanical pump characteristic extends into the higher vacuum range where diffusion pumps are feasible, but is also requires a forepump and is at a weight disadvantage over most of its pressure range.

Where the throughput line Q_1 intersects the mechanical pump characteristic determines the inlet pressure of the pump. The same throughput, however, flows through the duct before it reaches the pump and thereby experiences a small additional pressure drop. This is shown on the diagram by the extension of the throughput line to the duct characteristic. The pressure found there is added to the pump inlet pressure to obtain the first stage pressure, P_1=2.3 torr. This duct compensation is the only calculation on the diagram which is not completely graphical.

The procedure is the same in determining the pressures in subsequent stages. It is interesting to note that the duct losses for all the later stages are larger than the pump inlet pressure, rather than smaller, as it was in the first stage. This means that the stage pressures would be very little different if there were a pump of infinite speed at the end of each duct.

In each of the pumping stages after the first, a fore-vacuum requirement is met by the pump of the preceding stage, so that the fore-pressure tolerance of each pump must be kept in mind. For example; the MCF-60 oil diffusion pump must be backed by a pump which can maintain a pressure of 1.2×10^{-1} torr or lower. The mercury diffusion pump backing this pump maintains a pressure of 2×10^{-3} torr which is more than adequate.

Diffusion pumps may be classed as either fractionating or non-fractionating, but both employ the same basic operating principle. Molecules of gas move at random from the chamber being pumped into the inlet of the pump where they collide with a stream of hot vaporized pump fluid. The collisions propel the molecules toward the pump outlet where they collect and are compressed to a pressure level high enough for a fore-pump to handle. The vapor stream hits the cooled wall of the pump, condenses and flows back to the boiler at the base of the pump.

In the fractionating type of diffusion pump the condensed pump fluid is so directed that the most volatile components are vaporized and fed to nozzles nearest the pump outlet. This is done in a series of steps until the least volatile fractions are fed to the nozzle nearest the pump inlet. The fractionating type diffusion pump produces a lower ultimate pressure than the non-fractionating.

Cooled baffles are often used on the inlet of diffusion pumps to attain a lower ultimate pressure and also to reduce the back streaming of pump fluid to the chamber being evacuated. Baffles introduce a restriction to the pump inlet and consequently reduce the pumping speed of the pump. It is handled just the same as a duct loss. It is important to point out here a note of caution in considering the characteristic of diffusion pumps. As the inlet pressure rises the speed drops off and

tends to follow a line of constant throughput. In a dynamically pumped system, if the pump is required to operate near this portion of the characteristic, the system will most likely be unstable. If the throughput is increased slightly (and only for a short time), the result will be the same as though there were no pump at all. The system will fill with gas until the pressure rises above the fore-pump pressure.

Two other kinds of vacuum pumps used in the pumped gun program are not shown in Fig. 3.02.01(d). They were used in both of the installed gun systems, and their characteristics are plotted in Fig. 3.04.03 of the next section.

The air ejector is a type of pump which requires no moving mechanical parts and is generally used in the low vacuum regions. This pump uses the jet action of one fluid to entrain and compress another. Ejectors operate efficiently only up to a definite maximum ratio of compression. The maximum economical compression ratios vary from 6:1 to 10:1 depending on velocity profile. This type of pump becomes attractive when a relatively inexpensive supply of motive air is available and space and weight limitations preclude the use of mechanical pumps.*

Sorption pumping differs from the other types mentioned in that it is a batch process rather than continuous. The pumping rate is a function of the quantity of gas already taken up by the adsorbent.

This type of pump utilizes the gas sorption ability of a material such as alkali metal aluminosilicates, which is greatly enhanced at liquid nitrogen temperatures. The crystal structure is such that when the water of hydration is driven off, about one half of its volume becomes empty cavities which allow the material to adsorb gaseous products.

The ultimate pressure attainable with this type pump is a function of the number of molecules adsorbed, which implies that in a given system a low ultimate pressure will depend on the degree of prepumping.

*The pump labeled HG-45 in Fig. 3.02.01(d) contains an ejector to raise the fore-pressure tolerance of the entire unit. Unlike the air ejector, its working fluid (mercury) is condensed, again changing the characteristic somewhat.

This type of pump is ideally for applications where the operation of the pump must be self-sustaining.

With the pumping diagram as presented in Fig. 3.02.01, it is now possible to introduce design changes in orifices, pumping ducts or vacuum pumps and readily evaluate the significance of each change prior to actual testing.

In the preceding example of a dynamically pumped system, the vacuum pumps selected were, in part, readily available for the laboratory test set up. Each pump, as shown in Fig. 3.02.01, was used to fullest advantage, i.e., the pumps were not unnecessarily oversize. A Roots type pump could have replaced the mercury ejector but would not have been used to best advantage, since this pump is designed to maintain a high ultimate vacuum.

Proper pump selection may also depend on factors other than pressure and throughput. Limited size, weight, power and cooling capacity may all affect pump selection. System contamination tolerance due to diffusion pump back-streaming may preclude the use of mercury pumps or certain type oils and oil pumps. Start up and shut down procedures and times for some pumps could affect the overall operation sequence of a given system. All of these factors make pump selection a major and important effort in designing a dynamically pumped vacuum system.

3.04. Pumped Gun Application

Introduction:

The first approach to the use of a dynamically pumped gun for project experiments was by the purchase of a unit from W. C. Heraeus, Hanau, Germany. This filamentary cathode gun was designed for 150 kv maximum accelerating voltage and was provided with a three-stage vacuum system. The anode half of the accelerating gap could be moved laterally to trim up the beam alignment, and a magnetic lens, also movable, was used to focus the beam on the last orifice. Before the modification work was begun, the unit was checked out in the as-delivered condition. The currents obtained fell somewhat short of the manufacturer's indications, and some experimentation was required to discover the set of mechanical settings, lens current, bias and accelerating voltage which gave an adequate current, well focused for good transmission through the orifices.

Modifications:

Many details had to be modified to suit this gun to the system shown in Fig. 3.04.01. An extra vacuum stage was added, together with a shutter valve on the original outer orifice. This reduced the pumping requirements and made it possible to vacuum seal the gun for extended periods, thus improving the high voltage performance in operation. An insulating oil tank of lighter weight and smaller dimensions replaced the one supplied by Heraeus to shield the leads from the cable connector to the cathode feedthrough terminals. Enclosed in this oil tank were a filament isolation transformer and resistor to provide cathode bias for stabilization of the beam current. Because the power supplies were fitted with Seifert cable connectors from the window tube program, the same connector was used in the gun as well.

The gun was to be installed vertically, instead of horizontally as designed, so all the vacuum ducts had to be changed and adapted to the unconventional sources of fore-vacuum available in the installation.

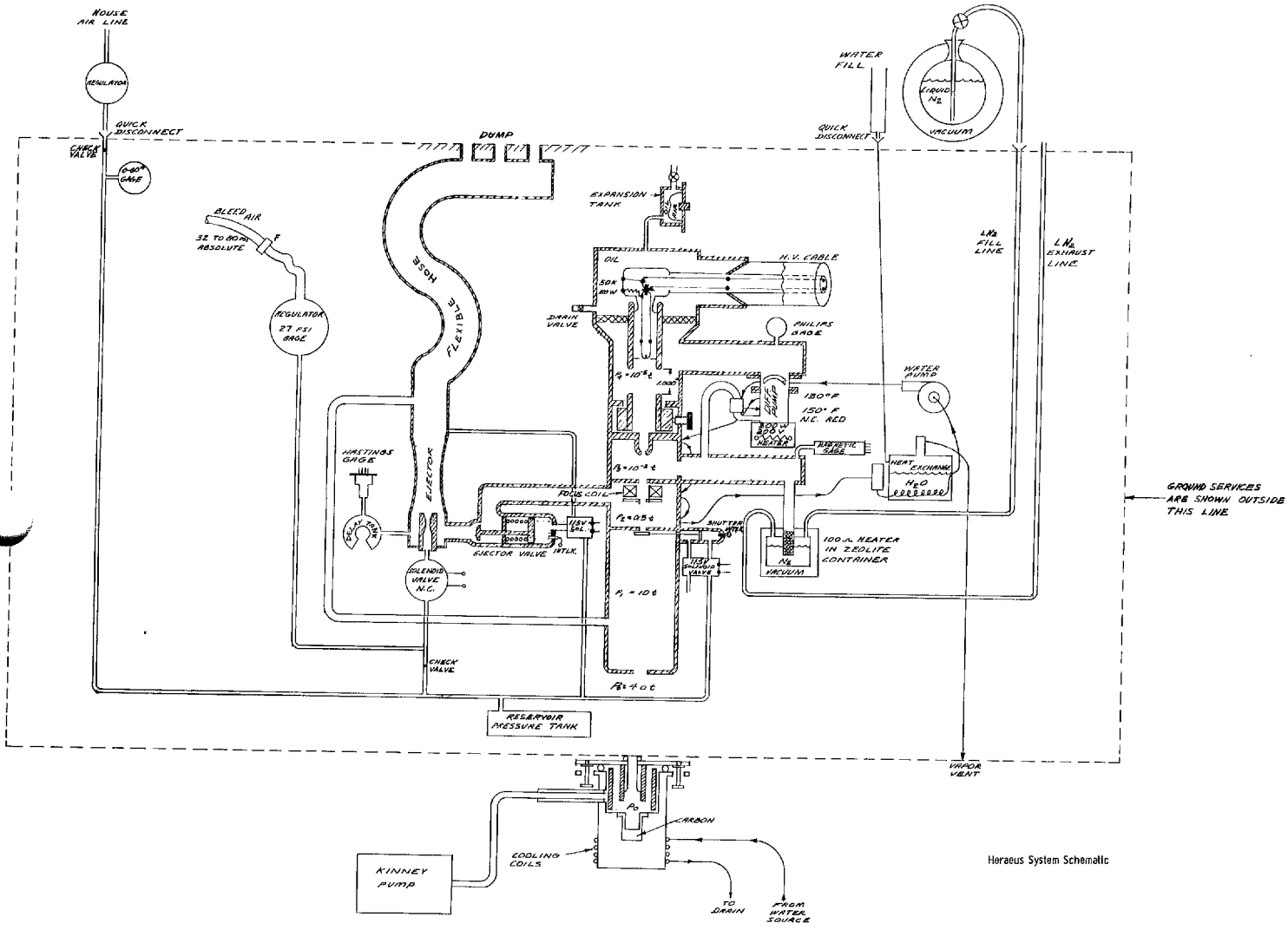

Heraeus System Schematic

Fig. 3.04.01

The changed attitude of the gun also made necessary a better vacuum seal at the magnetic lens, which previously had hung from its adjusting screws through the chamber wall without a positive seal.

The Heraeus gun in its original form, Fig. 3.04.02, required a large mechanical vacuum pump for each of its three stages. This pumping scheme was out of the question in the intended application, so a new set of smaller light weight pumps was incorporated in an optimum four-stage design. The original first stage was modified slightly and combined with a new first stage to form the front end and main support assembly.

A sliding shutter type air-operated valve was added to the N_2 nozzle and a Bellofram piston air-operated valve was added in the P_2 duct for vacuum control. The choice of air actuation was made after calculations showed how much weight and cooling would be involved with direct solenoid actuation.

Hand valves were installed in the air control system to permit operation of the unit for check out and test purposes.

A new recirculating flash evaporative type cooling system was added to the Heraeus to cool the gun nozzles and diffusion pumps.

The redesigned pumping complement had to be much lighter and smaller than the original mechanical pumps and yet maintain a P_4 pressure of 10^{-4} torr or less in the electron generating and accelerating chamber. The discharge pressure requirements, on the other hand, were reduced considerably because the unit was to operate into a pressure of 30 rather than 760 torr.

Numerous pumping schemes and combinations were considered before the following combination of four pumping stages were decided upon:

The first stage consisted of a wedge-shaped ramp mounted on the upper hatch of the Q-bay. The ramp performed well enough to be considered a pump capable of a 3:1 pressure reduction below ambient at operating conditions. This ramp pump then was capable of maintaining a pressure of 10 torr in the first stage chamber and also of providing the fore-vacuum for the second stage pump.

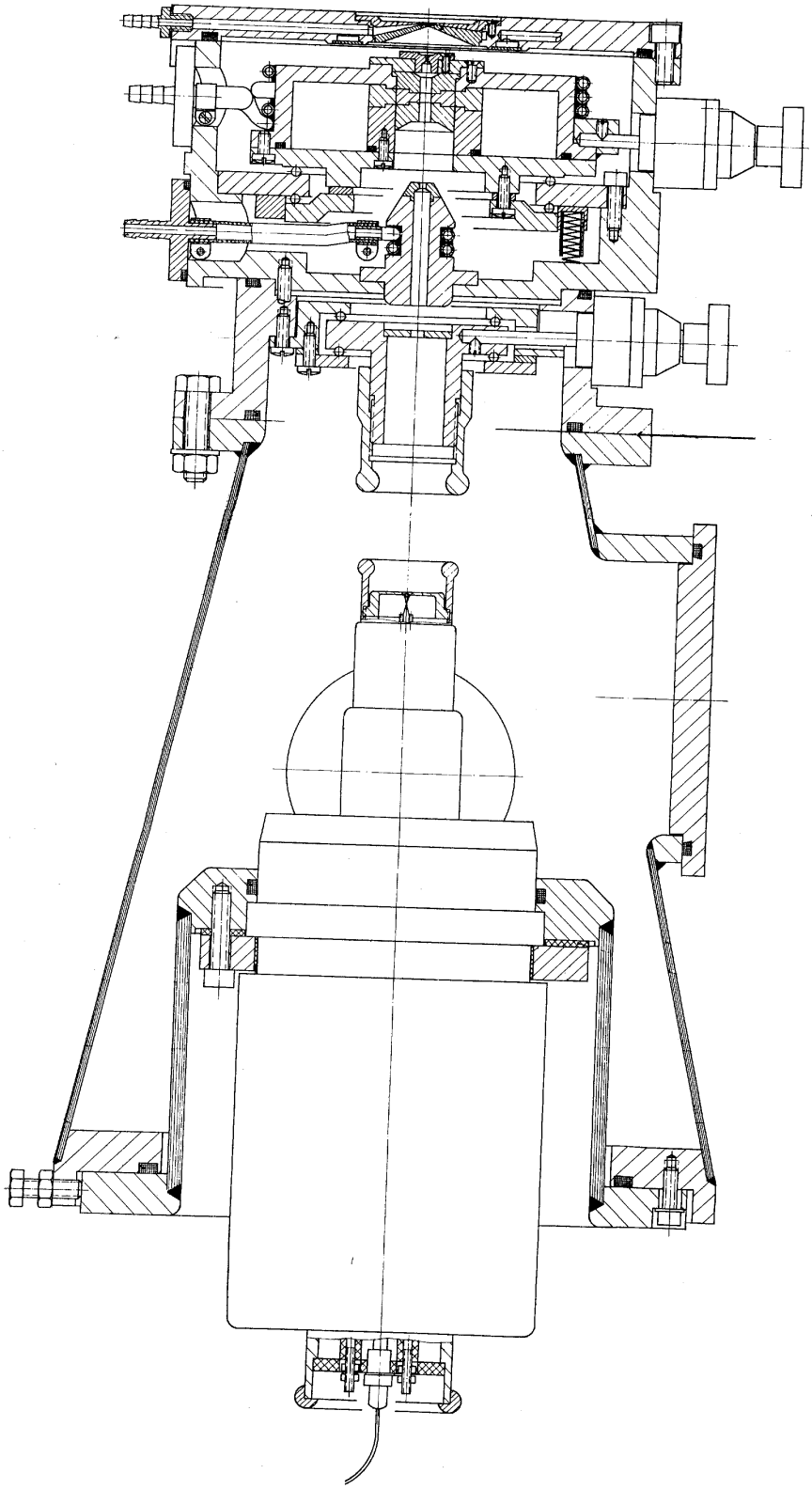

Heraeus Gun

Fig. 3.04.02

An air ejector designed and developed by Schutte and Koerting Company was used as a second stage vacuum pump. At altitude, air pressure at a minimum of 20 psia was available as a working fluid and proved a satisfactory motive air supply to operate the ejector. The ramp, or dump as it was otherwise called, was able as a fore pump for the ejector to maintain 10 torr in P_1 and also to handle the discharge from the ejector. The suction side of the ejector, P_2, could be maintained at approximately 0.5 torr.

The first version of the operational system incorporated a mercury diffusion pump in the third pumping stage. The lowest fore-pressure attainable for this stage was 500 microns of Hg, much too high for oil diffusion pumps. The fore-pressure tolerance for mercury pumps is of the order of 2 mm of Hg, well above that maintained by the ejector of the preceding stage. Unfortunately, the backstreaming of mercury into and through the orifice of the gun caused endless maintenance problems.

A sorption pump was substituted for the mercury pump to eliminate the mercury problem. Although this pump operates on a batch process and has a limited useful life between regenerations, it proved more than adequate for the intended service. A considerable improvement in operating procedure was realized also. The high vacuum P_3 and P_4 chamber could be pre-pumped prior to actual operation, greatly reducing the incidence of arc-over.

The main gun P_4 chamber was pumped on by an oil diffusion pump and adequately backed at 10^{-2} torr by either the mercury pump or sorption pump on the preceding stage. To minimize oil backstreaming to the cathode assembly or insulator, a water cooled baffle was used at the pump inlet. This reduced the chance for electrical arc-over. The ultimate vacuum maintained in the P_4 chamber with this pump and baffle combination was 3×10^{-5} torr.

A design diagram for the dynamic pumping system described for the Heraeus unit is shown in Fig. 3.04.03. The pressures shown are for

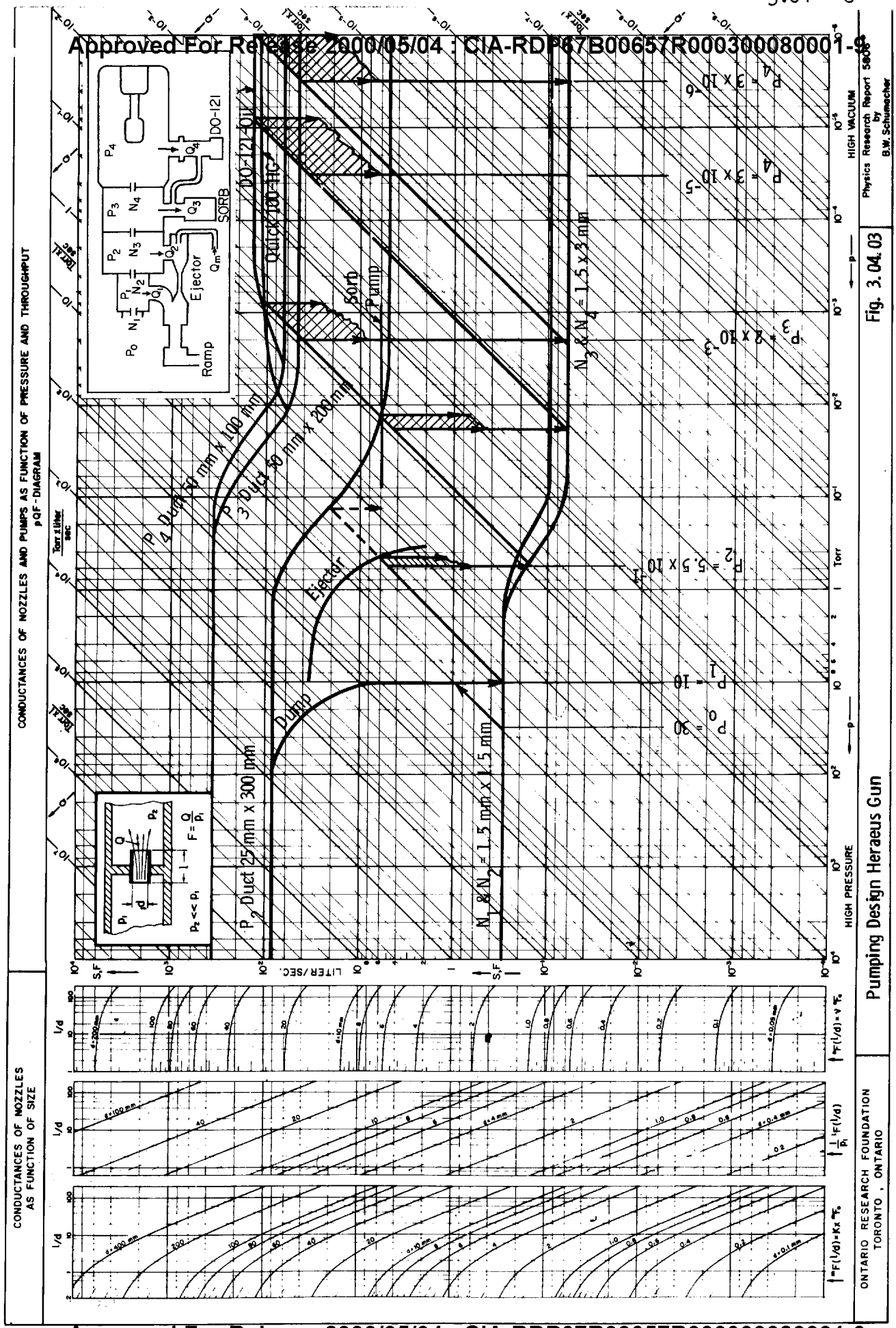

either pump on the fourth stage. Pressures shown for the sorption pump represent those attained after a typical regeneration and prepumping cycle.

Installation:

The Heraeus system was mounted in the aft end of the equipment bay as shown in Fig. 3.04.04. The front or lower end of the gun was mounted on the lower door and supported the total weight. Fore and aft loads were transmitted to the aft wall of the equipment bay through a yoke attached to the main body of the gun.

The ramp was mounted on the top door of the bay and sealed to prevent leakage. A flexible 2-1/2 inch line with enough slack was secured to the inner ramp tube with the top door partially open. The short excess dump line was then free to take a gradual bend when the door closed.

The first cooling system was completely open to the dump. The installation had all the water cooled components in series from the pump outlet at the high voltage tank to the inlet at the diffusion pump. Though basically a simple system, one outstanding drawback was that the low dump pressure created cavitation in the pump.

To remove this cavitation problem, a closed circulating cooling loop was substituted. The closed loop reservoir formed a constant temperature heat exchanger during operation, with the reservoir acting as a boiler at dump pressure. Boiler temperature in operation was estimated at 30-40°C, depending on altitude. An expansion chamber was included for the dual purpose of filling the closed loop and allowing for thermal expansion of the closed system. During system check-outs cooling water was run in and out of the reservoir to avoid any build up of temperatures during operation at atmospheric pressure.

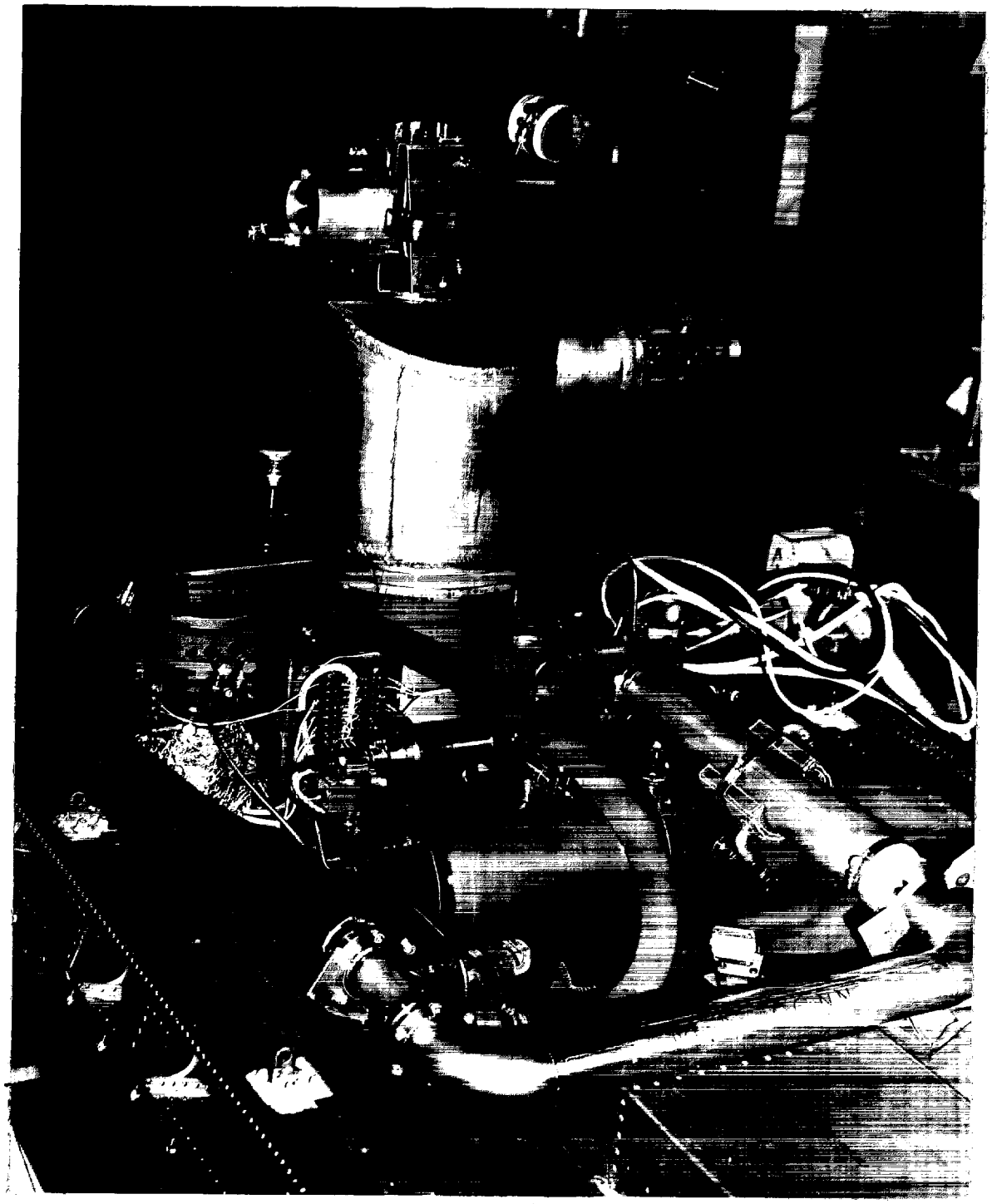

Q-Installation, Heraeus Gun

Fig. 3.04.04

CHAPTER 4

C-GUN AND BOLT CATHODE

4.01. Introduction

The intention to mount guns in the chines entailed radical changes in design from that of the modified Heraeus gun. Weight and space became prime concerns, and it was clear that all components must withstand the vibration, temperature and pressure conditions of the new environment with minimum assistance.

One of the most effective steps in meeting these needs was the integration of the gun and power supply cases, eliminating high voltage cables and connectors and providing a measure of cooling for the gun not otherwise available. This approach did impose space limitations on the power supply, however, and these could be met only by components for normal temperature ranges, so that thermal insulation and cooling had to be provided for the supply.

Considerably greater currents were desired from the C-guns than the Heraeus filament could provide, so another cathode with greater capabilities was sought. Development of the bolt cathode sub-system permitted currents in excess of 100 milliamperes to be supplied with reasonable tolerance to the ion bombardment that is inescapable in a dynamically pumped gun.

Operation of the Heraeus gun had heightened appreciation of the stamina that must be built into a system to be installed in such an inaccessible location as the chine bays. At the same time, constraints on space, weight, interference with existing structure, and development time forced a number of compromises. None of the particular forms in which the equipment is reported here represents an evolutionary dead-end; all the developments lead toward what would be considered an ideal form for an operational system.

4.02. The Bolt Cathode

Introduction:

The large emission currents required, with exposure to a stream of ions during operation, recommended the sturdy bolt cathode introduced by E. Bas.[1] This cathode is comprised of a rod of tungsten, surrounded near its emitting by a helical filament, from which an electron current can be drawn to heat the rod by bombardment. By a suitable choice of dimensions and materials, a rugged, long-lived cathode structure is obtained, Fig. 4.02.01. It is suitable for operation at moderate vacuum (less than 10^{-4} T), even in the presence of several milliamperes of positive ion bombardment and when frequently exposed to atmospheric air between operations. Some added complexity results from the need for bombardment power, rather than filament power, but the advantages gained by using this type of cathode far outweigh any such disadvantages.

Before accepting the extra complexity of the cathode heating supply, a check was made in the Heraeus gun with a filamentary cathode having several turns at the emitting knuckle instead of the 3/2 turns in the regular Heraeus filaments. When space-charge limited, the cathode supplied only about 45 ma at 150 kv. Greater extension of the filament, so that the beam was hopelessly unfocused, raised the emission current only to 50 ma. (These figures are extrapolated from performance at lower voltages and currents, since the Seifert power supply used was limited to 30 ma output current.)

In the cathode development program, the first step was to produce some cathodes suitable for use directly in a Heraeus gun, which was then being used as a test facility. Initial troubles with the auxiliary supply, mechanical stability of the grid ring support and failure of the filament contact springs in the Heraeus stem had to be cleaned up first. By the time a working state had been achieved, a modified cathode stem for the Heraeus gun was ready, permitting use of the 'final' form cathodes in the Heraeus gun. With the same form of

1. E. B. Bas, Z. angew. Phys. 6, 404 (1954).

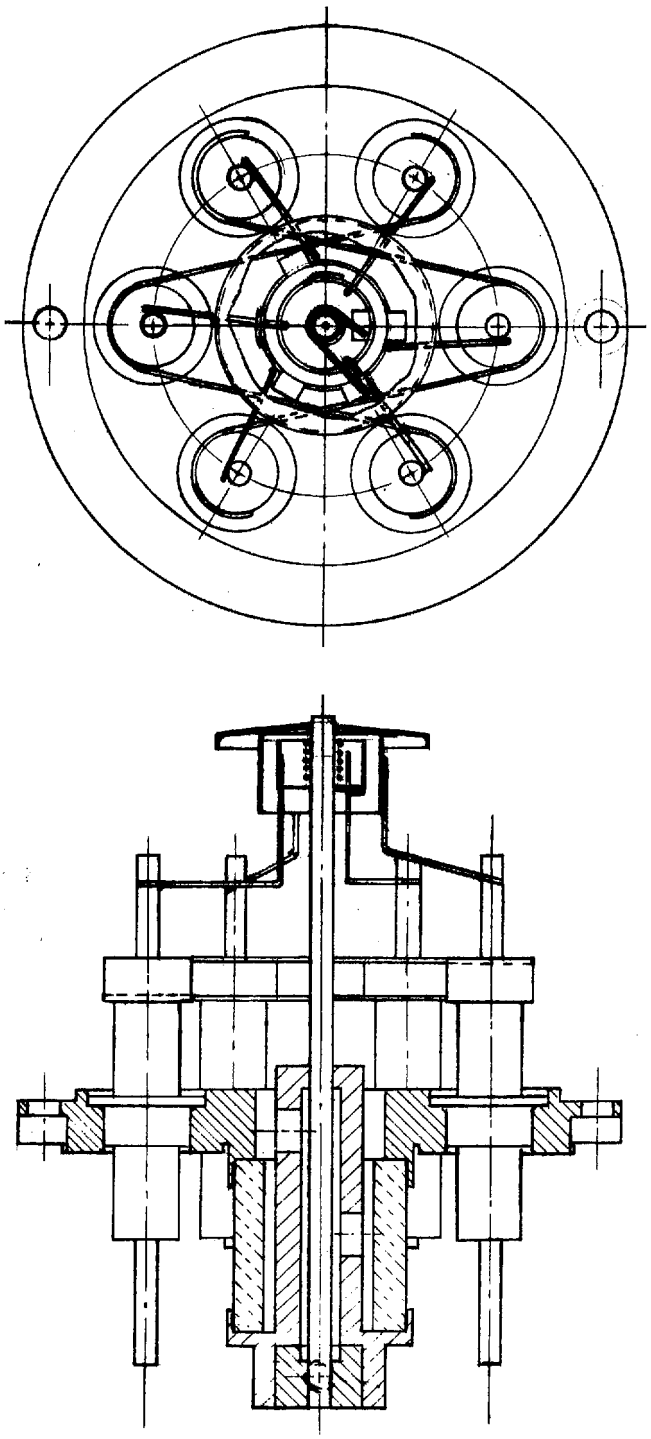

Bolt cathode construction

Fig. —4.02.01

grid structure preferred by Bas, the long focus required to traverse the series of orifices without excessive divergence of the beam envelope could not be obtained. An auxiliary grid was added, but this cut both the perveance and the high voltage capability of the structure. A Wehnelt cylinder, equivalent to the Heraeus electron optics, provided better perveance, more stable mechanical structure and almost 20 kv greater flashover.

A fully adjustable cathode structure of this type was made to accommodate the range of dimensions which might be desired and that design was employed throughout the remainder of the project. A simplified form, with spinnings substituted for the solid metal shapes, and fixed dimensions eliminating the troublesome threaded adjustable parts, has been built and would be recommended for any future operating.

General Design Considerations:

It was decided to adopt the Bas-type bolt cathode because of the relative simplicity of its structure shown in Fig. 4.02.01. However, certain modifications were necessary. A table of tungsten filament characteristics, Table 4.02.01, shows that a current density of about 5.1 amperes per square centimeter can be obtained from a tungsten cathode at a temperature of 2700° Kelvin or 2427° Centigrade. At this temperature the evaporation rate is not excessive, and the bolt diameter would have to be about .060". To minimize conduction losses it was decided to maintain the bolt face about one inch above its closest support.

The coil design presented some minor problems. Bas described a figure of merit for a coil[2] as the ratio of the coil inside diameter to the coil wire diameter and recommended values of 6:1 to 8:1. In our design it was decided to maintain about the same spacing between the bolt and the heater coil that Bas had used. That is about .016". Thus our coil I.D. became .092". To obtain a good figure of merit, the heater wire should have been 12 mil diameter, but this would have required

2. E. B. Bas, Z. angew. Phys. 7, 337 (1955).

Table 4.02.01: Specific Characteristics of Ideal Tungsten Filaments
(For a wire 1 cm in length and 1 cm in diameter)

T, °K	W', $\frac{W}{ld}$, watts/cm²	$R' \times 10^6$, $\frac{Rd}{l} \times 10^6$, ohm-cm	A', $\frac{A}{d^{3/2}}$, amp/cm$^{3/2}$	$V' \times 10^3$, $\frac{V\sqrt{d}}{l} \times 10^3$, volts/cm$^{1/2}$	I', $\frac{I}{ld}$, amp/cm²	M', $\frac{M}{ld}$, g/π cm²/sec, evaporation	$\frac{R'T}{R'_{293}}$, $\frac{RT}{R_{293}}$
							0.911
273		6.37					1.0
293	0.0	6.99	0	0			1.03
300	0.000100	7.20	3.727	0.02683			1.467
400	0.00624	10.26	24.67	0.2530			1.924
500	0.0305	13.45	47.62	0.6404			2.41
600	0.0954	16.85	75.25	1.268			4.93
700	0.240	20.49	108.2	2.218			3.46
800	0.530	24.19	148	3.581			4.0
900	1.041	27.94	193.1	5.393			4.54
1,000	1.891	31.74	244.1	7.749	3.36×10^{-16}	1.16×10^{-23}	5.08
1,100	3.223	35.58	301	10.71	4.77×10^{-13}	6.81×10^{-20}	5.65
1,200	5.210	39.46	363.4	14.34	3.06×10^{-11}	1.01×10^{-16}	6.22
1,300	8.060	43.40	430.9	18.70	1.01×10^{-9}	4.22×10^{-14}	6.78
1,400	12.01	47.37	503.5	23.85	2.08×10^{-8}	7.88×10^{-13}	7.36
1,500	17.33	51.40	580.6	29.85	2.87×10^{-7}	7.42×10^{-20}	7.93
1,600	24.32	55.46	662.2	36.73	2.91×10^{-6}	3.92×10^{-18}	8.52
1,700	33.28	59.58	747.3	44.52	2.22×10^{-5}	1.31×10^{-16}	9.12
1,800	44.54	63.74	836	53.28	1.40×10^{-4}	2.97×10^{-15}	9.72
1,900	58.45	67.94	927.4	63.02	7.15×10^{-4}	4.62×10^{-14}	10.33
2,000	75.37	72.19	1,022	73.75	3.15×10^{-3}	5.51×10^{-13}	10.93
2,100	95.69	76.49	1,119	85.57	1.23×10^{-2}	4.95×10^{-12}	11.57
2,200	119.8	80.83	1,217	98.40	4.17×10^{-2}	3.92×10^{-11}	12.19
2,300	148.2	85.22	1,319	112.4	1.28×10^{-1}	2.45×10^{-10}	12.83
2,400	181.2	89.65	1,422	127.5	0.364	1.37×10^{-9}	13.47
2,500	219.3	94.13	1,526	143.6	0.935	6.36×10^{-9}	14.12
2,600	263	98.66	1,632	161.1	2.25	2.76×10^{-8}	14.76
2,700	312.7	103.22	1,741	179.7	5.12	9.95×10^{-8}	15.43
2,800	368.9	107.85	1,849	199.5	11.11	3.51×10^{-7}	16.10
2,900	432.4	112.51	1,961	220.6	22.95	1.08×10^{-6}	16.77
3,000	503.5	117.21	2,072	243	44.40	3.04×10^{-6}	17.46
3,100	583	121.95	2,187	266.7	83	8.35×10^{-6}	18.15
3,200	671.5	126.76	2,301	291.7	150.2	2.09×10^{-5}	18.83
3,300	769.7	131.60	2,418	318.3	265.2	5.02×10^{-5}	19.53
3,400	878.3	136.49	2,537	346.2	446	1.12×10^{-4}	20.24
3,500	998	141.42	2,657	375.7	732	2.38×10^{-4}	20.95
3,600	1,130	146.40	2,777	406.7	1,173	4.86×10^{-4}	21.34
3,655	1,202	149.15	2,838	423.4	1,505	7.15×10^{-4}	

after Langmuir

inconveniently high heater currents. For this reason .010"-diameter heater wire, with a figure of merit of about 9, was used.

The inner heat shield, meanwhile, was designed to have an I.D. of about twice the heater coil O.D. The outer shield diameter was arbitrarily designed to be .100" larger than the inner. Both shields and the top shield as well were made of tantalum, because of its high melting point, low vapor pressure and ease of handling. The heat shield support legs were made of tantalum for the same reasons.

The specific design evolved from several considerations. One factor was the realization that the base might get as hot as 300°C after sustained operation. Under these circumstances, it was necessary to use only the best of hard vacuum, high-temperature materials and techniques. For this reason it was decided to use 94% (or better) alumina insulators. To obtain this type of insulator in relatively short time it is necessary to use simple, cylindrical shapes. Thus the cathode was designed around feed-thru-like structures. The metal parts were made of Kovar to match the ceramic expansion and the ceramic-to-metal seals were made by copper brazing.

The assembly was designed to permit replacement of the bolt. This was accomplished by means of a set screw in the bolt connection. Furthermore, it was considered essential that the location of the bolt should be accurately maintained relative to the circumference of the base. This was necessary to allow a bolt to be replaced without requiring re-alignment of the device.

The heater coil and shields were spot welded in place using jigs which had been designed to align them with the bolt axis and to locate them in their respective places in a strain-free condition. The heater coils made in the laboratory were severely stressed. To relieve this condition, a procedure was developed whereby the entire assembly (without the top shield) would be placed in an evacuated bell jar. Heater current would be applied, and the coil would move, relieving the winding stresses. Subsequently, the heater coil was re-aligned by

bending the supports. After this operation the top shield was welded in place. The use of commercial stress-free coils eliminated this step.

After completing the gun assembly it was found wise to operate the gun in a bell jar, drawing about 80 milliamperes from the cathode, for about one hour. This procedure culled out any defective assemblies prior to insertion in the final assembly.

Assembly Procedure:

One of the best ways to appreciate the details of design and performance of the bolt cathode is to follow the operations involved in preparing an assembly for use.

I. Reclaiming Used Assemblies
   - A. Cathode
     1. Cut off old shields
     2. Peel off tantalum wire welds on stem leads.
   - B. Grid Cup
     1. Polish outer surface of grid cup to remove oxide and possible pitmarks from arcs.

II. Parts Preparation
   - A. Stem Assemblies
     1. Liquid hone.
     2. Vapor degrease.
     3. Deionized water rinse.
     4. Methanol rinse.
   - B. Tantalum Shields and Tantalum Supports (1-1/2" long)
     1. Use treatment per "Materials and Technology for Electron Tubes" by Walter Kohl, page 220, or equivalent.
   - C. Tungsten Coil
     1. Use fired coil as is.

D. Grid Cup

1. Vapor degrease.
2. Deionized water rinse.
3. Methanol rinse.

E. After cleaning, all parts should be handled with gloves or tweezers and stored in dust-free containers.

III. Assembly

A. Inner Shield

1. Load the inner shield on the main welding jig.
2. Insert the bolt part of the main welding jig into the stem assembly.
3. Use the brass spacer to establish the location of the inner shield and lock the stem assembly set screw.
4. Preform and load three .025" diameter tantalum support rods. The upper ends of these rods should be inserted in the appropriate grooves in the main welding jig, under the inner heat shield.
5. Weld the lower end of each support rod to an alternate insulated pin on the stem assembly. Use welding heat 40 watt-sec, pressure 4 lbs. and set up A.
6. Now weld the inner heat shield to the upper end of the support rods. Use welding heat 29 watt-sec, pressure 4 lbs. and set up B. (Fig. 4.02.02)

B. Outer Shield

1. Load the outer shield onto the auxiliary electrode.
2. Slide the auxiliary electrode onto the main electrode.
3. Preform and load the upper ends of the three .025" diameter tantalum rods into appropriate holes in the auxiliary electrode.
4. Weld the lower end of these support rods to alternate stem leads as before. Use welding heat 40 watt-sec, pressure 4 lbs., set up A.

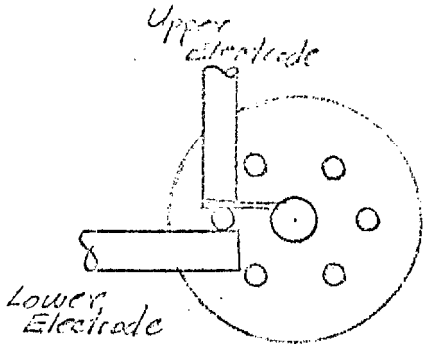

Set Up A

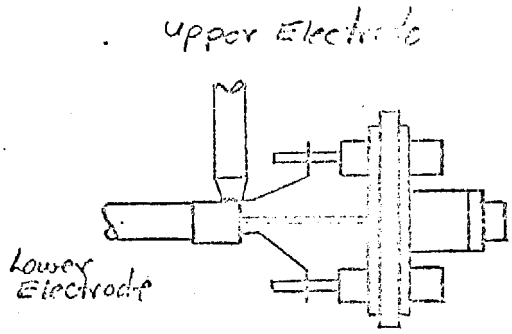

Set Up B

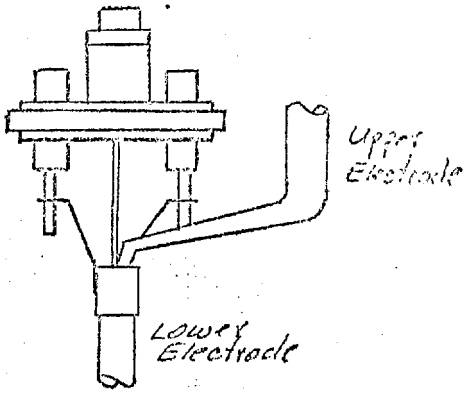

Set Up C

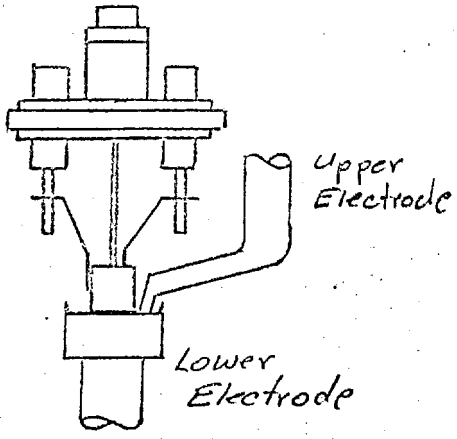

Set Up D

Electrode Set Ups for Welding Bolt Cathode Assembly.

Fig. 4.02.02

5. Now weld the outer heat shield to the support rods. Use welding heat 29 watt-sec, pressure 4 lbs., set up B.

C. Heater Coil

1. Load the heater coil on the mandrel of the heater welding jig.
2. Insert the jig into the inner heat shield and position the heater leg to lie on top of the inner heat shield tab.
3. Weld the heater leg to the heat shield. Use welding heat 19 watt-sec, pressure 3 lbs., set up C.
4. Weld the heater coil to the outer heat shield. Use heat 19 watt-sec, pressure 3 lbs., set up D.

D. Preliminary Inspection

1. Insert bolt into stem.
2. Reject if maximum bolt-to-coil spacing is greater than twice the minimum spacing.
3. Reject if there is any possibility of a coil turn to turn short.
4. Reject for any defective or questionable welds.

E. Top Heat Shield

1. Use top heat shield welding jig.
2. Weld three tabs on the outer shield to the top shield. Use heat 10 watt-sec, pressure 3 lbs., set up D.

F. Final Evaluation

1. Inspect under microscope.
2. Review items listed in preliminary inspection.

IV. Preliminary Operation

1. Assemble cathode into grid cup.
2. Locate bolt face with respect to grid cup.
3. Methanol rinse.

4. Operate in bell jar for approx. 1/2 hour.
5. Fill out file card on assembly providing spacing data and test information.
6. Pack assembly in clean dust-free container.

Performance:

To evaluate the cathodes, a setup was made in a bell jar with an anode close enough to the bolt to get emission at lower voltages. The anode for this test was initially made of copper and was set on a glass ring over the cathode. Later setups used a tungsten anode set in a large copper heat sink. The anode-to-cathode spacing was established by means of an adjustment. For our tests the spacing was established by means of a 0.020 inch shim. It was estimated that the bolt expanded 0.005 in. when heated, thus an approximately 0.015 in. cathode-to-anode spacing was reported. Typical bolt cathode characteristics are shown plotted in Fig. 4.02.03. The curve seems to deviate from the 3/2 power characteristics at about 150 volts. The linear characteristic in the temperature-limited region is similar to the "hollow cathode" characteristic. It probably represents the addition of current to the beam from the sides of the bolt.

A test was conducted to try to evaluate the amount of current going to the anode which originated from the heater coil, instead of the bolt. It was found that when the bombardment voltages were turned off, the anode current dropped to less than a few tenths of a milliampere. Thus at an operating condition of about 100 milliamperes plate current, the extraneous current originating from the heater coil would be less than 0.5%.

Fig. 4.02.04 is a round-robin chart of bolt-cathode characteristics. Chart 1 shows values of constant bolt current as a function of heater power and bombardment power with a spacing of approximately .015" and an anode voltage of 500 volts. From the curve it can be seen that there is a minimum heater power below which no bolt current can be obtained. This is because the coil gets so cool that no bombarding currents can be obtained. On the other hand, as the heater power is

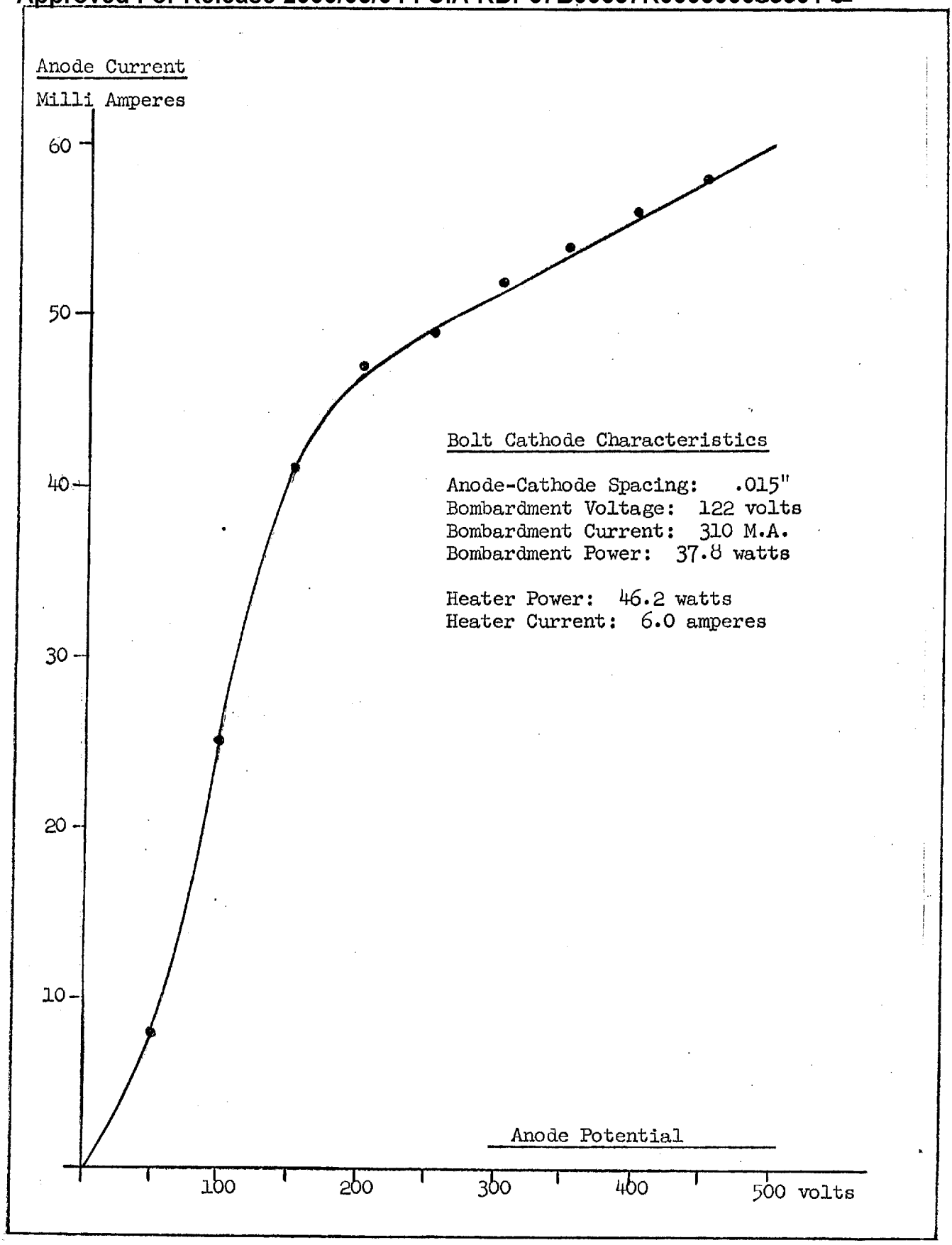

Figure 4.02.03

Approved For Release 2000/05/04 : CIA-RDP67B00657R000300080001-9

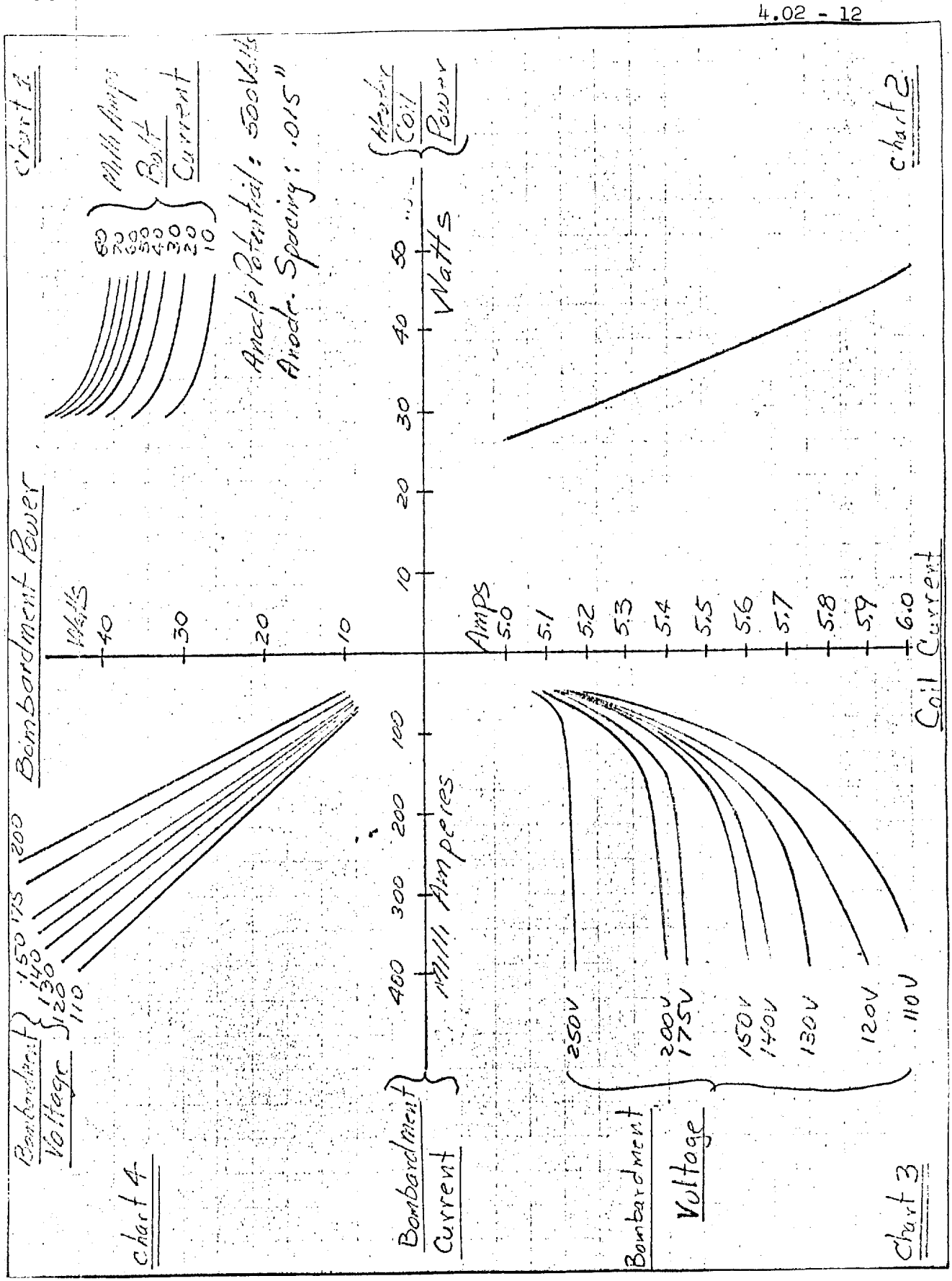

BOLT CATHODE CHARACTERISTICS

Fig. 4.02.04

increased, the increase in bolt current gets less. This is because the efficiency of the radiant heating from the coil falls off as the bolt gets hotter. This clearly shows the advantage of bombardment heating.

Chart 2 is a plot relating coil current to heater coil power. There may be as much as 5% error here, because this curve can also be a function of bolt temperature. When the bombarding power makes the bolt hotter than the heating coil, the bolt radiates heat to the heater. Under these conditions, the heater temperature increases and the coil resistance increases. As the power is equal to I^2R (square of the current multiplied by the resistance) the increase of coil resistance means an increase in heater power for a given coil current. This phenomenon will cause a shift in the slope of the curve. For illustrative purposes the curve shown is sufficiently accurate.

Chart 3 relates heater coil current to bombardment at several bombardment voltages. This plot is actually a portion of the standard graph of diode emission versus cathode temperature. This is the case as the bolt is actually the anode in the bombardment circuit. As the coil current increases, the temperature increases and the emission current at a given anode voltage goes up. However, at some value of current, the diode system should become space charge limited. At this point any increase in cathode temperature would have very little effect on anode current. Obviously, under the conditions plotted, the bombardment current was always temperature limited.

Chart 4 shows the linear relationship between bombardment current and power as a function of bombardment voltage.

Vibration Testing of Bolt Cathode:

One of the design objectives was a cathode which could withstand the vibration it might experience, and the units appeared rugged enough, except for the unavoidable brittleness of the filament after recrystallization in operation. To test the vibration resistance, a shaker was set up in a bell jar to excite a bolt at operating temperature. Vibration instruments for the temperature and pressure conditions were not

immediately available, so the following method of measuring displacement was adopted. Pairs of lines were scribed on the rod connecting the cathode to the shaker. Each pair spanned some measured axial distances, e.g., 0.010". Since the excitation was sinusoidal, an observer saw an image at each end of the displacement. Therefore, at a displacement equal to the separation of a pair of lines, that pair appeared to be three lines.

Vibration exposure corresponding to the "Design Vibration Envelope", Fig. 4.02.05, produced no ill effects in the bolt cathodes.

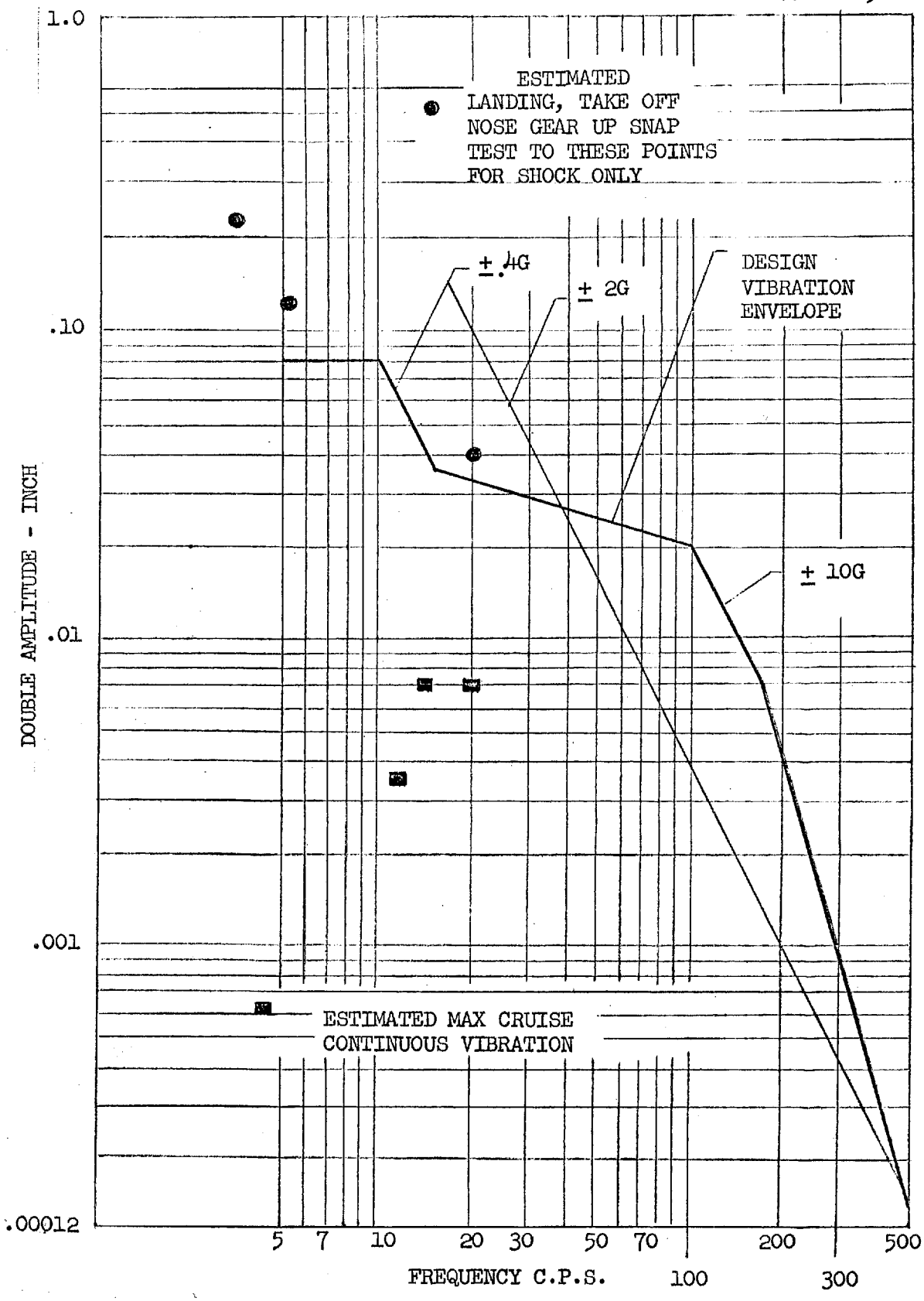

VIBRATION AND SHOCK SPECIFICATION

Fig. 4.02.05

4.03. Electron Optics

Summary:

The simple grid cup used by Bas[1] was adopted along with his cathode structure, but it proved to make too short a focus. The field in a flat cone, concave toward the anode, converges a beam emitted at the apex too quickly.

Next, an auxiliary cup recommended by Bas[1] for longer focus was added with good results, but the exact physical form was not too well suited to 150 kv operation, having been developed in work at much lower energy.

At this point in the development, it became evident that the new gun being designed for chine installation would be much simpler and more reliable if the anode elements could be tilted, rather than translated, for fine correction of the beam direction. A flat plate anode was far better in such a scheme than a toroidal shape, and it had the further beneficial effect of cutting in half the power of the electrostatic lens formed by the accelerating gap.

With a set of approximately correct dimensions established, a focusing assembly was desired which could be varied enough to verify the optimum settings at full voltage. This developed into Fig. 4.03.01, which was used throughout the experimental program. Interchangeable grid diaphragms were held between rings threaded inside the shell, and the focusing cup was internally threaded to go over the shell. The cathode assembly, Fig. 4.02.01, was held in the shell with two screws.

Laboratory Tests:

A preliminary laboratory apparatus to measure beam geometry and to understand control of this beam by varying cathode and anode dimensions was set up. It consisted of the following three units:

(1) Seifert High Voltage Supply (control unit and transformer).

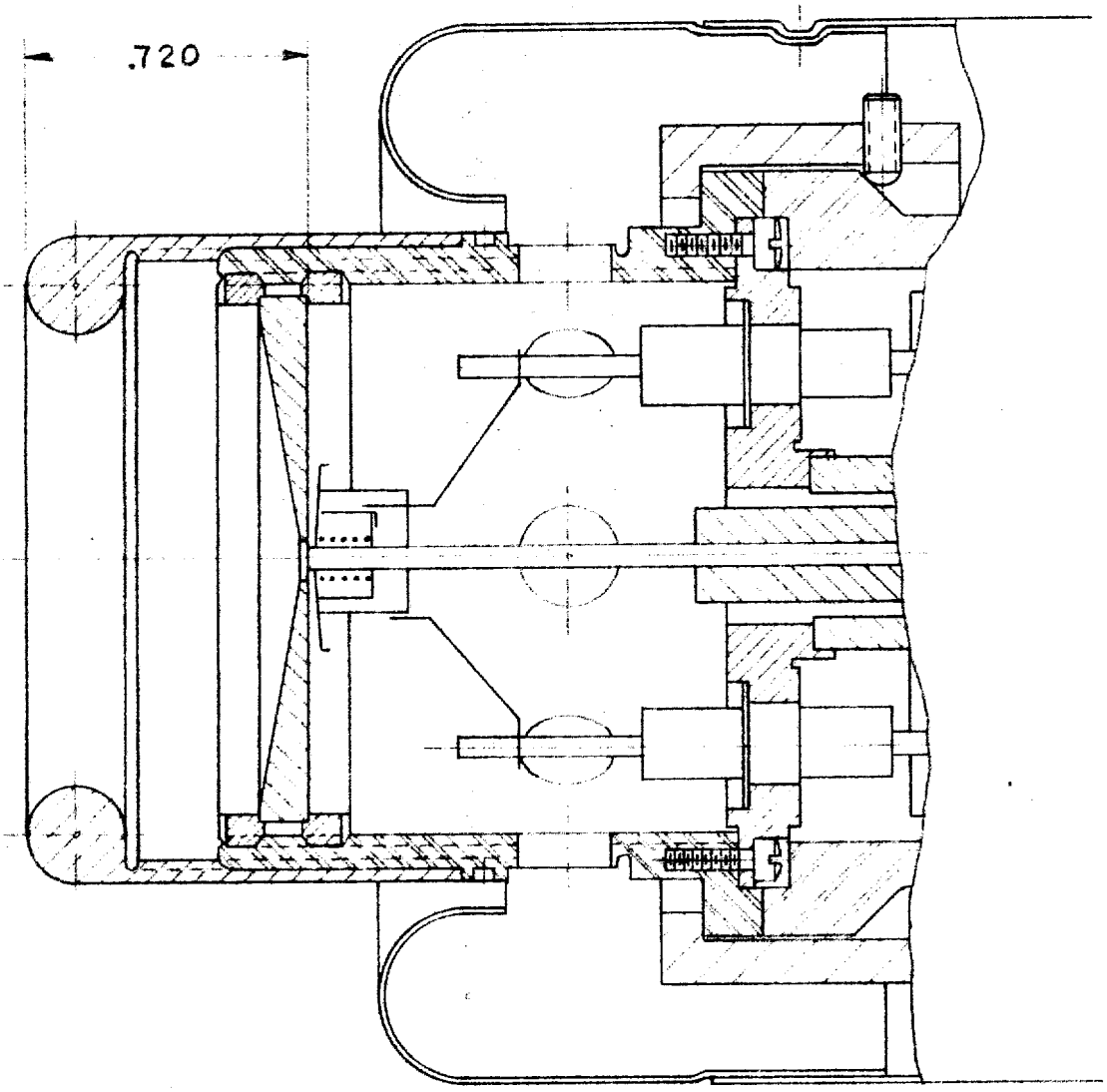

Adjustable Grid Assembly

Fig. 4.03.01

(2) An auxiliary power supply for producing filament heating, bombardment power and grid bias voltage.

(3) An Heraeus electron beam gun adapted to receive experimental cathodes.

The beam transfer section of the gun was replaced by a 4-inch-diameter glass pipe 2 feet long, terminated by a water-cooled copper cap attached to a graphite disc that acted as the high-energy electron collector. An independent vacuum pump on this volume removed it as a leakage source into the gun cathode chamber.

The envelope of the beam was studied by two methods. One method utilized the visible light produced by molecules of gas excited by collision with electrons in the beam. The beam was observed and photographically recorded by means of a periscope through the lead shielding to give maximum radiation protection to the operator. No attempt was made to relate the light intensity in the beam as a function of the beam cross section, since the major concern at the time was to locate the cross-over point of the beam and study its movements as a function of cathode dimensions.

The other method employed for beam geometry analysis involved the insertion of thin metal discs at various locations beyond the anode. The beam rapidly penetrated these discs and melted holes whose dimensions were simply taken as the extreme envelope of the electron beam. This system was the final one employed to determine cathode dimensions to be used in the C-gun, because the discs could be inserted at points along the beam axis inaccessible to visual observation.

Various disc thicknesses of different metals were inserted in the beam path to determine the optimum material and thickness that would most accurately define the beam envelope. Aluminum metal of less than one mil thickness proved to be unwieldy in that the electron beam did not cut a circular hole but rather an undefined aperture with an irregular, ragged appearance. When the metal thickness was increased to beyond 5 mils, excessive out-gassing occurred as the beam melted the metal and high-voltage operation became unstable. Instead of a thin

edge around the perimeter of the electron beam hole there was a circular aperture built up in the manner of a doughnut. It was felt that the beam diameter reported would be more credible if the perimeter of the melted area were minimized in thickness. After experimentation with various thicknesses of stainless steel and aluminum discs it was found that .005 in. aluminum or .0035 in. stainless steel discs produced the best defined holes.

Most of the tests on this system were run at 100 kv, because too much time would have been required to season the gun to a higher voltage. The mean on time was 30 secs to 60 secs, depending on how stable the target current had become (it was assumed that when target current became stable, the discs were melted out to their limits for the beam).

Data from these discs test are briefly summarized below (see facsimile of data book page K1674352 in Fig. 4.03.02) with the focus cup depth, S_{ggg} varied (all other variables fixed):

Run		
#12	S_{ggg} = 15/32",	crossover point 10" from anode
#13	S_{ggg} = 13/16",	crossover point 1-1/4" from anode
#14	S_{ggg} = 5/8",	crossover point between 2" and 2-3/4" from anode

These tests were taken at 100 kv, 10 ma, and zero bias. The discs used were 3-1/2 mil stainless steel and the ambient pressure surrounding the discs was in the order of one micron. The grid-to-anode spacing was varied from 1-1/32" to 1-5/16"; however, that change seemed to produce only small changes in the beam geometry compared to the change in focus cup depth.

This appears to be the case as long as the anode plate is flat, with a relatively small aperture compared to the extension grid aperture.

The effects of bias were checked on this particular cathode geometry. (See data book page K1674348 in Fig. 4.03.03).

K 1674352

SUBJECT: Note, measured $S_{gp} = 1\frac{26}{32}'' = S_{HV} + S_{ggg}$ cold setting

CUSTOMER: This page { S_{g2} = 14 mils ; S_{gb} = −1 mil }

SERIAL NO.

S. O. OR TEST NO. D. OR L. SPEC. NO. SHAFT NO. FRAME NO.

TO DETERMINE → By Dr. McCurdy's Calc., The Dynamic ("hot") Dimensions will Be → { S_{gb} = +2 mils }

(12th run)

Bias	KV	Ip	I_T	V_B	I_B	V_F	Press.	Time	S_{HV}	S_{ggg}	Discs
0	100	10 ma.	7.5 (cling/ly)	140	290	8.2	—	2 min	$1\frac{10}{32}''$	$\frac{15}{32}''$	$3\frac{1}{2}$ mil S.S. Discs

Purpose of Run #12 → Study effect of gg adjustment on Beam focal pt.
– Moved grid Extension Toward Bolt by $1/32''$ } New $S_{HV} = 1\frac{11}{32}''$, $S_{ggg} = \frac{15}{32}''$

$\frac{1}{8}''$ cu anode plate

$\frac{1}{4}''$

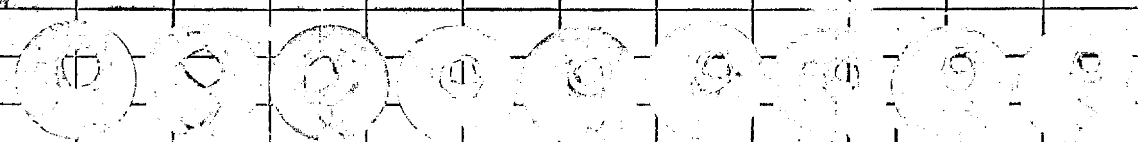

$S_1 = \frac{1}{4}''$ | $3/4''$ | $1\frac{1}{4}''$ | $1\frac{3}{4}''$ | $2\frac{3}{4}''$ | $3\frac{3}{4}''$ | $4\frac{3}{4}''$ | $5\frac{3}{4}''$ | $6\frac{3}{4}''$

205 mils (ave) — 165 mils (ave) — 82 mils (ave)

Beam ⇒ $D_{xd} = \frac{1}{2}''$

Focal pt. Beyond Exit

(13th Run)

Bias	KV	I_p	I_T	V_B	I_B	V_F	Press	Time	S_{HV}	S_{ggg}	Discs
0	100	10	7.5	150	270	8.2	2×10^{-4}	$1\frac{1}{2}$ min	$3\frac{1}{32}''$	$13/16''$	$3\frac{1}{2}$ mil S.S. Discs

Carefully Purpose of Run #13 → Check Repeatability of Standard Configuration Such as Run # 11 →
Made close agreement with #11 Keeping in mind Vacg This Run Was Than Vac. of #11

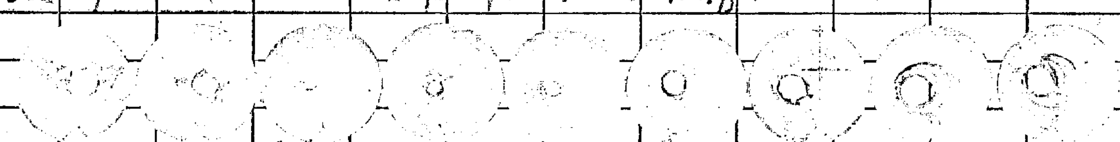

$S_1 = \frac{1}{4}''$ | $3/4''$ | $1\frac{1}{4}''$ (60 mils) | $1\frac{3}{4}''$ | $2\frac{3}{4}''$ (75 mils) | $3\frac{3}{4}''$ | $4\frac{3}{4}''$ | $5\frac{3}{4}''$ | $6\frac{3}{4}''$

$D_{xd} = \frac{1}{2}''$ ⇒ Beam

(14th Run)

Bias	KV	I_p	I_T	V_B	I_B	V_f	Press.	Time	S_{HV}	S_{ggg}	Discs
0	100	10	8	140	280	8.2	—	2 min	$\frac{37}{32}''$	$\frac{20}{32}''$	$3\frac{1}{2}$ mil S.S. Discs

(HV discharge > 15 ma I_p)

Note: In Run #12, Focal spot is Beyond discs Toward Collector outlet. In Run #13, Focal spot is Approx $1\frac{1}{4}''$ From Anode Plate. This Test is made with The Grid Extension Adj To A spot ≈ ½ way Between its Adj used in Nos 12 and 13. $\Delta Adj. = \frac{6}{32}''$.

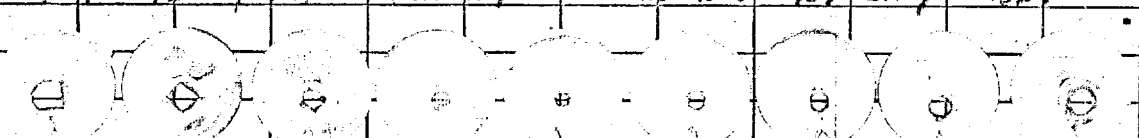

$D_{xd} = \frac{1}{2}''$ ⇒ Beam

$S_1 = \frac{1}{4}''$ | $3/4''$ | $1\frac{1}{4}''$ | $1\frac{3}{4}''$ | $2\frac{3}{4}''$ | $3\frac{3}{4}''$ | $4\frac{3}{4}''$ | $5\frac{3}{4}''$ | $6\frac{3}{4}''$ — 82 mils

Fig. 4.03.02

SGL = 10 mil D_{18} = 0

Note: add $\frac{1}{8}$" to all recorded Dis. to obtain [illegible]

4.03 - 6

(5 mil Discs) V_B = ?

THE SPACE ABOVE THIS LINE IS FOR FILING AND MUST NOT BE WRITTEN ON

K 1674348

SUBJECT: Burn 5 mil al. Discs ~~Super~~ Spaced $S_1 = 2\frac{1}{2}$", $S_2 = 6\frac{3}{4}$"

CUSTOMER: V_p = 100 KV (V_g = -180 Volts) I_p = 11 ma 80% transmission

SERIAL NO.: τ = 1 minute

S. O. OR TEST NO.: $D_{pd} = \frac{1}{4}$"

SHAFT NO.

FRAME: $D_{x\alpha} = \frac{1}{4}$" Beam ⇒

TO DETERMINE

$S_{HV} = 1\frac{1}{8}$" $S_{ggg} = \frac{5}{8}$" ← $2\frac{1}{2}$" = S_1 → $S_2 = 6\frac{3}{4}$" →

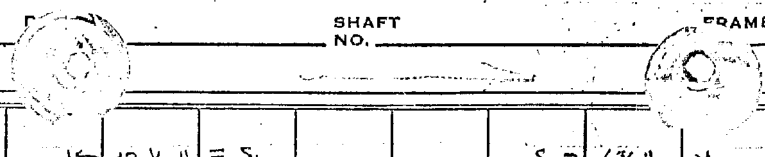

accident — Fil left on at atmos. Pressure – Burned out. Changed cathode units – Tried to set dimensions to equal old dimensions. S_{gb} = 0 ; S_{gl} = 10 mil

Estimate error of reproducibility ± 1 mil

V_p = 100 KV V_B = -120V, I_B = 300 ma (5 mil Discs) (2nd run)

I_p = 10 ma I_g = ? Press = 7×10⁻⁵ Torr τ = 30 secs $S_{HV} = 1\frac{1}{8}$"

Bias V_g = -120V S_{gl} = 10 mils S_{gb} = 0 $S_{ggg} = \frac{5}{8}$"

Beam ⇒ $D_{x\alpha} = \frac{1}{4}$"

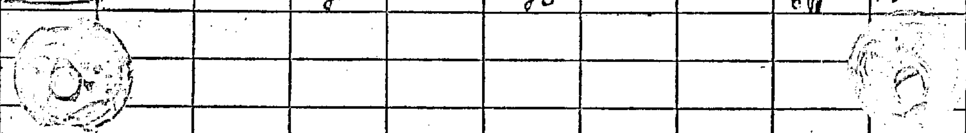

$D_{pd} = \frac{1}{4}$" $S_1 = 2\frac{3}{4}$" (10 mil [illegible]) $S_2 = 6\frac{3}{4}$"

$S_{HV} = 1\frac{1}{8}$" $S_{ggg} = \frac{5}{8}$"

V_p = 100 KV I_p = 10 ma, V_B = 110V, I_B = 280 ma, Press = 9×10⁻⁵ (3rd Run)

(V_g = -60V) Time = 35 secs Beam – good $S_{HV} = 1\frac{1}{8}$"

S_{gl} = 10 mils S_{gb} = 0 $S_{ggg} = \frac{5}{8}$"

Beam ⇒ $D_{x\alpha} = \frac{1}{4}$"

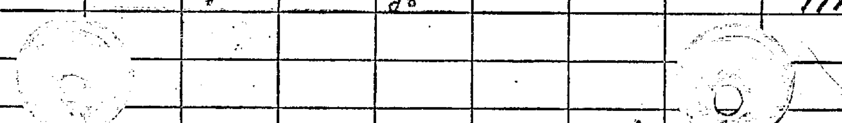

$S_1 = 2\frac{3}{4}$" 90 mils $S_2 = 6\frac{3}{4}$"

V_p = 100 KV, I_p = 10 ma, V_B = 110V, I_B = 280 ma Press = 6×10⁻⁵ (4th run)

(V_g = 0) Time = 35 secs $S_{HV} = 1\frac{1}{8}$" $S_{ggg} = \frac{5}{8}$"

S_{gl} = 10 mils S_{gb} = 0

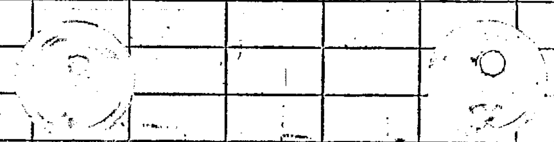

$S_1 = 2\frac{3}{4}$" 75 mil $S_2 = 6\frac{3}{4}$" 125 mil

Note: all data this page [illegible] $\frac{1}{4}$" thick [illegible]

Fig. 4.03.03

Grid bias was varied from -180 volts to zero volts in 4 steps and 5 mil aluminum discs were used at anode distances of 2-3/4" and 6-3/4". As the bias was decreased the beam aperture in the disc location of 2-3/4" became smaller. It was the smallest at zero bias and the beam crossover apparently was closer to this point at xero bias than any other. This data combined with beam visual data indicates that the crossover point approaches the cathode as the bias is increased.

By the use of such methods as these, the design converged to a cathode configuration which could be used in the new C-gun with reasonable transmission through the orifices.

C-Gun Laboratory Experiments:

Some means of monitoring the performance of the beam was needed in the compact C-gun, whose beam transfer section could have discs inserted for burnout measurements only with great difficulty. Viewing ports in the pumping ducts were finally adopted as superior to electrically insulated probes around the apertures or temperature instrumentation on the apertures, since the ports changed the performance of the gun in no way. The viewing ports were installed in the ducts of two chambers and gave a view of the beam as well as of the apertures, which quickly became incandescent when struck by a beam. This warning was the most direct warning to reduce power and trim up the beam direction. Another periscopic arrangement of mirrors was used to permit the observer to see around his x-ray shielding with a telescope for a very satisfactory view. The beam transfer section connected to a 6" dia., 12" long Pyrex cylinder. This chamber was observed through a shield of lead glass in the form of a rectangular brick 9" x 5" and 3" thick. With this system, the beam could easily be observed at any pressure desired, from microns to 40 torr. Beam cross section as a function of molecular species and pressure of the ambient gas could also be observed and measured through this window.

Tests in the Heraeus gun usually involved no more than 2 or 3 minutes running at any time. From these series of tests were determined the optimum dimensions of the electron optics to be used in the C-gun.

However, when longer running times were required in the C-gun a time dependent decrease in the emission current was experienced.

This decline of beam current with time was checked for repeatibility. As the cathode came up to terminal temperatures the current was noted and its rate of decline recorded. After terminal temperatures were reached (about 40 minutes after cathode turned on to space charge limit operation), the cathode was then shut off and left over night to cool. When the cathode was again turned on, beam current versus time was noted, and the plot repeated itself. This would indicate that the drift was due to temperature changes in the cathode and not due to any permanent change such as distortion, bombardment filament poisoning, or bolt emission face poisoning. An examination of the cathode individual components that might change enough in dimension with temperature to cause an appreciable change in the electron optics was then undertaken.

The first and most obvious component was the tungsten emitting bolt itself. It was fastened in the cathode by set screws 1-1/2" from its emitting face, where the approximate temperature was 2450°C. A temperature at the clamp of 500°C or less was assumed until terminal temperatures in the cathode were reached. Knowing the coefficient of thermal expansion of tungsten and using an average value for these two temperatures over a 1-1/2" length, the axial expansion of the bolt was calculated to be .008". Of course, most of this expansion would occur as soon as emission temperatures were reached at the emission face. Therefore, the change in length of this bolt over a period of 1/2 hour would be fairly insignificant. In any case, the change in dimension would be in the wrong direction to account for a decrease in beam current.

The second component considered was the focusing cup. If it were to increase in length, thereby causing an increase in S_{ggg}, the perveance of the system would decrease. Since the temperature of this

extension grid was unknown, the decision was made to construct one out of Invar instead of stainless steel. The coefficient of expansion of Invar is considerably less than that of stainless steel, and it was hoped that a test would show an appreciable change in the rate of decline of beam current with time. The tests showed no noticable difference in the current drift with cups of the two metals.

A third consideration was the body of the cathode itself. This, too, was stainless steel, so one structure was made of Invar and tested. Again, no change in drift was noted. Further investigations involved grinding down the main support stem of the bolt, clamping the bolt closer to the filament area, and removing the grid from the cathode. All of these efforts proved futile in controlling the drift. Since there was a schedule to be met, zero bias was relinquished, and the current control used in the Heraeus gun was adopted. Cathode bias resistors were added in the auxiliary power supply.

At this time in the program the requirement was advanced to 12 kilowatts of power or 80 ma at 150 kv, per gun. The first step was to run the cathode fully space charge limited and note the maximum current obtainable from this particular cathode geometry at 150 kv. As previously mentioned, the beam current, I_p, was 64 ma for the first few minutes of cathode operation and then began to deteriorate at an initial rate of approximately 1 ma/min. It eventually stabilized in around 40 min at an I_p of 40 ma. From this data, it was obvious that higher emission currents and a drastic improvement in stability were needed.

There are three basic adjustable dimensions (specified by large letter S in Fig. 4.03.04) that can be varied in the cathode to produce a change in perveance; S_{hv}, S_{ggg}, and S_{gb}. Experience has shown that high voltage arcing becomes a major problem if S_{hv} is adjusted to less than 1-1/8" so this dimension was fixed at 1-1/4". Variations in S_{gb} had also been tried but it was noted that transmission efficiency decreased if the bolt were adjusted any closer to the anode than its present setting. The remaining parameter S_{ggg} was then selected as the one with which to experiment.

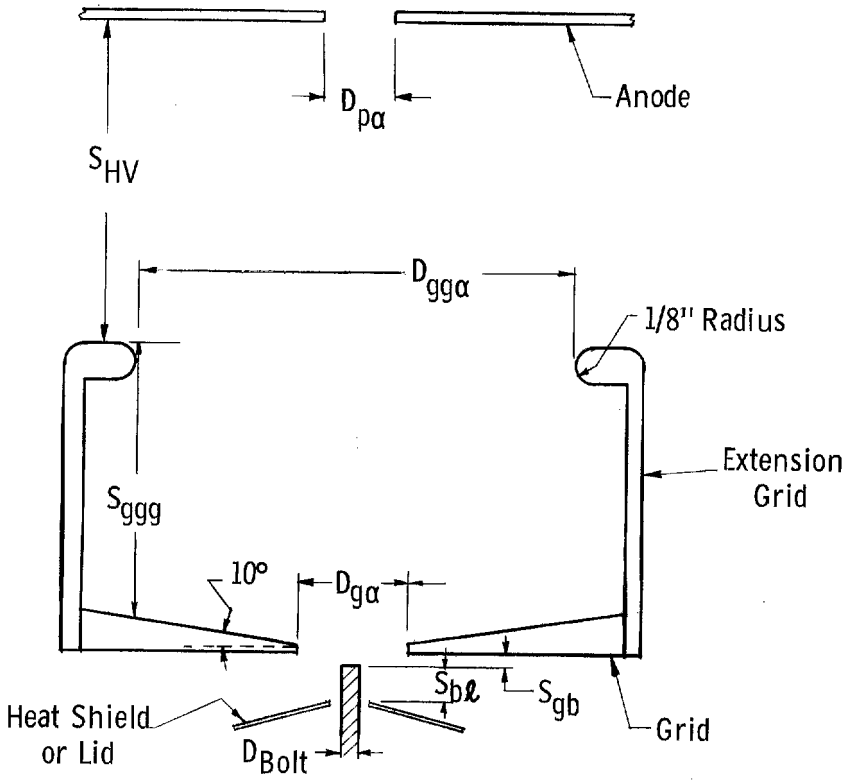

MA	KW	$S_{b\ell}$	S_{gb}	$D_{g\alpha}$	S_{ggg}	$D_{gg\alpha}$	S_{HV}	$D_{p\alpha}$	D_{Bolt}	R-BIAS
50	7.5	.014"	.001"	.250"	.578"	1.180"	1.594"	.312"	.062"	9K
70	10.5	.014"	.001"	.250"	.578"	1.180"	1.156"	.312"	.062"	7K
93	14.0	.014"	.001"	.250"	.398"	.961"	1.250"	.312"	.062"	5.2K

Note: Min. Shv 1 5/32"
Anode 0.2" per rev.

E-gun bolt nomenclature and settings

Fig. –4.03.04

It was apparent that S_{ggg} dimension alone could not be changed without causing loss of transmission, since tests on the Heraeus gun had revealed the dependency of the beam crossover location on the spacing of S_{ggg}. This crossover point then was a function of the shape of the equipotential lines surrounding the emission face of the bolt. As a first approximation, the S_{ggg} and D_{gg} combinations that exhibited 100% transmission were compared and found to fall on a rough parabola that intersected the emission face of the bolt(called the origin) at one point and the perimeter of the extension grid at the other point. The equation of this parabola with dimensions in inches was $y = 1.71 x^2$. Two more extension grids that would fall along this same parabolic envelope were then constructed but with the added advantage that the total distance from anode to emission face would be reduced. That is, S_{hv} was kept fixed, D_{gg} was reduced, thereby causing a reduction in S_{ggg} in order for the perimeter of the extension grid to intersect this envelope. The results were quite rewarding in that 100% transmission was maintained and higher emission currents produced.

The intermediate extension grid with a D_{gg} of 960 mils was set at S_{ggg} = 462 mils. The emission current was approximately 90 ma at 5 min of cathode running time and 70 ma at 15 minutes.

Transmission became 100% after 14 minutes. The other extension grid had a D_{gg} of 706 mils and S_{ggg} was set at 300 mils. Since we were set up to read only 100 ma of I_p at maximum, we could not determine the true I_p versus time for the first 16 minutes because the beam current was more than 100 ma. However, at 22 minutes the beam current was 87.5 ma and transmission was 98+%. The same drift problem in I_p was apparent. Even though these power levels were attainable it became obvious that a further step was required to produce a satisfactory electron gun.

Cathode self bias was selected as the most expedient method available to obtain more stable beam operation. Since biasing the present cathode only led to defocusing of the beam, some dimension had to be changed in the cathode in conjunction with the addition of bias. The

decision was made to change D_g from .100 inch to 1/4" as an attempt to pattern the area immediately surrounding the emission face after that of an Heraeus, filament type cathode because the filament cathode was known to operate with satisfactory stability.

The results of this redesign are summarized in Fig. 4.03.04. The beam stability became satisfactory, and the perveance was so increased by the change in D_g that the standard extension grid (D_{gg} = 1.18") could be used.

4.04 Insulator Development

Because of the temperatures expected in the cathode area, a high alumina insulator was desired. Simplicity of shape was emphasized, for there was not time to retrace the insulator development if troubles appeared, and the performance of the simpler shape could be predicted with more confidence. The shape which combined required surface leakage path length with mechanical strength was a cone, convex toward the pressure, Figure 4.04.01. Initial models made of Vycor borosilicate glass cracked when the cathode was heated, but the alumina units proved as effective as had been hoped. When subjected to the design maximum vibration environment, a cone and cathode assembly developed resonant displacements which would have severely degraded performance, but all joints remained sound and leak-tight.

The defects which did appear in operation fall into two classes: braze failures and electrical failures. In time, some cones began to leak at the ceramic-to-metal seal, apparently through failure of the metalized joint. Service life could be extended in these cases by coating the area with Dow Corning silicone varnish number 994 and baking over 150°C. The electrical failures divide in turn into two classes. A yellowish coating on the vacuum side of the insulator built up over a long period of time, apparently through decomposition of diffusion

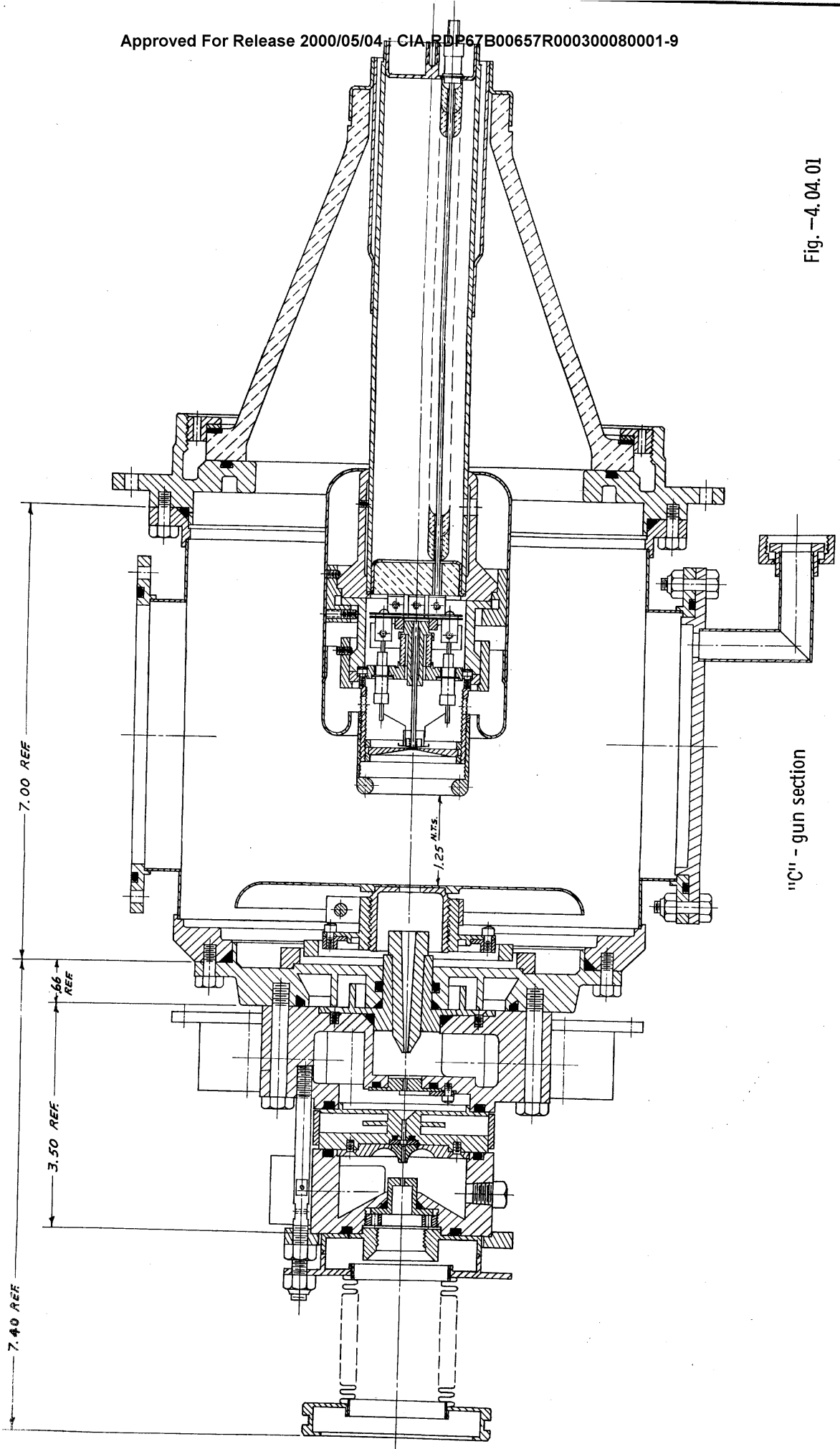

Fig. –4.04.01

"C" - gun section

pump oil. Unless removed with scouring powder and elbow grease, this layer eventually flashed over and developed low resistance tracks. The other kind of failure was an actual perforation of the insulator, which occurred in a region of high electrical stress.

In an effort to control voltage distribution and charge accumulation, the outside of one insulator was coated with a silicon carbide paint chosen for its nonlinear volt-ampere characteristic. The effects on steady dc test were good, but the operating experience was no better than with bare cones, and poorer when the paint began to come off.

An insulator in the form of a flattened cone with annular convolutions has been built, Figure 4.04.02. Laboratory tests of the insulator alone and operating tests of the insulator and cathode in a gun have proved the suitability of this design for extended service. No vibration tests have been run with this structure, but the shortened cathode stem permitted by this design raises the natural frequencies of the structure and greatly reduces the moments generated by shock loading. The wavy surface was necessary to provide the length of surface path 150 kv operation with a bare surface required.

Along with the more compact insulator, a new plug-in cathode (Figure 4.04.02) was designed to replace the existing complicated heavy and sensitive configuration. Replacement in the field was a major effort, which could greatly be simplified with

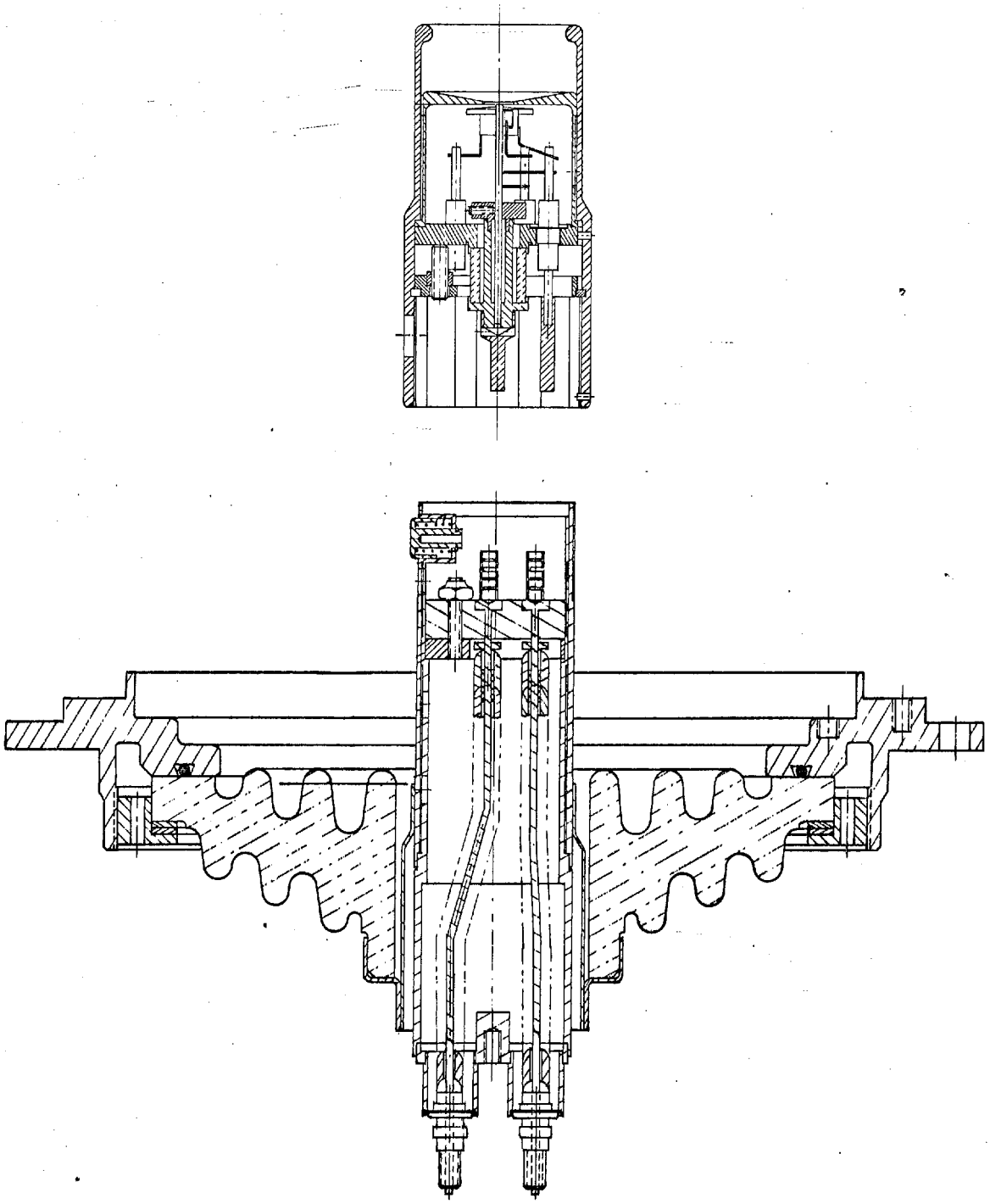

Plug in cathode and new insulator

Fig. 4.04.02

the plug-in feature, allowing replacement through a handhole instead of by disassembling the gun. All set screw type adjustments were replaced by proper dimensional tolerance and control thereby making all assemblies readily interchangeable. The new cathode is also much lighter in weight, raising the natural frequency of the cantilivered system.

Mechanical centering of the bolt is automatic once the stem and insulator are centered at initial build up. The bolt is centered with respect to the pilot diameter during manufacture, insuring automatic centering when the cathode assembly is plugged in place.

A new stem was designed to accommodate the plug-in cathode. A copper sleeve was incorporated in the stem to help transfer the heat generated by the bolt back to the gas cooling of the power supply.

The overall diameter of the new cathode assembly is much smaller than the old and can conceivably reduce the tendency for electrical arc-overs. The outside surface has no sharp edges or joints which also can minimize arc-overs.

Approximately one month of continual testing on two cathode assemblies has confirmed the practicality of the plug-in features and also indicated that performance was as good or better than the previous design.

Vibration Testing of Cone and Cathode Assembly:

While the alumina insulator looks extremely rugged and stress resistant, the weak spot is the brazed joint to the metal cup which begins the cathode structure. In addition, the means adopted to isolate the ceramic-to-metal seal from the cathode heat contributed a large compliance to the cantilevered cathode stem. The possible effects of vibration, both on the bolt cathode and on the insulator, were a source of concern. To put quantitative limits on these effects, a series of vibration tests was run. The cathode was not hot, nor was the space around the cathode evacuated, but the atmospheric damping was estimated as low enough to be neglected, and not nearly powerful enough equipment was available to shake the system needed to keep a cathode in operation.

The first step was a slow sweep from very low to very high frequencies to identify the natural frequencies of the vibrating structure. Two were found with low dynamic amplification. Then at each of these, the assembly was vibrated for two minutes at an excitation level defined by Figure 4.02.05, which was the guide in all questions of environmental vibration. After the vibration exposure, the assembly was retested for natural frequency and leak checked to discover any failure. None was discovered.

4.05 C-Gun Vacuum System

Refinements over Heraeus:

The C-gun system has several modifications in its pumping components from those in the Heraeus gun, although the pressures maintained at each comparable stage have been similar. These modifications can be listed as follows:

1) Use of MCF-60 diffusion pump or PMCS-2B diffusion pump and BCRU-20 baffle.
2) Completely redesigned sorb pump.
3) Redesigned ejector for compactness and lightweight.
4) Shorter dump connections.
5) Use of discharge tube through access door.

Sorb pump:

The redesigned sorb pump for the C-gun system is shown in Figure 4.05.01. It consists of three concentric tubes or containers, each with its own function. The center tube, of copper, contains the molecular sieve material and is, in turn, immersed in the second container, of stainless steel, holding the liquid nitrogen. The third tube, also of stainless steel, surrounds the first two, and contains the vacuum insulation, reducing the loss of liquid nitrogen to a minimum. The high polish on the surfaces surrounding the vacuum space is intended to reduce radiant heat loss through it. Two tubes, a fill and vent line, transfer the nitrogen into the second container.

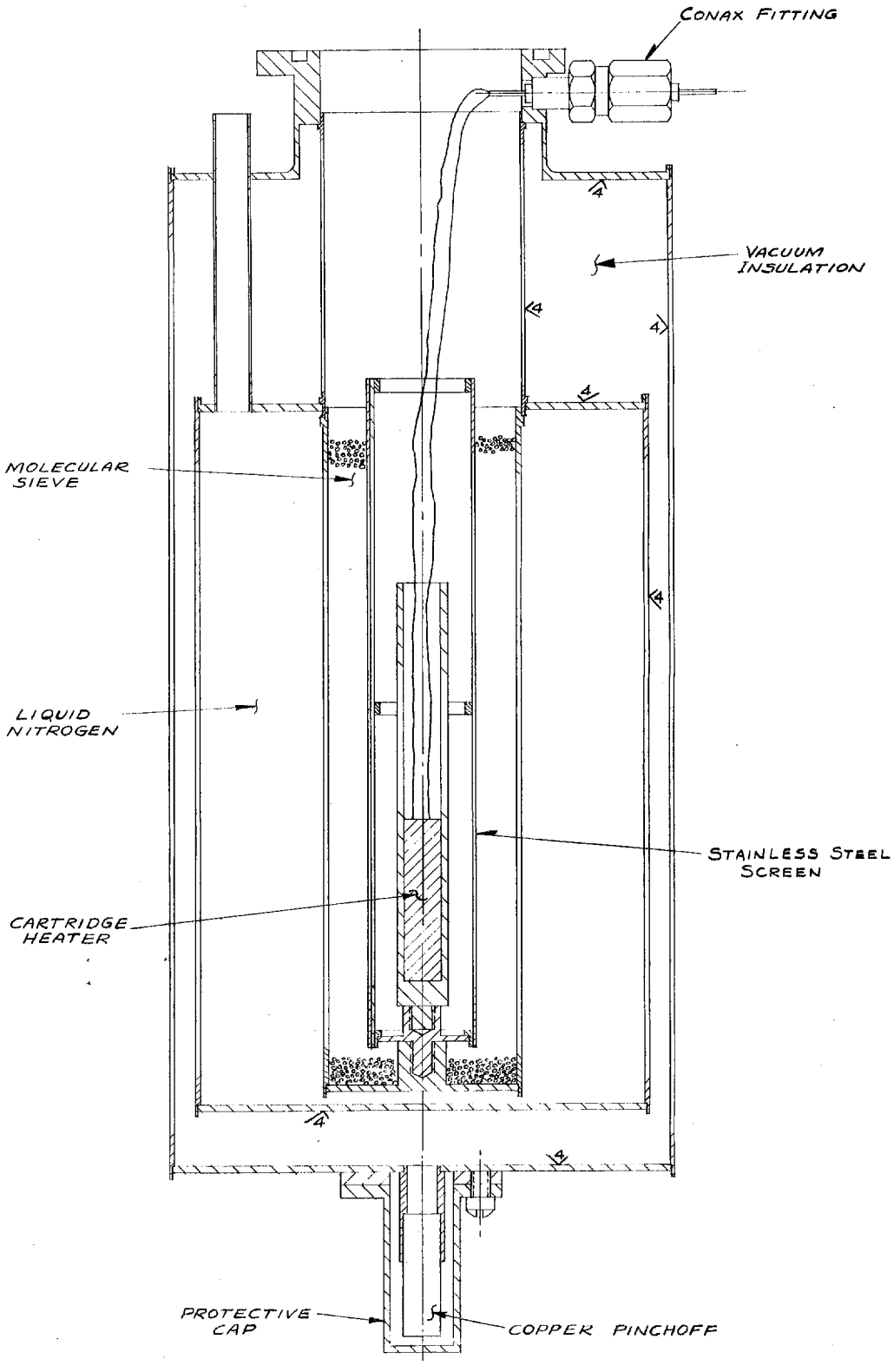

SECTION OF ASSEMBLED SORB PUMP

Fig. –4.05.01

As one of the features of the design was the liquid nitrogen container insulating vacuum, the attainment of this vacuum was very important. Several methods were available:

(1) A direct connection from system vacuum to container

This method as employed in standard liquid nitrogen traps is inconsistent with the use of the final vacuum system, since the high vacuum portion of the system is not always in operation.

(2) A closed system employing a final sealant

The vacuum chamber is to be pumped down and sealed off by either a valve or pinchoff. The final vacuum attained is limited by the cleanliness of the container as well as the pumping system used. In addition, outgassing of the valve or pinchoff upon sealing would increase the pressure of the sealed system.

(3) A closed system employing an internal absorbent and final sealant

A molecular sieve material is physically placed inside the vacuum chamber, which is pumped down and sealed off. As used on many commercial metal dewars, the material is in contact with the liquid nitrogen container and by its own pumping action would further reduce the pressure in the chamber. If proper assembly and pumping facilities were available, this method would be best, but its use demands prior baking of the molecular sieve, quick assembly, and pumpdown.

(4) A closed system employing bake-out and final sealant

Though long and relatively involved, this method is the best available at present to produce maximum results. It involves clean assembly procedures and pumpdown on an ion pump bake-out system. A 400°C bake produces ultra-high vacuum in the chamber and a copper pinchoff seals it.

The sorb pump must periodically be regenerated by heating to drive out the gases adsorbed in its active material. All the atmospheric gases but water will be desorbed at room temperature. Complete regeneration requires that the sorbent bed reach a temperature of 365°C. An electric heater was built into the pump for this purpose, but a series of failures of the heater lead wires prompted the adoption of a hot air baking. Air, heated to about 500°C, was blown into the fill pipe of the liquid nitrogen chamber, escaping from the vent, and the sorbent reached 270°C in 45 minutes, starting from liquid nitrogen temperatures. This proved to be hot enough for a satisfactory bake, even though it fell somewhat below the manufacturer's recommended temperature.

In the final system for which the pump is intended, an .059 in. diameter by .187 in. long aperture is used in the sorb pump's stage. The preceding (higher pressure) stage is maintained at .5 torr, or less, during operation of the system, and the pump must maintain at least .010 to .040 torr for the operation of the

following (lower pressure) stage. Fig. 4.05.02 shows the minimum characteristics the pump must maintain. The throughput presented is .04 torr liter/sec.

The performance of the sorb pump on test is summarized in Fig. 4.05.03.

Design Diagram:

Fig. 4.05.02 is the vacuum design diagram for the C-gun. A water cooled baffle on the oil diffusion pump was added to control oil backstreaming.

Control Valves:

The function of the control valves is to close the vacuum system when a beam is not required to permit maintaining a vacuum in the cathode space and avoid upsetting the pump cascade. There are two valves which perform this task together. One is the shutter valve which seals the P_2 chamber from ambient and the other is the ejector valve which seals the P_2 chamber from the ejector. Together they completely isolate the system.

The shutter valve seals the water cooled N_2 nozzle with a two-way pneumatically operated plate sliding on a stationary O-ring surrounding the nozzle opening. An insulated electrical contact at the top of the air cylinder indicates when the valve is opened, thereby disabling a high voltage lockout.

In use there have been several malfunctions of the valve, mostly attributable to assembly techniques. One of these is the use of a large amount of vacuum grease for lubrication, which eventually solidifies from the high temperatures caused by the beam, making the valve stick. For use at high power levels, the design will need modification, such as removing the O-ring completely from the orifice area when the valve is opened.

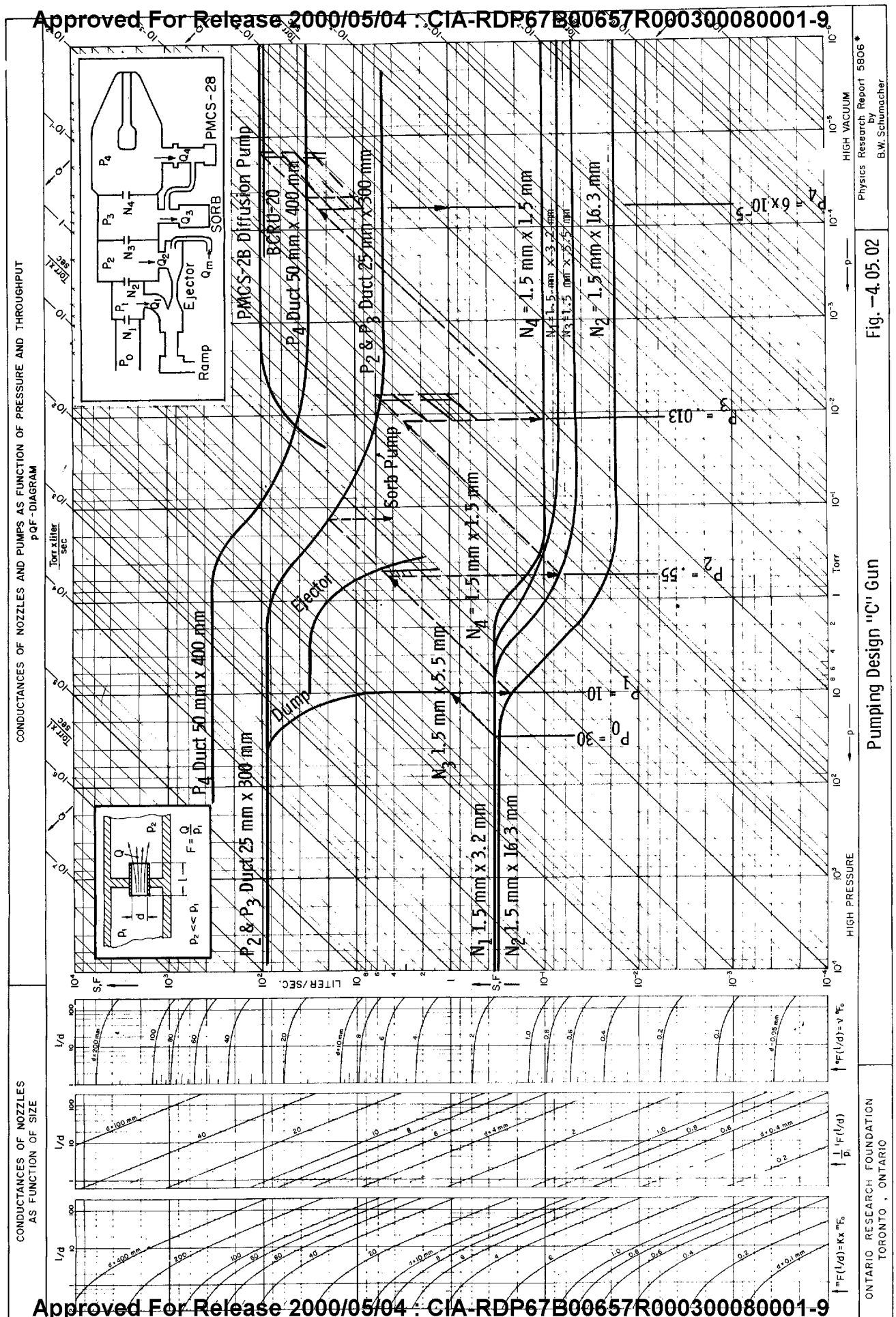

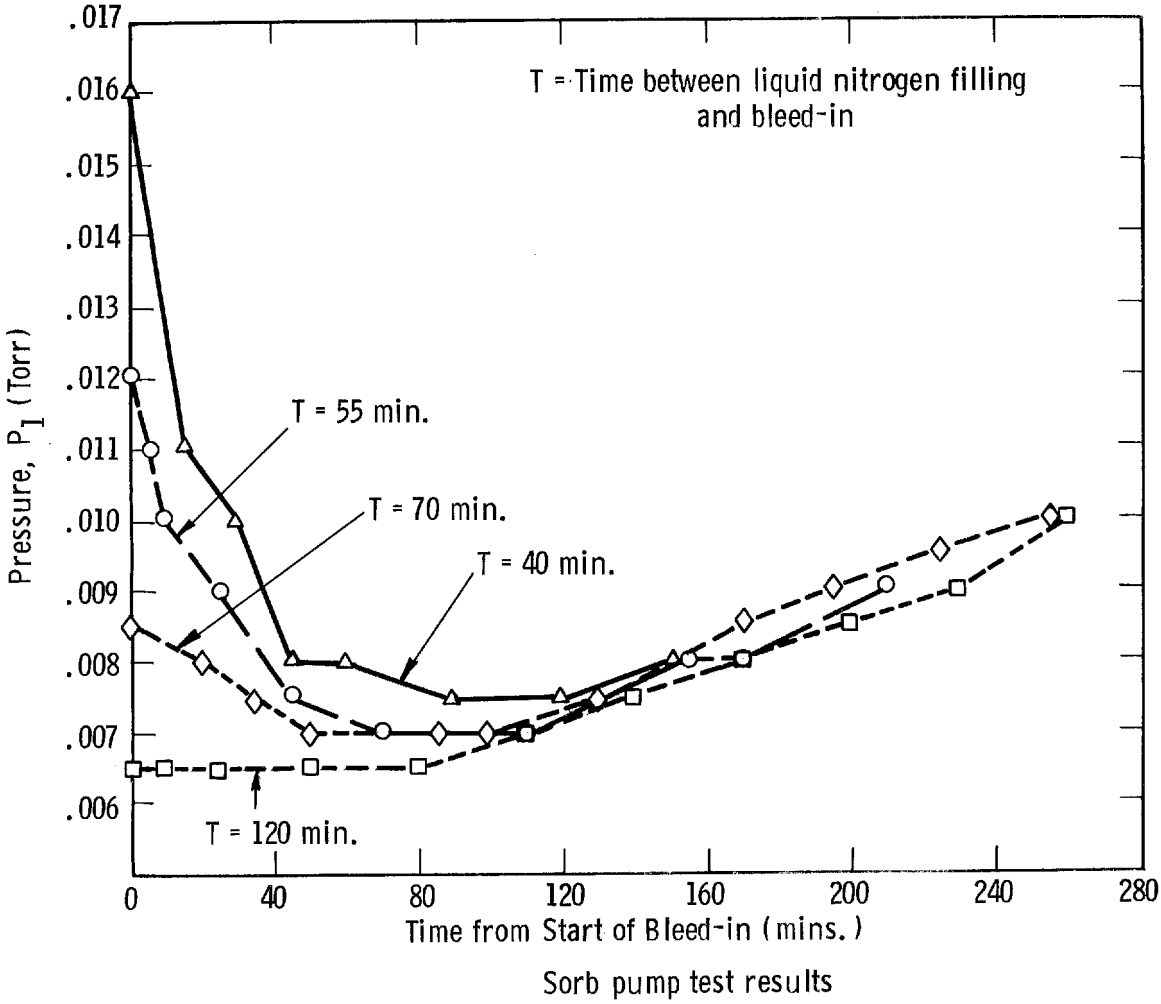

Sorb pump test results

Fig. —4.05.03

Ejector Valve:

The ejector valve is a spring loaded one-way pneumatic valve, connecting the air ejector and P_2 chamber. A spring loaded design was used to simplify the air line connections. (A similar design on the shutter valve required too great an air pressure for operation and the cramped location of this valve prohibited more surface area on the operating piston.) In operation, sticking has been a problem, again due to excessive use of vacuum grease. It has been found that a small amount of this grease will give good results but a non-gumming variety should be considered for future use.

The function performed by the two control valves described above could be taken over by one valve, sealing the system at the N_3 aperture. In this way, the system is not only simplified but the closed system is isolated from a large volume containing leak sources which would be tolerable in the dynamic system operation but intolerable to the closed system.

The present design is not readily adaptable to a single valve, mainly because of space limitations. However, a redesign of the beam transfer system could incorporate this valve. It will be essential to remove the O-ring from the nozzle area when the valve is opened and make it a part of the movable seal.

4.06. Beam Losses

Calculation of Single-Scatter Losses in Gun:

In calculating the electron losses to be expected inside the beam transfer section of the gun, especially in the P_1 stage, it is instructive to estimate the average number of collisions suffered by each electron.

For 150 kev electrons over a 1 cm path in air at 10 torr pressure, the estimate turns out to be 1.5 collisions.
As this neglects a number of factors, principally the effect on density of the power density of the beam, we can proceed with the calculation on the basis of single scattering and decide later whether the representation is valad.

The statistics for single-scattering have been summarized by Schumacher in Physics Research Report 6406 of the Ontario Research Foundation, Toronto Ontario. There, the proportion of electrons scattered from a beam into the annular space subtending unit angle at the scattering site by a layer of gas molecules is tabulated for values other than those of immediate interest. The report also gives the computation scheme, and parameters are plotted over a suitable range. Repeating the calculations of the report for the conditions found in the gun, the fraction lost from the beam on the basis of single-scatter is

$$F = \frac{D}{6}\left(\frac{D}{r}\right)^2 \times 1.3 \times 10^{-5} P$$

where:

P is pressure, torr,
D is path length, cm
r is radius of orifice, cm

For the various chambers of the gun, this results in the following values:

P (torr)	D (cm)	r (cm)	F
$P_1 = 10$	0.6	0.076	8×10^{-4}
$P_2 = 0.5$	1.1	0.076	2.5×10^{-4}
$P_3 = 0.01$	1.1	0.076	5×10^{-6}

These small figures can obviously be doubled to approximate the effect of the 1.5 collisions predicted above without giving cause for concern over the power which would be delivered to the apertures through which the orifices pass. The outermost, for example, might be expected to receive sixteen watts when the gun is operated at a ten kilowatt level. The aperture discs were, of course, designed to dissipate far greater power than this to survive the process of getting the gun lined up in the first place.

These calculations are corroborated by experience in running the guns in which the beam transfer section became generally warm, but not excessively hot when operated under simulated pressure conditions. A large error in the calculated losses would have been exposed by much greater rises of temperature than were actually experienced.

External Beam Scattering Measurements:

One assignment for the laboratory gun was to investigate the spread of the electron beam at a distance of 10" on beam axis from the last orifice. The particular cross section of primary interest, simulating the exit hole in the skin, was not perpendicular to the beam but at an angle of 22° with the beam axis. Consideration of the parameters effecting the beam would indicate that a perpendicular cross-section at any point in a field free region must be symmetrical and, therefore, circular in shape. Hence any oblique section must be nearly elliptical, if the divergence is small.

The experimental setup consisted of a water-cooled metal plate, inclined at 22° to the beam, with an elliptical hole 6.66 in x 2.42 in., ten inches from the outermost aperture of the gun measured along the cone axis. This was inserted in the Pyrex pipe experimental chamber and electrically insulated for measurement of intercepted current. The cooling water lines were likewise instrumented to indicate the amount of heat absorbed.

In operation, steady-state temperature conditions were reached in two or three minutes, and water flow, temperature rise and intercepted current could be measured. At a 40 torr discharge pressure (in air), and low current the simulated skin received about 8% of the power of a 150 kv beam. At higher current, the graphite beam collector at the end of the chamber glowed so brightly that considerably power was radiated to the plate. Since the effects of power density are to reduce scattering by reducing gas density, 8% was adopted as the maximum expected interception beyond the gun.

4.07. Installations

The C-unit as mounted in right chine is shown in Figs. 4.07.01 and 4.07.02. The optimum axis of the unit would have been made somewhat higher than shown, except that extensive changes would have been required to either the outer configuration of the aircraft structure or to the beam transfer section of the gun. The axis selected enabled the installation to be accomplished with a minimum of aircraft modifications, and yet was satisfactory for flight test purposes.

The left-hand installation was the same as the right with the exception of the ejector. Aircraft wiring and piping changes that would have been necessary to make the installations identical were much too complicated, so the ejector was removed from the C-unit and mounted separately in another bay. Dummy load resistors, required for pulsed operation, were also mounted in the left side, just forward of the water cooling system, as in Fig. 4.07.03.

On both sides, a small access door with the beam exit tube attached was fitted into the bottom chine to serve as a service entry for conducting performance tests, system check outs, and minor servicing. To provide a dump for the vacuum system, a ramp similar to the one used on the Q-bay was added to the structure at the outside edge of the chine. Three eliptical tubes were secured to the structure and formed a gas passage from an internal plenum to the ramp area. All open joints and connections to the outer structure were caulked by the aircraft ground crew with a silicone rubber sealant to insure proper operation of the ramp. Views of the ramp and pipes appear in Figs. 4.07.04(a) and (b).

The cooling water system for the C-gun, Fig. 4.07.05 and 4.07.06, is schematically similar to that of the Heraeus. One main difference was in the pump used. In tests at the low pressures that would be experienced during operation at altitude, the pump motor on the Heraeus system overheated quite badly. A 24 volt D.C. Moyno pump did not exhibit this deficiency and was used instead. Various problems later

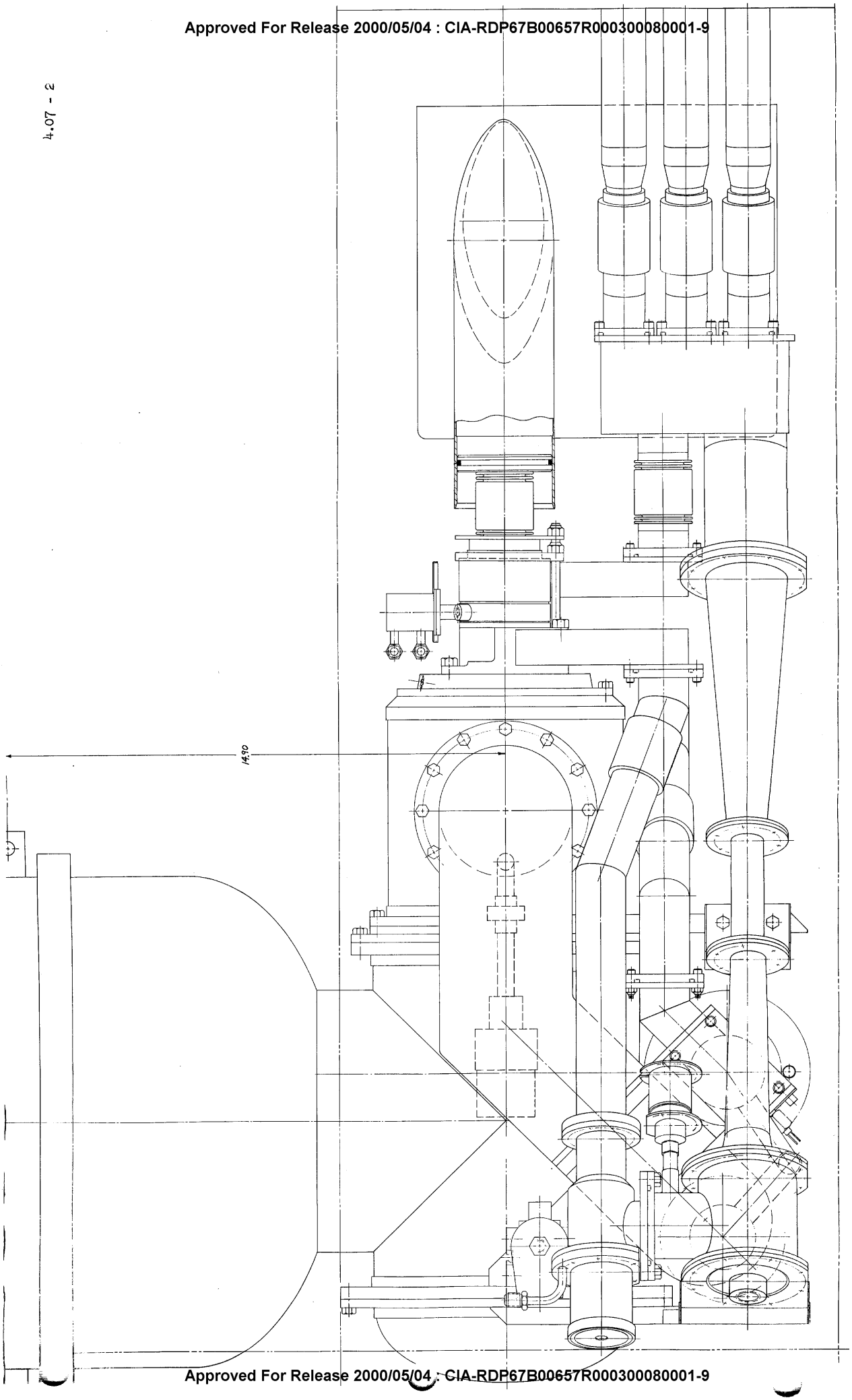

Fig. –4.07.01

"C" - installation

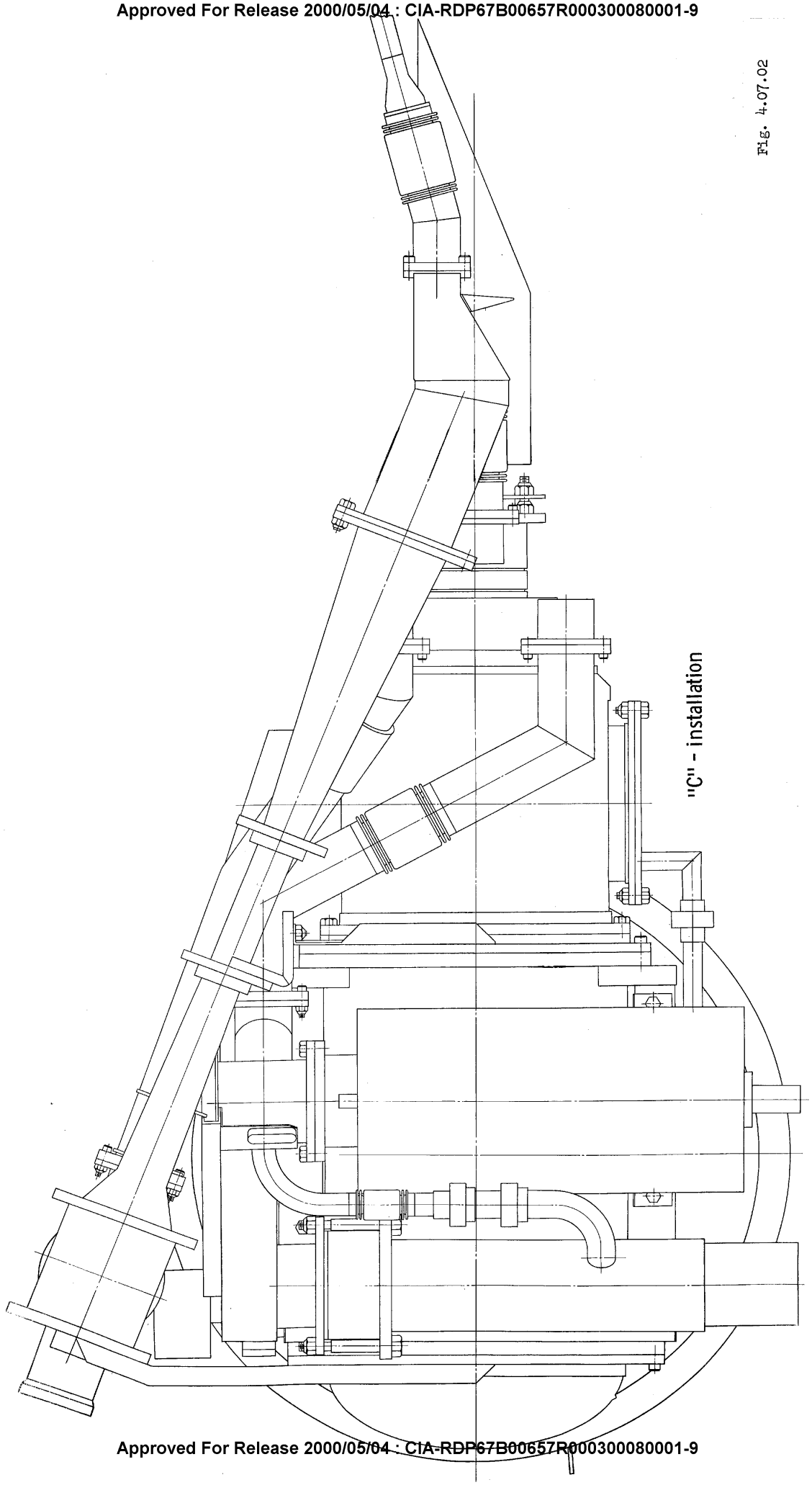

"C" - installation

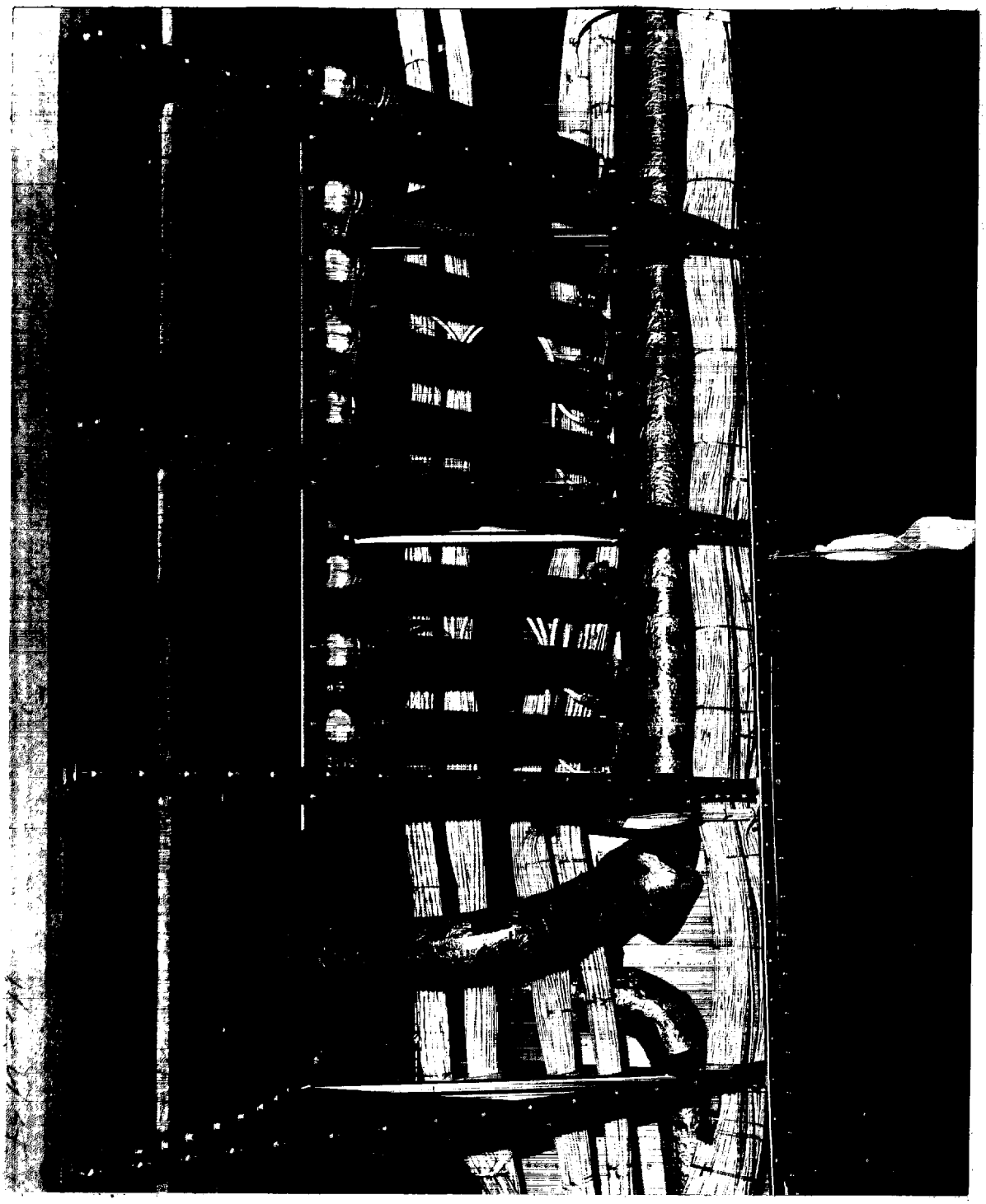

Dummy Load Resistor Bank

Fig. 4.07.03

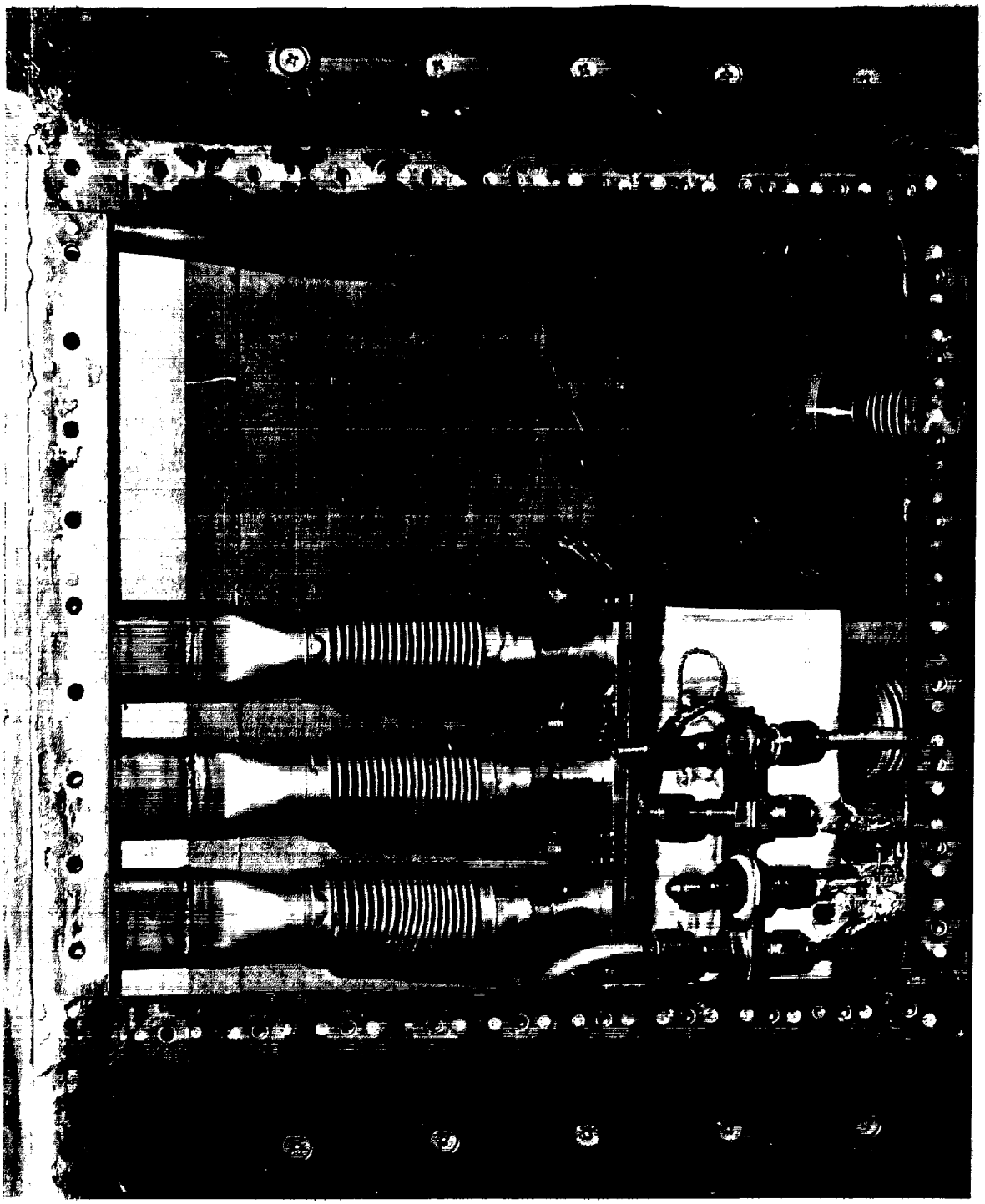

Access Opening Showing Lamp Tubes

Fig. 4.07.04(a)

Aft View of Ramp

Fig. 4.07.04(b)

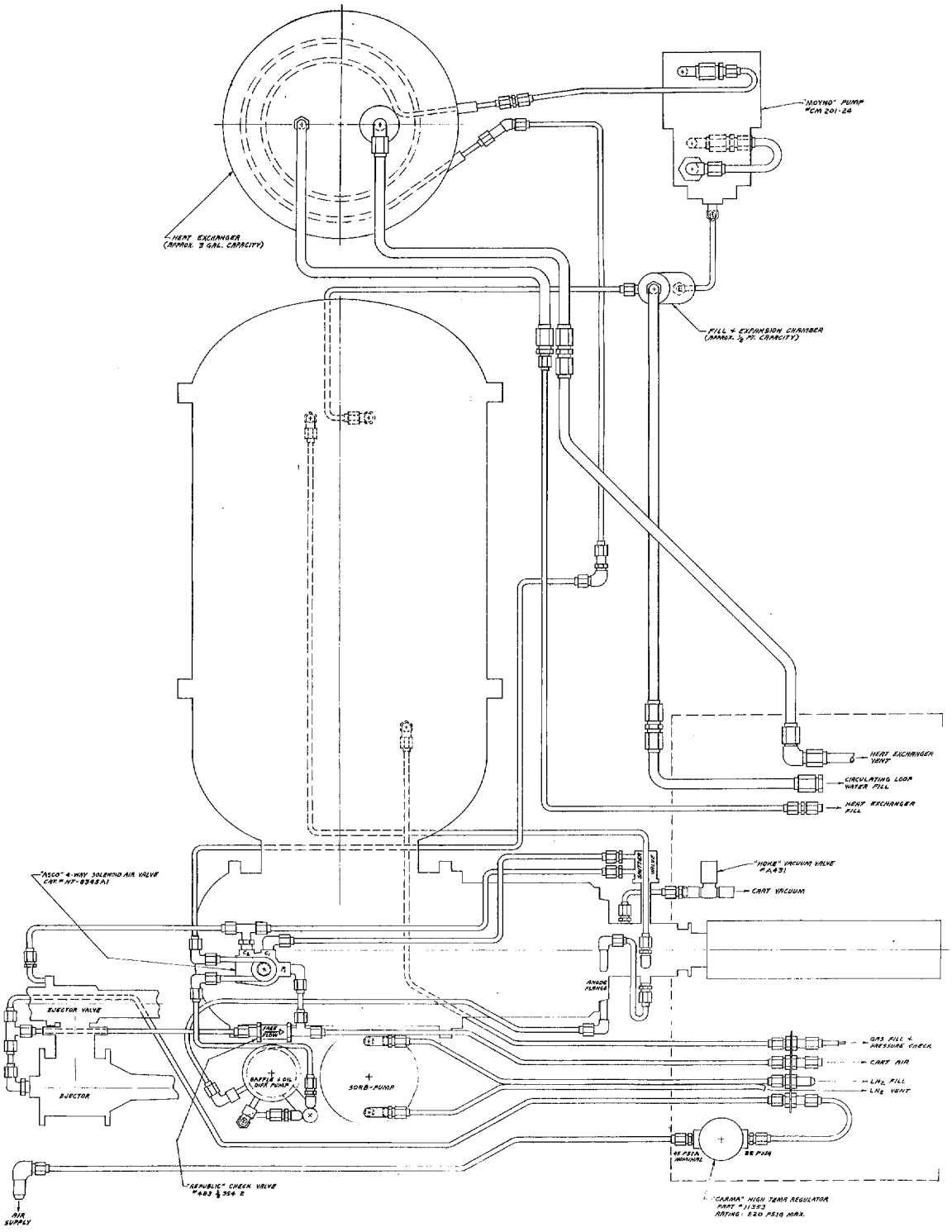

"C" - installation cooling schematic

Fig. –4.07.05

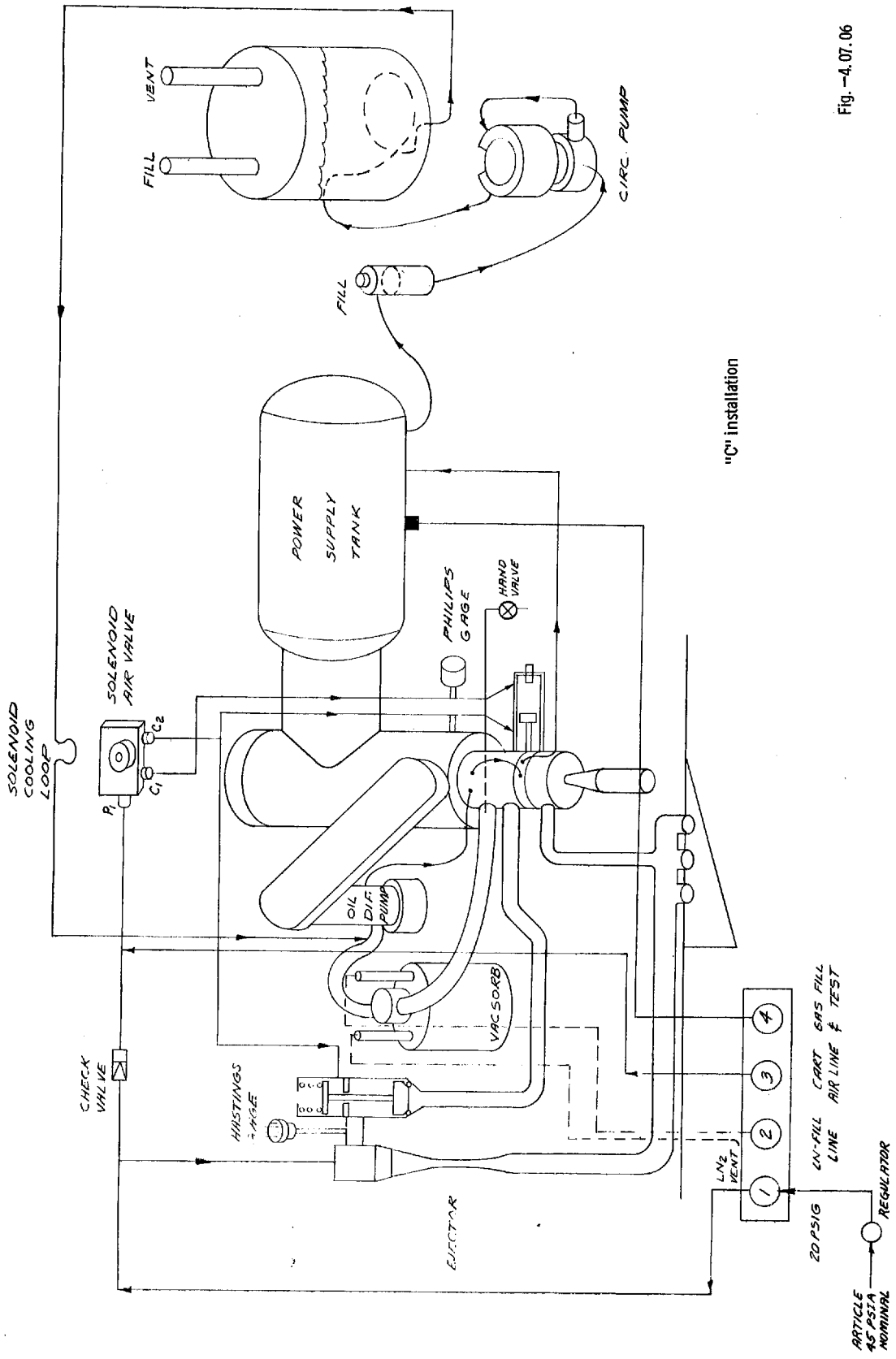

Fig. –4.07.06

"C" installation

encountered with this pump turned out to be due to assembly errors made when the pump was torn down for modification for the installation; otherwise it was quite satisfactory. The total system heat load was estimated at 2550 watts, and the heat exchanger was sized on the basis of this power and the diffusion pump cooling inlet temperature requirement. Operation of the system in flight showed this thermal design to be adequate for the loads encountered.

4.08. Operating Procedure

Introduction:

There is a body of technique developed in the course of using the electron beam equipment, which may properly be regarded as a part of the operating systems. Such procedures are outlined in this section.

Mechanical Centering of Bolt Cathode:

It was the objective of the design to provide a structure that would be electrically aligned when it was mechanically aligned. This entailed some means of centering the cathode structure on the mechanical axis of the gun after any radical re-adjustment of the system. As explained above, the cathode mount was provided with a translating stage (and flexible electrical connections) to permit such adjustment, and the part which was exchanged was merely seated in a circular fit to center it with respect to the cathode mount. The tool for checking the concentricity of the cathode in the gun used a cylindrical plug of which one end was turned to fit the seat, the other to fit into the grid cup with minimal play. The plug was drilled on a diameter to accept a rod to which a dial indicator could be fastened. In use, the plug was fitted with the dial indicator and dropped into the cathode mount seat. Concentricity with the mounting flange of the insulator cell was obtained by translating the cathode mount until the indicator runout was zero. (Usually $\pm$ 0.0005 in. was taken as good enough.) Then a cathode was installed, and the concentricity of its grid cup with respect to the same flange was measured, using the other end of the plug. Indicator runouts at this stage were ordinarily $\pm$ 0.001 in. After the insulator cell was installed in the gun case, the concentricity was checked once again, this time against the bore in which the anode assembly mounted. The runout at this stage was usually also about $\pm$ 0.001 in., although the tilting anode plate was able to compensate for eccentricities of 0.005 in. or more.

Removing Transition Section:

In the installation, the alignment of the gun axis with pertinent elements of the structure was fixed by the clamp which held the transition piece to the power supply tank. Once established, the correct orientation was worth preserving if the power supply case had to be opened for any reason. The means of doing this was an adjustable fixture, shown in Fig. 5.05.01, which also gave very welcome support to the gun, which was awkward to handle, even though light.

Use of the fixture entailed removing certain screws from either end of the transition section and attaching the plates at each end as indicated in the drawing. Then the adjusting screws lifted the weight of the gun until the power supply no longer bore any weight. At this setting, the fixture returned the gun to exact alignment.

Exhaust and Outgas:

The experimental system had special requirements in that the high vacuum area was often open to air for the purpose of changing dimensions, parts, and checking the cathode. The high voltage behavior during tests depended to a great extent on the length of time the P_4 chamber had been exposed to atmospheric pressure and the amount of humidity present at the time. Another important factor was the vacuum history of new parts installed in this chamber. If these parts had never before been heated inside a vacuum, then copious outgassing could be expected from them in a pressure range of 10^{-5} to 10^{-4} torr. Ideally, all parts should have been previously heat treated under vacuum before installation, but the means was not always available to accomplish this. Certain procedures, therefore, were adopted for the operation of the gun.

After closing the system, it was roughed out through a tap on the P_3 duct. Exhaust of the P_4 chamber usually would be completed in a matter of minutes to the roughing pump pressure level (10-15 microns), and the diffusion pump could be turned on. In a matter of 20 minutes the chamber was pumped to better than 10^{-4} torr. At this time the cathode was turned on full (60 watts bombardment power.) The cathode was allowed to run at this value until once again the pressure rose to

10^{-4} torr. The cathode was then cut back and if the pressure continued to rise, the cathode was shut off completely. When the vacuum had become better than 10^{-4} torr, then the cathode was energized again. This procedure continued for 30-40 minutes until the P_4 pressure reading fell, instead of rising. When it reached 5×10^{-5} torr with full (20% of standard) bombardment power, then the gun was ready for seasoning.

Seasoning:

The purpose of seasoning was to prepare the gun for stable operation at its highest voltage. Seasoning was always unavoidable after the high vacuum section of the gun had been opened to atmosphere or the system otherwise exposed to comparable pressures. There were two schemes of seasoning: cold seasoning and hot seasoning. Cold seasoning was accomplished by gradually increasing the high voltage with a cold cathode until the intended operating voltage was reached. Hot seasoning proceeded by outgassing the cathode as previously described, and then applying high voltage with the cathode running at its normal temperature. Of course, this produced a beam, but anode tuning of the beam at low voltages for 100% transmission was readily accomplished. Thereafter, hot seasoning up to 150 kv with the beam colleced in a shielded catcher could proceed with no damage to any part of the gun. Hot seasoning proved the generally more satisfactory procedure.

Anode Tuning:

The tilt screws for the anode gimbal passed through O-ring sealed glands, so that the anode plate could be tilted for fine beam adjustment while the gun was in operation. The usual drive for the screws was a pair of capacitor-split-phase synchronous motors, geared down to 2-3 rpm. This remote control enabled the beam to be centered very rapidly without exposing anyone to x-rays.

Catcher:

The beam at even partial power was a potent drill, and some provision had to be made to accept and dissipate the beam power, while minimizing the emission of x-rays. These objectives were met by a lead

shielded, water cooled copper tube inclined at a 5° angle to the beam axis. This was arranged to screw into a fitting at the outer gun orifice, sealing with an O-ring. The almost grazing incidence of the beam spread the focal spot enough to prevent any melting at the copper.

CHAPTER 5

POWER SUPPLIES AND CONTROLS

5.01. Introduction

The initial requirement for power supplies was conceived in terms of window tubes, with the only stringent requirement that of size. Weight reduction was later achieved by replacing oil insulation with a gas, C_4F_8, and by forming the tank walls of honeycomb panels. Transition to the Heraeus gun was straightforward: a filament isolation transformer was built into the gun to provide an impedance match, so that no internal changes in the power supply were required.

Moving out of the favorable conditions in the Q-bay presented problems of environment tolerance that were compounded by doubling the rating of each supply. The space available for mounting the supplies in the installation was severely limited, and weight objectives could be met only by eliminating cables and connectors, providing cooling to permit use of normal-temperature components, and utilizing light-weight materials and structures wherever practical. Because of the possibility of hot spots in the power supply, perfluoropropane, C_3F_8, was adopted as an insulating gas for its better thermal stability.

Before entering upon the development of power supply circuitry, an analysis was made of the relative weights of alternative schemes and the performance to be expected from each. An important element of the electrical system was the means used to distribute single-phase loads evenly over the three phases of the supply. These phase balancing networks may be present physically or disguised in the transformer connections of some circuit arrangements, but they must be there, since one of the system specifications was a balanced load. A proposal to make the total system a balanced load by scott-connecting the transformers of the two power supplies was rejected on grounds of the concentrated load that would present to one generator.

5.02. Comparative Weight Study

The initial study of component weights for the Q-supply was based on the following ratings:

Input: 520 cps, single phase or three phase

Output: 175 kv dc, 40 ma, 5% ripple (24.5 kv p-p), 20% duty

Table 5.02.01 lists the estimated weights of transformers, rectifiers, capacitors and the energy stored in capacitors. The calculated regulation shown does not include the effect of transformer or rectifier impedances, and is thus optimistic.

Capacitor weights were based on a nominal weight of 0.25 pounds per joule for units operating at 85°C. Rectifier weights were based on available high voltage silicon units, assumed the same for all single-phase supplies and multiplied by three for three phase circuits. (The rectifier currents are so low that no significant weight difference is realized by reducing the current rating.)

A phase balancing network weight of 28 pounds was assumed for all the single phase circuits.

Some attention was given to the question of the best distribution of power supplies for the several loads to be fed. Neglecting the weight of cables, the analysis showed a decided weight advantage in a single central supply for all loads. In the Q-bay environment the cable question was less pressing, and one power supply was actually built with twin outlets and a current balancing control to operate a pair of window tubes. Generally, though, the kind of experiments being run with all the Q-bay installations avoided the problem of central vs. individual supplies by having only one load to feed. For the C-guns, the prospect of terminating, installing, and possibly replacing a high temperature, high voltage cable gave strong backing to the concept of a directly connected power supply, which finally prevailed.

TABLE 5.02.01 WEIGHT COMPARISON FOR Q POWER SUPPLY ALTERNATIVES

Characteristic		Cascaded Xfmr. (3 stage) (6 level)	Full-Wave Voltage Quadrupler	Half-Wave Voltage Doubler	Half-Wave Voltage Quadrupler	Half-Wave Voltage Sextrupler	Three-Phase Doubler	Three-Phase Quadrupler
Transformer Weight	lb	72	33	28	24	27	46.5	40.5
Rectifier Weight	lb	14	14	14	14	14	42	28
Capacitor Weight	lb	4.5	9.0	15	30	42	6	13.5
Phase-Balancer Weight	lb	28	28	28	28	28	0	0
Total Component Weight	lb	118.5	84	85	96	111	94.5	82
Capacitor Stored Energy	joules	17	36	60	120	169	24	54
Regulation	kv	43	42	42	53	79	13	36.8
Circuit Diagram		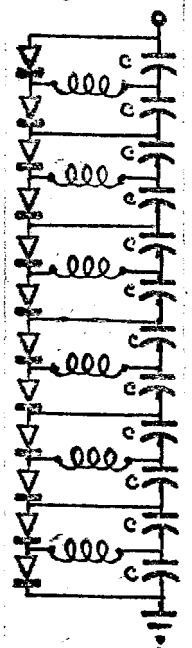	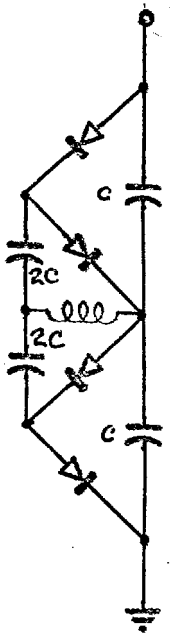	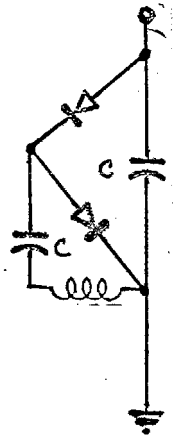	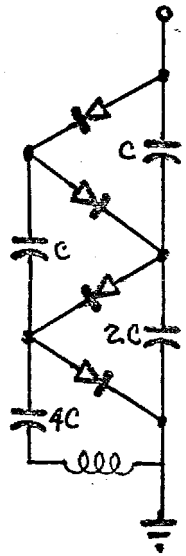	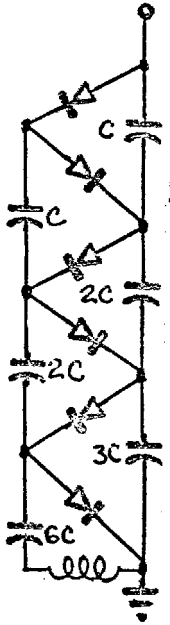	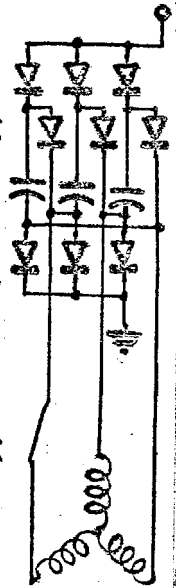	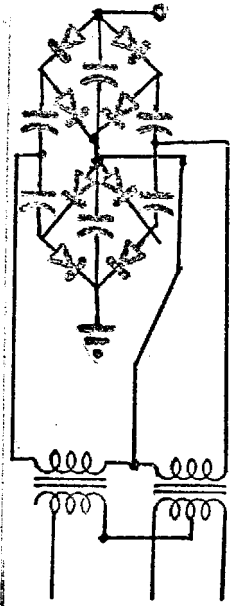

5.03. Q-Supplies*

The full-wave quadrupler circuit was adopted for the Q-supplies that were built for window tubes and later used also with the Heraeus gun. Photographs of an early, oil insulated version show the kind and disposition of components, Figures 5.03.01 and 5.03.02. The small box near the six feedthrough terminals houses lead-protective Zener diodes and bypass capacitors.

Compared to those shown, the components for the later gas insulated supplies are smoothly encapsulated and metal parts rounded off. The only component added in the gas insulated version is a circulating fan, which prevents stagnation of the insulating gas and keeps it moving between hot components and the cool walls to transfer heat to the Q-bay atmosphere.

*Throughout the project, equipment came to be known by the area in which is was installed. Thus, power supplies for the Q-bay were Q-supplies; those for the chine, C-supplies.

Fig. 5.03.01

Q-Supply

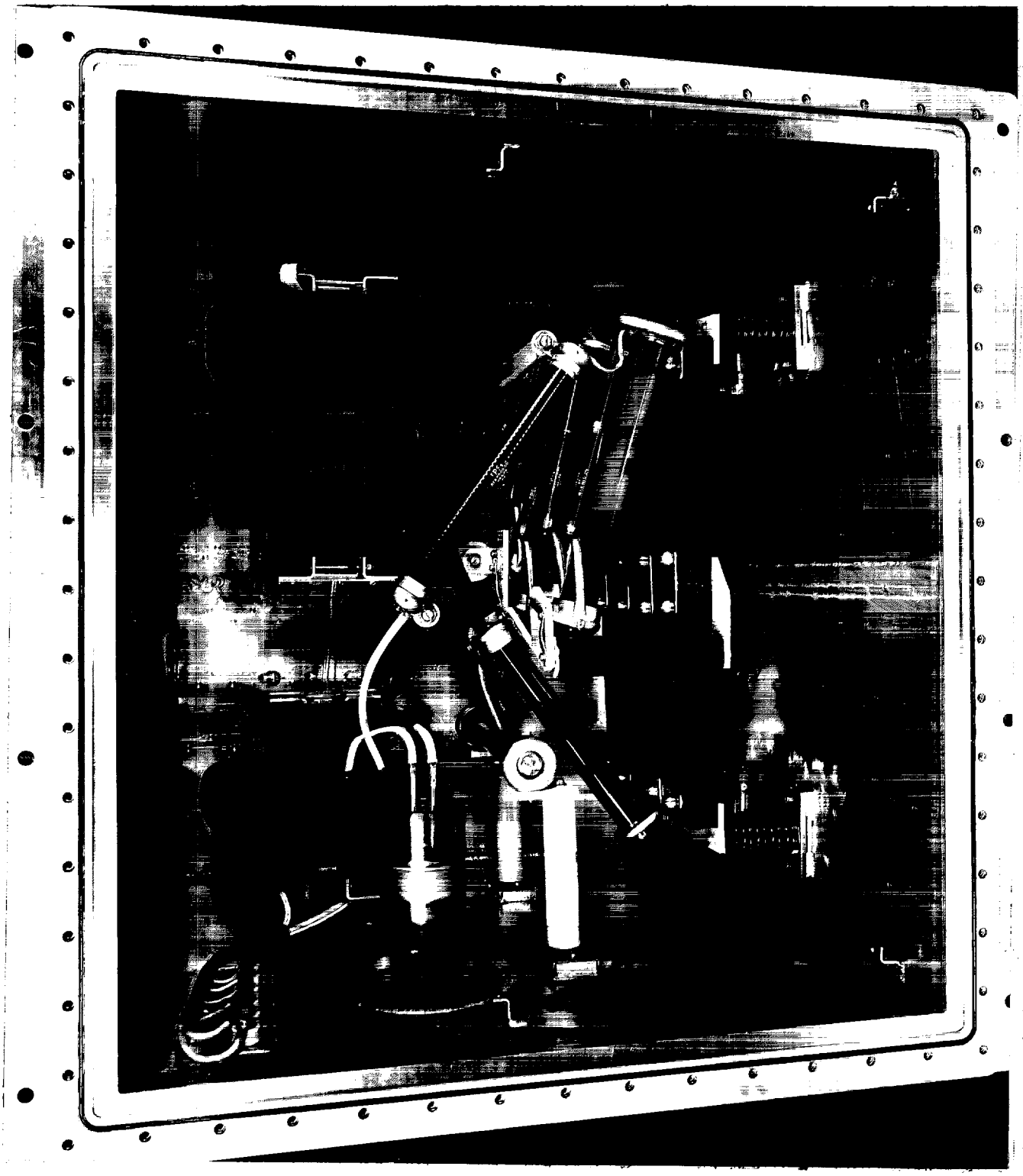

Q-Supply

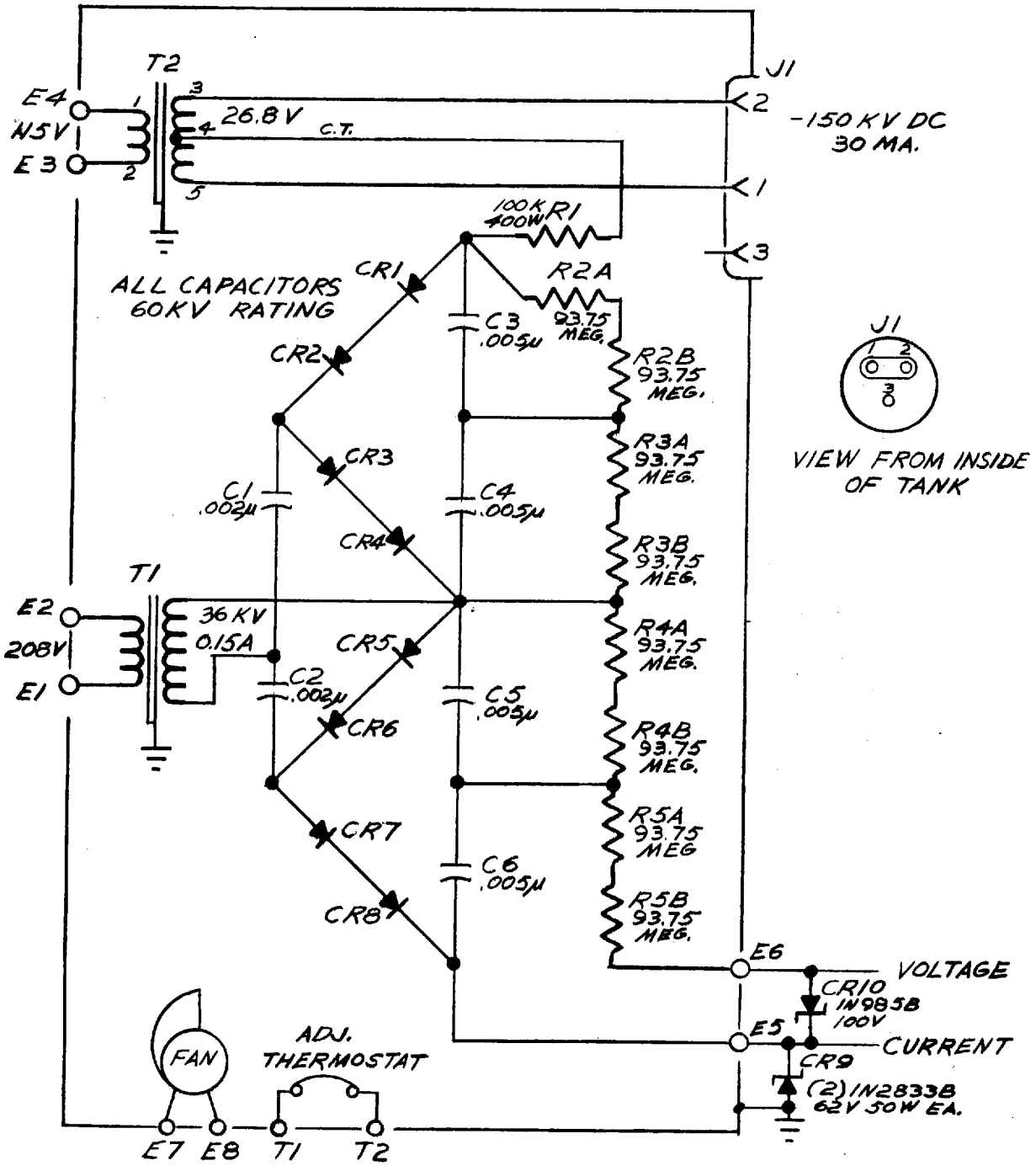

Q Supply Schematic

Fig. 5.03.03

5.04. C-Supply Circuit Selection

For the 12 kw power rating desired for each chine unit, a new comparison of the major contenders in the power supply group was made. The decision had not yet been made to unitize the gun and power supply on each side; consequently some of the supplies considered had double the unit power rating. Five basic points were taken as ground rules:

1. The load presented to the generator should be balanced three phase.
2. The insulating medium would be pressurized gas.
3. Cooling would be provided to permit use of normal temperature components. High temperature components had already been found to add more weight than a cooling system.
4. A small number of low energy arcs in the supply would not be harmful so long as it did not shut down as a result of the arcs.
5. A minimum number of control functions should be required.
6. Minimum operating life should be 500 hours.

With these starting points, the types of supply which had shown some promise were compared. Two approaches which had been rejected in designing the older Q-supplies were also included, the self-resonant transformer and the use of some higher basic supply frequency. The latter two techniques are discussed first below, followed by an intercomparison of all of the approaches.

Resonant Transformer Circuit:

This circuit utilizes a transformer similar in design to conventional types but operated with its secondary resonated, either by an external lumped capacitance or by distributed internal capacitance. Because of the resonance condition, the secondary voltage is not E_1N, but E_1NQ, where E_1 is the primary voltage, N is the turns ratio and Q is the quality factor of the tuned circuit.

The circuit's main disadvantage arises because the kva rating of the transformer is the kva rating of the supply multiplied by Q; for

a 24 kva supply with a Q of N, for example, the transformer rating would be 250 kva. Thus for operation at a given frequency, the transformer would be about 10 times heavier than a transformer for a conventional supply. Such a penalty more than offsets any advantage gained by not requiring voltage-multiplying components. Operation at higher frequencies would reduce required transformer weight proportionately, except that iron losses and consequent heating make necessary additional iron, in order to reduce flux density.

In practice, self-resonance occurs at about 3 kc x and higher frequency operation is not practical; the example in Table 5.04.01 is for this frequency, at which a transformer weighing 225 lbs is estimated to be needed.

Compared to the voltage-multiplier circuits, the resonant transformer approach also has these disadvantages:

1. The full voltage is developed across the transformer winding.
2. If half wave rectification is used, direct current flows in the winding. If full wave rectification is used the weight of rectifiers is increased, being at best the same as for a multiplier circuit.
3. To use voltage multiplication in addition to resonance requires that the multiplying capacitors be calculated as part of the resonant circuit with a resultant lowering of operating frequency and increase in transformer size.
4. The input frequency must be regulated within rather close limits.

Higher Freqeuncies for Conventional Circuits:

At higher frequencies, the size of the transformer is reduced, as shown in Table 5.04.01, until a minimum is reached at about 1000 cps. Above this frequency, the size is again increased due to the inability to utilize the iron fully. The reduction is about 10% of the 500 cps transformer weight or, for the 24 kw 24 quadrupler, 13.2 lb. The capacitors would be reduced by about 6 lb for a total weight reduction from

TABLE 5.04.01 HIGH FREQUENCY POWER SUPPLY COMPARISON

Weights in pounds for 24 kv-a output

Supply Frequency	Generator Weight	Generator Control Weight	Regulator Weight	Transformer Weight	Rectifier Weight	Capacitor Weight	System Weight
520 cps	90	10	0	132	13.0	12.0	257
1000 cps	50	10	0	119	13.0	6.0	198
2000 cps	60	10	0	140	13.0	4.0	227
3000 cps Self-resonant Transformer	70	10	20	225	6.5	8.0	340
10,000 cps Air Core Transformer	75	10	20(1)	(2)	13.0	2.0	400+

(1) Regulator not required if the transformer is not tuned. An untuned air core transformer would have too high leakage for these power levels. To add ferrite core takes the weight back about to the case of the self-resonant transformer.

(2) The coil would be about 8^{in} dia x 24^{in} long, requiring a container 24^{in} dia x 72^{in} long. A higher frequency would permit a smaller coil, but rotating machines of this rating are not practical at higher frequencies.

Approved For Release 2000/05/04 : CIA-RDP67B00657R000300080001-9

the 500 cps unit of about 19 lb. If a separate generator and control would weight about 60 lb, then, the net effect would be to increase the total system weight by about 4 lb.

Voltage Multiple Circuits:

Table 5.04.02 compares the high-frequency supplies with the voltage-multipliers. Assumptions used in component estimates, except as already described, are as follows:

Generator: The weight estimate of the aircraft generator is based on an increase of KVA of the present generator operating at its present frequency.

Transformers: These are of conventional design using wound cores, cut to accept the copper.

Rectifiers: Solid state rectifiers were assumed.

Capacitors: These were chosen for 500 hours life at an operating temperature of 150°C.

Tank and Structure: Two estimates are given, based on the use of stainless steel and of titanium.

Miscellaneous Structure: Since flanges, hardware, etc. are difficult to estimate accurately, appropriate allowances were made on the basis of the earlier gas-insulated units.

For the application, the total system weight advantage of the 2 phase quadrupler is offset by the weight of cables required with a central supply. The full-wave quadrupler was therefore again selected as the best overall choice.

TABLE 5.04.02 COMPARATIVE WEIGHTS OF POWER SUPPLIES

			TYPE OF CIRCUIT					
			Full-Wave Quadrupler	3φ Doubler	3φ Doubler	2φ Full-Wave Quadrupler	Self-Resonant Transformer	10 kc Air Core Supply
Power Rating		kw	12	12	24	24	24	24
Generator(1)		lb	34	34	34	34	90(2)	
Control		lb	30	30	30	30	30	
H.V. Transformer		lb	66	92	145	132	225	
Rectifiers		lb	6.5	19.5	19.5	13.0	6.5	
Capacitors		lb	8.0	5.5	10.5	12.0	8.0	
Tank and Structure	SStl	lb	72	87	90	87	90	(4)
	Ti	lb	49	57	59	57	59	
Fil. Transformer		lb	4.	4.	4.	4.	4.	
Misc. Structure		lb	10	10	40	40	40	
Insulating Gas		lb	5.	7.	8.	7.	8.	
Weight of Supply	SSt	lb	171.5(3)	225(3)	317	295	381.5	400+
	Ti	lb	148.5	195	286	265	350.5	
Total System Weight	SSt	lb	373	480	347	325	411.5	
	Ti	lb	329	420	316	295	380.5	

(1) It is estimated that the indicated weight would be added to the generator rating requirement. For the self-resonant transformer supply a separate 3 kc generator would be required.

(2) For a loaded Q of 10 the frequency would have to be regulated ± 0.25%.

(3) Two supplies required.

(4) Weight not estimated. For 10 kc, the highest practical frequency for rotating machines of this rating, the coil container would have minimum dimensions of 24" diameter x 72" long.

Approved For Release 2000/05/04 : CIA-RDP67B00657R000300080001-9

Phase Balancing Network:

The following discussion of the delta network used for phase balancing first derives the balance conditions algebraically, then considers the consequences of departure from the exact balance conditions.

No analysis was made of the overall weight penalty associated with some arbitrary degree of unbalance, since the ground rules specified that the ship's power system must be loaded in specified ways, which excluded in particular any significant unbalance.

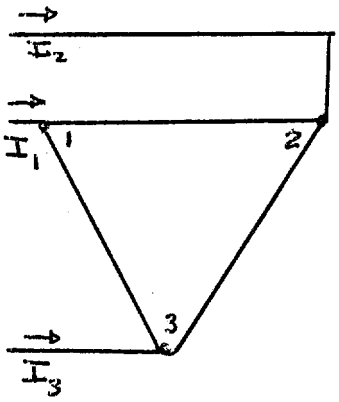

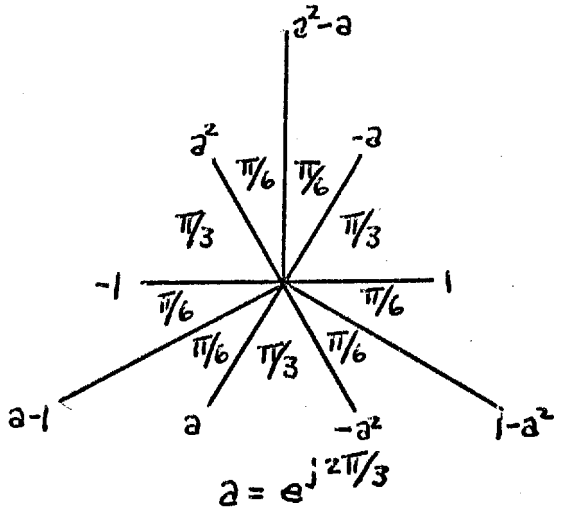

$$\begin{bmatrix} I_1 \\ I_2 \\ I_3 \end{bmatrix} = \begin{bmatrix} 1 & 0 & -1 \\ -1 & 1 & 0 \\ 0 & -1 & 1 \end{bmatrix} \begin{bmatrix} I_{12} \\ I_{23} \\ I_{31} \end{bmatrix}$$

$$\begin{bmatrix} I_{12} \\ I_{23} \\ I_{31} \end{bmatrix} = \begin{bmatrix} Y_{12} & 0 & 0 \\ 0 & Y_{23} & 0 \\ 0 & 0 & Y_{31} \end{bmatrix} \begin{bmatrix} E_{12} \\ E_{23} \\ E_{31} \end{bmatrix}$$

$$\begin{bmatrix} E_{12} \\ E_{23} \\ E_{31} \end{bmatrix} = \begin{bmatrix} 1 \\ a^2 \\ a \end{bmatrix} E_{12}$$

let $E_{12} = E$

$$\left.\begin{aligned} \text{But } I_o &= 1/3(I_1 + I_2 + I_3) \\ I_+ &= 1/3(I_1 + aI_2 + a^2 I_3) \\ I_- &= 1/3(I_1 + a^2 I_2 + aI_3) \end{aligned}\right\} \quad \text{The symmetrical components of the line currents}$$

$$\begin{bmatrix} I_o \\ I_+ \\ I_- \end{bmatrix} = 1/3 \begin{bmatrix} 1 & 1 & 1 \\ 1 & a & a^2 \\ 1 & a^2 & a \end{bmatrix} \begin{bmatrix} 1 & 0 & -1 \\ -1 & 1 & 0 \\ 0 & -1 & 1 \end{bmatrix} \begin{bmatrix} Y_{12} & 0 & 0 \\ 0 & Y_{23} & 0 \\ 0 & 0 & Y_{31} \end{bmatrix} \begin{bmatrix} 1 \\ a^2 \\ a \end{bmatrix} E$$

$$= 1/3 \begin{bmatrix} 0 \\ (1-2)\, Y_{12} + (a-a^2)\, a^2 Y_{23} + a(a^2-1)\, Y_{31} \\ (1-a^2)\, Y_{12} + (a^2-a) a^2 Y_{23} + a(a-1)\, Y_{31} \end{bmatrix} E$$

For no unbalance, $I_- = 0$.

If $Y_{12} = Y_{23}^*$, i.e., if $Y_{12} = Ye^{jb}$ and $Y_{23} = Y\ e^{-jb}$,

and if $Y_{31} = G$, then formally,

$$Y = \frac{(1-a^2)\, G}{(1-a^2)e^{jb} = (a-1)e^{-jb}}$$

Let the 12 and 23 admittances be pure susceptance, so that $b = \pm\pi/2$, and $Y = 0+jB$

$$jB = \frac{(a^2-a)\, G}{(1-a^2)e^{j3\pi/2} + (a-1)e^{-j\pi/2}} = \frac{\sqrt{3}\, e^{j\ /2}\, G}{(2-a^2-a)e^{j\pi/2}} = \frac{\sqrt{3}\, G}{3} = \frac{G}{\sqrt{3}}$$

Three different departures from the exact balance condition were studied: Ten percent load decrease at unity power factor and rated frequency, ten percent frequency increase at rated load and unity power factor, rated volt-amperes at 0.9 power factor and rated frequency.

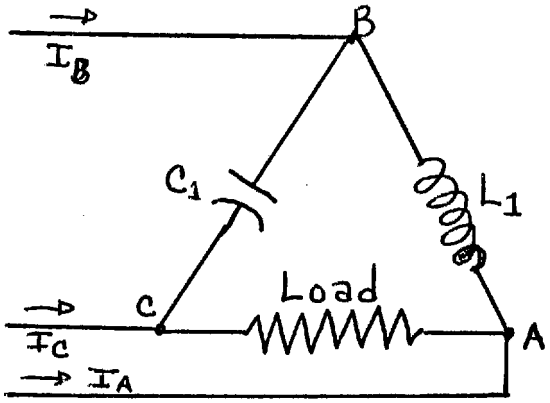

Case 1 Load with unity power factor

Case 1 is the vector diagram drawn for this case. The following relations hold true:

1. $V_{AB} = V_{bc} = V_{CA}$ } balanced 3 phase voltage input
2. $V_{CA} \angle 0 + V_{AB} \angle 120 + V_{BC} \angle 240 = 0$ } input
3. $\dot{I}_A = \dot{I}_{AB} - \dot{I}_{CA}$
4. $\dot{I}_B = \dot{I}_{BC} - \dot{I}_{AB}$
5. $\dot{I}_C = \dot{I}_{CA} - \dot{I}_{BC}$
6. I_{AB} lags V_{AB} by 90°
7. I_{BC} leads V_{BC} by 90°
8. $I_{AB} = I_{BC}$ [LI & Cl are chosen to make this true]
9. $I_{CA} = \sqrt{3}\, I_{BC}$ [Unless this is true, the system will not balance]

When conditions are set so that the above equations are valid, a balanced load is presented to the power system.

Case II. Load of the system (I_{CA}) decreased 10%, L1, C1, and the frequency remain constant.

Equations 1 through 8 still hold but 9 is modified by 10%. The resultant line current unbalance 10%.

$$\% \text{ unbalance} = \frac{\text{I max.} - \text{I avg.}}{\frac{I_A + I_B + I_C}{3}} \times 100$$

Case III. Line frequency is increased 10%

Equations 1 through 7 are still true; however, I_{AB} is decreased 10% and I_{BC} is increased 10%.

The resultant line current unbalance is 4%.

Case IV. Load with 0.9 power factor

Equations 1 through 8 are true. The resultant line current unbalance is 36%.

These four cases were set up in the laboratory and the results verified experimentally.

Case IV was made a balanced system in the lab by putting a capacitor in series with the load whose vars were equivalent to the load inductive vars.

This study was based on a system with fundamental sine waves. However, the load to which this system may be applied contains a capacitor multiplier which introduces load harmonics. The analysis therefore is not rigorous.

From this study, however, it can be concluded that it is load power factor which has the most influence on line current unbalance with this phase balancing technique.

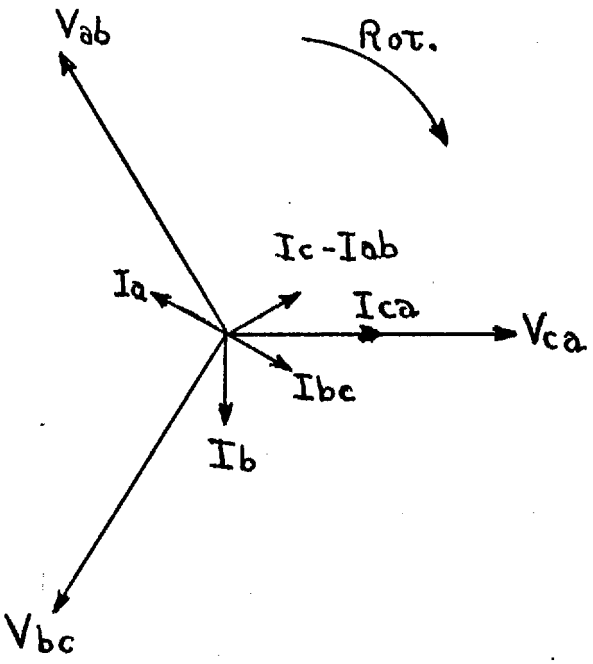

Case 1

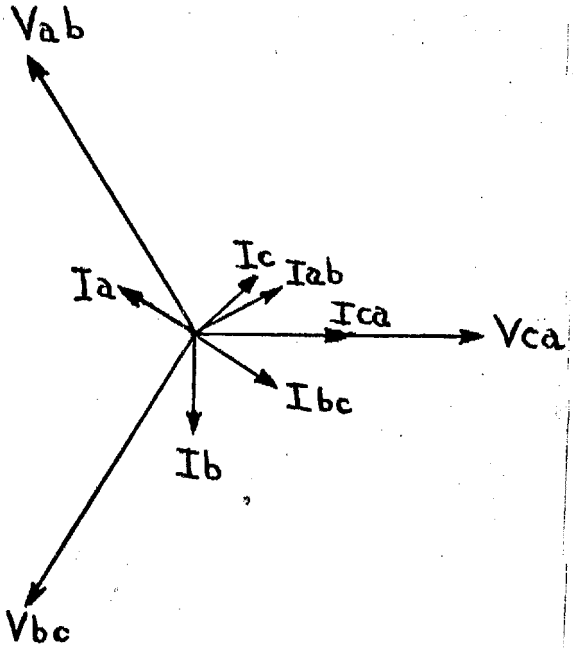

Case 2

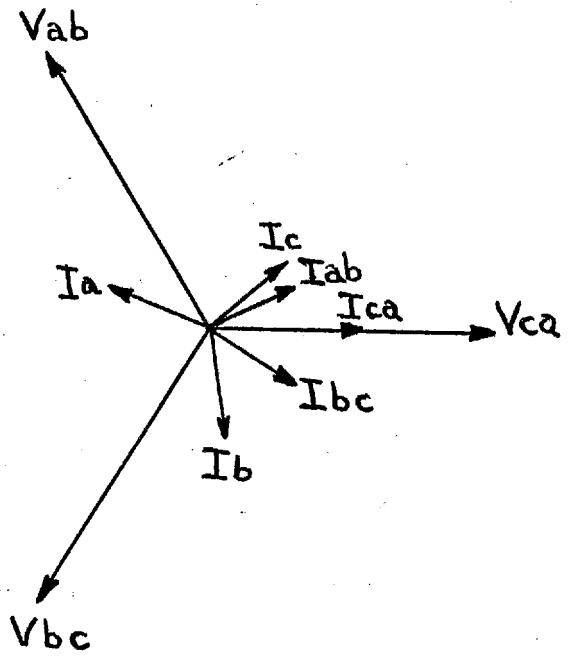

Case 3

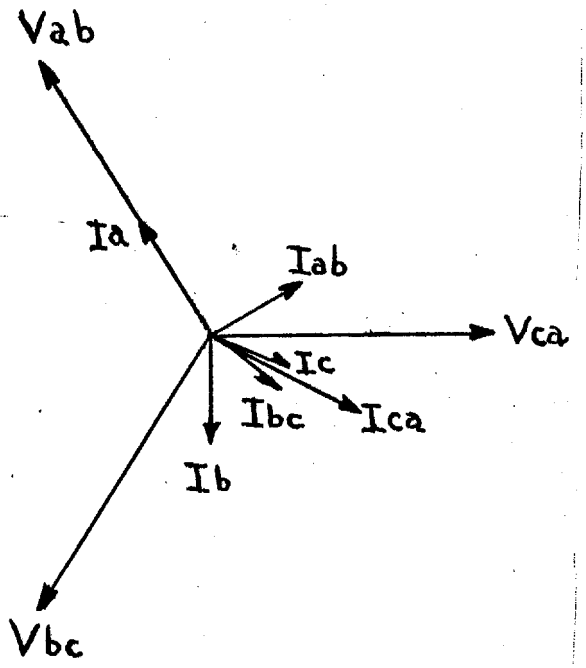

Case 4

5.05. C-Supply Description

The location of the prototype guns required either that long, high temperature, high voltage cables be employed, or that the power supplies be located at the gun positions. In view of the anticipated difficulties with cables, the radical-sounding idea of connecting the cases of the power supply and gun commanded serious consideration. It developed that this approach was entirely feasible, although the amount and shape of the available installation space dictated an arrangement other than the ideal one of direct axial continuation of the power supply case to form the gun housing. Instead, the gun was attached by means of a tee-shaped transition section; Fig. 5.05.01. This forced choice, however, eliminated the necessity of a connector for blind mating, which would have been required by the axial configuration. A removable cover at the opposite end of the run of the tee gave access to the terminals of the gun for connection.

The demand for small size and light weight led to an extension of the gas insulation technique used in the Q-supplies. Forced convection through a water-cooled heat exchanger permitted high ratings in small size. Because the most obvious gas, SF_6, will decompose at 300°C, and non-critical hotspots might reach this temperature, perfluoropropane was substituted. C_3F_8 has the additional advantage of slightly better electrical properties.

Substitution of titanium for steel, cooling to permit the use of normal-temperature components, and careful design to eliminate ineffective material brought the weight down to 108 pounds in the model actually installed. This could have been reduced further still to 87 pounds with technology at hand and is estimated at 78 pounds with reliance on developments as yet untried. It is interesting to note that the weight of each power supply was just the estimated weight of the two high temperature cables required had a central power supply been carried in the Q-bay.

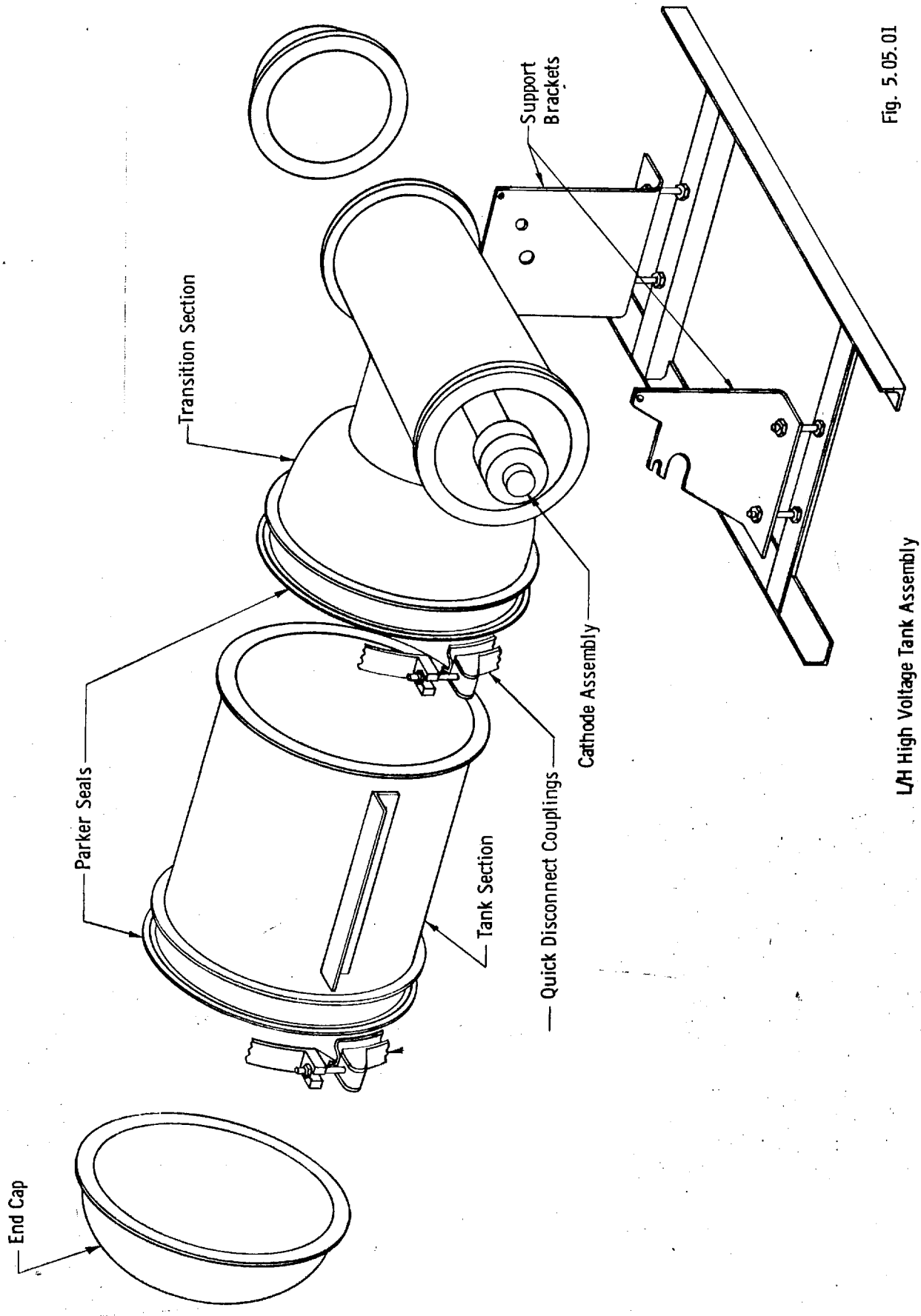

Fig. 5.05.01

L/H High Voltage Tank Assembly

The full-wave single phase voltage quadrupler was packaged in a cylindrical tank as shown in Figure 5.05.02, where the identity and weight of each major component can be read on the corresponding part of the mockup in the transparent tank. The auxiliary supply for cathode heating is located above the filament transformer at the end of the assembly away from the camera.

Weight, space, cooling and voltage problems required that the bleeder resistors which were incorporated into an output voltage measuring circuit in the Q-supplies be omitted in the C-supplies. Output voltage information was therefore obtained by measuring the ac input voltage and dc output current and entering a calibration chart with these arguments to obtain the output voltage.

The curves shown in Fig. 5.05.03 were obtained with a resistive load bank of 5 meghoms maximum, made up of 50 series-connected 100,000 ohm 100 watt resistors. Comparing the currents in the ground return leads of the power supply and load bank gave assurance that no significant currents were leaking from the load resistors. Smaller load resistors, down to the 1.875 megohms required to accept rated current of 80 ma at 150 kv dc, were obtained by shorting out selected resistors to maintain a reasonably uniform voltage distribution along the resistor string, although the limited power rating of the bank would not allow sustained operation at the higher currents.

The schematic of the C-supplies is shown in Fig. 5.05.04, which shows the arrangement with the final design auxiliary transformer. The full-wave voltage quadrupler was disposed in just four separate pieces: transformer, rectifier bank, ac capacitors, and dc capacitors. The auxiliary supply achieved control of cathode temperature by running the bombardment filament hot enough for its emission to be space-charge limited. Voltage changes at the input of the auxiliary supply transformer then had much greater effect on the bombardment voltage than on the current. Monitoring the auxiliary transformer primary current thus gave enough information to operate the cathode in its proper range. The

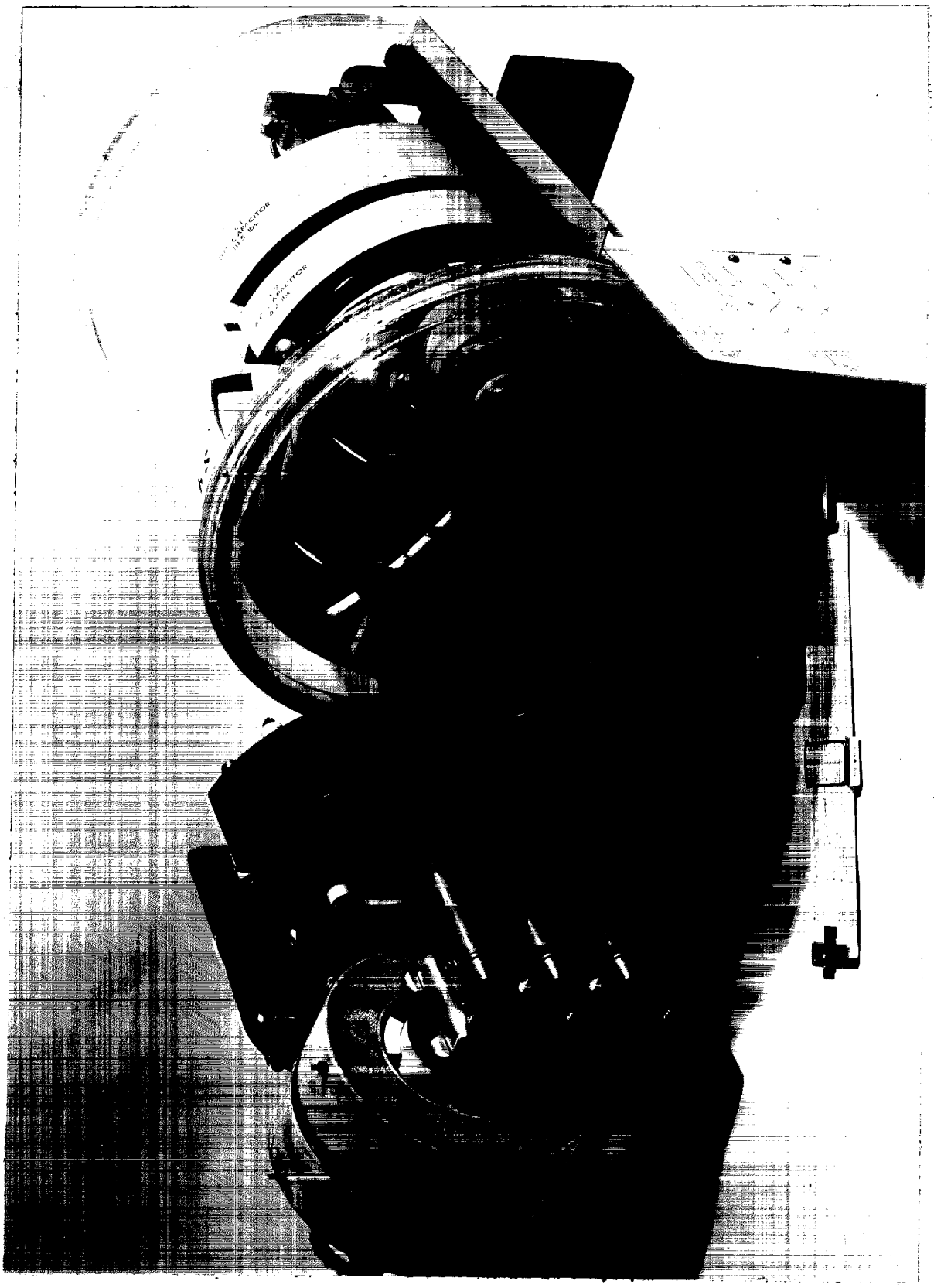

C-Supply, HV Parts and Mockup

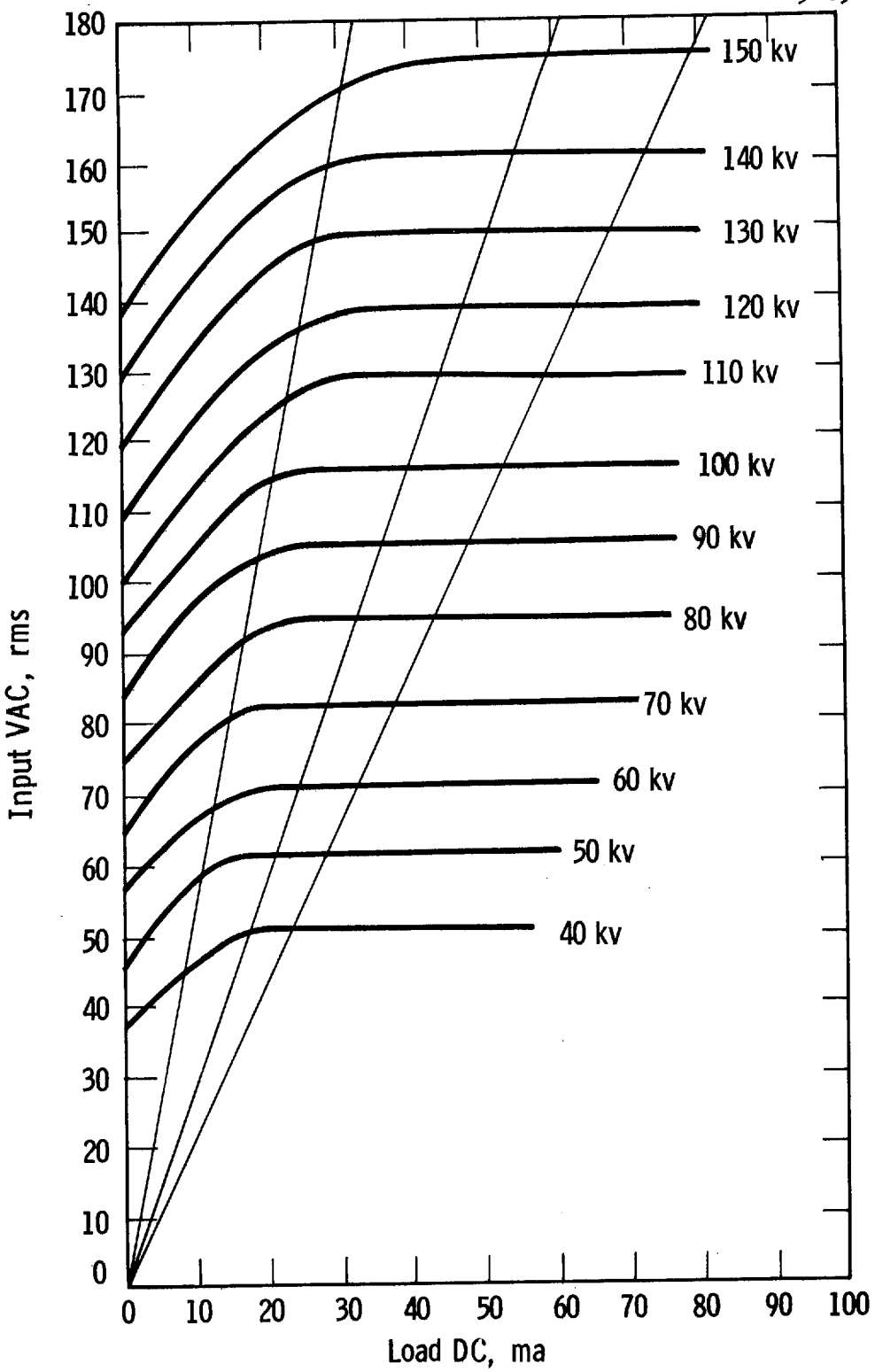

Fig. 5.05.03

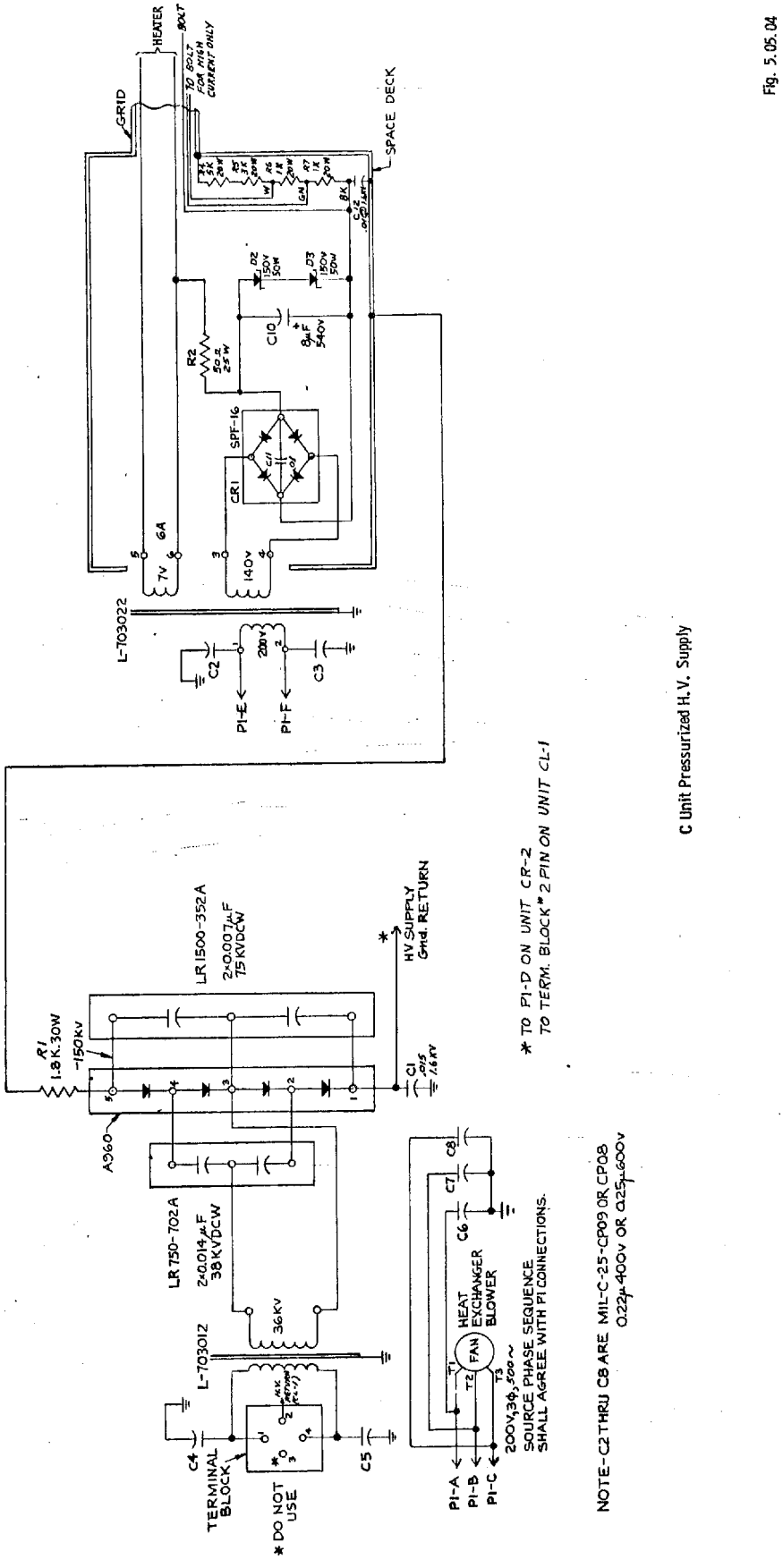

Fig. 5.05.04

C Unit Pressurized H.V. Supply

initial calibration was made by opening the power supply transition piece and inserting instruments to measure filament and bombardment current and voltage in both filament and bombardment circuits. This procedure, which was repeated every time a new cathode was installed, demonstrated, more than any other evidence, just how uniform the bolt cathodes were. All sets of data were virtually indistinguishable.

Experience:

With the exception of the items noted below, performance of the C-power supplies was quite satisfactory. None of the major high-voltage components failed in service, although the insulating support for the auxiliary transformer secondary did cause flashover problems for some time. This difficulty was finally traced to a grain in the mica-glass insulating material which had been ignored by a supplier in fabricating the item. Redesign to lengthen the breakdown path and substitution of a glass-reinforced epoxy remedied this defect.

The other major electrical problem involved the six-pin connector called P1 in the schematic. It was not able to withstand some of the surge voltages caused by flashovers in the gun. When this happened, there was a power follow from the fan circuit which burned up the connector. Replacing the connector with one with higher voltage rating and bypassing each lead entering the tank helped some, but at the termination of the experimental program it was not certain that that fix was permanent. Transferring the current monitoring lead from this small connector to an unused pin of the H.V. primary power connector seemed to eliminate the trouble, but additional consideration of the several contributing factors is needed.

A few early mechanical problems with fracture of insulating supports were cleared up by redesign to increase stressed sections, remove redundant constraints on brittle materials, and by substitution of semiflexible for brittle materials.

Two gas leakage problems were also encountered. The first of these involved the main shell of the supply known to have been dropped

in shipment. This tank later developed a leak at the spot welds joining the cylindrical tank shell and the support brackets. A heliarc weld beam repaired the leak, and extra beads at the ends of the brackets tied them to the sturdy flanges to share the load of the power supply components. Future models have been redesigned with longer brackets which extend up to the quick disconnect flanges, leaving just enough room for the clamping bands.

The other leakage problem was experienced with a transition section, which connects the gun and power supply cases together and partially supports the weight of the gun. When the particular section began to leak insulating gas, it was found that one of its welds was cracked. Each of the other three transitions was immediately checked but none showed any fault.

An intensive investigation into the history of this particular piece showed that the proper stress-relieving procedure for 12% Cr steel had not been followed, and that eventual failure due to stress corrosion could have been predicted if the departure from prescribed methods had been known initially. The defective part was scrapped, and a new part made by approved procedures. It exhibited no weld defects and served without incident.

The unit used for gun development accumulated far more than its rated 500 hours of service life without apparent distress, despite all of the nonstandard conditions encountered in laboratory service. It was also subjected on several occasions to two-hour continuous operation at 125% rated load. With normal cooling water flow, no overheating or electrical malfunctioning was observed, implying that there is apparently sufficient margin in the power supply design for adequate service reliability.

C-Supply Weights:

Between the time of the initial weight estimates (above) were made and actual construction of a power supply was begun, lighter components had become available, and experience with some of the structural elements and with electrical insulation in this service had accumulated so that much lighter power supplies could be designed and built. In Table 5.04.03 are listed the component weights for the C-supplies as constructed.*

For comparison with these "Present" weights, the column headed "Attainable" estimates the outcome of a straightforward redesign program based on present knowledge. The last column of the table indicates what might result from an extensive development program utilizing exotic materials and techniques such as aluminum foil transformer windings and high-strength thin-section structural members.

Additional system weight-saving can be expected of future supplies over the present version because of the fact that only about 9 additional pounds of transformer weight would be required to construct a balanced-load 3-phase-input supply, compared to the 20 lb phase balancing network presently employed with the single phase supply. Thus, the total of about 152 lbs for the present supply plus network would be reduced to about 101 lbs for a next generator supply not requiring a network.

*The improvements in Table 5.05.01 over the Table 5.04.02 estimates would affect each of the alternate choices about equally, and thus cause no change in choice of circuit.

TABLE 5.05.01

Present and Future C-Supply Weights

12 kw, Single Phase Units

Item	Present Wt lb	Attainable Wt lb	Conjectural Wt lb
AC Capacitor	4.5	4.5	4.5
DC Capacitor	7.5	7.5	7.5
Rectifier	6.0	4.5	4.5
HV Xfmr	48.0	35.3	30.0
Aux Supply	4.0	1.5	1.5
Isolation Xfmr	6.7	4.5	4.1
Gas	4.0	4.0	4.0
Heat Exchanger	1.3	1.3	1.3
Supports	2.1	1.1	1.1
Wiring	1.0	0.5	0.5
Misc Hdwr	15.0	5.0	5.0
Supply Weight	100.1	69.7	64.0
Shell + Flanges	8.8	8.8	5.7
Dome	2.4	2.4	1.6
Transition	12.5	7.0	4.0
Clamp(s)	7.8	3.5	1.9
Seals	0.5	0.5	0.5
Tank Weight	32.0	22.2	13.7
Total Weight	132.1	91.9	77.7

5.06. Control and Telemetry

Apparatus for in-flight control of the high voltage power supplies and of the incidental power for items such as cathodes, cooling pumps, solenoid valves, etc. was carried in the Q-bay. Initially, this space was used because it was the location of the power supply and gun. When the C-system was first designed, the intention was to locate the control units in the chines, adjacent to the power supplies. Later, however, it was decided to retain the Q-bay location for the controls, in order to avoid the time and expense that would otherwise be needed to prove out a unit usable in the high-temperature chine environment.

The control system was founded on a few basic functions, which remained almost constant through the many revisions to accommodate the successive beam generating systems as they were developed:

Sensing and discrimination of voltages and currents was done with Sigma series 8300 magnetic amplifier relays, which will operate on differences between a signal and reference of less than a microwatt. With these, direct-current quantities were sensed directly, and ac quantities were measured by adding suitable rectification and filtering. More rapid detection of current or voltage than the magnetic amplifier affords was secured by using SCR's with dc supplies to control relays. The principal use of this circuit was for overcurrent (fault) sensing.

For vacuum monitoring of P_2, a thermocouple gauge was used. Its output could have been fed to a magnetic amplifier relay of suitable sensing coil impedance, except that for checkout a visual indication of pressure was also required. Accordingly, a contact-making indicator (Hastings Model CVT-4) was used with the gauge tubes (Hastings DV-4D) appropriate to the 0.1-2.0 torr range of interest.

High vacuum, P_4, was sensed by a Philips ionization gauge (CVC type PHG-06). This cold-cathode tube has the advantages of simple power supply requirements and absence of elements which can be damaged by vibration or exposure to atmosphere. A 1500 volt supply was incorporated in the control to power each of these gauges, interconnections suitable

to this voltage being made by coaxial cable and HN connectors. The tubes themselves were modified for use at high altitude by replacing the connecting cable supplied by the manufacturer with a bulkhead HN connector, whose leads were potted in Silastic.

A low resolution (3 bit) analog-to-digital converter was built to provide the telemetering signal for a continuous range variable, x-ray intensity in the tube system, and beam current for the pumped guns. An offset bias was built in to the converters to permit the linear scale characteristic to span the range of maximum interest. For reliability and circuit convenience, all other variables were arranged to be sensed as contact closures.

The ways in which signals, obtained from these sensing elements, from limit switches, from interlock contacts, and from external controls were combined to exercise the desired control are shown in the accompanying figures. Actual connections of the hybrid signals are inconvenient to trace, so logic diagrams are used to symbolize the control system relations.

The control built for the window tube installation was used in all the subsequent stages of evolution. Because most of the equipment phases actually overlapped, radical revision of the hardware was possibly only twice. Other changes were accommodated by cunning artifice that sometimes resulted in startling responses to component malfunctions or to operationally impossible inputs (ϕ-conditions).

The detailed functional organization of each version of the control system can be understood by examining the control logic diagrams. Fig. 5.06.01 is the version used for the chine installation. Several sub-groups enclosed in dotted lines appear as independent functional blocks in the other systems, where they are shown as single components with the same labels. Fig. 5.06.02 is the version for the Heraeus gun installed in the Q-bay, and Fig. 5.06.03 is the version originally designed to control the window tube. Each of these is taken from the corresponding operating system, and duplicates the response of the

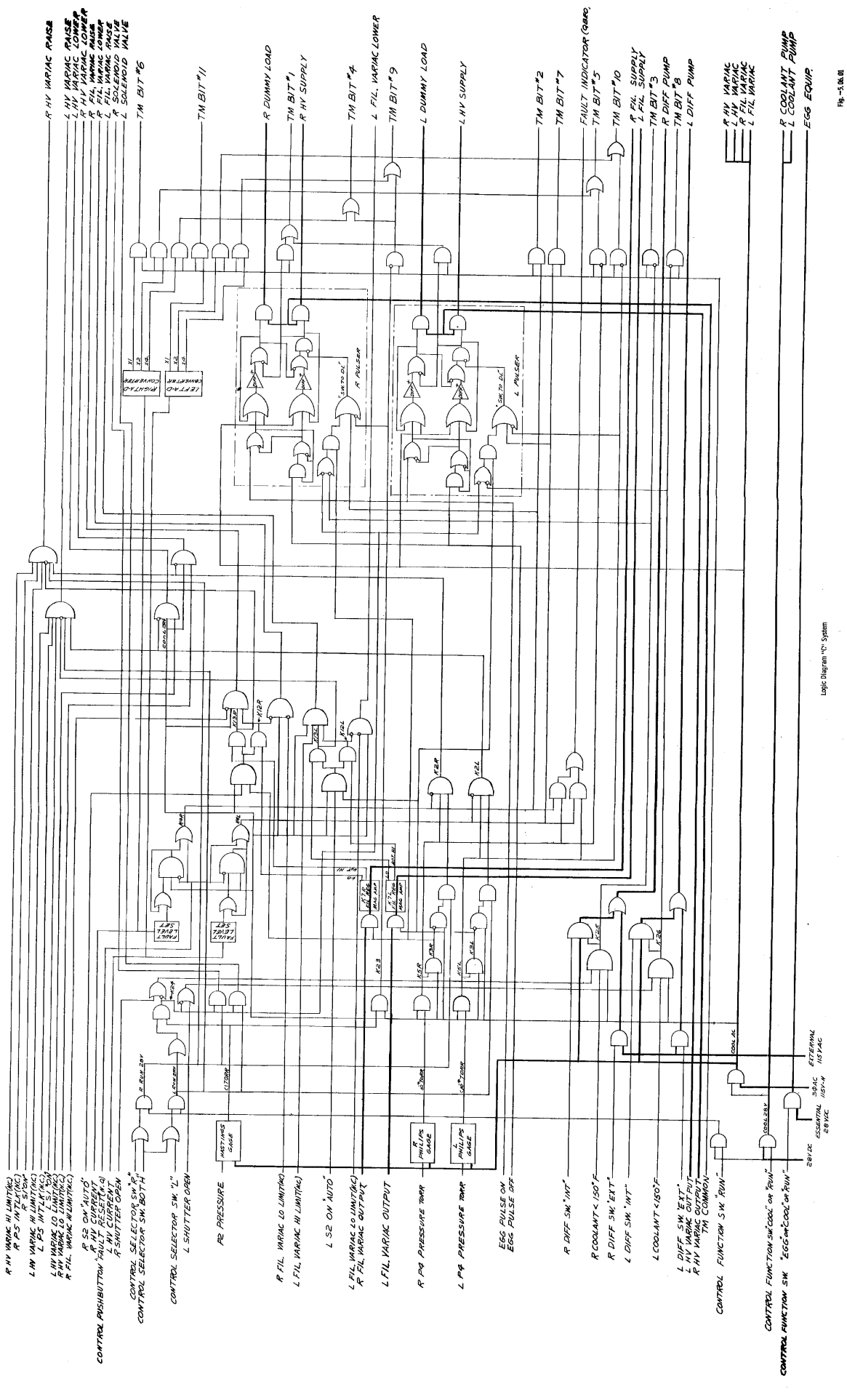

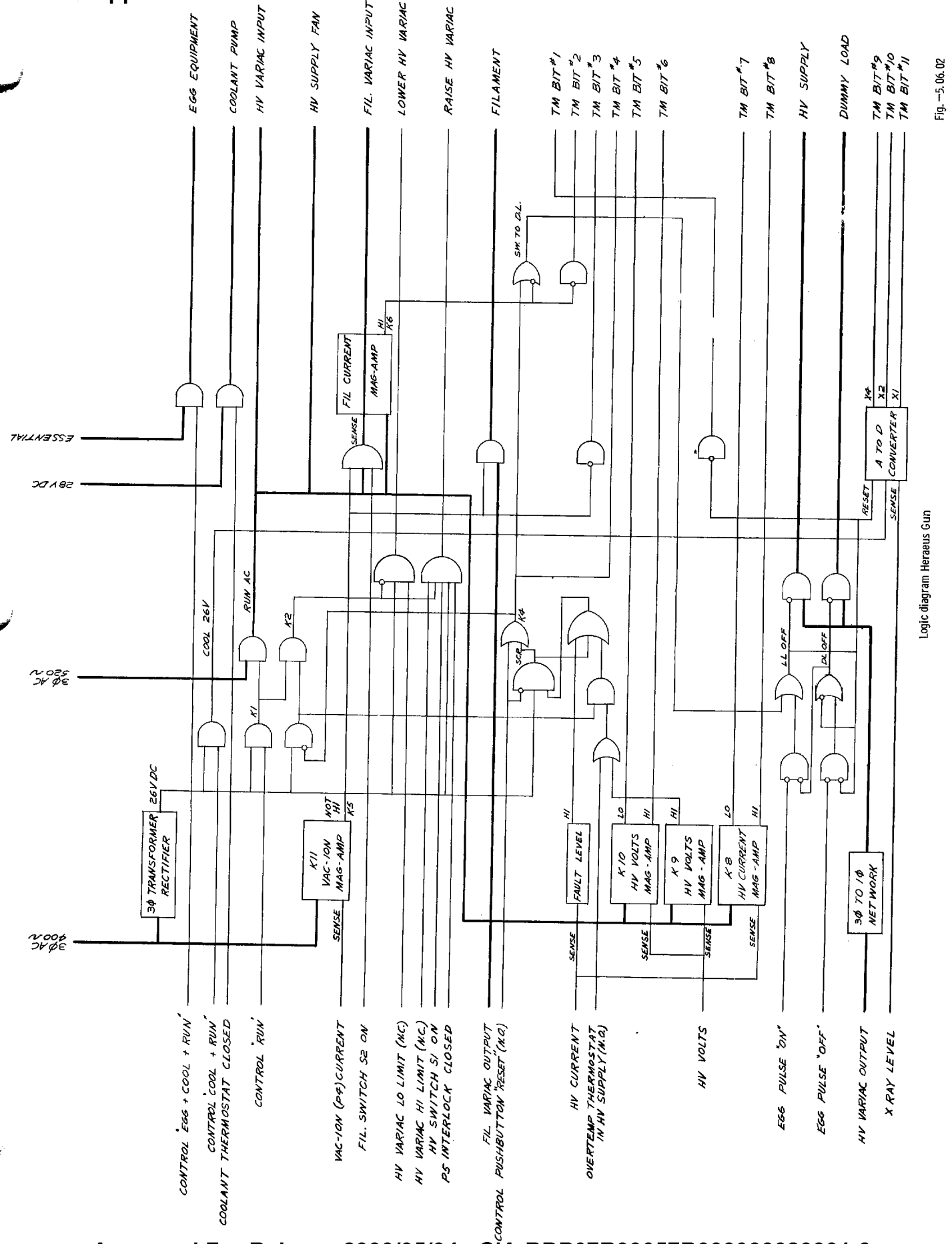

Fig. —5. 06. 02

Logic diagram Hereaus Gun

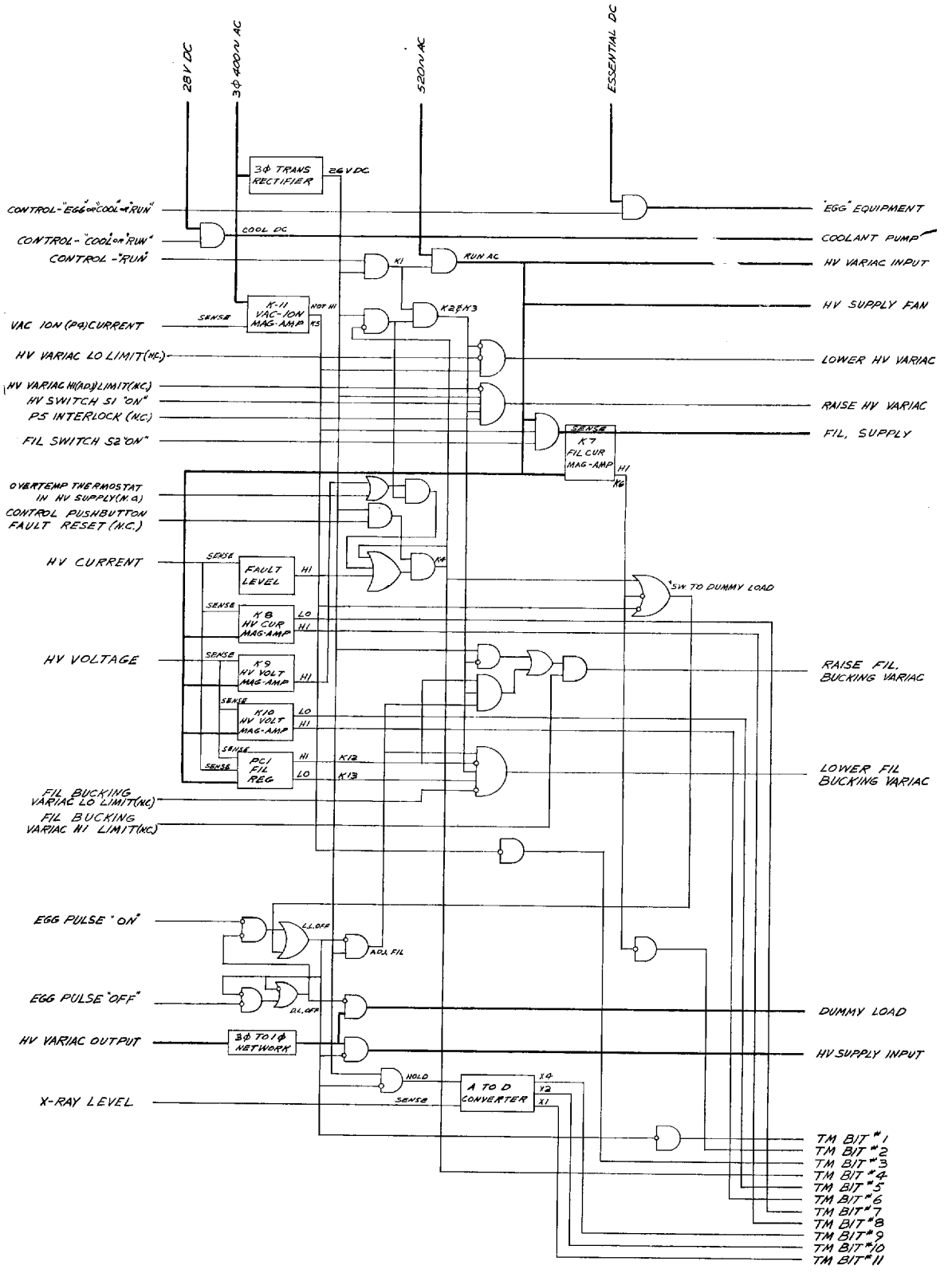

Logic diagram window tube

Fig. —5.06.03

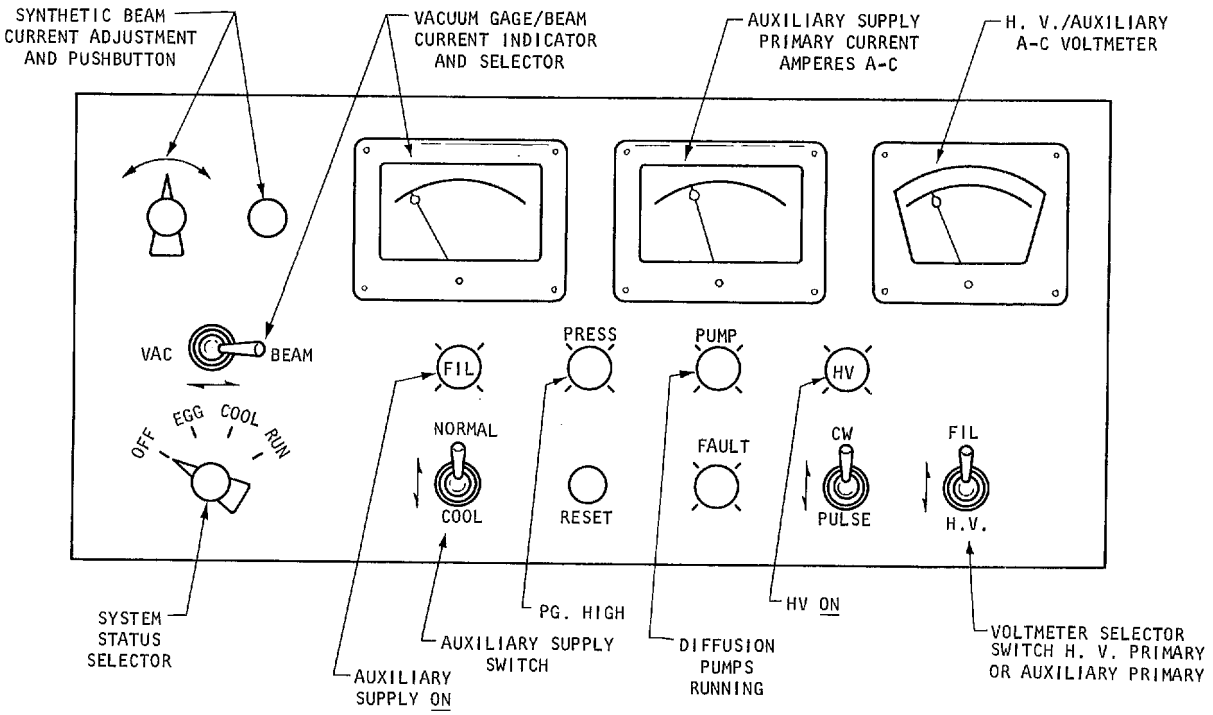

Laboratory control box

Fig. —5.06.04

physical system for all contemplated inputs. The response to ϕ-condition inputs may be different in the hardware and on the schematic.

In addition to its operating mode, every control system required modes for checking, testing and trouble shooting. These were provided by special jumper wires in the control input cable connector, which enabled the control to distinguish which mode of behavior to adopt. These jumpers, backed up by a few special switches and strategic clip leads, permitted almost any mode of control operation that was needed. Fig. 5.06.04 is a drawing of the panel of the laboratory control box, which contained all the controls requisite to starting up, checking the system in or out of the vehicle, or seeking out troubles in the apparatus. In a piece of servicing apparatus such as this, it is easy to be convinced that more and more direct control over the functions of the system is necessary, but the circuit complexity that entails, the extra hazard of failure it imposes on the operating control system, and the opportunities that it provides for human error to damage the system draw the line far short of the point at which technical problems begin to limit the special functions that can be introduced.

In contrast to the laboratory control panel, intended for testing and checkout, the pilot's control panel for in-flight operation of the equipment was made as simple as possible. It contained only a status selector (OFF / EGG / COOL / RUN), a gun selector (LEFT/BOTH/RIGHT), and a FAULT RESET button. The latter was included to permit manual restoration of high voltage after a fault, before the automatic reset circuits had passed through their complete cycle, a feature included to allow a minimum of down time during the relatively short data taking portion of a flight. To inform the pilot of fault conditions requiring reset action, use was made of the ship's Q-BAY EQUIPMENT OUT warning light. With this exception, all auxiliary systems were made automatic in operation and all status information was telemetered to the ground, rather than displayed in the cockpit, so that the pilot needed to have practically no concern about the operation of the Kempster system.

The telemetry consisted of eleven bits which could be assigned to whatever functions were of the greatest interest. The actual assignment was a compromise between eleven on-off indications and a completely encoded eleven bit telemetry word. Some bits changed significance, depending on the state of other bits; others retained their assignment. The logic diagrams include the bit assignments for each system.

CHAPTER 6
FIELD SUPPORT EQUIPMENT AND PROCEDURES

6.01. Introduction

A large fraction of the testing and checkout work in the field was done with the equipment installed in the aircraft, rather than in the laboratory. To facilitate this work, portable service and support equipment was needed.

No less important than adequate service equipment was sound service procedure. This was provided by a comprehensive set of check sheets, which were used to control all routines pertaining to preparations for flight tests.

Because most personnel were assigned to the field on a rotating basis, formalized procedures were essential, not only in checkout, but in maintainance and modification of equipment. Changes on all chine-mounted equipment were systematically administered, in order to prevent errors, uncertainties, and omissions.

One aspect of the operation of the equipment presented unusual requirements for field personnel. This was the incidental production of x-rays in normal operation and in checkout of the guns. Means were employed to assure safe conditions for all personnel concerned.

Field operation disclosed a number of items in the system needing improvement, some expected because of only limited testing prior to shipment, and some unexpected. Where time permitted, changes were made in the field. In other cases, however, schedule requirements dictated that compromises or temporary expedients be adopted. To aid in planning future work with the same or similar equipment, this chapter concludes with a summary of the additional changes believed desirable, as of the conclusion of the program.

6.02. Ground Support Equipment

In preparing the installed equipment for a flight, a number of different facilities were utilized:

1. A small motor-driven water pump to fill the system's coolant-circulating loop on reinstallation; also to circulate cooling water through the electron-beam catcher during ground operation.
2. Compressed air, supplied at low flow by a small air pump and at higher rates from the shop lines - to actuate the system's pneumatic valves and to furnish motive air for the ejector; also, as hot air, in reconditioning the sorbent in the sorb pump.
3. A general-purpose type vacuum pump, capable of an ultimate vacuum of 1-10 microns and having a displacement of about 15 cfm for sorb pump regeneration and for maintaining vacuum in the P_1 and P_2 spaces during ground operation into a vacuum-tight beam catcher.
4. Pressure-measuring means covering the range 1 micron to 1 atmosphere - for use with item 3.
5. A light-duty (5 ampere) 28 v dc power supply - for routine checking and special, temporary checkout requirements, especially when ship's power was not available.
6. A supply of liquid nitrogen - for filling the sorb pump.
7. An in-line air heater - for attachment to the system's LN2 fill port to provide hot air for sorb pump bake-out.
8. A supply of liquified insulating gas - for refilling or pressuring the power supply.

9. A source of 3-phase 515 cps 35 amp power - for full-power ground operation of the system power supplies without the core saturation that otherwise occurs if operated at 400 cps.

The first five requirements were provided by assembling appropriate equipment on a 2 ft x 3 ft cart which could be rolled to the side of the installation for connection to installed units. Fig. 6.02.01 shows this arrangement schematically. Items 6, 7, and 8 were carried on this same cart, although not built-in.

The last item was met by modifying an aircraft generator test stand, type AG108, equipped with a ship's generator, type 31121-000. A ship's generator controller, type 51133-000 was added to the stand, together with an output circuit breaker, reed-type frequency meter, output connectors, and dry batteries for field flashing.

To handle the C-units and move them safely in and out of the chines, an adapter was made to permit an aircraft generator ground-handling unit to be used. By this means, the equipment, mounted on the handler, could be rolled into place beneath the aircraft and hydraulically raised into position.

A final, major item for support equipment that was needed only in the laboratory was a high-capacity rotary pump. A Kinney KD4-250, 250 cpm pump was used for bench testing whenever the ejector was operated. This pump was able to produce the required ejector exhaust pressure of about 10 Torr at the operating throughput. A somewhat smaller pump, 100 to 150 cpm, would probably have been adequate, but the larger size was on hand, and additional capacity proved useful for some of the tests that were run.

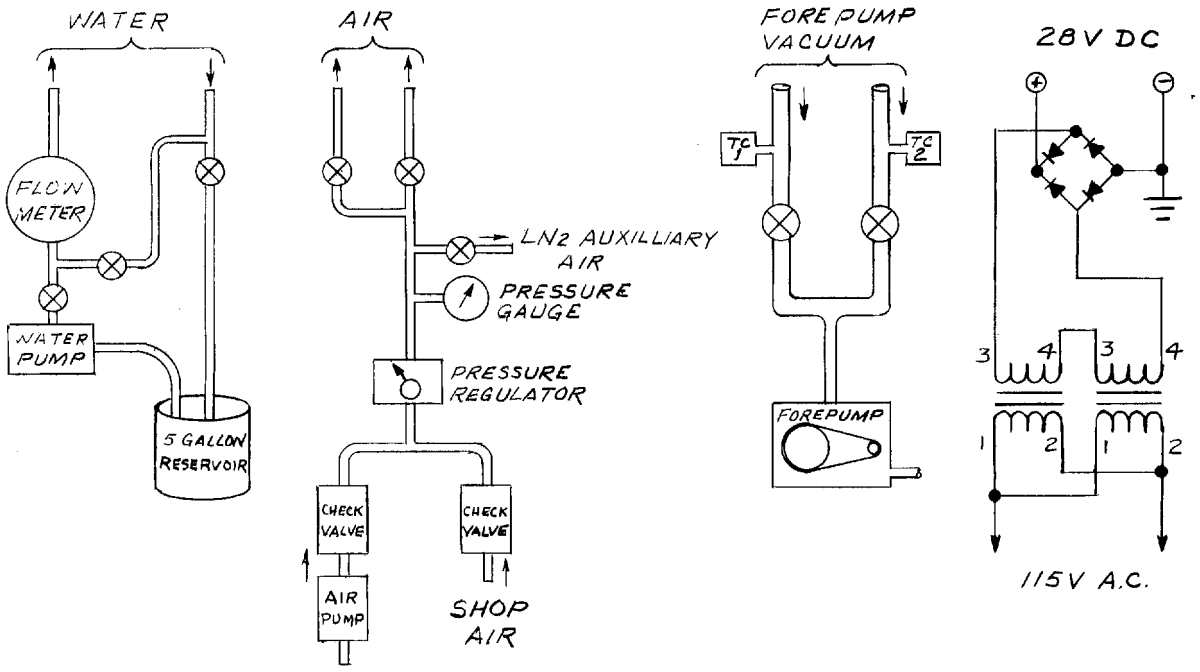

Ground Support Cut Service Systems

Fig. 6.02.01

6.03. Flight Test Operating Techniques

Preflight preparation:

The preflight procedures believed necessary for successful operation in flight varied widely over the course of the program. In the initial phase utilizing sealed-off solid anode (dummy window) tubes, operating the equipment was very much like operating commercial x-ray equipment, and almost no special preflight process was followed. Of course, the various components and interconnections were checked to insure no failures due to oversights. When the more complex differerentially pumped guns replaced the sealed tubes in the field, a more complex check out procedure became necessary, and a start-up phase had to be added.

The additional complexity was especially needed for the first pumped gun, the Heraeus system. This unit had been converted for flight use in as short a time as possible, and little attention was paid to making it operationally fool-proof. Accordingly, the check list for preflighting the system included step-by-step instructions, carefully planned and ordered to prevent inadvertent failures because of such oversights as admitting full atmospheric pressure to the sorb pump when cooled, or to the high vacuum space when the filament was heated. Experience with modifying the gun also pointed out a number of possible trouble spots in its operation. To insure a successful test, as many as possible of these were checked as a part of each preflight, with some additional steps being added to the check list accordingly.

When the field operation converted from the Heraeus gun to the C guns, there was a strong tendency to carry over most of the former check list. As time went on, however, it was found that few of the system's individual functions actually required preflight checking to verify proper operation, and some shortening of the list was possible. In addition, attention to fool-proofing, both in the basic unit and in the control system (which was drastically modified from the version used with the Heraeus gun) allowed most of the step-by-step instructions to be eliminated from the list. During the last few weeks of flight testing,

changes in procedure were made to simplify and speed up those parts of the preflight done on the last one or two hours prior to launch.

Fig. 6.03.01 is the "Flight Test Record" form used in the last two flights, with late changes incorporated. Some further simplification of the form would probably have been order, had the field program continued, but it was felt that no useful purpose would be served by making revisions after the conclusion of the tests, since there was no intention of using in the future exactly the same support and control systems, both of which interact strongly with the check list.

Basic objectives of the preflight procedures are fourfold:

1) To verify proper installation
2) To initiate pumping and to pump down the vacuum space
3) To condition the accelerator to tolerate operating voltages
4) To verify proper overall operation

The first of these is covered by pages 3 and 4 of the form and was carried out in the hangar; the next three utilize page 5, again in the hangar; while page 6 covers last minute operations and checks outdoors on the pad. The calibration data of page 2 is needed for telemetry interpretation and for experimental purposes. Page 1 summarizes the checkout and test results.

For the last few flights of the program, the preflight philosophy was changed so that all pumping down was done indoors, and the system vacuum was held after checkout by the sorb pump (which was then periodically serviced up to flight time). By this means, the most time consuming part of the immediate preflight list was eliminated, in addition to which the conditioned state of the guns seemed to be better retained.

Procedures during flight:

Flight paths employed in the test program consisted of three portions: outbound, turn-around, and inbound. On the outbound leg, which was limited in altitude over its initial portion, tracking lock and telemetry were usually lost, beginning at about 5 to 15 minutes after takeoff, to be reacquired following turn around on the initial part of the inbound

TEST FLIGHT RECORD

(Check one) Left___ Right___ Unit

Our Flight No._____

Scheduled Date/Time_____

Rescheduled Date/Time_____

Rescheduled Date/Time_____

Takeoff Date/Time_____

Landing Date/Time_____

TEST OBJECTIVES:

RESULTS:

EQUIPMENT:

Gun No.____ Power Supply No.____ Main Control No.____ Pulser No.___

Gun Location_____ Cathode Assy. No._____ A-D Converter No._____

Boiler Fluid_____ Circulating Fluid_____

Special Equipment_____

SETTINGS (NOMINAL)

E_p_____KV, I_p_____ma

Dummy Load_____ohms, Terminal Numbers_____

ϕBalance Circuit_____ Component Valves_____

Duty Cycle_____ Cycle Length_____msec.

CALIBRATION Date/Time _____/_____ Initials_____

GUN INSTALLATION Date/Time _____/_____ Initials_____

RACK INSTALLATION Date/Time _____/_____ Initials_____

OPERATION CHECKOUT Date/Time _____/_____ Initials_____

STARTUP Date/Time _____/_____ Initials_____

POSTFLIGHT Date/Time _____/_____ Initials_____

CHECK IF ADDITIONAL NOTES ON REVERSE SIDE _____

Fig. 6.03.01

"C" CALIBRATION

Left___ Right___Unit

Date_____

1. Power Supply Gas _____ At _____ psig at room Temperature.
2. Gun No. ____ Power Supply No. ____ Main Control No.____ Pulser No.___
   Test conditions desired: _____ KV, _____ma.
   Test conditions attained: HV pri ____ vac at ____cps (nom 151 cps)
   I_p_____ ma, I_t _____ma, V_{hv}_____KV
   I_{aux}_____ amp, E_{aux}_____ vac
   P_4 _____ Torr, R_k_____ohms
   Running Time _____Min.
   Radiation Level _____mr/hr at 1 Meter
   Line Volts _____
3.* Under frequency control setpoints: _____cps off, _____ cps on
4. Aux. power supply Man Level _____ volts, Auto Level _____ amps
5. Beam current trip level _____ ma.
6. Philips Gauge (P_4 trip level (____X10$^-$ Torr.) _____ ma.
7. A-D Converter No. _____

Count	000	001	010	011	100	101	110	111
Input 0 to								

Should be nominal current.

8. All potentiometers locked._____

NOTES:

*Not usually checked

Fig. 6.03.01 (continued)

"C" RACK INSTALLATION

Date _____

	Left	Right
1. Install control(s) and pulser(s) in rack.	____	____
a. Mate PL/R4. (See note 1)	____	____
b. Mate PL/R5.	____	____
c. Mate PL/R7	____	____
d. Mate PL/R8.	____	____
e. Mate PL/R9.	____	____
f. Mate PL/R10.	____	____
g. Connect both EGG coax lines.	____	____
2. Install A-D converter(s) in rack.	____	____
a. Mate PL/R41.	____	____
3. Install rack in Q-bay, mating Q4 on rack (Y-cable) with Q4 on article before hoisting last 18 inches.	____	____
4. Mate Q5 on rack (Y-cable) with DC cable Q5 on article.	____	____
5. Mate article AC cable(s) PL/R3 with PL/R3 on control(s).	____	____
6. Install gun control (Hastings) box on rack.	____	____
a. Mate P28.	____	____
b. Mate PL/R21.	____	____
c. Mate PL/R22	____	____
d. Mate PL/R26.	____	____
7. Mate KL/R1.	____	____
8. Connect KL/R3 terminals 1, 2 or 3, 4, 5, 6, and 8.	____	____
9. Connect strip chart recorder(s). Check paper supply.	____	____
10. Tie down all slack cables.	____	____

Note 1. Connections duplicated on both sides are shown L/R.

Note 2. EGG will usually handle their own connections and will close lower hatch.

Fig. 6.03.01 (continued)

"C" GUN INSTALLATION

Date _____

		Left	Right
1.	Check angular position of both clamping bands on HV tank.	____	____
2.	Check gun inclination angle.	____	____
3.	Check hardware for tightness and locking devices.	____	____
4.	Check air and water loops for continuity and tightness.	____	____
5.	Check insulating blanket for completeness, fit, and ties.	____	____
6.	Get alternator lift. Bolt lift stand onto lift head.	____	____
7.	Put gun on lift stand and move to article.	____	____
8.	Check that hoist path is clear and line up basket nuts.	____	____
9.	Be certain outer cylinder of lift is not stuck to center post. Jack gun into place, seated on brackets.	____	____
10.	Install three mounting bolts (forward, outboard).	____	____
11.	Have crew member install aft support bracket.	____	____
12.	Drop frame on hoist; install aft inboard mounting bolt.	____	____
13.	Loosen and retighten aft gun support to relieve strain.	____	____
14.	Hook up ship's air line.	____	____
15.	Fill the circulating coolant loop with fluid.	____	____
16.	Connect Philips gauge co-ax cable.	____	____
17.	Connect five heavy wires to terminals 1, 4, 5, 6, & 7 of KL/R4.	____	____
18.	Mate connector(s) KL/R2.	____	____
19.	Install X-ray monitor, if used.	____	____
20.	Have crew install rib gap sections and blanket.	____	____
21.	Have crew seal vent ports. Inspect. This must be done at least four hours before rollout in cold weather to allow seal to cure.	____	____
22.	Have crew install and seal ramp. Inspect.	____	____
23.	Reinstall alternator platform on lift and return.	____	____

Fig. 6.03.01 (continued)

"C" OPERATIONAL CHECKOUT Date _____ Left - Right

1. Have crew put 400 power on article and remove door (if on) Time ____
2. Connect TM light box to P9. Set lab control box to OFF, connect to P8. ____
3. Connect vacuum pump to P3 tap. Pump out hose. ____
4. Valve off pump, open P3 tap and note P3. Energize P4 jacket heater. ____
5. Connect 20 psig air thru air heater to sorb pump. Open pump valve to P3 and turn on heater. Time _____
6. In about 1/2 hour, P3 will peat at ___ and then fall. Turn off heater when P3 heads down below 100 μ. Time _____
7. When sorb pump exit air cools back down, disconnect air. Note P3. Disconnect P4 jacket heater. _____μ
8. Turn control to COOL. Diffusion pump should take hold within 10 min. Time _____
9. Throw S1 to OFF, control to RUN. Check A-D battery (5.9v min) _____v
10. Return control to COOL. Plug 2 holes in P1 manifold and connect cart's other vacuum hose to the third hole. ____
11. Remove ship's air line and cap ship's air inlet. ____
12. Install catcher with cooling lines. ____
13. Close valve to P3. Open valve to P1. With P1 less than P3, reopen P3. ____
14. Install and connect tuning motors and target current meter. ____
15. Connect 12 psig air to ground air inlet. (Shutter should be operable) ____
16. Change over to 520 power. Turn on catcher water and run beam. Note pri ____v, Ip ____ ma, It ____ma. Time _____

DO NOT SWITCH OUT OF "RUN' WITHOUT 2 MIN OF 0 CURRENT (shutter seal)

17. Turn control to OFF and disconnect pump from P1. ____
18. Remove tuning motors and catcher. ____
19. Remate P3, P8, and P9. Temporarily gnd. TB2-9 to check QBEO lite up front ____
20. Check recorder paper supply and connect to signal and power. ____
21. Connect all 3 bellows and boiler vent line. ____
22. Inspect seal at vents and ramp. Check for leakage if questionable ____
23. Disconnect ground air supply and cap inlet. Reconnect ship's air supply. ____
24. Close P3 valve, turn off and disconnect vacuum pump. ____
25. Fill cooling system boiler. ____

Fig. 6.03.01 (continued)

"C" PREFLIGHT STARTUP Date_____ Left Right

1. Connect vacuum pump to Ps tap. Pump out hose. Time _____ _____
2. Valve off pump, open P3 tap, note P3 _____μ _____μ
3. If above 50 μ, pump down and record _____μ _____μ
4. Close P3 tap, disconnect pump _____ _____
5. Fill sorb pump with LN2. Time _____ _____
6. Note HV tank pressure ____/ ____. If below 30, fill to 35 psig. _____
7. Check that ship's air line is connected and ground air line capped. _____ _____

REPEAT ON OTHER SIDE

8. Check that wheel well breakers are closed. _____ _____
9. On Gun Control Box note (a) Hastings set point _____T
   (b) Diffusion pump switch on INTERNAL _____ _____
   (c) Hastings power switch on LEFT RIGHT
   (d) Hastings Gauge Head selection LEFT RIGHT
10. On control units note (a) Switch S1 is ON _____ _____
    (b) Switch S2 is AUTOmatic _____ _____
11. Request clock pulses from EGG. _____
12. Set PCB to COOL. Time _____
13. Check for sound of chine water pumps. _____ _____
14. Check for flashing G bit by depressing G test button. (EGG unit must be on) _____
15. Check that P4 comes down (should be less than 10 min). Time _____
16. Check all fuses. Check diffusion pump lights on Hastings box. _____
17. Check misc. word from EGG. Should be Left only 0200, right only 0004, Both 0204 _____
18. Turn PCB to EGG. Misc. word should be L-0016, R-0700, Both 0716 _____
19. Top off sorb pumps with LN2. Help crew replace doors. (Use bellows tool). _____
20. Notify crew OK to close Q-bay hatches. Time _____

Fig. 6.03.01 (continued)

FLIGHT DATA

Our flight no. _____ A/C no. _____ Flight no. _____ Date _____

Time off _____ Time down _____ Pilot _____ EGG no. ___

Time	OFF	EGG	COOL	RUN	G	F	T+ S_x	X_4 PS+	X_2 P+	X_1	REMARKS

Debriefing notes:

Fig. 6.03.01 (continued)

"C" POSTFLIGHT CHECKSHEET

Date _____

		Left	Right
1.	Remove recorder strip chart(s) if used.	____	____
2.	Remove door, using bellows holding tool.	____	____
3.	Connect vacuum pump and gauge to P3 tap. Pump down hose.	____	____
4.	Valve off pump and open P3 tap. Record P3 pressure. P3 (left) = _____T P3 (right) = _____T	____	____
5.	Blow out residual LN_2. If none, so note.	____	____
6.	Note apparent mechanical damage.	____	____
7.	Recover X-Ray monitor if used.	____	____
8.	Refil boiler. Record amount used. Left _____ cc Right _____cc	____	____
9.	Check all fuses.	____	____
10.	Check pressure in HV tank and record. Left ____psig Right _____ psig.	____	____

Fig. 6.03.01 (concluded)

leg, usually at 30 minutes after takeoff. During as much as possible of the next 15 minutes data was taken so that it was desirable that the diffusion pumps be started immediately after takeoff to allow ample time for the system to attain its operating pressure and for the cathode temperatures to stabilize. On the other hand, it was not desired to start the pumps before takeoff because of the possibility of subsequent unscheduled delays prior to takeoff, which might result in overheating the cooling systems. Accordingly, the preflight concluded with all power removed from the units. This had the added advantages that removal of ground power from the ship, if necessary, had no effect on the system, and that no power was present when the ac frequency (at engine idle rpm) was below the transformer saturation frequencies (a safety factor in addition to the underfrequency trip device incorporated in the unit controls).

Immediately after takeoff, the pilot switched the system to COOL, starting the cooling system circulators and energizing the diffusion pump heaters. Approximately 7 minutes later, the cathode of each gun was automatically energized, in response to a "pressure OK" signal from the respective P_4 pressure sensor. This allowed about 23 minutes for cathode warm-up prior to use. For the data run, the pilot actuated the guns by switching to RUN, either at a prearranged altitude and position, or on radio command from the EC&G test control room. On completion of the run, the pilot returned the system to COOL, usually by prearrangement, but occasionally on radio command. Prior to landing

25X1A

he de-energized the [redacted] system, leaving the telemetry system operating, however, until after touch-down.

During the flight, the status of each gun was monitored visually at the EC&G test control point by means of a remote indicator for the 11-bit "miscellaneous" telemetry word. The form used for recording relevant events appears on page 7 of the test sheets, Fig. 6.03.01. By this means, it was possible to spot and diagnose troubles immediately in the field, without having to wait several days for a data reduction printout from the magnetic tape recording of the same telemetered information.

To assure accuracy in spite of the speed with which some of the indications changed, the register readings were read into a dictating machine, for later transcription to the form. This technique also permitted other comments to be recorded. The [redacted] controller, in addition to monitoring his system status indicator, was included in the EC&G intercommunications net, from which aircraft range, heading, and status could be obtained, and through which messages to and from the pilot could be relayed. 25X1A

In general, the procedures employed at the EC&G control point worked quite smoothly and the support rendered was very satisfactory. One facility that was provided turned out to be particularly helpful: a 4-channel pen recorder was utilized to record real time (for later reference to taped data), aircraft range, the "gun on" telemetry bit, and the log-i.f. dc output of the rf-data receiver. This information, with the [redacted] status data, gave a preliminary idea of the results of the test and allowed interesting time intervals to be identified for data reduction from the magnetic tape. Interpretation was aided by including a db calibration on the rf-data channel of the pen recording. 25X1A

Postflight Items:

Following engine shutdown, the units were inspected for any visible mechanical or electrical discrepancies, and the amounts of cooling fluids used up in flight were noted. These items were recorded on the last page of the log sheets. Additional data, such as altitude and speed attained during the data run and any unusual occurrences, were obtained at the formal debriefing about one hour after landing and noted in the log sheets.

Recommendations:

In retrospect, extensive simplification of both the check forms used and the procedures followed now appear desirable. Specific changes depend on the exact nature of future systems and on the use to which they are put, i.e., operational or experimental, and so cannot realistically be set down at this time.

6.04. Maintenance and Modifications

Records and Systems:

As work progressed, the need for improvements occurred to the laboratory-based group, and field operation pointed out deficiencies which should be remedied. In order to keep the records straight, every major event in the life of each piece of equipment was recorded in a notebook, physically attached to the equipment when possible.

Changes which were agreed upon were documented and carried out for all C-units through a formal modification kit system.

When a change was accepted as desirable, kits of all the new parts required were made up with a form which indicated the exact change to be made. Even if no new material was required, a form was used to document compliance with the modification instructions.

Maintenance Philosophy:

A good preventative maintenance program, if properly executed, should assure reliable equipment operation and cause off or down time to be practically eliminated. Such a program requires that a thorough evaluation of all electrical and mechanical units be made in preparing a maintenance manual. Certain items should have daily, weekly and monthly checks. Strict adherence to all charts and check sheets and workmanship of the highest order should be employed. The spare parts supplied should carry sufficient information for easy identification, installation and reordering. With good recommended procedure and qualified personnel the trouble-free upkeep of any equipment should be routine.

Throughout the field phase of the program, this philosophy was implemented wherever possible, although developmental aspects of the effort frequently required compromises. It is recommended that future efforts seek to identify necessary maintenance procedures prior to beginning field tests, and that equipment development in the field be held to an absolute minimum.

6.05. X-ray Protection of Personnel

In flight operation, the electron beam becomes a source of x-rays produced by electron collisions with air molecules. Personnel and radiation sensitive items such as film are accordingly protected by a combination of natural shielding, proper distance limitations, and, in a few instances, special shielding. During ground checking and testing, the source is more intense, because of the higher production efficiency of the targets encountered. In order to protect the personnel who are near the equipment, several steps were taken.

1. Radiation was contained as much as possible at the source, by thoroughly shielding the electron beam catcher. Using a low-atomic-number beam stopping material (graphite) also minimized radiation from that source.
2. Rope barriers were erected to keep personnel a safe distance away from the source. (Radiation decreases as the inverse square of distance).
3. Adequate monitoring instruments were kept available and continuously utilized to measure the radiation flux in occupied areas. Both ionization chamber and geiger counter radiation instruments were utilized for survey work, and all personnel associated with the project were issued film badges. In addition, a supply of pocket ionization chamber dosimeters was obtained to help any individual estimate the dosage received during actual operation of the gun.
4. Supplementary portable lead shields were used, especially in the laboratory, for those few instances when close proximity to the equipment was required for observation or adjustment.

With these procedures and precautions, no excess radiation exposures were experienced, as evidenced by the film badge records.

6.06. Recommended Modifications

Introduction:

Experience with the elements of the system during the development phase and in operation suggested many points which could be improved in any extension of the approach. Many of these points have been recognized from the time they were adopted as quick substitutes for more satisfactory solutions with unacceptably long lead times; others were dividends of the experimental programs.

Gun:

1. Insulator

   Incorporating the new "pancake" style insulator will allow the use of a much shorter stem and thereby raise the natural frequency of the cathode and stem support assembly. The successful laboratory trial of the prototype suggests concentration on this approach. The short insulator will also allow a considerable weight and size reduction in the transition section on future designs.

2. Cathode Assembly and Stem

   The plug-in cathode assembly replaces a heavy, complicated and sensitive cathode. Replacement in the field is currently a major effort which will be greatly simplified with the plug-in feature. The new design is also much lighter in weight, which further raises the natural frequency of the cathode and stem support assembly.

   The stem design is shorter to keep the cathode-to-anode spacing the same as the present unit, while incorporating the new insulator. The new stem also is lined with copper to help transfer heat from the cathode assembly back to the gas cooling of the power supply.

3. Anode Tilt and Adjustment

   Some rework in this area is necessary to insure positive motion of the anode plate with no conceivable backlash or play. Some

simplification is also warranted in this area since not all of the incorporated features are presently used.

4. Isolation Valves

The N_3 orifice should be valved rather than N_2 plus the ejector. This will completely eliminate the ejector valve. This was not done on the first units because of the complexity of the design and the short time available.

Power Supply:

1. High Voltage Surge Resistor

The high voltage surge resistor has failed a number of times and should be redesigned to take the load more reliably. The mechanical support and spacing surely add to the problem and should be redesigned.

2. Six Pin Connector

If it proves impractical to relocate the power supply positive lead, the six pin connector on the tank should be changed to one which will withstand the gas pressure load, high temperature and low ambient pressure.

3. Gas Cooling Loop

The gas cooling loop in the power supply should be modified to provide cool gas to hot spot areas. The present configuration just pulls the gas across a heat exchanger and cools but does not direct the gas to any particular location.

4. Lead Channels

The internal leads to the power supply connector are presently taped to the walls of the power supply housing and can come loose and possibly cause arcing. Channels securely fastened to the housing should be provided for all leads.

5. Modify Current-Monitoring Technique

Under fault conditions, the present arrangement gives unacceptably high voltages on the current monitoring lead. These in turn damage connectors, especially at low ambient pressure, and

cause failure of other parts wired to the same connectors. Cursory attempts to limit the voltage rise on this lead have not been completely successful. A thorough analysis of the problem is expected to produce a satisfactory solution, however.

Cooling System:

1. Pump

   A new pump should be considered for use in the cooling loop. The motor should be 500 cycle, 3 phase to get away from the brush wear problem encountered with the 24 volt dc motor in the present system.

2. Sight Glass

   There is no way of checking the water flow in the closed loop portion of the cooling system. A sight glass in the system at an accessable position would enable a visual water check.

3. General

   A complete re-evaluation of the cooling system should be made in view of past problems. Consideration should be given to the possibility of steady state operation.

Mounting:

1. Slip Joints

   Beam axis movement should be considered if slip joints in the chine blankets are to be incorporated in the installation.

2. Access

   Better access should be provided to facilitate maintenance and check-out. The present access door is just large enough to permit check out but not large enough or located to permit minor maintenance.

3. Ramp

   A permanent ramp should be installed to eliminate the need for re-sealing every time the skin panel is removed and re-installed.

Environmental Test, Loads and Temperatures:

The gun should be subjected to the vibration loads and temperatures encountered during actual operation to determine structural integrity. The gun should also be operated and performance checked at actual conditions expected.

Support Equipment:

1. Service Cart

   The carts should be redesigned so units can be checked out more readily and also be more presentable. More safety devices should be added to prevent check-out failures.

2. Catcher

   A heavy duty catcher should be designed to handle the full output of the gun. The present catcher was not designed to handle full power.

With the inclusion of these modifications, either in the presently existing equipment, or in a new, redesigned system, it is felt that trouble-free, reliable operation would be obtained.